

Isolation and Structure Elucidation of Secondary Metabolites from Fungi

Inaugural-Dissertation

Zur Erlangung des Doktorgrades
der Mathematisch-Naturwissenschaftlichen Fakultät
der Heinrich-Heine-Universität Düsseldorf

vorgelegt von

Yang Liu

aus Dalian, China

Düsseldorf, Jun, 2016

Aus dem Institut für Pharmazeutische Biologie und Biotechnologie der
Heinrich-Heine Universität Düsseldorf

Gedruckt mit der Genehmigung der
Mathematisch-Naturwissenschaftlichen Fakultät der
Heinrich-Heine-Universität Düsseldorf

Gedruckt mit der Unterstützung des
China Scholarship Council, the Ministry of Education of China

Referent: Prof. Dr. Peter Proksch

Co- Referent: Prof. Dr. Rainer Kalscheuer

Tag der mündlichen Prüfung: 22. 08. 2016

Erklärung

Hiermit erkläre ich ehrenwörtlich, dass ich die vorliegende Dissertation mit dem Titel „Isolation und Strukturaufklärung von Sekundärmetaboliten aus Pilzen“ selbst angefertigt habe. Außer den angegebenen Quellen und Hilfsmitteln wurden keine weiteren verwendet. Diese Dissertation wurde weder in gleicher noch in abgewandelter Form in einem anderen Prüfungsverfahren vorgelegt.

Düsseldorf, den 28. 06. 2016

Yang Liu

Abstract

Endophytic fungi are microorganisms that colonize the inner tissues of healthy plants without causing any apparent disease symptoms. In recent years, the focus of bioactive natural products research has shifted from plants to endophytic fungi, as the latter of them have the capacity to produce the same bioactive agents originally found in their host plants. Several fungal secondary metabolites are already used as drugs or lead compounds, such as plinabulin, cyclosporin A, simvastatin or cephalosporin C, indicating that endophytes are a rich source of bioactive natural products with a huge pharmaceutical potential.

The projects involved in this dissertation mainly focus on the isolation of bioactive secondary metabolites from axenic cultures of endophytic or soil-derived fungi, as well as from fungal-bacterial co-cultivation experiments, with the aim of activating silent gene clusters that are not expressed under standard laboratory culture conditions. The structures of the isolated secondary metabolites were elucidated by 1D (^1H and ^{13}C), 2D (HSQC, HMBC, COSY, ROESY) NMR spectroscopy, and HRESIMS spectrometry, as well as by electronic circular dichroism (ECD) spectroscopy. The pure substances were investigated for their cytotoxicity toward the murine lymphoma cell line L5178Y, and against human lymphoma Ramos and Jurkat J16 cell lines, as well as for their antibiotic activity against *Staphylococcus aureus*, *Escherichia coli*, *Pseudomonas aeruginosa*, *Enterococcus faecalis*, and *Mycobacterium tuberculosis*.

In summary, 26 secondary metabolites were obtained from two endophytic fungi *Stemphylium globuliferum* and *Annulohypoxylon* sp., as well as from the hypersaline lake derived fungus *Cladosporium cladosporioides*. Nine of the isolated metabolites were identified as new natural products. This dissertation consists of the following three parts, which have led to four publications.

Metabolites from the endophytic fungus *Stemphylium globuliferum*

Stemphylium globuliferum was isolated from the plant *Juncus actus*, which was collected from the shore of the hypersaline lake El Hamra located in Wadi el Natrun in Egypt. Thirteen secondary metabolites were isolated from the crude extract, including six new natural products, stemphylanthranol A, stemphylanthranol B, dihydroaltersolanol B, dihydroaltersolanol C, and the atropisomers acetylalterporriol D and acetylalterporriol E. Notably, stemphylanthranols A and B were identified as the first naturally occurring trimeric anthraquinone derivatives. Altersolanols A–C, dihydroaltersolanol C, acetylalterporriol E, alterporriol E, and 6-*O*-methylalaternin showed strong cytotoxicity against the murine lymphoma (L5178Y) cell line with IC₅₀ values ranging from 1.25 to 10.4 μM. Furthermore, dihydroaltersolanol C exhibited moderate antibacterial activity against *S. aureus* with a minimum inhibitory concentration (MIC) of 49.7 μM.

Metabolites from the hypersaline lake derived fungus *Cladosporium cladosporioides*

The fungus *Cladosporium cladosporioides* was isolated from the sediment of the hypersaline lake El Hamra located in Wadi el Natrun in Egypt. Four secondary metabolites were isolated from the crude extract of *C. cladosporioides*, one of which was identified as a new viriditoxin derivative, designated cladosporinone. All isolated compounds were investigated for their cytotoxicity against the murine lymphoma cell line L5187Y and for their antibiotic activity against several pathogenic bacteria. Viriditoxin was by far the most active compound, exhibiting selective activity against *Staphylococcus aureus* ATCC 29213 with an MIC value of 0.015 μg/mL (0.023 μM). Moreover, viriditoxin and its new congener cladosporinone showed strong cytotoxicity with IC₅₀ values of 0.15 and 0.88 μM, respectively. The structure activity relationships of the isolated compounds were discussed based on their activities in the respective cell lines.

Metabolites from the mangrove-derived endophytic fungus *Annulohypoxyton* sp.

The endophytic fungus *Annulohypoxyton* sp. was isolated from the Mangrove plant *Rhizophora racemosa* collected in Cameroon. Nine secondary metabolites were obtained from the crude extract, including two new benzo[*j*]fluoranthene-based metabolites daldinone E and daldinone G, as well as an artefact, daldinone F, which originated from daldinone E during the isolation procedure. Co-cultivation of *Annulohypoxyton* sp. with *Streptomyces lividans* or with *Streptomyces coelicolor* resulted in an up to 38-fold increase of 1-hydroxy-8-methoxynaphthalene, while no significant induction was detected when the fungus was co-cultivated with either *Bacillus subtilis* or with *Bacillus cereus*. Daldinone F exhibited strong to moderate cytotoxicity against Ramos and Jurkat J16 cell lines with IC₅₀ values of 8.5 and 13.9 μ M, respectively. Mechanistic studies suggested that daldinone F caused apoptosis by activating caspase-3 via the intrinsic pathway. Moreover, daldinone F potently blocks autophagy, a potential pro-survival pathway for cancer cells. The biogenetic pathway of the isolated benzo[*j*]fluoranthene derivatives is suggested to start with the oxidative coupling between 1,3,8-trihydroxynaphthalene (3HN) and 1,8-dihydroxynaphthalene (DHN). Feeding experiments with DHN which was added to the growing fungal culture increased the accumulation of daldinone B, which is in accordance with the proposed biogenetic pathway of benzo[*j*]fluoranthene derivatives.

Zusammenfassung

Endophytische Pilze sind Mikroorganismen, die in gesunden Pflanzen leben und ihrem Wirt keinen Schaden zufügen. In den letzten Jahren entdeckte man, dass endophytische Pilze die Fähigkeit besitzen, die gleichen Verbindungen wie ihre Wirte zu produzieren, was den Fokus von bioaktiven Naturprodukten von Pflanzen auf endophytische Pilze verschob. Viele Sekundärmetabolite aus Pilzen z.B. Plinabulin, Cyclosporin A, Simvastatin oder Cephalosporin C werden bereits als Arzneimittel oder Prodrugs verwendet. Die erfolgreiche Anwendung dieser Verbindungen verstärkte die Forschung in Richtung bioaktiver Sekundärmetabolite aus endophytischen Pilzen.

Die einzelnen Untersuchungen, die diese Dissertation beinhaltet, konzentrieren sich hauptsächlich auf bioaktive Sekundärmetabolite aus endophytischen Pilzen, sowie Ko-Kultivierung, um unter Laborbedingungen nicht-exprimierte Gen-Cluster zu aktivieren. Es konnten mehrere zytotoxische und antibakterielle Verbindungen aus den bearbeiteten Endophyten isoliert werden, welche für weitere Studien interessant sind. Die Strukturen der Sekundärmetabolite wurden per 1D (^1H und ^{13}C), 2D (HSQC, HMBC, COSY, ROESY) NMR-Spektroskopie, sowie HR-ESI-MS-Spektrometrie, als auch mittels Circular dichroismus Spektroskopie (ECD) bestimmt. Darüber hinaus wurden die Reinsubstanzen hinsichtlich ihrer Zytotoxizität gegenüber der murinen Lymphomzelllinie L5178Y und der menschlichen Lymphomzelllinien Ramos und Jurkat J16, sowie hinsichtlich ihrer antibiotischen Aktivität gegenüber *Staphylococcus aureus*, *Escherichia coli*, *Pseudomonas aeruginosa*, *Enterococcus faecalis* und *Mycobacterium tuberculosis* getestet.

Insgesamt konnten 26 Sekundärmetabolite aus zwei endophytischen Pilzen, *Stemphylium globuliferum* und *Annulohyphoxylon* sp., sowie einem hypersalinen Bodenpilz *Cladosporium cladosporioides* isoliert werden. Neun dieser Verbindungen wurden als neue Naturprodukte identifiziert und eine als neu beschriebenes Artefakt. Alle Substanzen wurden hinsichtlich ihrer antibiotischen und zytotoxischen Aktivität evaluiert. Diese Dissertation besteht aus den folgenden vier Teilen, die bereits in wissenschaftlichen Journalen publiziert oder zum

Publizieren eingereicht wurden:

Endophytischer Pilz *Stemphylium globuliferum*

Der Pilz *Stemphylium globuliferum* wurde aus der Pflanze *Juncus actus* isoliert, welche am Ufer des hypersalinen Sees El Hamra im Wadi El Natrun, Ägypten, gesammelt wurde. Es konnten dreizehn Sekundärmetabolite aus dem Rohextrakt isoliert werden. Sechs davon wurden als neue Naturprodukte identifiziert, namens Stemphyanthranol A, Stemphyanthranol B, Dihydroaltersolanol B, Dihydroaltersolanol C und die Atropisomere Acetylalterporriol D und Acetylalterporriol E. Hierbei wurden Stemphyanthranol A und B als erste natürlich vorkommende trimere Anthrachinonderivate identifiziert. Dihydroaltersolanol B und C sind Derivate von Altersolanol B und C, bei denen die Doppelbindung des aliphatischen Rings hydriert wurde. Der Unterschied der neuen Atropisomere Acetylalterporriol D und E zu den Alterporriolen D und E war die Acetylierung der Hydroxygruppe (3-OH). Altersolanol A-C, Dihydroaltersolanol C, Acetylalterporriol E, Alterporriol E und 6-O-methylalaternin zeigten starke zytotoxische Aktivität gegenüber der murinen Lymphomzelle L5178Y mit IC₅₀-Werten zwischen 1,25 und 10,4 µM. Zudem zeigte Dihydroaltersolanol C auch moderate antibakterielle Aktivität gegen *S. aureus* mit einer minimalen Hemmkonzentration (MIC) von 49.7 µM.

Boden-Pilz *Cladosporium cladosporioides*

Der Pilz *Cladosporium cladosporioides* wurde aus dem Sediment des hypersalinen Sees El Hamra in Wadi El Natrun, Ägypten isoliert. Vier Sekundärmetabolite wurden aus dem Rohextrakt von *C. cladosporioides* isoliert, von denen einer der neue Sekundärmetabolit Cladosporinon war. Alle isolierten Verbindungen wurden hinsichtlich ihrer zytotoxischen Aktivität gegenüber der murinen Lymphomzelllinie L5178Y und ihrer antibiotischen Aktivität gegen mehrere pathogene Bakterien untersucht. Viriditoxin, der Hauptsekundärmetabolit des Rohextraktes, fiel besonders auf Grund seiner selektiven Aktivität gegenüber *Staphylococcus aureus* ATCC 29213 mit einem MIC-Wert von 0.015 µg/mL (0.023 µM) auf. Der neue

Sekundärmetabolit Cladosporinon ist ein Viriditoxin-Derivat, welches nur zytotoxische Aktivität zeigte. Die Struktur-Wirkungs-Beziehung der Verbindungen wurde anhand ihrer zytotoxischen und antibiotischen Aktivität erörtert. Der vorgeschlagene Polyketid-Biosyntheseweg des Viriditoxins und seiner Derivate wird diskutiert.

Mangroven-Endophyt *Annulohyphoxylon* sp.

Der endophytische Pilz *Annulohyphoxylon* sp. wurde aus der Mangrovenpflanze *Rhizophora racemosa*, die in Kamerun gesammelt wurde, isoliert. Aus dem Rohextrakt konnten neun Sekundärmetabolite isoliert werden. Es handelte sich hierbei um zwei neue Benzo[*j*]fluoranthen-basierende Metabolite (Daldinon E und Daldinon G), sowie ein neues Artefakt (Daldinon F), das während des Isolierungsprozesses aus Daldinon E entstand. Kultivierungsexperimente von *Annulohyphoxylon* sp. mit dem Aktinomyzeten *Streptomyces lividans* resultierten in einer 38-fachen Zunahme von 1-Hydroxy-8-methoxynaphthalen. Im Gegensatz dazu konnte während der Ko-kultivierung des Pilzes mit *Bacillus subtilis* oder mit *Bacillus cereus* keine signifikante Induktion detektiert werden. Daldinon F zeigte starke bis moderate Zytotoxizität gegenüber den Ramos- und Jurkat J16-Zelllinien mit IC₅₀ Werten von 8,5, bzw. 13,89 µM. Weitere Untersuchungen zeigten, dass Daldinon F über den intrinsischen Weg eine Caspase-3-Aktivierung bewirkt und somit die Apoptose induziert. Desweiteren blockiert Daldinon F wirksam die Autophagie, welche einen potentiellen Signalweg für das Überleben der Krebszellen darstellt. Ein Biosyntheseweg für die Benzo[*j*]fluoranthen-Derivate beinhaltet die oxidative Kopplung zwischen 1,3,8-Trihydroxynaphthalen (3HN) und 1,8-Dihydroxynaphthalen (DHN). Ein Fütterungsexperiment mit DHN erhöhte die Akkumulation von Daldinon B im Pilzextrakt, was dem vorgeschlagenen Biosyntheseweg der Benzo[*j*]fluoranthen Derivate entspricht.

Contents

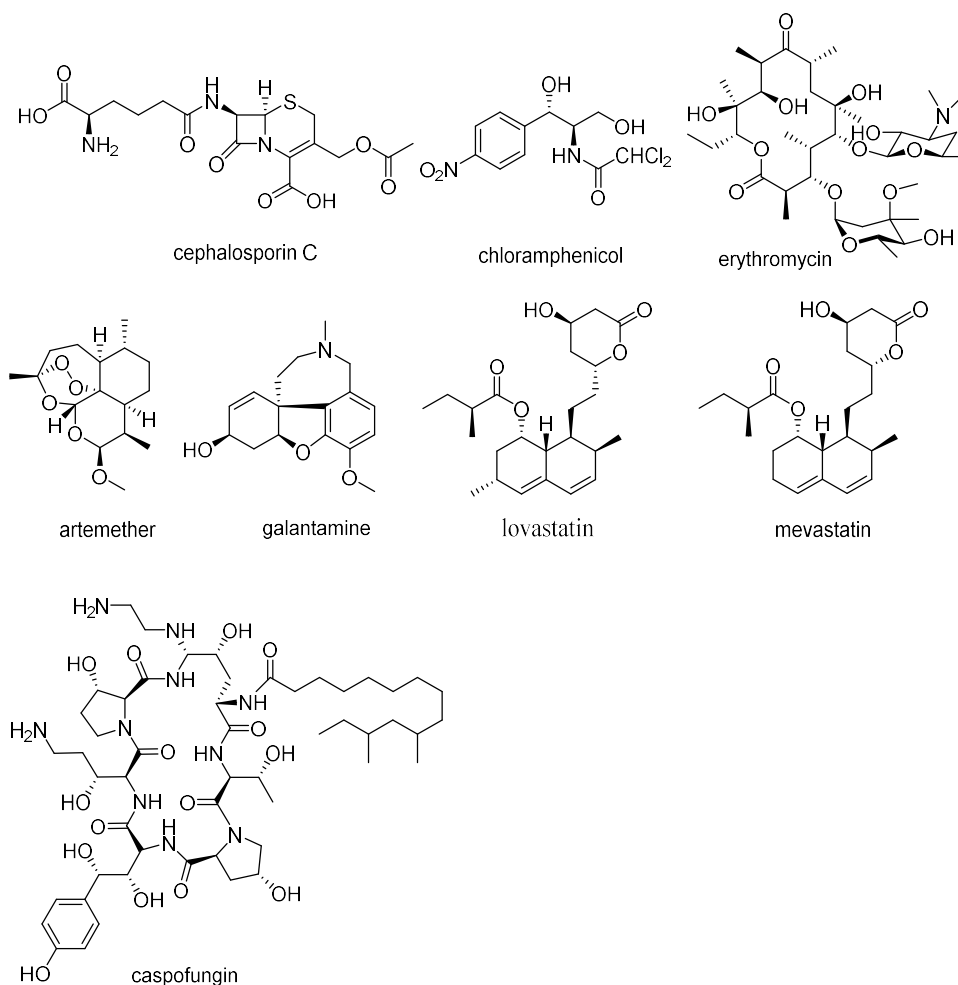
1 General Introduction	1
1.1 Natural products and drug discovery	1
1.2 Endophytes: a rich source of bioactive metabolites	2
1.2.1 Fungi derived from terrestrial plants	4
1.2.2 Fungi derived from the marine environment	4
1.3 Anti-cancer drugs derived from fungal secondary metabolites	5
1.3.1 Fungal anticancer drugs with anti-angiogenesis activity	5
1.3.1.1 Plinabulin	6
1.3.2 Fungal anticancer drugs with antitubulin activity	6
1.3.2.1 Paclitaxel	7
1.3.2.2 Vinca alkaloids	8
1.3.3 Fungal anticancer drugs with DNA topoisomerase inhibition	8
1.3.3.1 Camptothecin	9
1.4 Strategies to maximize the diversity of fungal secondary metabolites	10
1.4.1 Medium optimization	10
1.4.2 Co-cultivation as a useful tool to activate silent gene clusters	11
1.5 Aim of the study	11
2 Publication 1	14
2.1 Trimeric Anthracenes from the Endophytic Fungus <i>Stemphylium globuliferum</i>	15
3 Publication 2	40
3.1 Tetrahydroanthraquinone Derivatives from the Endophytic Fungus <i>Stemphylium globuliferum</i>	41
4 Publication 3	79
4.1 Cladosporinone, a new viriditoxin derivative from the hypersaline lake derived fungus <i>Cladosporium cladosporioides</i>	80
5 Publication 4	93
5.1 Benzo[j]fluoranthene Metabolites from a Mangrove Derived Endophytic Fungus	

<i>Annulohypoxyton</i> sp.	94
6 General discussion	170
6.1 Endophytic fungi produce secondary metabolites through the polyketide biogenetic pathway	170
6.2 Co-cultivation: an ecological perspective to stimulate the secondary metabolites accumulation of the endophytic fungus <i>Annulohypoxyton</i> sp.	173
6.3 Structure and activity relationships of the isolated compounds	175
6.3.1 Anthraquinone derivatives isolated from <i>Stemphylium globuliferum</i>	175
6.3.2 Naphthopyranone derivatives isolated from <i>Cladosporium cladosporioides</i>	176
6.3.3 Benzo[<i>j</i>]fluoranthene derivatives isolated from <i>Annulohypoxyton</i> sp.	178
7 Bibliography	179
8 Abbreviations	191
9 Acknowledgements	194
10 Curriculum vitae	197

1 General Introduction

1.1 Natural products and drug discovery

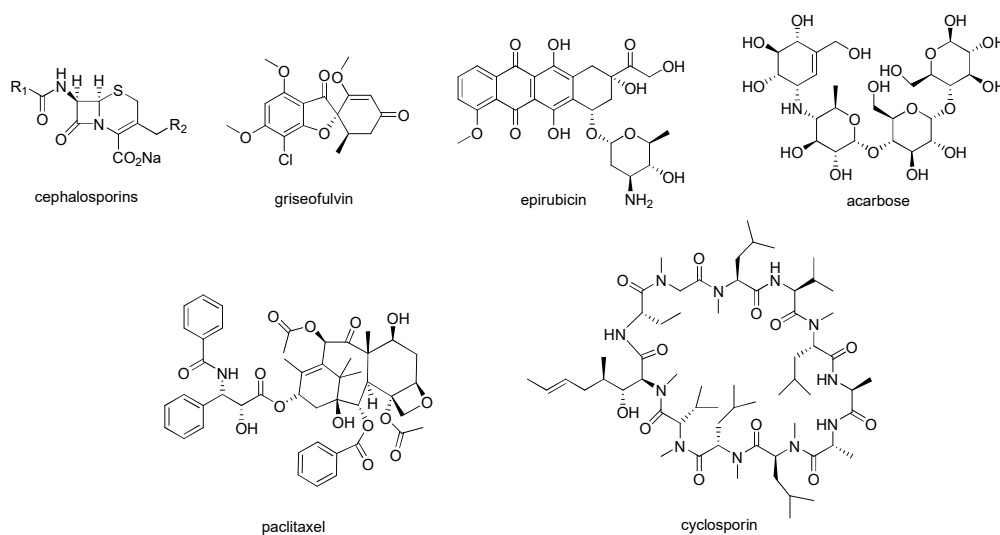
Nature is a vital source of compounds that have found many applications in the fields of medicine, pharmacy, and biology (Butler, 2004). Natural products have been used to treat diseases since ancient times with the first record dating back to 2600 BC from Mesopotamia (Newman *et al.*, 2000). A lot of drugs were derived from natural products, such as the antibiotics cephalosporin C (Aoki and Okuhara, 1980), chloramphenicol, and erythromycin (Butler, 2004), the antilipidemic drugs lovastatin and mevastatin (Alberts, 1988), the antimalarial drug artemisin (Klayman, 1985), and the antifungal drug caspofungin (Stone *et al.*, 2002). Around 56% of the worldwide drugs, particularly anticancer and anti-infective drugs, were derived or inspired by natural products (Cragg and Newman, 2013; Chin *et al.*, 2006). Remarkably, above 60% of these drugs were only developed during the period 1989-1995 (Grabley and Thiericke, 1999). Natural products, acting as leads in the development of new drugs, have their own special advantages. The unique value of natural products in drug discovery can be concluded in three criteria: (1) natural products have been the largest source of front-line drugs (Newman and Cragg, 2012; Cragg *et al.*, 1997), (2) natural products have found to possess a wide variety of biological activities (Ortholand and Ganesan, 2004; Lam, 2007), (3) natural products feature privileged structures that have evolved over millions of years (Ganesan, 2008; Ariëns, 1984).



1.2 Endophytes: a rich source of bioactive metabolites

Endophytes are microorganisms that spend the whole or part of their life cycle colonizing inter and/or intra-cellular healthy tissues of host plants without causing any apparent symptoms of disease (Tan and Zou, 2001; Faeth, 2002). These microorganisms have attracted considerable attention in the last 20 years due to their medicinal and agricultural potential (Jalgaonwala *et al.*, 2011). Secondary metabolites produced by endophytes are viewed as outstanding sources of bioactive natural products. Microbial secondary metabolites as a source of lead structures in drug discovery were not explored until the discovery of penicillin. In 1928, Alexander Fleming discovered that *Staphylococcus aureus*, seeded in a petri dish, was susceptible to mold. The mold, later was identified as *Penicillium notatum*, and was found to produce an active agent that was named penicillin (Demain and Sanchez, 2009). Since then, a large number of terrestrial and marine microorganisms have been investigated for the

production of new bioactive secondary metabolites, as potential agents in drug discovery. This is especially true if we consider that approximately 40 % of the biologically active natural products are derived from microbes (Demain, 2014). In addition, bioactive secondary metabolites from microorganisms have found a wide application in drug discovery, such as the antibacterial agent cephalosporin (Sweet and Dahl, 1970), the antidiabetic agent acarbose (Wehmeier and Piepersberg, 2004), the anticancer agent plinabulin (Ji *et al.*, 2015), the antifungal agent griseofulvin (Gull and Trinci, 1973) or the immunosuppressant agent ciclosporin (Laupacis *et al.*, 1982).



Endophytic fungi, which asymptotically colonize plant tissues, have been investigated from numerous plant species, especially from medicinal plants (Nisa *et al.*, 2015). Fungi and their secondary metabolites used in drug discovery have several benefits: (1) fungi already existed over a billion years, and have evolved special biosynthetic mechanisms for the production of a variety of secondary metabolites (Kharwar *et al.*, 2011); (2) fungi are an inexhaustible and renewable source of bioactive secondary metabolites with less than 16% of the described fungal species being investigated so far (Pimentel *et al.*, 2011; Kharwar *et al.*, 2011); (3) Based on modern biotechnology methods (e.g. genetic engineering, metabolic technology, and microbial fermentation process), the fungal cultures can be manipulated to abundantly produce the metabolites of interest (Zhao, 2011).

Only 7% of the estimated 1.5 million fungal species are known (Hawksworth, 2004), and only a limited amount of those known fungi can be cultured and screened to investigate the secondary metabolites (Suryanarayanan *et al.*, 2009). Thus, fungi are an important group of eukaryotic microorganisms in drug discovery and an increasing number of fungal secondary metabolites with novel structures and biological targets are being reported (Suryanarayanan *et al.*, 2009).

1.2.1 Fungi derived from terrestrial plants

The multi-billion dollar anti-cancer compound paclitaxel was isolated from the bark of the yew tree *Taxus brevifolia*, but later, it was also reported as a constituent of many endophytic fungi, such as *Pestalotiopsis microspora*, *Seimatoantlerium tepuiense*, and *Seimatoantlerium nepalense* (Nisa *et al.*, 2015). Endophytic fungi are suggested to have a mutualistic relationship with their hosts. Host plants provide nutrients to endophytic fungi, which in return, protect the host plants against pathogens and feeding damage caused by herbivores (Aly *et al.*, 2011). This complex interspecies crosstalk between endophytic fungi and host plants leads to a huge variety of fungal metabolites with medicinal, agricultural, or industrial applications (Aly *et al.*, 2011). Thus, the fact that fungal endophytes are considered to be the real contributors of bioactive plant metabolites has shifted the focus of many natural product researchers from plants to fungal endophytes (Cragg and Newman, 2013; Strobel and Daisy, 2003).

1.2.2 Fungi derived from the marine environment

Oceans cover approximately 70% of the Earth surface and contain an exceptional biological diversity (Subramani and Aalbersberg, 2012). A total of 530 species of marine-derived fungi were reported so far which belong to 321 genera, 424 species of which are Ascomycota (in 251 genera), 94 species are anamorphic fungi (in 61 genera), and 12 species are Basidiomycota (in 9 genera) (Rateb and Ebel, 2011; Overy *et al.*, 2014). In the last decades, around 1300 bioactive compounds with antitumor, antibacterial, anticoagulant, anti-inflammatory, antifungal, and antiviral activities have been isolated and reported from marine-derived fungi (Lee *et al.*, 2013; Bhatnagar and Kim, 2012). The ecological habitats of marine-derived fungi mainly include submerged wood, mangroves, sands, sediment, algae, estuary

plants, invertebrates, and plankton (Overy *et al.*, 2014; Rateb and Ebel, 2011). Moreover, marine-derived fungi may have a strong symbiotic relationship with their invertebrate hosts. It is assumed that numerous bioactive secondary metabolites isolated from sponges, sea squirts, corals and other invertebrates are actually produced by symbiotic microorganisms, including fungi (Oliveira *et al.*, 2012).

1.3 Anti-cancer drugs derived from fungal secondary metabolites

Cancer is defined as the uncontrolled growth of cells, commonly followed by metastasis increasing the possibility of spreading to other tissues or organs. (Chandra, 2012). Each cancer starts with changes in one cell or a small group of cells. Cancer cells lose a number of vital control systems, due to the fact that genes in the cell have been damaged or lost, followed by unregulated growth (Hanahan and Weinberg, 2000). There are several kinds of cancer, for example common carcinomas in tissues or organs, such as lung, breast, colon, bladder and prostate carcinomas or common sarcomas, such as fat, bone, and muscle sarcomas (Bosch *et al.*, 1995; Parker *et al.*, 1996; Sikora *et al.*, 1999). Cancer causes a high mortality rate all over the world and each year more than six million new cases are reported. Natural products as potential anticancer agents can be dated back to early reports from 1550 BC (Chandra, 2012). However, serious scientific research of anticancer drugs only began in the 1950s since the discovery and development of the vinca alkaloids (Chandra, 2012). These drugs control the growth of cancer by targeting the more rapidly dividing cancer cells by blocking the spindle apparatus (Kharwar *et al.*, 2011), and therefore they are less toxic towards normal tissue cells (Helleday *et al.*, 2008).

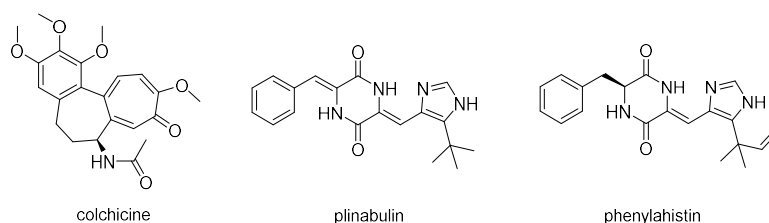
1.3.1 Fungal anticancer drugs with anti-angiogenesis activity

Cancer cells obtain nutrients and oxygen by developing their own blood supply process known as angiogenesis, which is a tightly regulated process to generate new blood vessels from the pre-existing ones (Wang *et al.*, 2015; Ma and Waxman, 2008). Angiogenesis plays an important role for tumor development and metastasis in tumors (Bertolini, 2011). Therefore, inhibition of tumor angiogenesis is considered as a valuable target for anti-cancer therapy

(Kerbel, 2000; Vasudev and Reynolds, 2014). Several anti-angiogenesis inhibitors have been developed, such as sunitinib and bevacizumab, which have been approved by FDA (Yamazaki *et al.*, 2012; Mita *et al.*, 2010).

1.3.1.1 Plinabulin

Plinabulin is a synthetic derivative based on the natural product phenylahistin (also known as halimide). Phenylahistin was isolated from the fungus *Aspergillus ustus* in 1997. It showed potent anti-microtubule activity in HT-29 cells with IC₅₀ value of 300 nM (Yakushiji *et al.*, 2011). Plinabulin was already shown to be a novel vascular-disrupting agent that can inhibit tumor blood supply through disruption of tumor vascular generation from endothelial cells. Furthermore, plinabulin showed inhibitory activity on tubulin polymerization (Wang *et al.*, 2016; Singh *et al.*, 2011). Interestingly, the structure of plinabulin even though it is different from that of colchicine, shows antitubulin activity by binding to the colchicine site of β -tubulin (Ji *et al.*, 2015; Millward *et al.*, 2012). Plinabulin is currently under phase II clinical trials (Ji *et al.*, 2015).



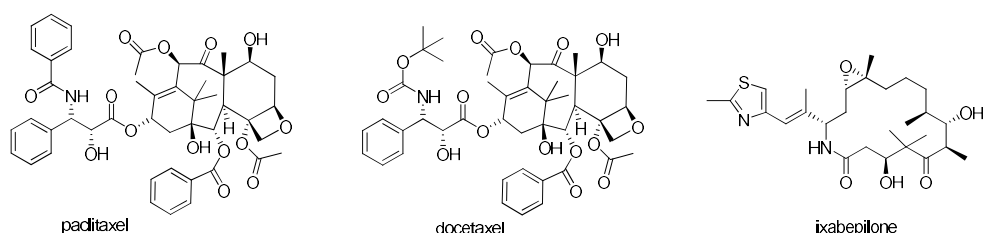
1.3.2 Fungal anticancer drugs with antitubulin activity

Microtubules are noncovalent polymers of α - and β -tubulin heterodimers that form key components of the cytoskeleton in all eukaryotic cells. Microtubules play an important role in cellular functions (Yamazaki *et al.*, 2011), such as cell shape maintenance, intracellular transport, and mitosis (Yamazaki *et al.*, 2012). Most anti-microtubule agents are divided into three main groups. The first group includes micro-tubule stabilizing agents, which bind to the taxane domain of tubulin. The second group includes micro-depolymerizing vinca agents, which bind to the vinca alkaloid domain of tubulin. Finally, the third group also includes micro-

tubule depolymerizing agents, however, via binding to the colchicine domain (Lu *et al.*, 2012). The latter group exhibits selective vascular collapse resulting in the prevention of blood supply to tumor tissues, thus suppressing the tumor (Yamazaki *et al.*, 2012).

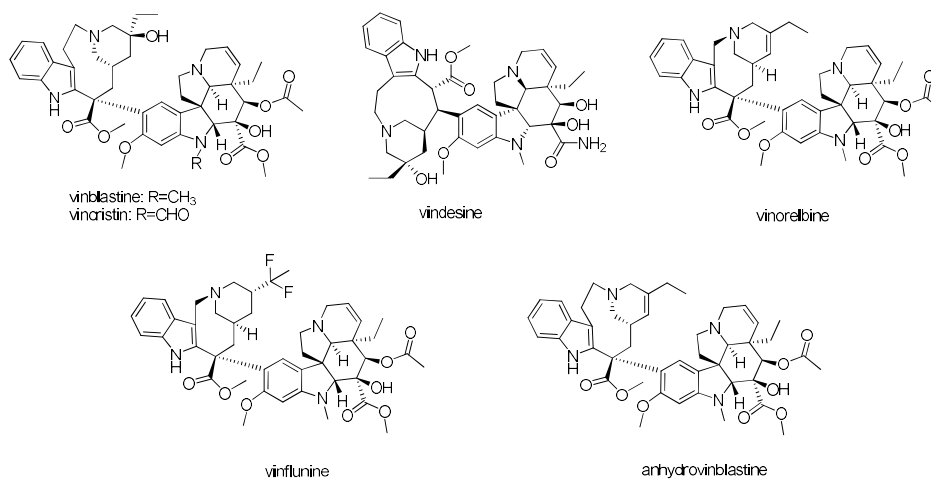
1.3.2.1 Paclitaxel

Paclitaxel was isolated from the stem bark of the Pacific yew tree *Taxus brevifolia* (Taxaceae) in 1969, and its structure elucidation was reported in 1971 (Wani *et al.*, 1971; Cragg, 1998).. Later, in 1993, paclitaxel was reported as a secondary metabolite of the endophytic fungus *Taxomyces andreanae*, which was isolated from *Taxus brevifolia* (Stierle *et al.*, 1993; Jalgaonwala *et al.*, 2011,; Xiong *et al.*, 2013). Paclitaxel was also obtained from other endophytic fungi, such as *Paraconiothyrium variabile* and *Epicoccum nigrum*, both isolated from the English yew *Taxus baccata* (Somjaipeng *et al.*, 2015). Until now, paclitaxel was reported to be synthesized by at least 18 different fungal genera, primarily endophytes that live asymptotically within *Taxus* or other plant genera (Soliman *et al.*, 2013). Paclitaxel promotes microtubule polymerization by inhibiting their disassembly, thus disrupting important cellular processes and inducing apoptosis. As an anti-microtubule drug, paclitaxel (Taxol[®]) is used for the treatment of a broad range of human tumors, including ovarian, breast, lung, bladder, head, and neck cancers (Sreekanth *et al.*, 2011; Bhanot *et al.*, 2011). It took 21 years from the original landmark paper on the isolation and structural determination of taxol to its approval in 1992 by the FDA for the treatment of ovarian cancer (Wani and Horwitz, 2014). Other microtubule-targeting agents are docetaxel (paclitaxel analogue) and ixabepilone (epothilone analogue) (Harzstark *et al.*, 2011; Pusztai, 2007).



1.3.2.2 Vinca alkaloids

Vinca alkaloids, including vinblastine and vincristine, were isolated from the Madagascar periwinkle *Catharanthus roseus* in the late 1950s and early 1960s by two independent groups (Cragg and Newman, 2003; Cragg *et al.*, 2009). Interestingly, vinblastine was also reported from the endophytic fungus *Alternaria* sp. isolated from *Catharanthus roseus* in 1998 (Guo *et al.*, 1998; Kumar *et al.*, 2013; Kumar *et al.*, 2013). Vinblastine and vincristine inhibit tubulin assembly via binding to β -tubulin at a different site from that of taxane drugs. Both compounds inhibit mitosis by destroying the microtubules of the mitotic apparatus at the metaphase stage followed by disruption of many biological functions, which depend upon the class of subcellular organelles (Wilson *et al.*, 1975). Vinca alkaloids have been used in clinical oncology for almost 50 years. Vincristine is used in combination chemotherapy for the treatment of acute lymphoblastic leukemias and lymphomas, whereas vinblastine is used in combination chemotherapy for the treatment of bladder and breast cancers (Kingston, 2009). In addition, several vinca alkaloid analogues, such as vindesine, vinorelbine, vinflunine, and anhydrovinblastine, have been developed as anticancer agents.



1.3.3 Fungal anticancer drugs with DNA topoisomerase inhibition

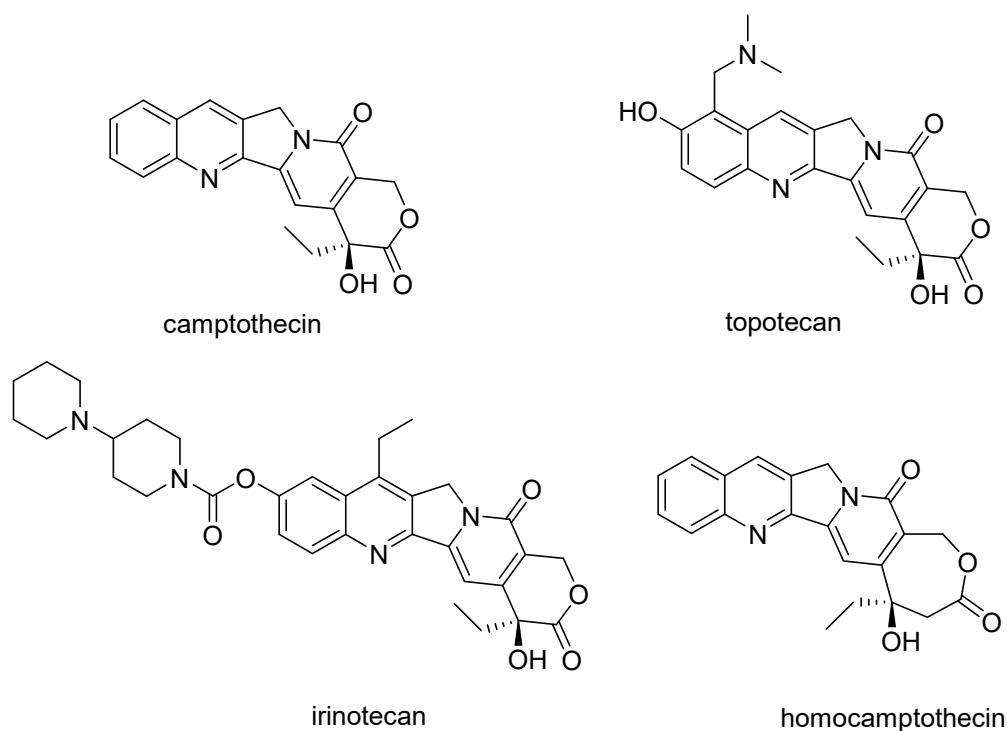
DNA topoisomerases are specific nuclear enzymes that modulate the topological state of DNA during transcription, replication and recombination (Deweese and Osheroff, 2009).

Particularly, DNA topoisomerase I regulates a single-strand of the DNA helix, whereas DNA topoisomerase II regulates both strands of the DNA helix, removing both negative and positive superhelical turns from DNA (Zuma *et al.*, 2011; Kato and Kikuchi, 1998). Thus, DNA topoisomerases are considered as potential targets for anticancer therapy (Cortés *et al.*, 2003).

1.3.3.1 Camptothecin

Camptothecin, a quinoline alkaloid, was first isolated from the stem bark of *Camptotheca acuminata* (Nysaceae) in 1966 (Goodman and McGahren, 1966). Camptothecin was also found in several different species of unrelated families of plants, such as *Merrilliodendron megacarpum* (Icacinaceae), *Ophiorrhiza pumila* (Rubiaceae), *Ervatamia heyneana* (Apocynaceae) and *Mostuea brunonis* (Gelsemiaceae) (Lorence and Nessler, 2004; Sirikantaramas *et al.*, 2009). Interestingly, camptothecin was reported from the endophytic fungus *Entrophospora infrequens*, which was isolated from the plant *Nothapodytes foetida*. Moreover, the endophytic fungus *Neurospora* sp., isolated from the seeds of the same plant (*N. foetida*) was also reported to produce camptothecin (Wall and Wani, 1996; Rehman *et al.*, 2008; Chandra, 2012). Subsequently, a series of camptothecin-producing endophytic fungi like *Fomitopsis* sp., *Alternaria alternata*, *Phomopsis* sp. (Shweta *et al.*, 2013), and *Fusarium solani* were reported (Kusari *et al.*, 2009).

Camptothecin showed strong inhibitory activity against DNA topoisomerase I (Wall and Wani, 1996; Kitajima *et al.*, 2002; Efferth *et al.*, 2007). In addition, a number of reports indicate the therapeutic potential of camptothecin against colon, uterine, cervical, and ovarian cancer (Kusari *et al.*, 2009). The first-generation of camptothecin analogues irinotecan and topotecan as water-soluble derivatives were approved by the US Food and Drug Administration (FDA) in 1996 (Lorence and Nessler, 2004; Sirikantaramas *et al.*, 2009). Later, a new family of camptothecin derivatives, homocamptothecins, with an expanded seven-membered lactone ring were developed. Homocamptothecins enhance plasma stability and induce inhibition of topoisomerase I compared to the conventional six-membered ring camptothecin derivatives (Lorence and Nessler, 2004; Bailly, 2003; Lavergne *et al.*, 1998).



1.4 Strategies to maximize the diversity of fungal secondary metabolites

Fungi are found worldwide, including extreme environments with high temperature, high salt concentration, and high or low pH conditions. It is considered that the pattern of fungal secondary metabolites is heavily influenced by different environmental conditions, in which fungi are adapted to live. Likewise, the production of secondary metabolites from fungi is strongly influenced by culture conditions, such as medium source, phosphate, trace elements, and incubation time. Therefore, adjusting the cultural conditions is considered as a powerful method to maximize the diversity of fungal secondary metabolites (Mathan *et al.*, 2013). There are several different ways to regulate the cultural conditions. The most common methods are OSMAC approach, mostly depending on different cultural media, or co-culture of different microbes (also called co-cultivation) that imitates the natural competitive conditions (Marmann *et al.*, 2014).

1.4.1 Medium optimization

Medium optimization mainly depends on the OSMAC (One Strain, MAny Compounds) approach (Bode *et al.*, 2002; Scherlach and Hertweck, 2009). Microbial genome sequence

analysis suggested that most gene biosynthesis clusters remain silent under standard laboratory culture conditions (Schroeckha et al., 2009), resulting in limited chemical diversity of fungal secondary metabolites. It is also widely recognized that the biosynthesis of fungal secondary metabolites can be influenced by different cultural conditions, such as media composition, pH value, temperature, oxygen, light, even cultural vessel. There are many ways to optimize the medium of a fungal culture, including component replacing, biological mimicry, artificial neural networks, continuous fermentation, and stoichiometric analysis (Kennedy et al., 1999). Therefore, setting the cultural parameters that influence the biosynthesis of fungal secondary metabolites is a useful technique to enhance the chemical diversity of microorganisms.

1.4.2 Co-cultivation as a useful tool to activate silent gene clusters

Bacteria and fungi co-exist in natural habitats, such as soil, water and plants as endophytes (Netzker *et al.*, 2015). It is suggested that endophytes compete for living space and nutrients by producing a wide array of bioactive secondary metabolites to inhibit other antagonistic microorganisms. Therefore, co-cultivation by forcing direct interactions between different microbes, may trigger the expression of silent biosynthetic pathways for the production of new secondary metabolites or enhance the accumulation of constitutively present metabolites in prokaryotes and eukaryotes alike (Ola *et al.*, 2013; Nützmänn *et al.*, 2011; Schroeckh *et al.*, 2009). For example, glionitrin A was only detected when the marine-derived fungus *Aspergillus fumigatus* was co-cultured with a marine-derived bacterium of the genus *Sphingomonas*. Glionitrin A showed strong antibacterial activity against MRSA with an MIC value of 0.78 µg/mL (Marmann *et al.*, 2014). Moreover, the known antibacterial compounds enniatin B, enniatin B1, and enniatin A1 were enhanced up to 78-fold during co-cultivation of the fungus *Fusarium tricinctum* and the bacterium *Bacillus subtilis* (Ola *et al.*, 2013).

1.5 Aim of the study

It has been estimated that there are as many as 1.5 million fungal species on Earth, of which only 74,000 species have been described (Hawksworth, 1991). Thus, endophytic fungi are considered as a prolific source of bioactive secondary metabolites with high medicinal and agricultural potential (Jalgaonwala *et al.*, 2011). The aim of this study was mainly focused on

the isolation and identification of bioactive secondary metabolites from co-culture and/or axenic cultures of endophytic fungi with different bacteria.

Based on the activities of fungal crude extracts in different bioassays and based on HPLC analysis, three fungal strains were investigated: (1) *Stemphylium globuliferum*, isolated from the plant *Juncus actus*, which was collected from the shore of Lake Wadi el Natrun in Egypt; (2) *Cladosporium cladosporioides*, which was isolated from the sediment of hypersaline lake Wadi el Natrun; (3) *Annulohyphoxylon* sp., isolated from the mangrove *Rhizophora racemose*, which was collected in Cameroon. The secondary metabolites of these fungi were purified by chromatography on silica gel, reversed phase silica gel, Sephadex LH-20, Diol-functionalized silica gel, and by semi-preparative HPLC. The structures were elucidated on the basis of 1D and 2D (^1H , ^{13}C , COSY, HSQC, HMBC, ROSSY) NMR spectroscopy, HRESIMS spectrometry, UV and circular dichroism (CD) spectroscopy. Subsequently, the pure substances were evaluated for their antibacterial activity and cytotoxicity against the murine lymphoma (L5178Y), human ovarian tumor (A2780 sens and A2780 cis), Jukart J16, and Ramos cell lines.

Chapter 2 and chapter 3 (Publication 1 and 2) describe the first two naturally occurring trimeric anthracene derivatives stemphyllanthranols A and B, two new anthracene dimers and two new anthracene monomers that were isolated from the endophytic fungus *S. globuliferum*. The structures of the new derivatives were unambiguously elucidated by 1D and 2D NMR, by HRESIMS, as well as by ECD spectroscopy. Furthermore, the proposed biogenetic pathways were discussed.

Chapter 4 (publication 3) describes the isolation of one new cytotoxic viriditoxin derivative cladosporinone, together with viriditoxin and two viriditoxin derivatives that were isolated from the hypersaline sediment fungus *Cladosporium cladosporioides*. In this part, the structure elucidation, the biogenetic pathway, as well as the antibiotic and cytotoxic activities of the isolated compounds were evaluated.

Chapter 5 (manuscript 4) describes two new benzo[*j*]fluoranthene-based metabolites, daldinones E and G, together with one new artefact daldinone F that were isolated from the

endophytic fungus *Annulohyphoxylon* sp. The proposed biogenetic pathway was discussed according to the literature. Daldinone F exhibited strong cytotoxicity against Ramos and Jurkat J16 cells, by inducing the intrinsic apoptotic pathway.

2 Publication 1

2.1 Trimeric Anthracenes from the Endophytic Fungus *Stemphylium globuliferum*

Published in: “Journal of Natural Products”

Impact factor: 3.662

Contribution: 70 %, first author, conducting most of the experiments, literature research, manuscript writing.

Reprinted with permission from “Liu Y., Wray V., Abdel-Aziz M. S., Wang C. Y., Lai D., Proksch P. (2014) Trimeric Anthracenes from the Endophytic Fungus *Stemphylium globuliferum*.” *J. Nat. Prod.*, 77, 1734–1738. Copyright 2014 American Chemical Society and American Society of Pharmacognosy

Trimeric Anthracenes from the Endophytic Fungus *Stemphylium globuliferum*

Yang Liu,^{†,‡} Victor Wray,[‡] Mohamed S. Abdel-Aziz,[§] Chang-Yun Wang,[‡] Daowan Lai,^{*,†,||} and Peter Proksch^{*,†}

[†]Institute of Pharmaceutical Biology and Biotechnology, Heinrich-Heine University, Universitaetsstrasse 1, 40225 Duesseldorf, Germany

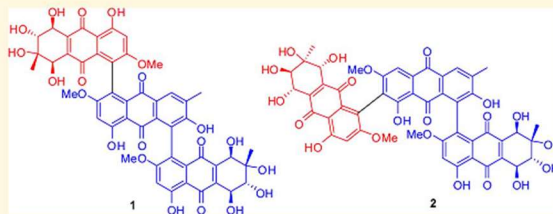
[‡]Helmholtz Centre for Infection Research, Inhoffenstraße 7, D-38124 Braunschweig, Germany

[§]Microbial Chemistry Department, Genetic Engineering and Biotechnology Division, National Research Center, El-Behoos Street 33, Dokki-Giza 12622, Egypt

[‡]Key Laboratory of Marine Drugs, The Ministry of Education of China, School of Medicine and Pharmacy, Ocean University of China, Qingdao 266003, People's Republic of China

Supporting Information

ABSTRACT: The first naturally occurring trimeric anthracene derivatives, stemphyanthranols A and B (1 and 2), were obtained from the endophytic fungus *Stemphylium globuliferum* that had been isolated from *Juncus actus* growing in Egypt. The structures of the new compounds were unambiguously determined by 1D and 2D NMR, and by HRMS. A hypothetical biosynthetic pathway for the new trimers is proposed.



Endophytes are fungal and bacterial microorganisms that colonize asymptotically the intercellular and/or intracellular parts of healthy plants.^{1,2} In natural ecosystems, endophytic fungi are symbiotic in all plants so far investigated and exhibit complex interactions with their hosts.³ In recent years, endophytes have attracted considerable attention as prolific sources of novel bioactive compounds.^{4,5} In some cases, these unique substances have promising potential for future agricultural or pharmaceutical applications. Fungi of the genus *Stemphylium* occur as pathogens and saprobes in a wide range of plants⁶ but have also been described as endophytes.⁷ *Stemphylium* species are known to accumulate a plethora of polyketide compounds, such as macrosporin, stemphypyrone, stemphyperlenol, altersolanols A, K, L, and N, alterporriols A, B, D, E, G, and H, stemphytoxins I–IV, and stemphyloxins I and II.^{7–11} These compounds exhibited a wide range of activities, such as cytotoxicity, protein kinase inhibitory activities, and antimicrobial activities.^{7,9}

Of particular interest among the metabolites produced by the genus *Stemphylium* are anthraquinone and preanthraquinone derivatives. Our previous investigation of *S. globuliferum* (strain no. DA-8) isolated from the Moroccan medicinal plant *Mentha pulegium* had afforded several new bioactive anthracene monomers and dimers,^{7,9} raising the question whether trimeric anthracenes can also be produced by this fungal strain. However, fermentation of this strain on different solid or in liquid culture media failed to give the expected trimeric products as monitored by LC-MS. Fortunately, a further strain (no. WN9L-3) of *S. globuliferum* obtained from *Juncus actus*

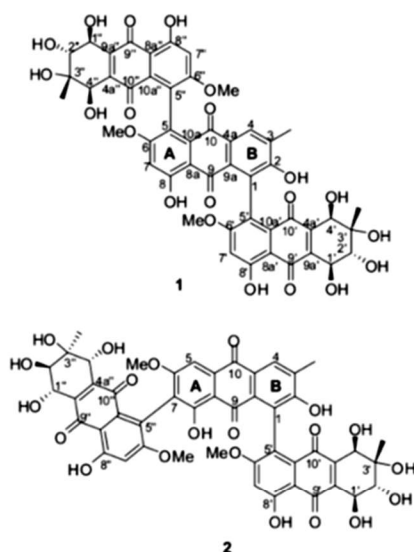
(Juncaceae) growing in Egypt was capable of producing such trimeric compounds albeit at low yields (1: 3.4 mg; 2: 1.5 mg). In this study, we describe the structure elucidation of the first two trimeric anthracene compounds (1 and 2) isolated from nature and propose their biogenetic origin.

The fungal extract was subjected to liquid–liquid partition, column chromatography over silica gel, and Sephadex LH-20, followed by semipreparative HPLC to afford two compounds, 1 and 2.

Stemphyanthranol A (1) was isolated as a red, amorphous powder. Its molecular mass was determined to be 952 amu, as prominent pseudomolecular ion peaks were seen at m/z 953.0 $[M + H]^+$ and 951.3 $[M - H]^-$ in the ESIMS spectra. Its molecular formula was established as $C_{48}H_{40}O_{21}$ on the basis of a prominent pseudomolecular ion peak observed at m/z 953.21367 $[M + H]^+$ in the HRESIMS spectrum. In the downfield region of the 1H NMR spectrum, three singlets at δ_H 13.29, 13.11, and 13.05, which were attributable to three chelated OH groups, gave a first hint to a trimeric anthracene nature of 1, as the monomeric or dimeric anthracenes identified from this species so far showed one or two characteristic chelated OH signals, respectively.^{7,9} This speculation was corroborated by analysis of the ^{13}C NMR and mass data. In the ^{13}C NMR spectrum, the resonances at δ_C 189.1, 188.8, 187.7, 184.3, 184.2, and 181.5 were assignable to six ketone groups originating from three monomeric anthracene units (Table 1).

Received: February 6, 2014

Published: July 10, 2014



Further analysis of the 1D (^1H , ^{13}C) and 2D NMR (HSQC, HMBC, COSY) data, as well as comparison of the data with the literature,^{12–15} allowed the assignment of two identical tetrahydroanthraquinone moieties and one macrosporin unit in 1. The unequivocal assignments of the ^1H and ^{13}C NMR data for each tetrahydroanthraquinone unit were completed by analysis of the COSY, HSQC, and HMBC spectra (Table 1). In the COSY spectrum, H-1' ($1''$) showed correlation to H-2' ($2''$), while key HMBC correlations of 3' ($3''$)-Me to C-2' ($2''$), C-3' ($3''$), and C-4' ($4''$) allowed the assignments of the 1,2,3,4-tetrahydroxyl-3-methylbutyl fragments. Further HMBC correlations of H-4' ($4''$) to C-9a' ($9a''$), C-4a' ($4a''$), and C-10' ($10''$), of H-1' ($1''$) to C-9' ($9''$), C-9a' ($9a''$), and C-4a' ($4a''$), and of H-2' ($2''$) to C-9a' ($9a''$) established the linkage between the above-mentioned butyl fragments and the ketone groups as shown in Figure 1. The HMBC correlations from the chelated OH groups ($8'/8''$ -OH) to C-8' ($8''$), C-8a' ($8a''$), and C-7' ($7''$) indicated that H-7' ($7''$) was located at the *ortho* position of $8'/8''$ -OH. In addition, HMBC correlations were observed from H-7' ($7''$) to C-5' ($5''$), C-8a' ($8a''$), C-6' ($6''$), and C-8' ($8''$) and from 6' ($6''$)-OMe to C-6' ($6''$); thus methoxy groups were located at C-6' ($6''$), while the substitutions at C-5' ($5''$) remained to be defined (Figure 1). These assignments were supported by the ROESY spectrum, in which the correlations of $8'/8''$ -OH to H-7' ($7''$) and of 6' ($6''$)-OMe to H-7' ($7''$) were clearly seen (Figure 2).

Apart from the aforementioned NMR signals, the remaining signals were assigned to a macrosporin unit, which incorporated two benzene rings, two ketone groups (δ_{C} 187.7, 181.5), one methyl group (δ_{C} 17.1; δ_{H} 2.22, s), and one methoxy group (δ_{C} 56.74; δ_{H} 3.66, s). In this anthraquinone unit, a long-range COSY correlation was found between the aromatic methyl (δ_{H} 2.22, s) and H-4 (δ_{H} 7.77, s), while the latter proton (H-4) showed further HMBC correlation to one ketone group (C-10, δ_{C} 181.5). Thus, the methyl group had to be located at C-3. The correlations of 3-Me to C-3, C-4, and the oxygenated carbon (C-2, δ_{C} 158.0) suggested that C-2 was substituted by a hydroxyl group. The correlations from OH-2 (δ_{H} 9.34, s) to C-1, C-2, and C-3 not only confirmed the location of the hydroxyl group but also revealed that C-1 was substituted. Similarly, the

HMBC correlations (Figure 1) from the chelated OH group (OH-8, δ_{H} 13.29, s) to C-7, C-8, and C-8a, from H-7 (δ_{H} 6.87, s) to C-5, C-8a, C-6, and C-8, and from 6-OMe (δ_{H} 3.66, s) to C-6 indicated the presence of 6-methoxy and 8-hydroxyl substituents, while C-5 was substituted. To complete the structure, the two tetrahydroanthraquinone units have to be connected to the macrosporin unit via C-1 and C-5, respectively.

The relative configuration of each tetrahydroanthraquinone unit was determined to be the same as that of altersolanol A by analysis of the coupling constants and ROESY correlations. The large coupling constant (7.4 Hz) between H-1' ($1''$) and H-2' ($2''$) indicated their axial orientations. The ROESY correlations between 3' ($3''$)-Me, H-4' ($4''$), and 4' ($4''$)-OH indicated that 3' ($3''$)-Me was equatorially oriented, which was consistent with the ROESY correlations observed between 1' ($1''$)-OH, H-2' ($2''$), and 3' ($3''$)-Me. Further correlation of H-4' ($4''$) to 3' ($3''$)-OH suggested that 4' ($4''$)-OH was axially oriented (Figure 2). Since compound 1 was co-isolated with its putative biogenetic precursors—macrosporin and altersolanol A—the absolute configuration of the central chirality in 1 is assumed to be the same as that of altersolanol A.

Stemphyllanthranol B (2) was isolated as an isomer of stemphyllanthranol A (1), as both compounds exhibited similar UV absorption maxima and shared the same molecular formula $\text{C}_{48}\text{H}_{40}\text{O}_{21}$ based on the HRESIMS measurements. The ^1H and ^{13}C NMR data of 2 were closely related to those of 1, suggesting that 2 was also a trimeric anthracene. Comparison of the chemical shifts for both compounds, as well as analysis of the 1D and 2D NMR data revealed that compound 2 also contained one macrosporin and two altersolanol A moieties. However, the chemical shifts for the A ring of the macrosporin moiety were significantly different for both compounds (Table 1), thus indicating a different substitution pattern. Indeed, the sole aromatic proton in the A ring of 2 was found to correlate with the ketone group (C-10) in the HMBC spectrum, which allowed the assignment of this proton to H-5. This proton further showed a ROESY correlation to a methoxy group (6-OMe, δ_{H} 3.83), which is consistent with the 6-methoxy substitution. Therefore, the second altersolanol A moiety of 2 has to be linked to macrosporin at C-7 instead of C-5 as in 1. This was further corroborated by analysis of the HMBC spectrum, in which correlations from H-5 to C-6, C-7, and C-8a, from 6-OMe to C-6, and from 8-OH to C-7, C-8, and C-8a were discerned (Figure 3).

Compound 1 is structurally related to the dimeric anthracenes alterporriols A and B that were isolated as atropisomers from the pathogenic fungus *Alternaria porri*,^{12,13} while 1 has an additional altersolanol A unit substituted to C-1 of the macrosporin moiety. Similarly, 2 contains one additional altersolanol A unit attached to C-1 of the putative atropisomeric anthranoid precursors alterporriols G and H, which were previously obtained from *S. globuliferum*.⁷ The rotation hindrance around the biaryl axis in the bianthraquinones has allowed the identification of several pairs of alterporriol-type atropisomers, such as alterporriols A¹³/B,¹² C¹⁴/atropisomer C,¹⁵ D/E,¹⁶ and G/H.⁷ In the present study, 1 and 2 seem to be present as a single compound, as detected by HPLC and LC-MS, rather than atropisomeric mixtures. The axial chirality of several dimeric anthranoids has in the past been successfully determined by comparing the calculated and experimental ECD spectra as demonstrated in our previous

Table 1. ^1H and ^{13}C NMR Data of 1 and 2 (DMSO- d_6)

position	1		2	
	δ_{H} (600 MHz), mult. (J in Hz) ^a	δ_{C} (150 MHz) ^a	δ_{H} (700 MHz), mult. (J in Hz) ^a	δ_{C} (176 MHz) ^a
1		124.8,C		125.8,C
2		158.0,C		158.4,C
3		131.7,C		131.7,C
4	7.77, s	129.6,CH	8.09, s	129.7,CH
4a		126.5,C		125.9,C
5		121.2,C	7.42, s	102.1,CH
6		163.9,C		163.2,C
7	6.87, s	104.3,CH		111.0,C
8		164.7,C		160.4,C
8a		110.2,C		118.9,C
9		187.7,C		187.9,C
9a		130.3,C		130.6,C
10		181.5,C		180.8,C
10a		130.9,C		133.2,C
1'/1''	4.49, dd (7.4, 5.3)/4.50, dd (7.4, 5.2)	68.4,CH/68.4,CH	4.43, d (7.1)/4.46, d (7.1)	68.28,CH/68.33,CH
2'/2''	3.58, m/3.58, m	73.7,CH/73.8,CH	3.53, d (7.1)/3.57, d (7.1)	73.7,CH/73.8,CH
3'/3''		72.88,C/72.94,C		72.9,C/73.0,C
4'/4''	4.07, d (7.1) /4.09, d (7.2)	68.2,CH/68.3,CH	4.06, d (6.8) / 4.09, d (7.0)	68.1,CH/68.2,CH
4a'/4a''		142.8,C/142.6,C		142.7,C/142.5,C
5'/5''		122.97,C/123.05,C		122.8,C/116.0,C
6'/6''		164.2,C/164.4,C		164.0,C/163.85,C
7'/7''	6.94, s/6.98, s	103.8,CH/104.1,CH	6.93, s/6.97, s	104.4,CH/104.1,CH
8'/8''		163.7,C/163.7,C		163.85,C/163.88,C
8a'/8a''		109.3,C/110.2,C		109.7,C/109.5,C
9'/9''		188.8,C/189.1,C		189.0,C/189.0,C
9a'/9a''		143.53,C/143.48,C		143.4,C/143.7,C
10'/10''		184.2,C/184.3,C		184.0,C/184.6,C
10a'/10a''		128.7,C/129.2,C		130.0,C/129.4,C
3-Me	2.22, s	17.1,CH ₃	2.34, s	17.2,CH ₃
3'-Me/3''-Me	1.15, s/1.14, s	22.3,CH ₃ /22.2,CH ₃	1.11, s/1.13, s	22.2,CH ₃ /22.3,CH ₃
6-OMe	3.66, s	56.74,CH ₃ ^b	3.83, s	56.5,CH ₃
6'-OMe/6''-OMe	3.72, s/3.73, s	56.73,CH ₃ ^b /56.71,CH ₃ ^b	3.70, s/3.76, s	56.9,CH ₃ /56.8,CH ₃
2-OH	9.34, s		9.47, s	
8-OH	13.29, s		12.38, s	
1'-OH/1''-OH	4.82, d (5.3) /4.84, d (5.2)			
2'-OH/2''-OH	5.02, d (5.2) / 5.02, d (5.2)			
3'-OH/3''-OH	4.39, s/4.35, s			
4'-OH/4''-OH	5.61, d (7.1) / 5.70, d (7.2)		5.63, d (6.8) / 5.76, d (7.0)	
8'-OH/8''-OH	13.05, s/13.11, s		12.86, s/13.03, s	

^aThe NMR data assigned for the two altersolanol A units could be interchanged. ^bAssignments may be interchanged within a column.

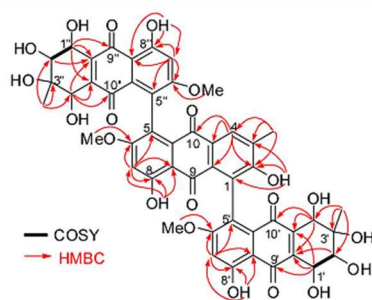


Figure 1. Key COSY and HMBC correlations of 1.

investigations.^{9,17} However, in the cases of 1 and 2, the presence of two biaryl axes makes the calculation of ECD spectra considerably more complex and was hence not

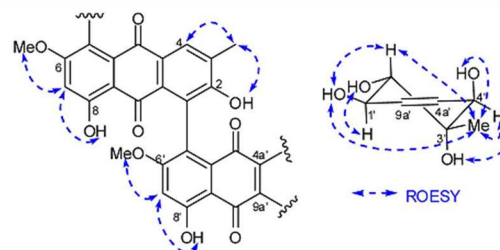


Figure 2. Selected ROESY correlations of 1.

attempted in this study. Thus, the absolute configuration for 1 and 2 remains unclear.

From a structural point of view, compounds 1 and 2 are derivatives of alterporriols A/B^{12,13} and G/H,⁷ as the addition of one additional altersolanol A unit to C-1 of the latter would give rise to 1 and 2, respectively. In our previous investigation,⁷

chromatography over Sephadex LH-20 using DCM–MeOH (1:1) as mobile phase to remove pigments. Further purification carried out on a semipreparative HPLC column (C₁₈) with MeOH–H₂O (55:45) as mobile phase yielded compounds **1** (3.4 mg) and **2** (1.5 mg). Altersolanol A (around 1 g) was isolated as the major compound from the more polar fraction eluted with DCM–MeOH (6:4).

Stemphylianthranol A (1): red, amorphous powder; $[\alpha]_D^{25}$ –35.2 (c 0.175, MeOH); UV (λ_{max} , MeOH) log ϵ 204 (4.28), 225 (4.21), 276 (3.93), 439 (3.51) nm; CD (MeOH) ($\Delta\epsilon$) 474 (+1.99), 406 (–3.21), 355 (–2.09), 315 (–3.28), 286 (–9.44), 259 (+10.14) nm; ¹H (600 MHz) and ¹³C (150 MHz) NMR, see Table 1; ESIMS *m/z* 953.0 [M + H]⁺, 951.3 [M – H][–]; HRESIMS *m/z* 953.21367 [M + H]⁺ (calcd for C₄₈H₄₁O₂₁, 953.21348).

Stemphylianthranol B (2): red, amorphous powder; $[\alpha]_D^{25}$ –8.1 (c 0.15, MeOH); UV (λ_{max} , MeOH) log ϵ 204 (4.04), 222 (3.95), 291 (3.74), 422 (3.23) nm; CD (MeOH) ($\Delta\epsilon$) 499 (+1.27), 423 (–4.35), 386 (–2.25), 352 (–3.13), 319 (–0.37), 292 (–7.56), 274 (+2.63), 264 (+0.06), 250 (+3.22) nm; ¹H (700 MHz) and ¹³C (176 MHz) NMR, see Table 1; ESIMS *m/z* 952.8 [M + H]⁺, 951.4 [M – H][–]; HRESIMS *m/z* 953.21321 [M + H]⁺ (calcd for C₄₈H₄₁O₂₁, 953.21348).

Bioassay. The cytotoxic and antibacterial assays were performed as described previously.²³ Kahalalide F (IC₅₀ 4.3 μ M) was used as the positive control in the cytotoxic assay. In the antibacterial assay, tetracycline was used as the positive control, which showed inhibition against *S. aureus*, *E. coli*, and *P. aeruginosa* with MIC values (μ g/mL) of 0.25, 0.5, and 32, respectively.

■ ASSOCIATED CONTENT

Supporting Information

Copies of 1D and 2D NMR and MS spectra of **1** and **2**. This material is available free of charge via the Internet at <http://pubs.acs.org>.

■ AUTHOR INFORMATION

Corresponding Authors

*E-mail: laidaowan123@gmail.com.

*Tel: +49 211 81 14163. Fax: +49 211 81 11923. E-mail: proksch@uni-duesseldorf.de.

Present Address

^{||}MOA Key Laboratory of Plant Pathology, Department of Plant Pathology, College of Agronomy and Biotechnology, China Agricultural University, Beijing 100193, People's Republic of China.

Notes

The authors declare no competing financial interest.

■ ACKNOWLEDGMENTS

The financial support from BMBF granted to P.P. is gratefully acknowledged. Y.L. wants to thank the China Scholarship Council, the Ministry of Education of China, for a doctoral scholarship. We thank H. Niemann and C.-D. Pham (Heinrich-Heine University, Düsseldorf, Germany) for collecting the plant in Egypt with support from DAAD. We are indebted to Prof. W. E. G. Müller (Johannes Gutenberg University, Mainz, Germany) for cytotoxicity assays and to Prof. H. Brötz-Oesterhelt (Heinrich-Heine University, Düsseldorf, Germany) for antibacterial assays.

■ REFERENCES

- (1) Faeth, S. H. *Oikos* **2002**, *98*, 25–36.
- (2) Wilson, D. *Oikos* **1995**, *73*, 274–276.
- (3) Rodríguez, R. J.; White, J. F., Jr.; Arnold, A. E.; Redman, R. S. *New Phytol.* **2009**, *182*, 314–330.
- (4) Zhang, H. W.; Song, Y. C.; Tan, R. X. *Nat. Prod. Rep.* **2006**, *23*, 753–771.
- (5) Aly, A. H.; Debbab, A.; Kjer, J.; Proksch, P. *Fungal Diversity* **2010**, *41*, 1–16.
- (6) Camara, M. P.; O'Neill, N. R.; van Berkum, P. *Mycologia* **2002**, *94*, 660–672.
- (7) Debbab, A.; Aly, A. H.; Edrada-Ebel, R.; Wray, V.; Mueller, W. E. G.; Totzke, F.; Zirrgiebel, U.; Schaechtele, C.; Kubbutat, M. H. G.; Lin, W. H.; Mosaddak, M.; Hakiki, A.; Proksch, P.; Ebel, R. *J. Nat. Prod.* **2009**, *72*, 626–631.
- (8) Arnone, A.; Nasini, G.; Merlini, L.; Assante, G. *J. Chem. Soc., Perkin Trans. 1* **1986**, 525–530.
- (9) Debbab, A.; Aly, A. H.; Edrada-Ebel, R.; Wray, V.; Pretsch, A.; Pescitelli, G.; Kurtan, T.; Proksch, P. *Eur. J. Org. Chem.* **2012**, *2012*, 1351–1359.
- (10) Barash, I.; Manulis, S.; Kashman, Y.; Springer, J. P.; Chen, M. H.; Clardy, J.; Strobel, G. A. *Science* **1983**, *220*, 1065–1066.
- (11) Manulis, S.; Kashman, Y.; Netzert, D.; Barash, I. *Phytochemistry* **1984**, *23*, 2193–2198.
- (12) Suemitsu, R.; Sano, T.; Yamamoto, M.; Arimoto, Y.; Morimatsu, F.; Nabeshima, T. *Agric. Biol. Chem.* **1984**, *48*, 2611–2613.
- (13) Suemitsu, R.; Yamamoto, T.; Miyai, T.; Ueshima, T. *Phytochemistry* **1987**, *26*, 3221–3224.
- (14) Suemitsu, R.; Ueshima, T.; Yamamoto, T.; Yanagawase, S. *Phytochemistry* **1988**, *27*, 3251–3254.
- (15) Okamura, N.; Haraguchi, H.; Hashimoto, K.; Yagi, A. *Phytochemistry* **1993**, *34*, 1005–1009.
- (16) Suemitsu, R.; Sakurai, Y.; Nakachi, K.; Miyoshi, I.; Kubota, M.; Ohnishi, K. *Agric. Biol. Chem.* **1989**, *53*, 1301–1304.
- (17) Bara, R.; Zerfass, I.; Aly, A. H.; Goldbach-Gecke, H.; Raghavan, V.; Sass, P.; Mándi, A.; Wray, V.; Polavarapu, P. L.; Pretsch, A.; Lin, W.; Kurtan, T.; Debbab, A.; Brötz-Oesterhelt, H.; Proksch, P. *J. Med. Chem.* **2013**, *56*, 3257–3272.
- (18) Stoessl, A.; Unwin, C. H.; Stothers, J. B. *Tetrahedron Lett.* **1979**, *20*, 2481–2484.
- (19) Stoessl, A.; Unwin, C. H.; Stothers, J. B. *Can. J. Chem.* **1983**, *61*, 372–377.
- (20) Ohnishi, K.; Tanabe, H.; Hayashi, S.; Suemitsu, R. *Biosci. Biotechnol. Biochem.* **1992**, *56*, 42–43.
- (21) Ohnishi, K.; Suemitsu, R.; Kubota, M.; Matano, H.; Yamada, Y. *Phytochemistry* **1991**, *30*, 2593–2595.
- (22) Kjer, J.; Debbab, A.; Aly, A. H.; Proksch, P. *Nat. Protoc.* **2010**, *5*, 479–490.
- (23) El-Neketi, M.; Ebrahim, W.; Lin, W.; Gedara, S.; Badria, F.; Saad, H.-E. A.; Lai, D.; Proksch, P. *J. Nat. Prod.* **2013**, *76*, 1099–1104.

Supporting Information

The First Trimeric Anthracenes from the Endophytic Fungus *Stemphylium Globuliferum*

Yang Liu,^{†,‡} Victor Wray,[‡] Mohamed S. Abdel-Aziz,[§] Chang-Yun Wang,[‡] Daowan Lai^{*,†,||} and Peter Proksch^{*,†}

[†] Institute of Pharmaceutical Biology and Biotechnology, Heinrich-Heine University, Universitätsstrasse 1, 40225 Duesseldorf, Germany

[‡] Helmholtz Centre for Infection Research, Inhoffenstraße 7, D-38124 Braunschweig, Germany

[§] Microbial Chemistry Department, Genetic Engineering and Biotechnology Division, National Research Center, El-Behoos st.33, Dokki-Giza 12622, Egypt

[‡] Key Laboratory of Marine Drugs, The Ministry of Education of China, School of Medicine and Pharmacy, Ocean University of China, Qingdao 266003, PR China

Corresponding Author:

*E-mail: laidaowan123@gmail.com (D.L.), proksch@uni-duesseldorf.de (P.P.)

Present Address

^{||} MOA Key Laboratory of Plant Pathology, Department of Plant Pathology, College of Agronomy and Biotechnology, China Agricultural University, Beijing 100193, PR China

Contents

Figure S1-1. ^1H NMR spectrum of 1 (DMSO- d_6 , 600MHz).....	S3
Figure S1-2. ^1H NMR spectrum of 1 with assignments (expansion).....	S4
Figure S2. ^{13}C NMR spectrum of 1 (DMSO- d_6 , 150MHz).....	S5
Figure S3. COSY spectrum of 1	S6
Figure S4. HSQC spectrum of 1	S7
Figure S5. HMBC spectrum of 1	S8
Figure S6. ROESY spectrum of 1	S9
Figure S7. LC/ESIMS spectrum of 1	S10
Figure S8. HRESIMS spectrum of 1	S11
Figure S9-1. ^1H NMR spectrum of 2 (700MHz, DMSO- d_6).....	S12
Figure S9-2. ^1H NMR spectrum of 2 with assignments (expansion).....	S13
Figure S10. ^{13}C NMR spectrum of 2 (176 MHz, DMSO- d_6).....	S14
Figure S11. COSY spectrum of 2	S15
Figure S12. HSQC spectrum of 2	S16
Figure S13. HMBC spectrum of 2	S17
Figure S14. ROESY spectrum of 2	S18
Figure S15. ESIMS spectrum of 2	S19
Figure S16. HRESIMS spectrum of 2	S20

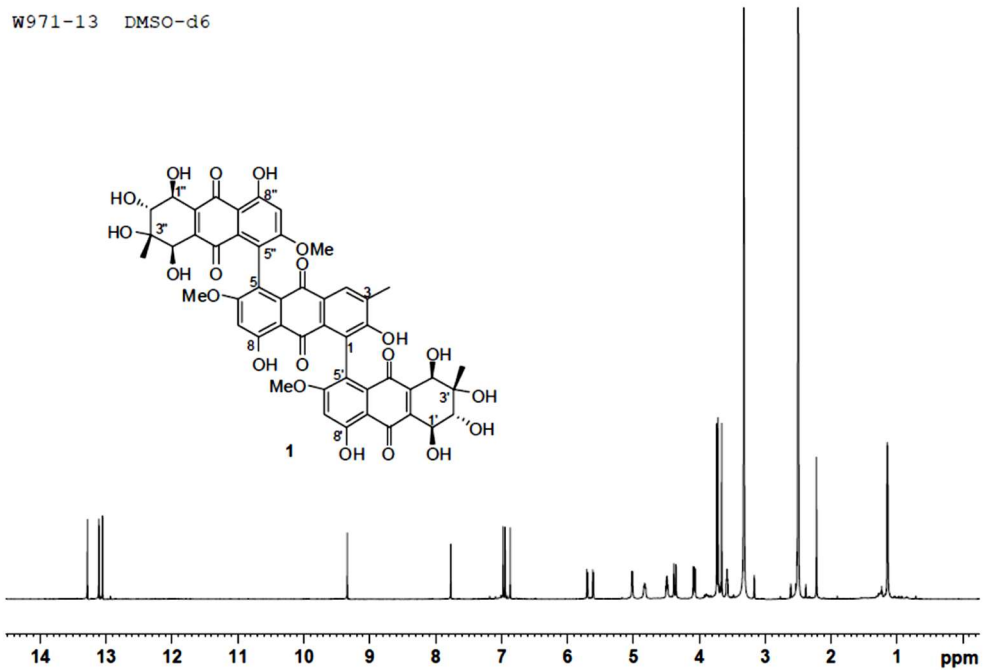


Figure S1-1. ¹H NMR spectrum of 1 (DMSO-d₆, 600MHz).

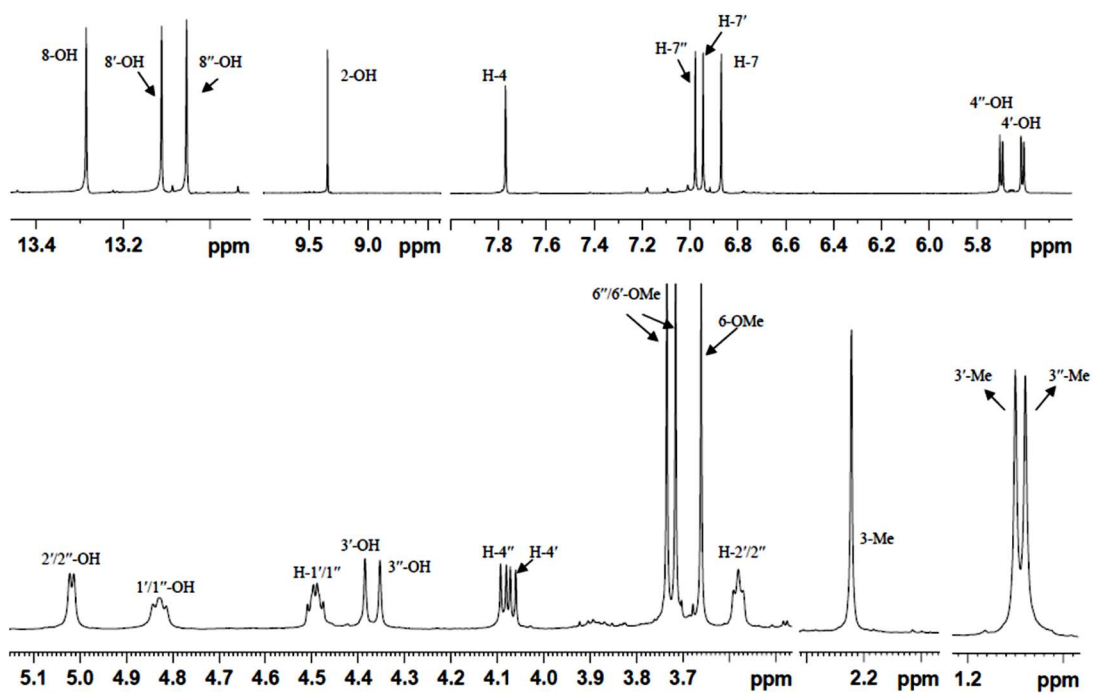
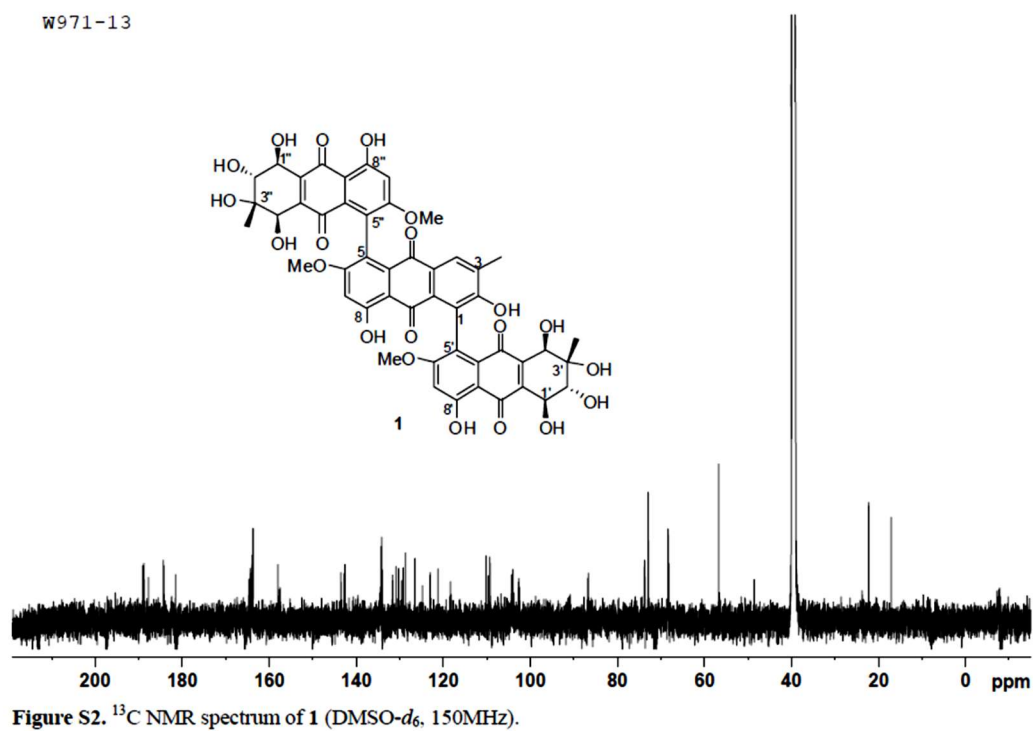
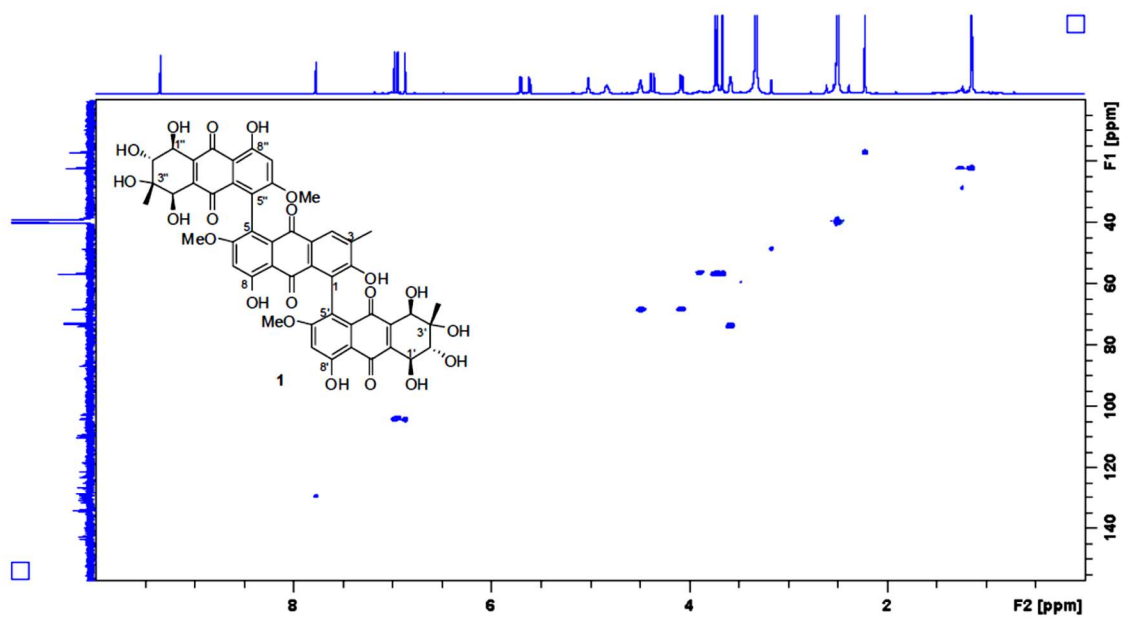


Figure S1-2. ¹H NMR spectrum of 1 with assignments (expansion).





S7

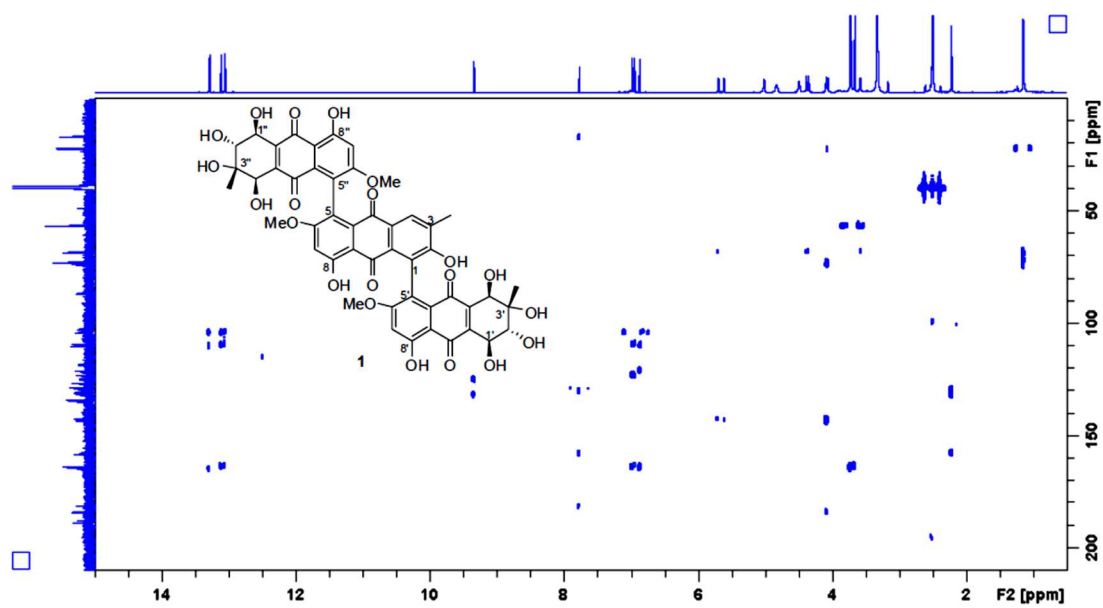


Figure S5. HMBC spectrum of 1.

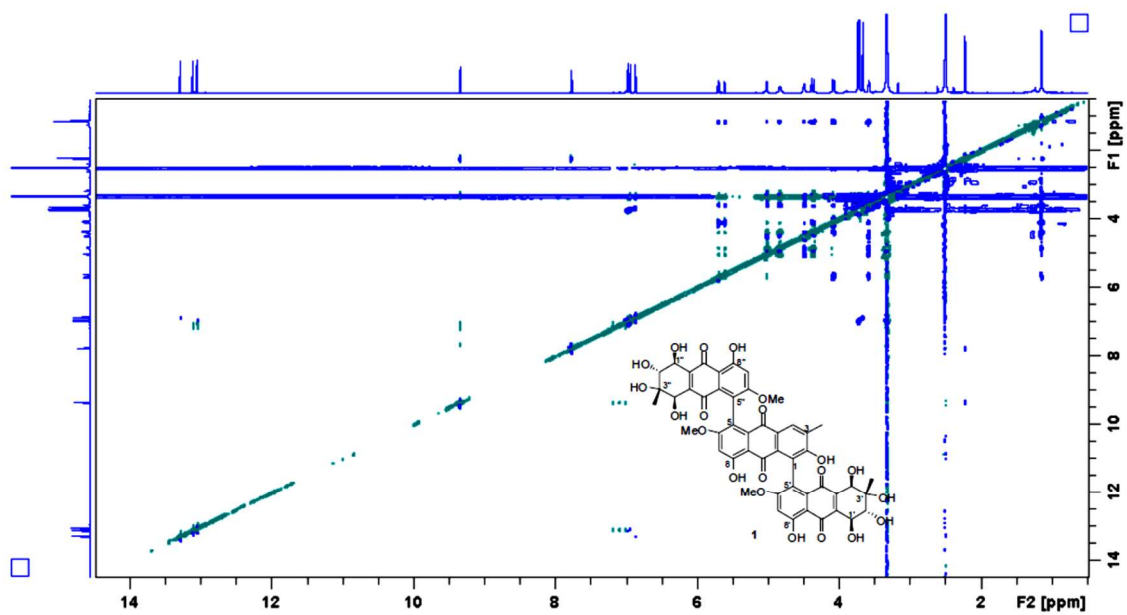


Figure S6. ROESY spectrum of 1.

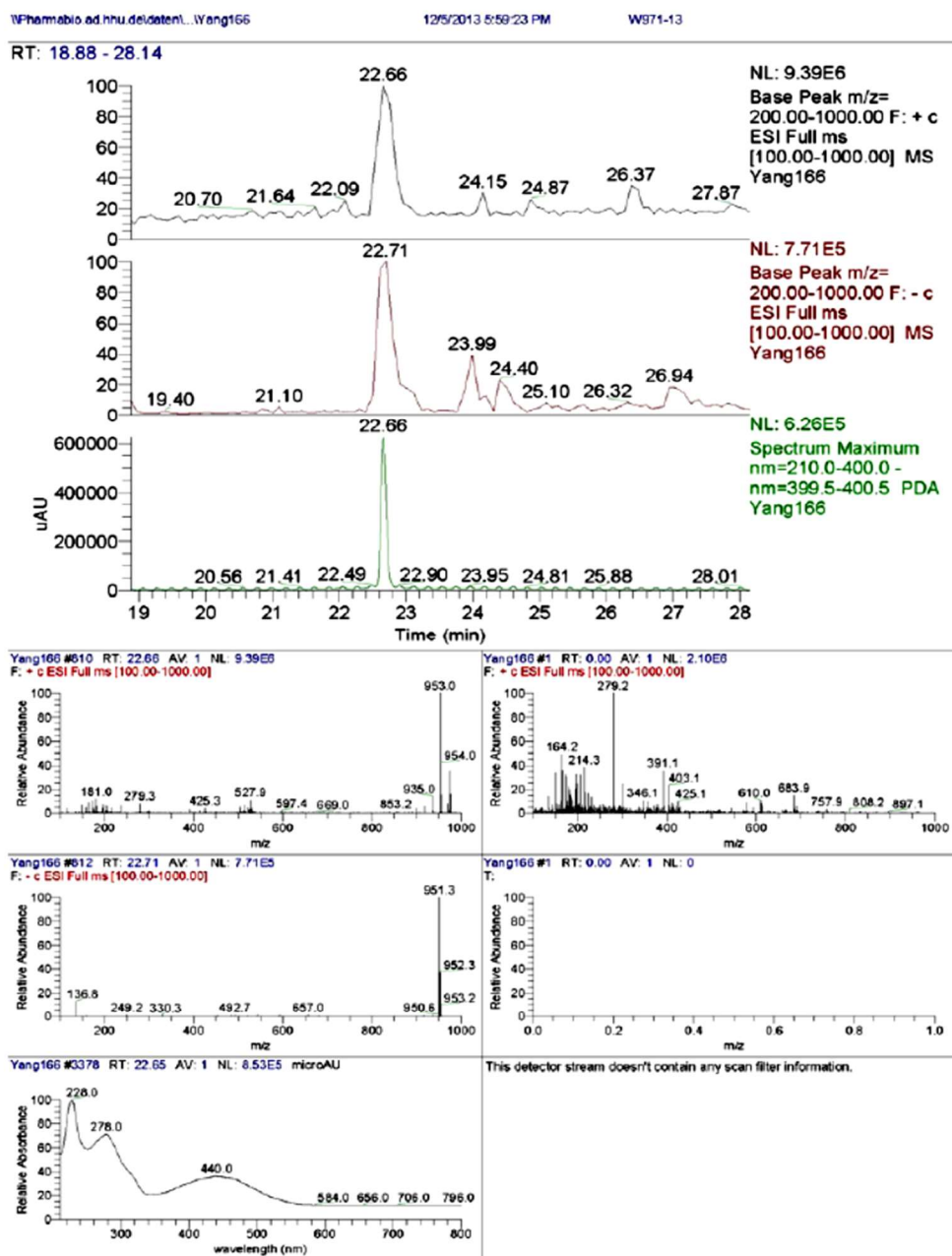


Figure S7. LC/ESIMS spectrum of 1.

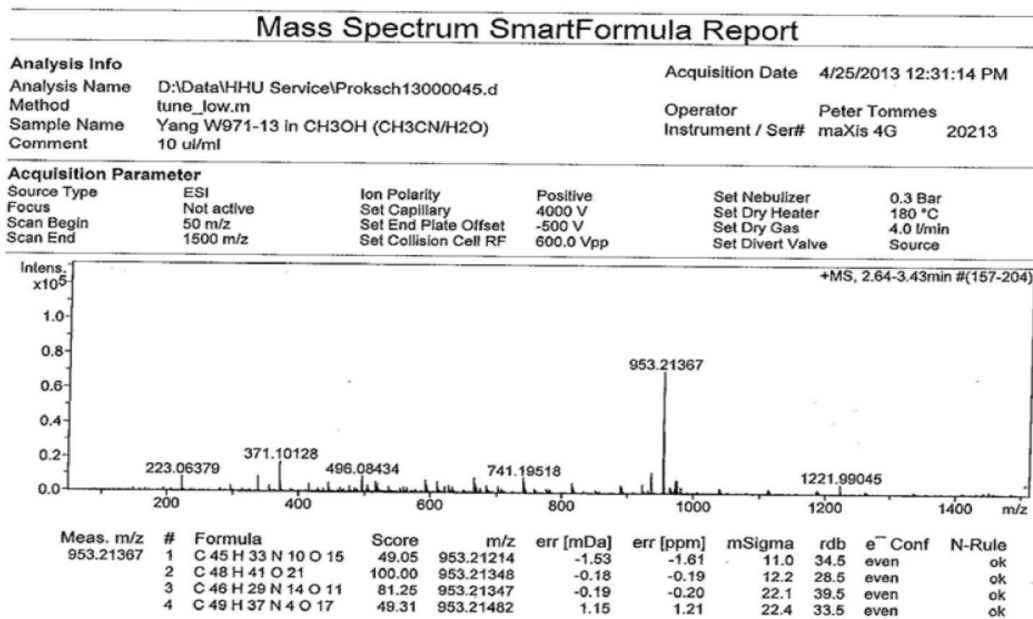


Figure S8. HRESIMS spectrum of 1.

SBCS0506 1 1

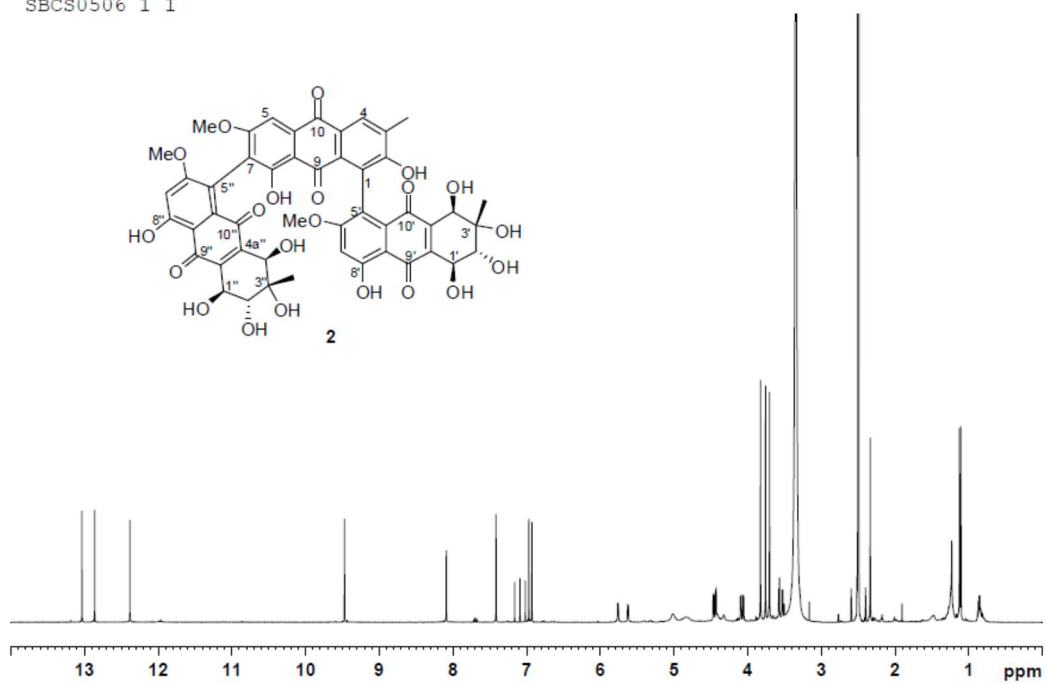


Figure S9-1. ^1H NMR spectrum of 2 (700MHz, $\text{DMSO-}d_6$).

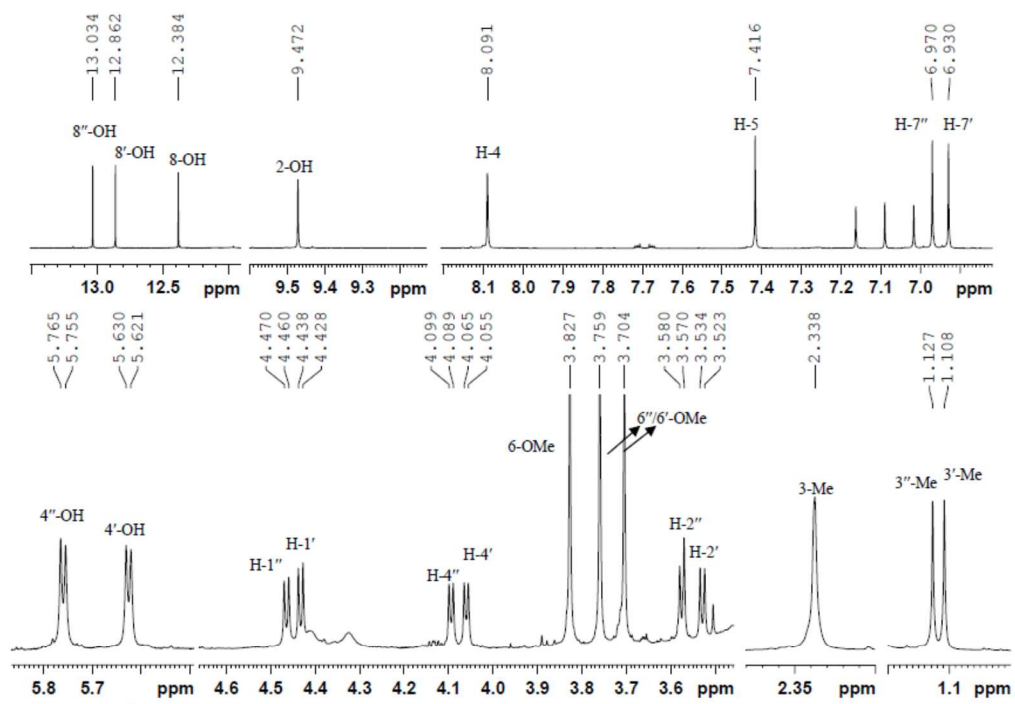
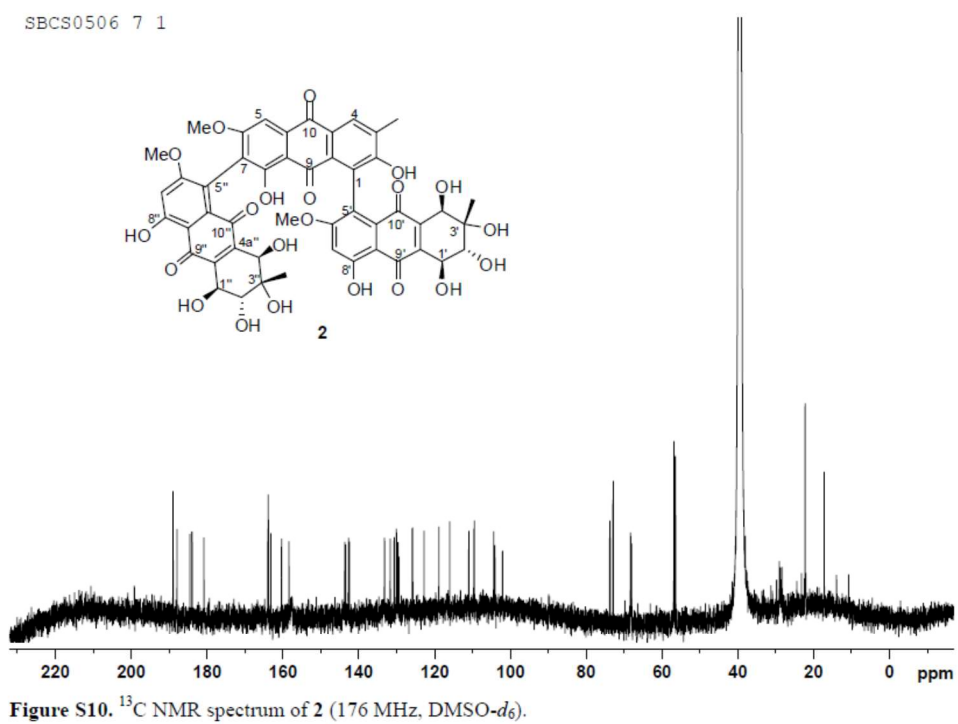


Figure S9-2. ^1H NMR spectrum of 2 with assignments (expansion).



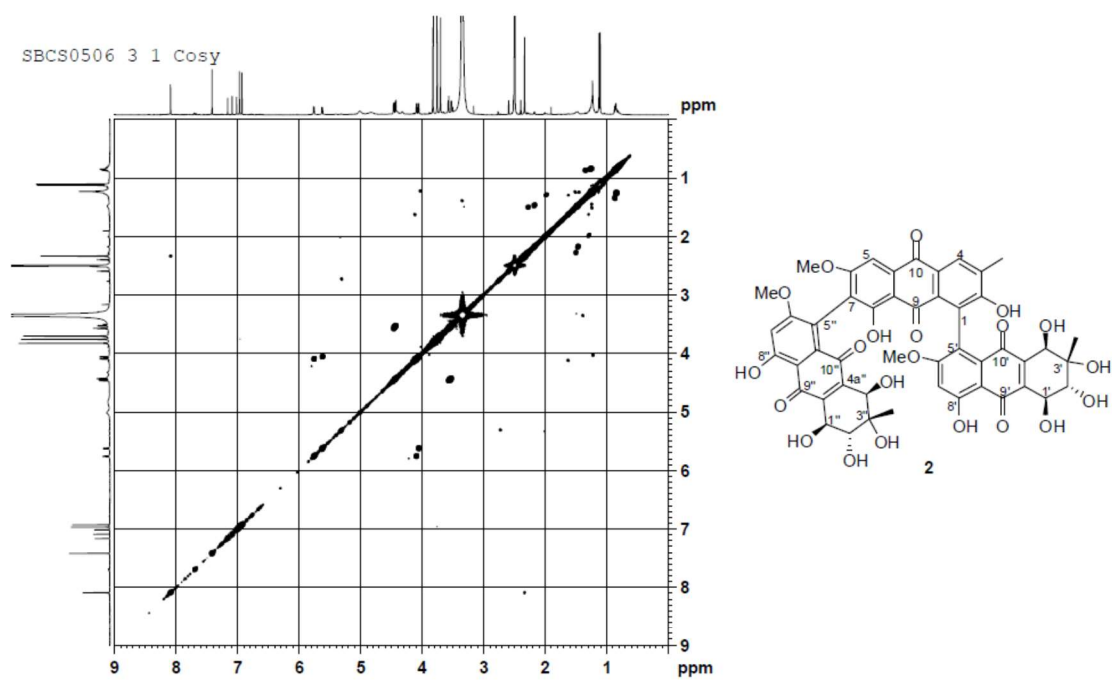


Figure S11. COSY spectrum of 2.

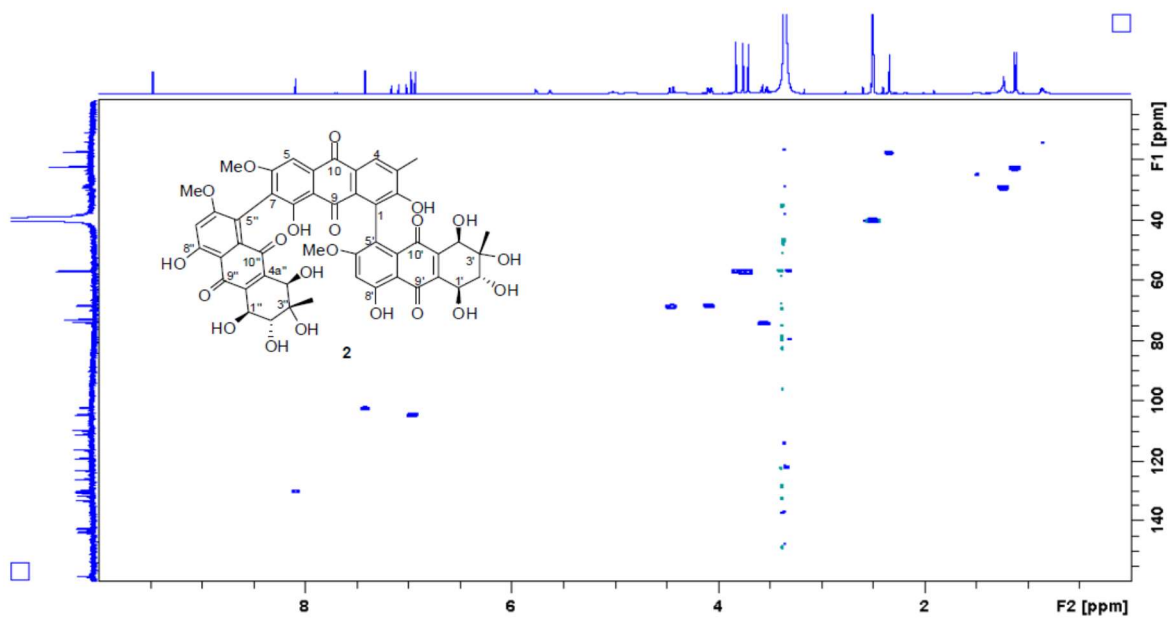
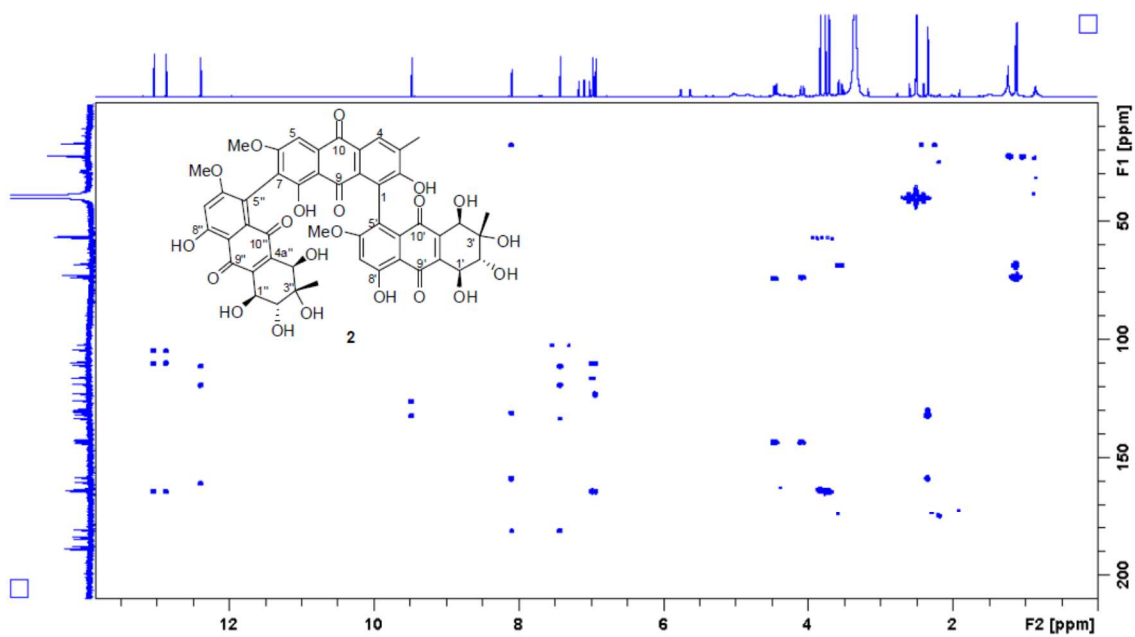
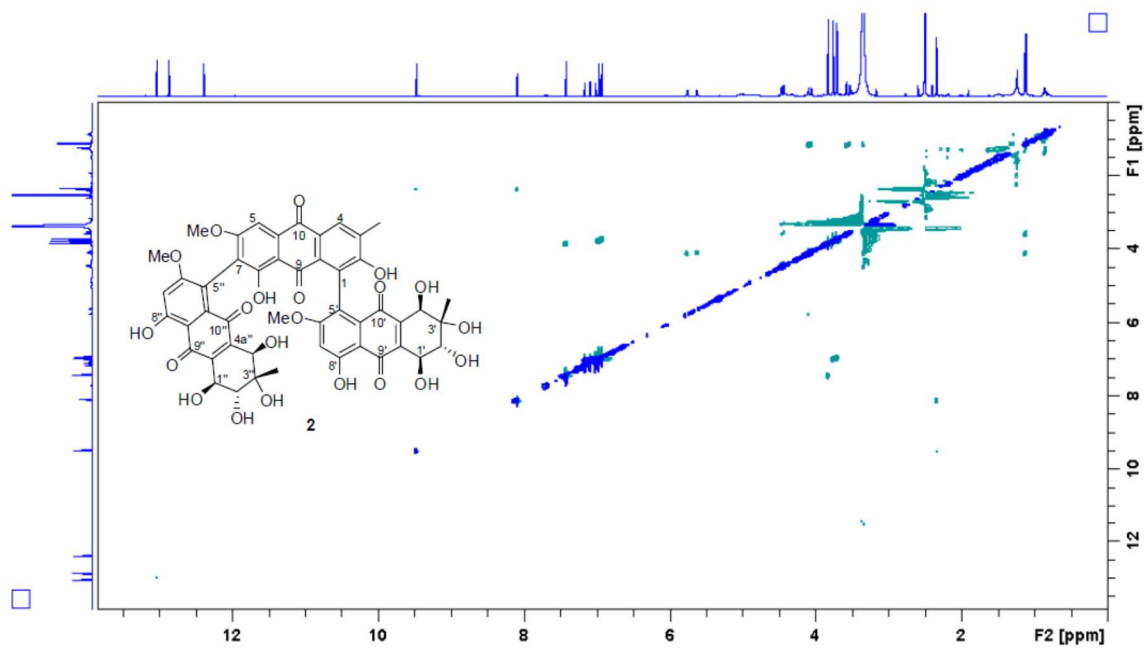


Figure S12. HSQC spectrum of 2.



S17



S18

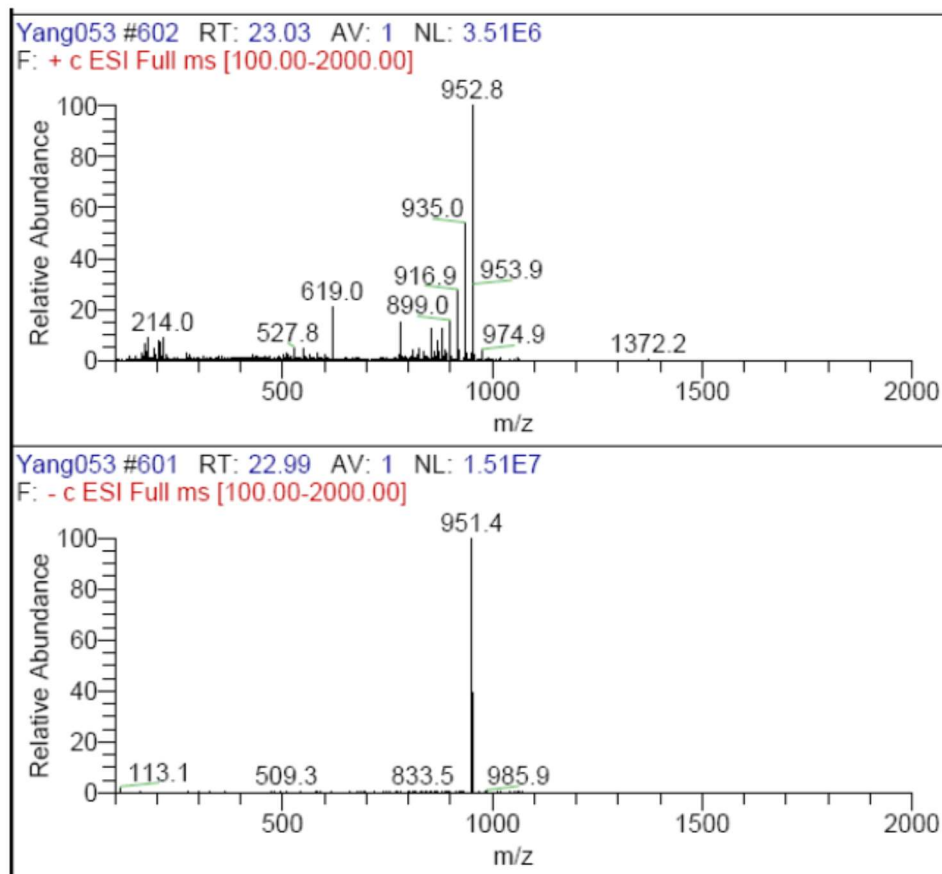


Figure S15. ESIMS spectrum of 2.

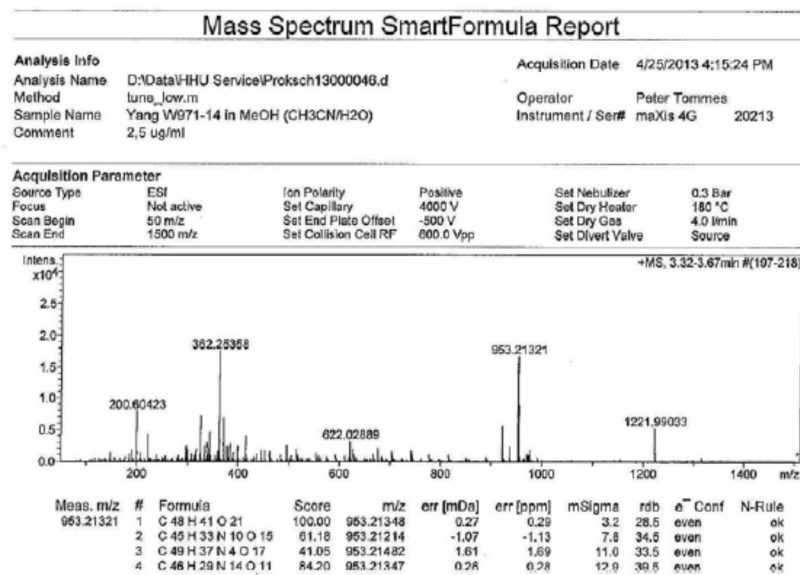


Figure S16. HRESIMS spectrum of 2.

3 Publication 2

3.1 Tetrahydroanthraquinone Derivatives from the Endophytic Fungus *Stemphylium globuliferum*

Published in: “European Journal of Organic Chemistry”

Impact factor: 3.065

Contribution: 80 %, first author, conducting most of the experiments, literature research, manuscript writing.

Reprinted with permission from “Liu Y., Marmann A., Abdel-Aziz M. S., Wang C. Y., Müller W. E. G., Lin W. H., Mándi A., Kurtán T., Daletos G., Proksch P. Tetrahydroanthraquinone Derivatives from the Endophytic Fungus *Stemphylium globuliferum*.” *Eur. J. Org. Chem.*, 12, 2646–2653. Copyright 2015 Wiley-VCH Verlag GmbH & Co. KGaA, Weinheim

DOI: 10.1002/ejoc.201500079

Tetrahydroanthraquinone Derivatives from the Endophytic Fungus *Stemphylium globuliferum*

Yang Liu,^[a,b] Andreas Marmann,^[a] Mohamed S. Abdel-Aziz,^[c] Chang Yun Wang,^[b]
Werner E. G. Müller,^[d] Wen Han Lin,^[e] Attila Mándi,^[f] Tibor Kurtán,^[f]
Georgios Daletos,^{*[a]} and Peter Proksch^{*[a]}

Keywords: Natural products / Endophytic fungi / Quinones / Cytotoxicity / Antibacterial activity / Atropisomerism

Four new tetrahydroanthraquinone derivatives, namely, dihydroaltersolanol B (**1**), dihydroaltersolanol C (**2**), and the atropisomers acetylalterporriol D (**3**) and acetylalterporriol E (**4**), were obtained from the endophytic fungus *Stemphylium globuliferum*, which was isolated from *Juncus acutus* growing in Egypt. The structures of the new compounds were unambiguously elucidated on the basis of one- and two-dimensional NMR spectroscopy, as well as by high-resolution mass spectrometry and electronic circular dichroism (ECD) spectroscopy. In addition, seven known anthraquinone deriva-

tives **5–11** were isolated and identified on the basis of their spectral characteristics and by comparison with literature data. Compounds **2**, **4–7**, **9**, and **11** showed strong cytotoxicity against the murine lymphoma cell line L5178Y with IC₅₀ values ranging from 1.25 to 10.4 μM. Compounds **1–4** were also tested for their antibacterial activity against *Staphylococcus aureus*, *Escherichia coli*, and *Pseudomonas aeruginosa*. Only **2** exhibited moderate growth inhibition against *S. aureus* with a minimum inhibitory concentration (MIC) of 49.7 μM.

Introduction

Endophytic fungi are present in all higher plants from the tropics to the arctic regions.^[1] Molecular biological methods have demonstrated that up to several hundred different endophytes can be associated with a single host plant and colonize all of the tissues.^[2,3] Fossilized tissues of higher plants have indicated that plant–endophyte associations have existed for at least 400 million years.^[4] This symbiotic interaction between the host plant and endophytic fungi is often described to have positive effects on the host.

For example, whereas the host plant provides water, nutrients, and a special economic niche for endophytes, the fungal secondary metabolites may stimulate plant growth^[5,6] and protect the host plant against pathogens^[6,7] and feeding damage caused by herbivores.^[8,9] This complex interspecies crosstalk leads to the production of a huge variety of structurally diverse fungal metabolites with potential medicinal or agricultural applications.^[10–14] In particular, endophytes from extreme habitats that exist under high ecological pressure, such as those present in mangrove plants or in plants that grow in salt lakes, have been suggested to be promising sources for new metabolites.^[15–17]

During our ongoing search for new, bioactive compounds from endophytic fungi,^[18–21] we investigated the endophytic fungus *Stemphylium globuliferum*, which was isolated from *Juncus acutus* collected from the shore of the hypersaline lake El Hamra in Wadi el Natrun, Egypt. The fungal extract caused a significant growth inhibition of the murine lymphoma cell line L5178Y, which prompted us to investigate the compounds produced by this endophyte. *Stemphylium* sp. produce a broad spectrum of polyketide secondary metabolites with different bioactivities, such as the antimicrobial stemphyllotoxin I–IV,^[22] the phytotoxic chromone glucosides stemphyloxin I and II,^[23,24] the cytotoxic altersolanol A, B, and C,^[25,26] as well as the protein kinase inhibitors alterporriol G and H.^[25–27] In our previous study, the first naturally occurring trimeric anthraquinone derivatives, stemphyllanthranol A and B, were isolated from *S. globuliferum*.^[28] As a continuation of this work, four new tetrahydroanthraquinone derivatives were

[a] Institute of Pharmaceutical Biology and Biotechnology, Heinrich Heine University, Universitätsstrasse 1, 40225 Düsseldorf, Germany
E-mail: proksch@uni-duesseldorf.de

georgios.daletos@uni-duesseldorf.de
<http://www.pharmazie.hhu.de/institute/institut-fuer-pharmazeutische-biologie-und-biotechnologie/arbeitskreise/ak-proksch.html>

[b] Key Laboratory of Marine Drugs, The Ministry of Education of China, School of Medicine and Pharmacy, Ocean University of China, Qingdao 266003, P. R. China

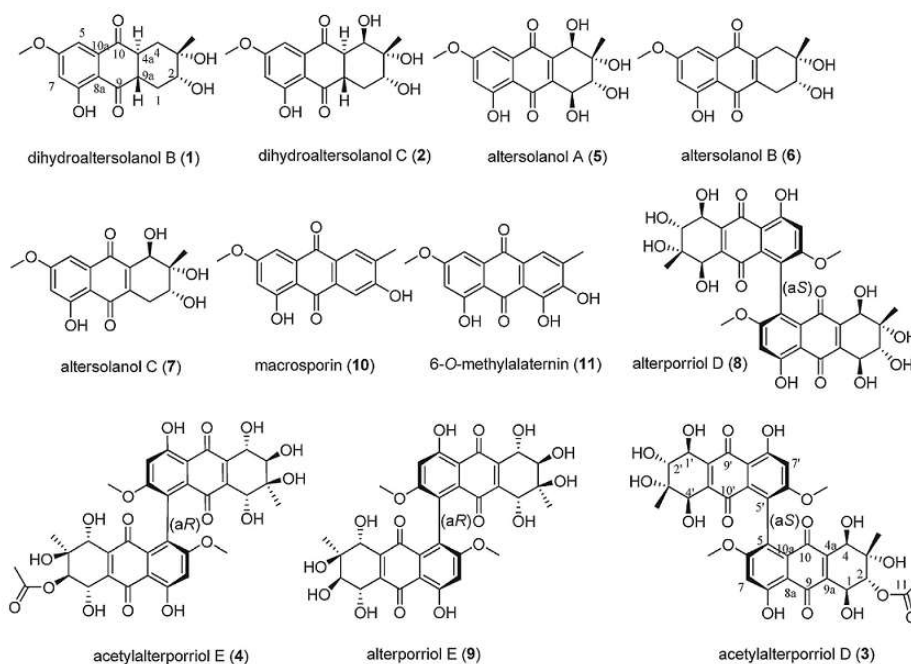
[c] Microbial Chemistry Department, Genetic Engineering and Biotechnology Division, National Research Center, Dokki-Giza 12622, Egypt

[d] Institute of Physiological Chemistry and Pathobiochemistry, Johannes Gutenberg University, Duesbergweg 6, 55128 Mainz, Germany

[e] State Key Laboratory of Natural and Biomimetic Drugs, Peking University, Beijing 100191, P. R. China

[f] Department of Organic Chemistry, University of Debrecen, P. O. B. 20, 4010 Debrecen, Hungary

Supporting information for this article is available on the WWW under <http://dx.doi.org/10.1002/ejoc.201500079>.



isolated, namely, dihydroaltersolanol B (**1**) and C (**2**) and the atropisomers acetylalterporriol D (**3**) and E (**4**), together with the seven known anthraquinone derivatives altersolanol A–C (**5–7**), alterporriol D and E (**8–9**), macrosporin (**10**), and 6-*O*-methylalternerin (**11**).^[26,29–35] The structure elucidation of the new compounds as well as results of cytotoxic and antibacterial bioassays are reported.

Results and Discussion

The EtOAc extract of the endophytic fungus *S. globuliferum* grown on solid rice medium was partitioned between *n*-hexane and 90% aqueous MeOH. The resulting MeOH phase was fractionated by vacuum liquid chromatography (VLC) on silica gel, followed by size exclusion chromatography with Sephadex LH-20 and semipreparative reversed-phase HPLC to yield four new tetrahydroanthraquinone derivatives (**1–4**) and seven known compounds (**5–11**).^[26,29–35]

Compound **1** was obtained as a yellow powder. The molecular formula of **1** was determined as C₁₆H₁₈O₆ on the basis of the prominent ion peak at *m/z* = 307.1174 [M + H]⁺ in the HRMS (ESI) spectrum. It exhibited UV absorption maxima at λ_{max} (MeOH) = 241, 288, and 345 nm, which suggest a tetrahydroanthraquinone as the basic structure. The ¹H NMR and COSY spectra revealed signals representative of two *meta*-coupled aromatic protons at δ_H = 6.71 (d, *J* = 2.5 Hz, 1 H, 7-H) and 6.95 ppm (d, *J* = 2.5 Hz, 1 H, 5-H), a methoxy group at δ_H = 3.94 ppm (s, 3 H, 6-OCH₃), an aliphatic methyl group at δ_H = 1.31 ppm (s, 3 H, 3-CH₃), as well as a continuous spin system composed of two methylene groups (1-CH₂ and 4-CH₂), two aliphatic

methine protons (4a-H and 9a-H), and one oxymethine proton, as indicated by its downfield chemical shift at δ_H = 3.48 ppm (dd, *J* = 11.8, 4.5 Hz, 1 H, 2-H). The ¹³C NMR and heteronuclear single quantum coherence (HSQC) spectra of **1** confirmed the corresponding carbon signals, including two sp² carbon atoms [δ_C = 106.4 (C-7) and 105.5 ppm (C-5)], five sp³ carbon atoms [δ_C = 38.3 (C-4), 74.2 (C-2), 30.8 (C-1), 48.6 (C-9a), and 46.8 ppm (C-4a)], one aliphatic methyl group at δ_C = 27.2 ppm (3-CH₃), and one methoxy group at δ_C = 56.6 ppm (6-OCH₃). The remaining signals included those of four aromatic sp² quaternary carbon atoms [δ_C = 138.8 (C-10a), 113.2 (C-8a), 165.0 (C-8), and 167.1 ppm (C-6)], one oxygenated sp³ quaternary carbon atom at δ_C = 70.7 ppm (C-3), and two carbonyl groups at δ_C = 197.7 (C-10) and 203.1 ppm (C-9). These data were in agreement with those observed for the known altersolanol B (**6**),^[30,31] apart from the additional methine proton signals at δ_H = 3.03 (ddd, *J* = 12.5, 11.6, 3.5 Hz, 1 H, 9a-H) and 3.20 ppm (ddd, *J* = 12.5, 11.8, 3.7 Hz, 1 H, 4a-H) in the ¹H NMR spectrum of **1**; these data suggest that the double bond between C-9a and C-4a in **1** is reduced compared to that in **6**. In the HMBC spectrum of **1**, the correlations from 9a-H to C-9, C-1, and C-4a and from 4a-H to C-9a and C-10 corroborated this assumption, which is in accordance with the molecular weight difference of 2 amu observed between both compounds. The remaining HMBC correlations from 5-H to C-7, C-6, C-10a, C-8a, and C-10; 7-H to C-8, C-5, C-6, and C-8a; 6-OCH₃ to C-6; 4-H to C-4a, C-9a, C-10, C-3, C-2, and 3-CH₃; 1-H to C-2, C-3, C-4a, C-9a, and C-9; and 3-CH₃ to C-4, C-3, C-2, and C-4a fully support the attachment of the methyl

HRMS (ESI) on the basis of the prominent peak at $m/z = 713.17108$ $[M + H]^+$. In the 1H and ^{13}C NMR spectra of **3** (Table 2), the presence of two chelated OH groups at $\delta_H = 12.96$ and 12.92 ppm (8-OH and 8'-OH) as well as the presence of four ketone groups at $\delta_C = 190.4$, 190.9 , 185.0 , and 185.4 ppm (C-9, C-9', C-10, and C-10') suggested the dimeric tetrahydroanthraquinone nature of **3**. Further inspection of the 1D (1H and ^{13}C) and 2D NMR (COSY, HSQC, and HMBC) data of **3** allowed the assignment of two tetrahydroanthraquinone units corresponding to **5**^[29,30] and the known altersolanol N.^[25]

Accordingly, in the 1H NMR of **3**, the resonances of a tertiary methyl group at $\delta_H = 1.38$ ppm (s, 3 H, 3'-CH₃), three carbinolic protons at $\delta_H = 4.32$ (d, $J = 6.6$, 1 H, 4'-H), 3.86 (dd, $J = 7.2, 5.0$ Hz, 1 H, 2'-H), and 4.76 ppm (dd, $J = 7.2, 3.1$ Hz, 1 H, 1'-H), an aromatic proton at $\delta_H =$

6.82 ppm (d, $J = 2.1$ Hz, 1 H, 7'-H), and an aromatic methoxy group at $\delta_H = 3.75$ ppm (s, 3 H, 6'-OCH₃) were attributed to an altersolanol A (**5**) unit. The HMBC cross-peaks detected from 4'-H to C-2', C-3', C-10', C-4a', C-9a', and 3'-CH₃; 3'-CH₃ to C-4' and C-3'; 7'-H to C-5', C-6', C-8', and C-8a'; and 6'-OCH₃ to C-6' fully supported this assignment (Figure 3). The ROESY correlation between 6'-OCH₃ and 7'-H in addition to the chelated proton resonance at $\delta_H = 12.9$ ppm (s, 1 H, 8'-OH) further supported the 6'-methoxy and 8'-hydroxy substitutions and, thus, indicated that the altersolanol A unit was connected to the second unit through C-5'.

The remaining signals included those of a tertiary methyl group at $\delta_H = 1.27$ ppm (s, 3 H, 3-CH₃), three carbinolic protons at $\delta_H = 4.37$ (d, $J = 6.6$ Hz, 1 H, 4-H), 5.45 (d, $J = 7.8$ Hz, 1 H, 2-H), and 4.95 ppm (dd, $J = 7.8, 3.0$ Hz, 1

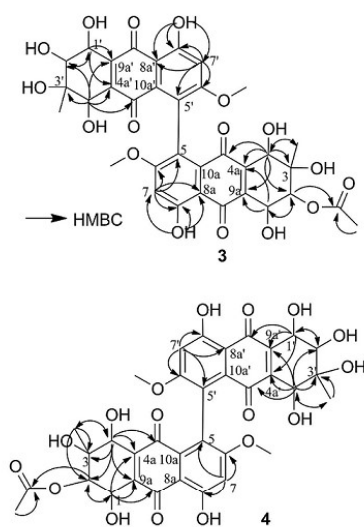
Table 2. NMR spectroscopic data of **3** in [D₆]acetone (δ in ppm, J in Hz; 1H at 700 MHz for **3** and 600 MHz for **4**; ^{13}C at 175 MHz for **3** and 150 MHz for **4**).^[a]

			3		4		
Position	δ_H , multiplicity (J)	δ_C	HMBC	δ_H multiplicity (J)	δ_C	HMBC	
1	4.95, dd (7.8, 3.0)	68.1, CH	C-2, C-9a, C-4a	4.96, d (7.8)	68.2, CH	C-2, C-9, C-4a, C-9a	
2	5.45, d (7.8)	76.9, CH	C-1, C-11	5.43, d (7.8)	76.9, CH	C-1, C-11	
3		73.7, C			73.6, C		
4	4.37, d (6.6)	70.1, CH	C-2, C-3, C-10, C-4a, C-9a, 3-CH ₃	4.36, s	69.9, CH	C-2, C-3, C-10, C-4a, C-9a, 3-CH ₃	
5		123.3, C ^d			124.0, C ^b		
6		165.6, C			166.3, C ^b		
7	6.83, d (2.1) ^a	104.74, C ^c	C-8, C-6, C-5, C-8a	6.86, s	104.44, CH ^e	C-5, C-6, C-8, C-8a	
8		165.6, C			165.8, C ^d		
9		190.4, C ^f			190.3, C		
10		185.0, C			184.8, C		
11		170.9, C			170.7, C		
4a		143.3, C ^b			143.4, C		
8a		110.56, C ^g			110.53, C ^e		
9a		143.5, C ^b			143.1, C		
10a		131.4, C ^h			130.6, C ^f		
3-CH ₃	1.27, s	22.4, CH ₃	C-4, C-2, C-3	1.27, s	22.4, CH ₃	C-4, C-3, C-2	
6-OCH ₃	3.75, s ^b	57.3, CH ₃	C-6	3.78, s	57.19, CH ₃	C-6	
11-CH ₃	2.11, s	21.0, CH ₃	C-11	2.10, s	20.9, CH ₃	C-11	
8-OH	12.96, s ^c		C-8, C-7, C-8a				
1-OH	4.37, d (3.0)						
3-OH	4.09, s						
4-OH	4.96, d (6.6)						
1'	4.76, dd (7.2, 3.1)	70.7, CH	C-2', C-9a', C-4a'	4.76, d (7.2)	70.7, CH	C-2', C-9', C-4a', C-9a'	
2'	3.86, dd (7.2, 5.0)	74.8, CH	C-1'	3.84, d (7.2)	74.6, CH	C-1'	
3'		74.1, C			73.9, C		
4'	4.32, d (6.6)	69.8, CH	C-2', C-3', C-10', C-4a', C-9a', 3'-CH ₃	4.32, s	69.6, CH	C-3', C-10', C-4a', C-9a', 3'-CH ₃	
5'		123.1, C ^d			123.7, C ^e		
6'		165.5, C			166.2, C ^b		
7'	6.82, d (2.1) ^a	104.67, CH ^e	C-8', C-6', C-5', C-8a'	6.87, s	104.37, CH	C-5', C-6', C-8', C-8a'	
8'		165.5, C			165.7, C		
9'		190.9, C ^f			190.9, C		
10'		185.4, C			185.1, C		
4a'		143.8, C ^b			143.8, C		
8a'		110.58, C ^g			110.47, C ^e		
9a'		144.1, C ^b			143.8, C		
10a'		131.3, C ^h			130.5, C ^f		
3'-CH ₃	1.38, s	22.7, CH ₃	C-4', C-3'	1.39, s	22.7, CH ₃	C-4', C-3'	
6'-OCH ₃	3.75, s ^b	57.2, CH ₃	C-6'	3.78, s	57.22, CH ₃	C-6'	
8'-OH	12.92, s ^c		C-8', C-6', C-7', C-8a'				
1'-OH	4.25, d (3.1)						
2'-OH	4.13, br. d (5.0)						
3'-OH	3.70, s						
4'-OH	4.70, d (6.6)						

[a] The assignments marked with a-h may be interchanged. [b] The assignments for C-4a, C-4a', C-9a, and C-9a' may be interchanged.

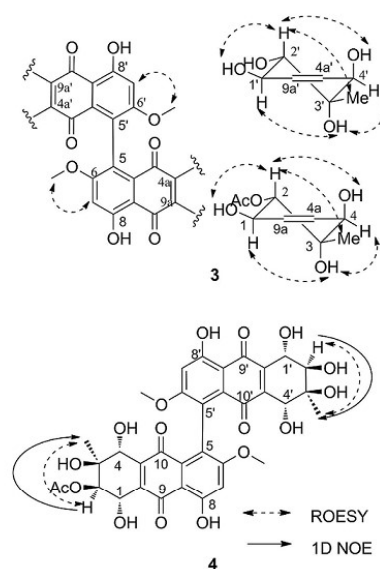
FULL PAPER

G. Daletos, P. Proksch et al.

Figure 3. Selected HMBC correlations of **3** and **4**.

H, 1-H), an acetyl group at $\delta_{\text{H}} = 2.11$ ppm (s, 3 H, 11-CH₃), an aromatic proton at $\delta_{\text{H}} = 6.83$ ppm (d, $J = 2.1$ Hz, 1 H, 7-H), as well as an aromatic methoxy group at $\delta_{\text{H}} = 3.75$ ppm (s, 3 H, 6-OCH₃). These signals were indicative of an altersolanol N moiety as confirmed by the COSY correlation between 2-H and 1-H and by the HMBC correlations from 7-H to C-5, C-6, C-8, and C-8a; 4-H to C-2, C-3, C-10, C-4a, C-9a, and 3-CH₃; 3-CH₃ to C-4, C-3, and C-2; 2-H to C-1 and C-11; 6-OCH₃ to C-6; and 11-CH₃ to C-11. The location of the acetyl group (11-CH₃) at C-2 ($\delta_{\text{C}} = 76.9$ ppm) was further corroborated by the marked downfield shift observed for 2-H ($\Delta\delta = 1.59$ ppm) compared with the corresponding chemical shift in the altersolanol A unit (Table 2). In a similar manner, the ROESY correlation of 6-OCH₃ to the aromatic proton 7-H, in addition to the chelated proton at $\delta_{\text{H}} = 12.9$ ppm (s, 1 H, 8-OH), indicated the presence of 6-methoxy and 8-hydroxy substituents in the aromatic ring; therefore, only C-5 remains for the connection of the two tetrahydroanthraquinone units. Thus, **3** was assigned as an asymmetric dimer consisting of one altersolanol A unit (**5**) and one altersolanol N unit connected through a 5',5'-biaryl linkage.

The relative configuration of the aliphatic rings in **3** (Figure 4) was determined by analysis of the coupling constants and the NOE correlations observed in the ROESY spectrum. The large vicinal coupling constant ($J = 7.8/7.2$ Hz) between 2-H/2'-H and 1-H/1'-H suggested their *trans* diaxial orientations, which was corroborated by the correlations of 2-H/2'-H with 1(1')-OH in the ROESY spectrum of **3**. In addition, key ROESY correlations between 2-H/2'-H, 3(3')-CH₃, and 4(4')-OH indicated their cofacial orientation. On the other hand, correlations of both 1-H/1'-H and 4-H/4'-H to 3(3')-OH suggested that they were directed to the opposite face with the same relative configuration as that observed for **5** and altersolanol N. Hence, **3** was identified as a new natural heterodimer for which the name acetylalterporriol D was proposed.

Figure 4. ROESY correlations of **3** and **4**.

The axial chirality of **3** was determined by comparing its ECD spectrum with that of alterporriol D, which has (aS) axial chirality (Figure 5, a).^[25] The axial chirality of alterporriol D and E was deduced previously by comparison with the ECD spectrum of alterporriol N, for which time-dependent DFT (TDDFT) ECD calculations were performed.^[25] The near-congruent ECD curves of **3** and alterporriol D allowed the assignment of the axial chirality of **3** as (aS), as the ECD spectra are governed predominantly by the axial chirality element.

Acetylalterporriol E (**4**) was obtained as a red powder and displayed the same UV absorption spectrum and shared the molecular formula C₃₄H₃₂O₁₇ with **3** on the basis of HRMS (ESI) measurement ($m/z = 713.17126$ [M + H]⁺). Moreover, the ¹H and ¹³C NMR spectra of **4** (Table 2) were almost superimposable with those of **3**, and the analysis of the 2D NMR spectra of **4** indicated that both compounds shared the same planar structure. However, **4** eluted ca. 2 min later than **3** upon HPLC analysis. These data suggest that **4** is a stereoisomer of **3** differing either in the configuration of the biaryl axis or in the chiral centers for each tetrahydroanthraquinone unit. The relative configuration of **4** was determined by detailed analysis of the ROESY data (Figure 4) as well as the coupling constants of the relevant protons (Table 2). Owing to the lack of the hydroxy signals in the ¹H NMR spectrum of **4** in [D₆]acetone, further 1D NOE experiments were performed. The enhancement of only the signal assigned to 3-CH₃(3'-CH₃) upon irradiation of 2-H(2'-H) indicates their cofacial orientation. Accordingly, the relative configuration of the aliphatic ring in **4** was found to be identical to that of **3**. A detailed analysis of the CD spectrum of **4** revealed that the difference between those two compounds was caused by chirality of the 5,5'-axis. The ECD spectra of **4** and alterporriol E^[25] showed similar ECD patterns in the range $\lambda = 200$ –600 nm

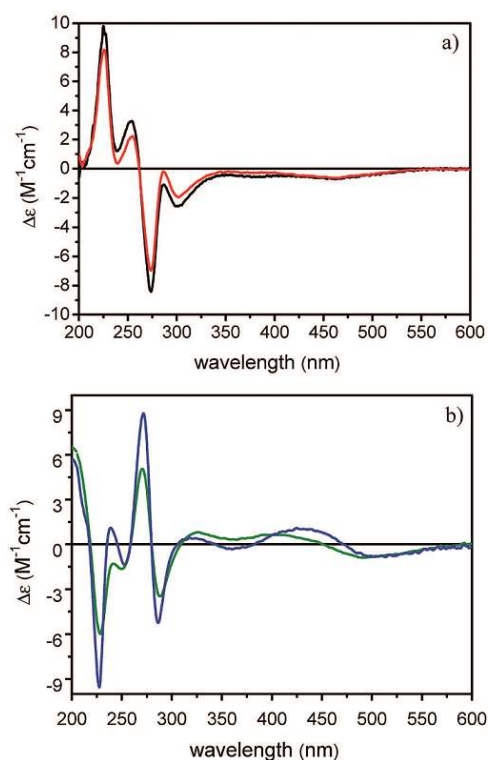


Figure 5. (a) ECD spectrum of acetylalterporriol D (**3**, red) in acetonitrile compared with that of alterporriol D (**8**, black). (b) ECD spectrum of acetylalterporriol E (**4**, blue) in acetonitrile compared with that of alterporriol E (**9**, green).

(Figure 5, b) and, therefore, the axial chirality of **4** was assigned as (aR). Thus, **4** was identified as the atropisomer of **3** and was given the name acetylalterporriol E.

On the basis of their NMR and mass spectroscopic data and by comparison with the literature data, the remaining compounds were identified as altersolanol A (**5**),^[29–31] altersolanol B (**6**),^[30,31] altersolanol C (**7**),^[32] alterporriol D (**8**),^[33–35] alterporriol E (**9**),^[32–35] macrosporin (**10**),^[30] and 6-*O*-methylalaternin (**11**).^[26]

Compounds **1–11** were examined for their effects on the growth of the murine lymphoma L5178Y cell line through 3-(4,5-dimethylthiazol-2-yl)-2,5-diphenyltetrazolium bromide (MTT) assays (Table 3). Compound **2** showed potent activity with an IC_{50} value of 3.4 μM , whereas **1** was not active; therefore the 1-hydroxy substitution in dihydroalterolanol-type derivatives is important for mediating cytotoxicity. Furthermore, the anthraquinone derivative **11** possesses considerable cytotoxicity (IC_{50} = 1.25 μM), whereas its analogue macrosporin (**10**) displayed only weak activity, which suggests that the *ortho*-dihydroxy substitution pattern of **11** greatly increases the observed cytotoxicity. On the other hand, all altersolanol-type derivatives (**5–7**) showed potent activity, which indicates that the substituents at the aliphatic ring are not essential structural features for the activity of these compounds. To prove this assumption,

derivatization of **5** and **7** with the diol protecting group acetone was carried out. The slight decrease in the activity of the corresponding acetone derivatives (10.6 and 3.4% relative to the activities of **5** and **7**, respectively) further supported that the OH groups at the 2- and 3-positions did not mediate the cytotoxicity. Notably, **4** and **9** with (aR) axial chirality exhibited marked activity with IC_{50} values of 10.4 and 6.9 μM , respectively, whereas their (aS) congeners were inactive. These results suggest that the biaryl chirality of tetrahydroanthraquinone dimeric derivatives plays a crucial role for the mode of action of these compounds.

Table 3. Cytotoxicity assay for isolated compounds.

	L5178Y growth inhibition [%] (10 $\mu\text{g/mL}$)	IC_{50} [μM]
1	10.5	–
2	99.2	3.4
3	–5.4	–
4	71.8	10.4
5	100	2.53
6	100	3.78
7	100	4.68
8	8.3	–
9	96.8	6.9
10 ^[a]	45.5	–
11 ^[a]	98.1	1.25
Altersolanol A acetone	89.4	–
Altersolanol C acetone	96.6	–

[a] Data from ref.^[26].

The new compounds **1–4** were also tested for their antibacterial activity against *Staphylococcus aureus* ATCC 29213, *Escherichia coli* ATCC 25213, and *Pseudomonas aeruginosa* ATCC 27853. Only **2** exhibited moderate growth inhibition against *S. aureus* with a minimum inhibitory concentration (MIC) value of 49.7 μM , whereas the other compounds were inactive in this bioassay (IC_{50} > 64 $\mu\text{g/mL}$).

Experimental Section

General Experimental Procedures: Optical rotations were determined with a Perkin–Elmer-241 MC polarimeter. The ^1H , ^{13}C , and 2D NMR spectra were recorded at 25 $^{\circ}\text{C}$ with samples in $[\text{D}_6]\text{acetone}$ with Bruker AVANCE DMX 600 or Bruker ARX 700 NMR spectrometers. Chemical shifts were referenced to the solvent residual peaks ($\delta_{\text{H}} = 2.05$ ppm for ^1H , $\delta_{\text{C}} = 29.92$ ppm for ^{13}C). Mass spectra (ESI) were recorded with a Finnigan LCQ Deca mass spectrometer, and HRMS (ESI) spectra were obtained with a FTIRMS-Orbitrap (Thermo-Finnigan) mass spectrometer. Solvents were distilled before use, and spectral-grade solvents were used for spectroscopic measurements. HPLC analysis was performed with a Dionex UltiMate3400 SD with a LPG-3400SD Pump coupled to a photodiode array detector (DAD3000RS); routine detection was at $\lambda = 235, 254, 280,$ and 340 nm. The separation column (125 \times 4 mm) was pre-filled with Eurosphere-10 C18 (Knauer, Germany), and the following gradient was used (MeOH, 0.02% HCOOH in H_2O): 0 min: 10% MeOH, 5 min: 10% MeOH, 35 min: 100% MeOH, 45 min: 100% MeOH. Semipreparative HPLC was performed with a Merck Hitachi HPLC System (UV detector L-7400; pump L-7100; Eurosphere-100 C18, 300 \times 8 mm, Knauer, Germany). Column chromatography included LH-20 Sephadex and Merck MN Silica gel 60 M (0.04–0.063 mm). TLC

FULL PAPER

G. Daletos, P. Proksch et al.

plates with silica gel F₂₅₄ (Merck, Darmstadt, Germany) were used to monitor fractions; detection was under UV at $\lambda = 254$ and 366 nm or by spraying the plates with anisaldehyde reagent followed by heating.

Fungal Material: The endophytic fungus *S. globuliferum* was isolated from fresh *J. acutus* collected in November 2012 from the shore of the salt lake El Hamra in Wadi el Natrun, Egypt. The plant was twice rinsed with autoclaved distilled water and dried, followed by surface sterilization by twice immersing the plant in 70% ethanol (1 min) under clean-bench conditions. After drying, blades of disinfected *J. acutus* were cut into small pieces ca. 1 cm long, placed on the fungal isolation medium (medium composition: 15 g/L malt extract, 15 g/L agar, 0.2 mg/L chloramphenicol, 10 g/L sea salt, pH 7.4–7.8), and then incubated for several days at room temperature. The purified fungus was later transferred to solid rice medium for large scale fermentation.

Identification of Fungal Cultures: The fungus was identified as *S. globuliferum* according to a molecular biological protocol by DNA amplification and sequencing of the internal transcribed spacer (ITS) region, as described previously.^[36] The sequence data was submitted to the GenBank with accession number EU859960. The fungal strain was kept in the laboratory of one of the authors (P. P.).

Fermentation: The fungus was cultivated by using solid rice medium in six Erlenmeyer flasks. The solid rice medium was prepared by mixing rice (100 g) and demineralized water (110 mL) in a flask, followed by treatment in an autoclave (121 °C, 20 min). The fungus, which nearly covered the whole surface of a Petri dish, was inoculated onto sterile rice medium under clean-bench conditions and grown (20 °C) for 30 d.

Extraction and Isolation: The culture was diced and extracted with EtOAc. The crude extract was evaporated to dryness, and then subjected to liquid–liquid partitioning between *n*-hexane and 90% aqueous MeOH. The 90% MeOH fraction amounted to 2.80 g and was further separated by vacuum liquid chromatography on silica gel with solvents in a gradient of increasing polarity (*n*-hexane/ethyl acetate/dichloromethane/methanol) to obtain a total of 11 fractions. The fractions eluted with dichloromethane/MeOH (DCM/MeOH, 9:1–8:2) were then subjected to column chromatography with Sephadex LH-20 as the stationary phase and DCM/MeOH (1:1) as the mobile phase to remove pigments. Further purification was performed by reversed-phase HPLC (silica-based, semipreparative column) with MeOH/H₂O (50:50, 42:58, 40:60, 35:65) as the mobile phase to yield the four compounds **1** (8.2 mg), **2** (13 mg), **3** (1.8 mg), and **4** (3.9 mg), respectively.

Dihydroaltersolanol B (1): Yellow powder. $[\alpha]_D^{25} = 5.87$ ($c = 0.175$, MeOH). UV [MeOH, photodiode array (PDA)]: $\lambda_{\max} = 241, 288, 345$ nm. ECD (MeCN, $c = 5.44 \times 10^{-4}$ M): λ ($\Delta\epsilon$) = 357 (–0.35), 328 (1.83), 248 (–0.67), 229 (0.89), 207 (–3.11), 198 (–3.16) nm. ¹H (600 MHz) and ¹³C (150 MHz) NMR, see Table 1. ESI-MS: $m/z = 307.0$ [M + H]⁺, 305.4 [M – H][–]. HRMS (ESI): calcd. for C₁₆H₁₉O₆ [M + H]⁺ 307.1176; found 307.1174.

Dihydroaltersolanol C (2): Yellow powder. $[\alpha]_D^{25} = 69.63$ ($c = 0.44$, MeOH). UV (MeOH, PDA): $\lambda_{\max} = 241, 288, 345$ nm. ECD (MeCN, $c = 5.17 \times 10^{-4}$ M): λ ($\Delta\epsilon$) = 363 (sh, –1.21), 356 (–1.34), 325 (2.06), 297 (sh, 0.99), 286 (sh, 0.76), 263 (0.76), 243 (sh, 0.57), 228 (0.65), 197 (–5.32) nm. ¹H (600 MHz) and ¹³C (150 MHz) NMR, see Table 1. ESI-MS: $m/z = 323.0$ [M + H]⁺, 321.3 [M – H][–]. HRMS (ESI): calcd. for C₁₆H₁₉O₇ [M + H]⁺ 323.11253; found 323.11249.

Acetylalterporriol D (3): Yellow powder. $[\alpha]_D^{25} = -64.44$ ($c = 0.25$, MeOH). UV (MeOH, PDA) $\lambda_{\max} = 225, 276, 459$ nm. ECD

(MeCN, $c = 2.11 \times 10^{-4}$ M): λ ($\Delta\epsilon$) = 466 (–0.64), 302 (–1.94), 273 (–6.97), 255 (–2.23), 225 (8.18) nm. ¹H (700 MHz) and ¹³C (175 MHz) NMR, see Table 2. ESI-MS: $m/z = 713.0$ [M + H]⁺, 711.3 [M – H][–]. HRMS (ESI): calcd. for C₃₄H₃₃O₁₇ [M + H]⁺ 713.17123; found 713.17108.

Acetylalterporriol E (4): Yellow powder. $[\alpha]_D^{25} = -127.96$ ($c = 0.27$, MeOH). UV (MeOH, PDA): $\lambda_{\max} = 225, 276, 459$ nm. ECD (MeCN, $c = 2.33 \times 10^{-4}$ M): λ ($\Delta\epsilon$) = 505 (–0.79), 425 (+1.08), 360 (–0.33), 318 (+0.44), 286 (–5.24), 271 (+8.78), 253 (–1.38), 239 (+1.11), 227 (–9.56), 201 (5.71) nm. ¹H (600 MHz) and ¹³C (150 MHz) NMR, see Table 2. ESI-MS: $m/z = 713$ [M + H]⁺, 711.2 [M – H][–]. HRMS (ESI): calcd. for C₃₄H₃₃O₁₇ [M + H]⁺ 713.17123; found 713.17126.

Bioassays: The cytotoxic and antibacterial assays were performed as described previously.^[37,38]

Supporting Information (see footnote on the first page of this article): 1D (¹H and ¹³C) and 2D (HMQC, HMBBC, ROESY) NMR spectroscopic data and high-resolution mass spectra of **1–4**, ECD spectra of **1–4**, **8**, and **9**.

Acknowledgments

Financial support from the German Bundesministerium für Bildung und Forschung (BMBF) granted to P. P. and from Ministry of Science and Technology (MOST) to W. H. L. is gratefully acknowledged. Y. L. wishes to thank the China Scholarship Council, the Ministry of Education of China for a doctoral scholarship. We are indebted to Prof. Heike Brötz-Oesterhelt (Heinrich-Heine University, Düsseldorf, Germany) for antibacterial assays, to Hendrik Niemann and Cong-Dat Pham (Heinrich-Heine University, Düsseldorf, Germany) for collecting the samples from Wadi El Natrun in Egypt, and to Dr. Victor Wray (Helmholtz Centre for Infection Research, Braunschweig, Germany) for NMR measurements. T. K. thanks the Hungarian National Research Foundation (OTKA K105871) for financial support and the National Infrastructure Development Institute (NIIFI 10038) for CPU time.

- [1] K. L. Higgins, A. E. Arnold, J. Miadlikowska, S. D. Sarvate, F. Lutzoni, *Mol. Phylogenet. Evol.* **2007**, *42*, 543–555.
- [2] I. Zabalgoatza, *Span. J. Agric. Res.* **2008**, *6*, 138–146.
- [3] R. J. Rodriguez, J. F. White Jr., A. E. Arnold, R. S. Redman, *New Phytol.* **2009**, *182*, 314–330.
- [4] H. W. Zhang, Y. C. Song, R. X. Tan, *Nat. Prod. Rep.* **2006**, *23*, 753–771.
- [5] G. V. Bloembergen, B. J. J. Lugtenberg, *Curr. Opin. Plant Biol.* **2001**, *4*, 343–350.
- [6] B. Lugtenberg, F. Kamilova, *Annu. Rev. Microbiol.* **2009**, *63*, 541–556.
- [7] H. P. Bais, S. W. Park, T. L. Weir, R. M. Callaway, J. M. Vivanco, *Trends Plant Sci.* **2004**, *9*, 26–32.
- [8] M. Rohlf, A. C. L. Churchill, *Fungal Genet. Biol.* **2011**, *48*, 23–34.
- [9] T. L. Bultman, G. D. Bell, *Oikos* **2003**, *103*, 182–190.
- [10] B. Schulz, C. Boyle, S. Draeger, A. K. Römmer, K. Krohn, *Mycol. Res.* **2002**, *106*, 996–1004.
- [11] K. Ananda, K. R. Sridhar, *Can. J. Microbiol.* **2002**, *48*, 871–878.
- [12] L. Hammerschmidt, V. Wray, W. H. Lin, E. Kamilova, P. Proksch, A. H. Aly, *Phytochem. Lett.* **2012**, *5*, 600–603.
- [13] A. H. Aly, A. Debbab, P. Proksch, *Appl. Microbiol. Biotechnol.* **2011**, *90*, 1829–1845.
- [14] H. Thatoi, B. C. Behera, R. R. Mishra, *Mycologia* **2013**, *4*, 54–71.

- [15] M. E. Rateb, R. Ebel, *Nat. Prod. Rep.* **2011**, *28*, 290–344.
- [16] A. S. S. Ibrahim, A. A. Al-Salamah, M. A. El-Tayeb, Y. B. El-Badawi, G. Antranikian, *Int. J. Mol. Sci.* **2012**, *13*, 10505–10522.
- [17] N. Gunde-Cimerman, J. Ramos, A. Plemenitaš, *Mycol. Res.* **2009**, *113*, 1231–1241.
- [18] A. R. B. Ola, A. Debbab, A. H. Aly, A. Mandi, I. Zerfass, A. Hamacher, M. U. Kassack, H. Broetz-Oesterhelt, T. Kurtan, P. Proksch, *Tetrahedron Lett.* **2014**, *55*, 1020–1023.
- [19] A. R. B. Ola, A. Debbab, T. Kurtán, H. Brötz-Oesterhelt, A. H. Aly, P. Proksch, *Tetrahedron Lett.* **2014**, *55*, 3147–3150.
- [20] Y. M. Zhou, A. Debbab, V. Wray, W. H. Lin, B. Schulz, R. Trepos, C. Pile, C. Hellio, P. Proksch, A. H. Aly, *Tetrahedron Lett.* **2014**, *55*, 2789–2792.
- [21] W. Ebrahim, A. H. Aly, V. Wray, P. Proksch, A. Debbab, *Tetrahedron Lett.* **2013**, *54*, 6611–6614.
- [22] A. Arnone, G. Nasini, L. Merlini, G. Assante, *J. Chem. Soc. Perkin Trans. 1* **1986**, 525–530.
- [23] I. Barash, S. Manulis, Y. Kashman, J. P. Springer, M. H. Chen, J. Clardy, G. A. Strobel, *Science* **1983**, *220*, 1065–1066.
- [24] S. Manulis, Y. Kashman, D. Netzer, I. Brash, *Phytochemistry* **1984**, *23*, 2193–2198.
- [25] A. Debbab, A. H. Aly, R. A. Edrada-Ebel, V. Wray, A. Pretsch, G. Pescitelli, T. Kurtan, P. Proksch, *Eur. J. Org. Chem.* **2012**, 1351–1359.
- [26] A. Debbab, A. H. Aly, R. A. Edrada-Ebel, V. Wray, W. E. G. Müller, F. Totzke, U. Zirrgiebel, C. Schächtele, M. H. G. Kubbutat, W. H. Lin, M. Mosaddak, A. Hakiki, P. Proksch, R. Ebel, *J. Nat. Prod.* **2009**, *72*, 626–631.
- [27] A. H. Aly, A. Debbab, R. A. Edrada-Ebel, W. E. G. Müller, M. H. G. Kubbutat, V. Wray, R. Ebel, P. Proksch, *Mycosphere* **2010**, *1*, 153–162.
- [28] Y. Liu, V. Wray, M. S. Abdel-Aziz, C. Y. Wang, D. W. Lai, P. Proksch, *J. Nat. Prod.* **2014**, *77*, 1734–1738.
- [29] A. Stoess, *Can. J. Chem.* **1969**, *47*, 777–784.
- [30] A. Stoess, C. H. Unwin, J. B. Stothers, *Can. J. Chem.* **1983**, *61*, 372–377.
- [31] A. M. Becker, R. W. Rickards, K. J. Schmalzl, H. C. Yick, *J. Antibiot.* **1978**, *31*, 324–329.
- [32] N. Okamura, K. Mimura, A. Yagi, H. Haraguchi, K. Shingu, K. Miyahara, *Phytochemistry* **1996**, *42*, 77–80.
- [33] A. H. Aly, R. A. Edrada-Ebel, V. Wray, W. E. G. Müller, S. Kozyska, U. Hentschel, P. Proksch, R. Ebel, *Phytochemistry* **2008**, *69*, 1716–1725.
- [34] R. Suemitsu, K. Horiuchi, M. Kubota, T. Okamatsu, *Phytochemistry* **1990**, *29*, 1509–1511.
- [35] G. Lazarovits, R. W. Steele, A. Stoessl, *Z. Naturforsch., C* **1988**, *43*, 813–817.
- [36] S. Wang, X. M. Li, F. Teuscher, D. L. Li, A. Diesel, R. Ebel, P. Proksch, B. G. Wang, *J. Nat. Prod.* **2006**, *69*, 1622–1625.
- [37] M. Ashour, R. Edrada, R. Ebel, V. Wray, W. Wätjen, K. Padmakumar, W. E. G. Müller, W. H. Lin, P. Proksch, *J. Nat. Prod.* **2006**, *69*, 1547–1553.
- [38] M. El-Neketi, W. Ebrahim, W. H. Lin, S. Gedara, F. Badria, H. E. A. Saad, D. W. Lai, P. Proksch, *J. Nat. Prod.* **2013**, *76*, 1099–1104.

Received: January 17, 2015
Published Online: March 5, 2015

Eur. J. Org. Chem. **2015** · ISSN 1099–0682

SUPPORTING INFORMATION

DOI: 10.1002/ejoc.201500079

Title: Tetrahydroanthraquinone Derivatives from the Endophytic Fungus *Stemphylium globuliferum*

Author(s): Yang Liu, Andreas Marmann, Mohamed S. Abdel-Aziz, Chang Yun Wang, Werner E. G. Müller, Wen Han Lin, Attila Mándi, Tibor Kurtán, Georgios Daletos,* Peter Proksch*

Table of contents

Figure S1 ^1H NMR spectrum of 1 (acetone- d_6 , 600 MHz)	3
Figure S2 ^{13}C NMR spectrum of 1 (acetone- d_6 , 150 MHz)	4
Figure S3 HSQC spectrum of 1	5
Figure S4 HMBC spectrum of 1	6
Figure S5 ROESY spectrum of 1	7
Figure S6 HRESIMS spectrum of 1	8
Figure S7 ^1H NMR spectrum of 2 (acetone- d_6 , 600 MHz)	9
Figure S8 ^{13}C NMR spectrum of 2 (acetone- d_6 , 150 MHz)	10
Figure S9 HSQC spectrum of 2	11
Figure S10 HMBC spectrum of 2	12
Figure S11 ROESY spectrum of 2	13
Figure S12 HRESIMS spectrum of 2	14
Figure S13 ^1H NMR spectrum of 3 (acetone- d_6 , 700 MHz)	15
Figure S14 ^{13}C NMR spectrum of 3 (acetone- d_6 , 175 MHz)	16
Figure S15 HSQC spectrum of 3	17
Figure S16 HMBC spectrum of 3	18
Figure S17 ROESY spectrum of 3	19
Figure S18 HRESIMS spectrum of 3	20
Figure S19 ^1H NMR spectrum of 4 (acetone- d_6 , 600 MHz)	21
Figure S20 ^{13}C NMR spectrum of 4 (acetone- d_6 , 150 MHz)	22
Figure S21 HSQC spectrum of 4	23
Figure S22 HMBC spectrum of 4	24
Figure S23 ROESY spectrum of 4	25
Figure S24 1D NOE spectrum of 4	26
Figure S25 HRESIMS spectrum of 4	27
Figure S26 ECD spectra of 1 and 2 in acetonitrile	28
Figure S27 ECD spectra of 3 , 4 , 8 , 9 in acetonitrile	29
Figure S28 ECD spectra of 3 and 4 . in acetonitrile	30

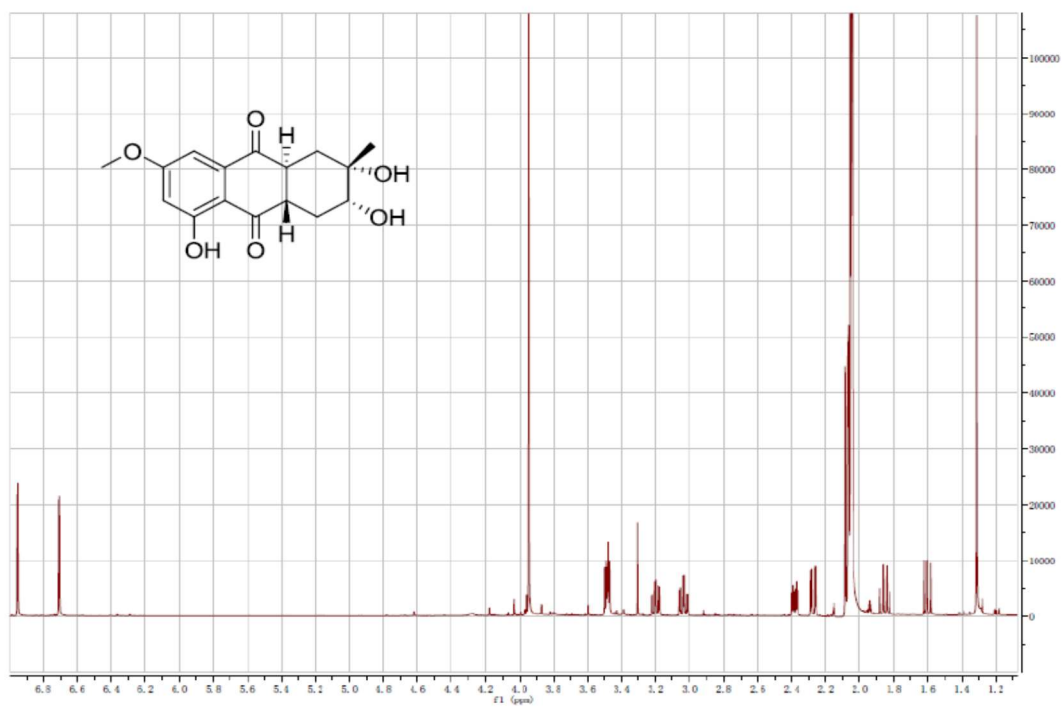
Figure S1 ^1H NMR spectrum of **1** (acetone- d_6 , 600 MHz)

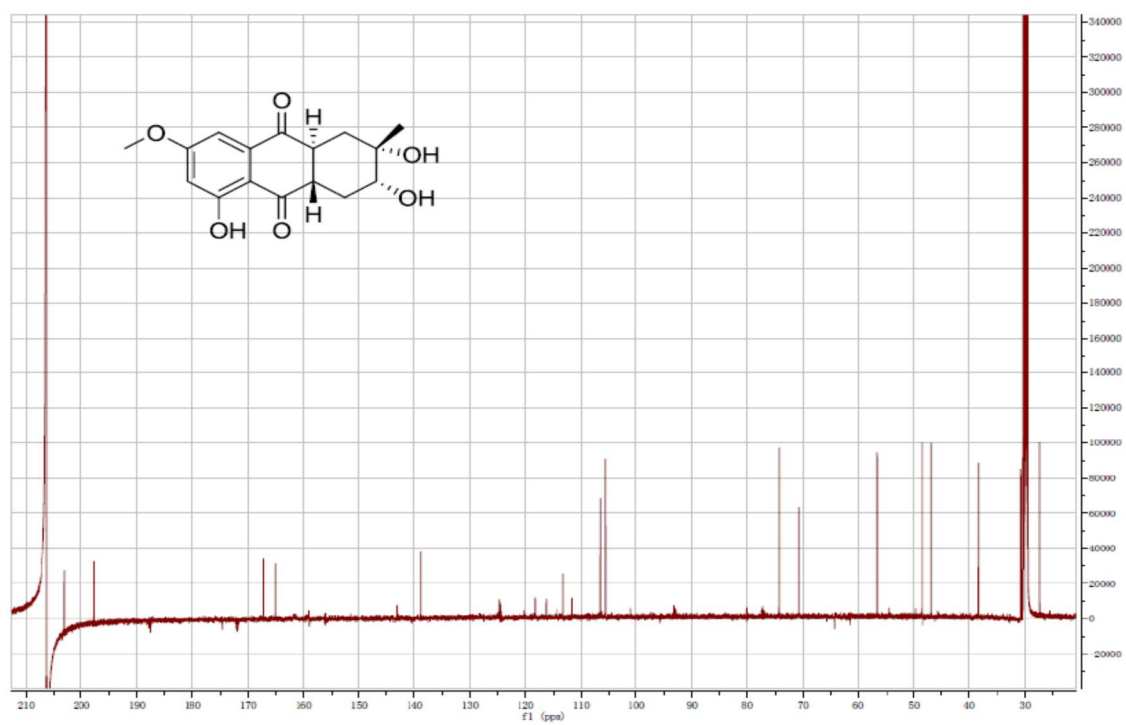
Figure S2 ^{13}C NMR spectrum of **1** (acetone- d_6 , 150 MHz)

Figure S3 HSQC spectrum of 1

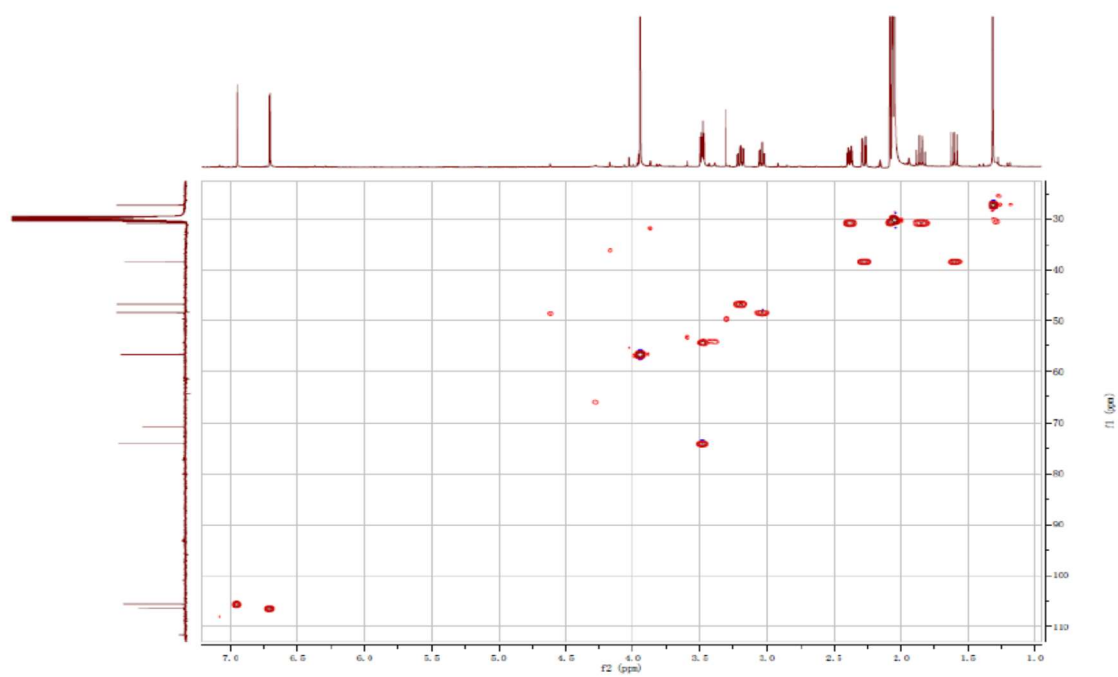


Figure S4 HMBC spectrum of 1

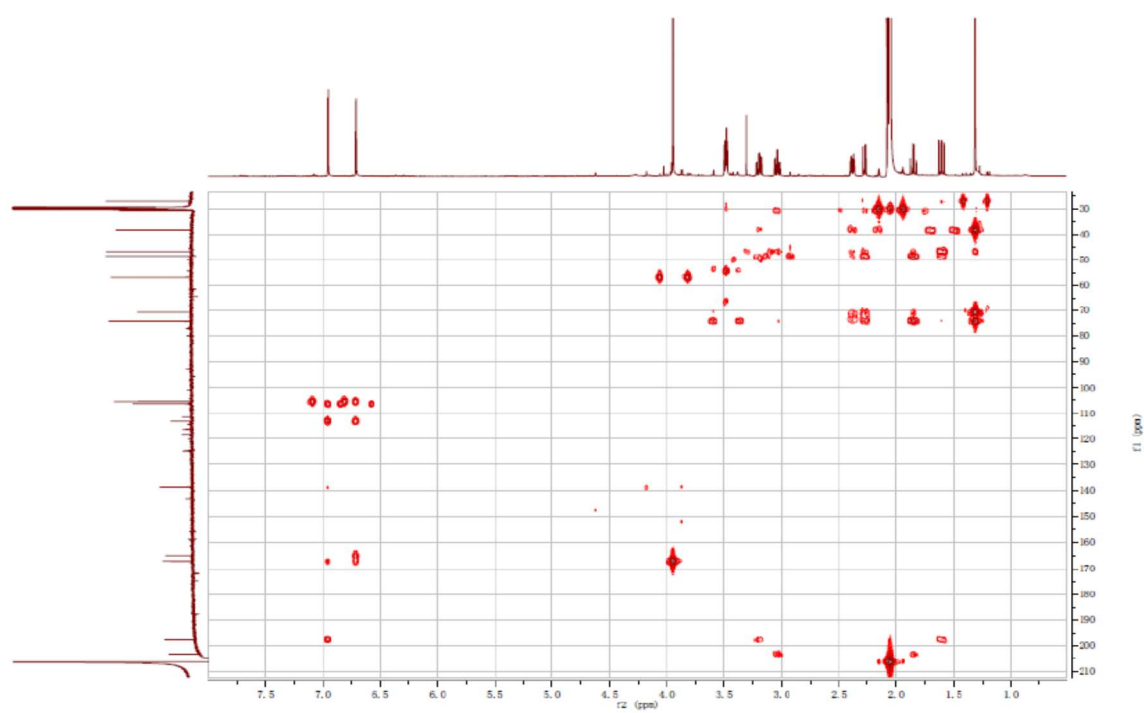


Figure S5 ROESY spectrum of 1

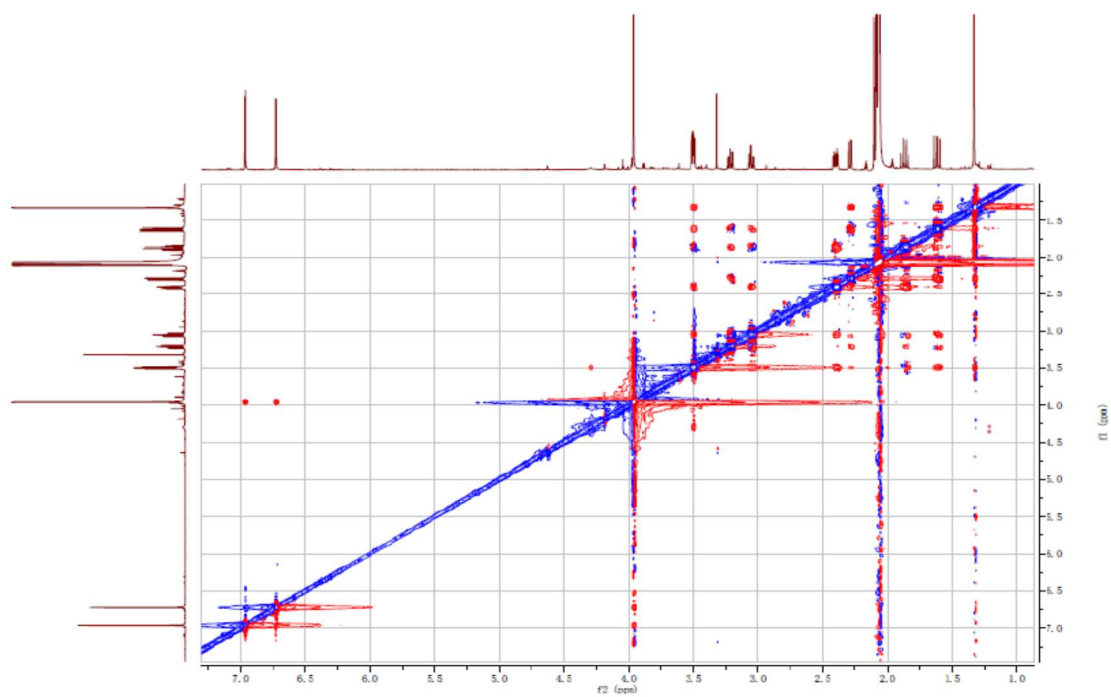


Figure S6 HRESIMS spectrum of 1

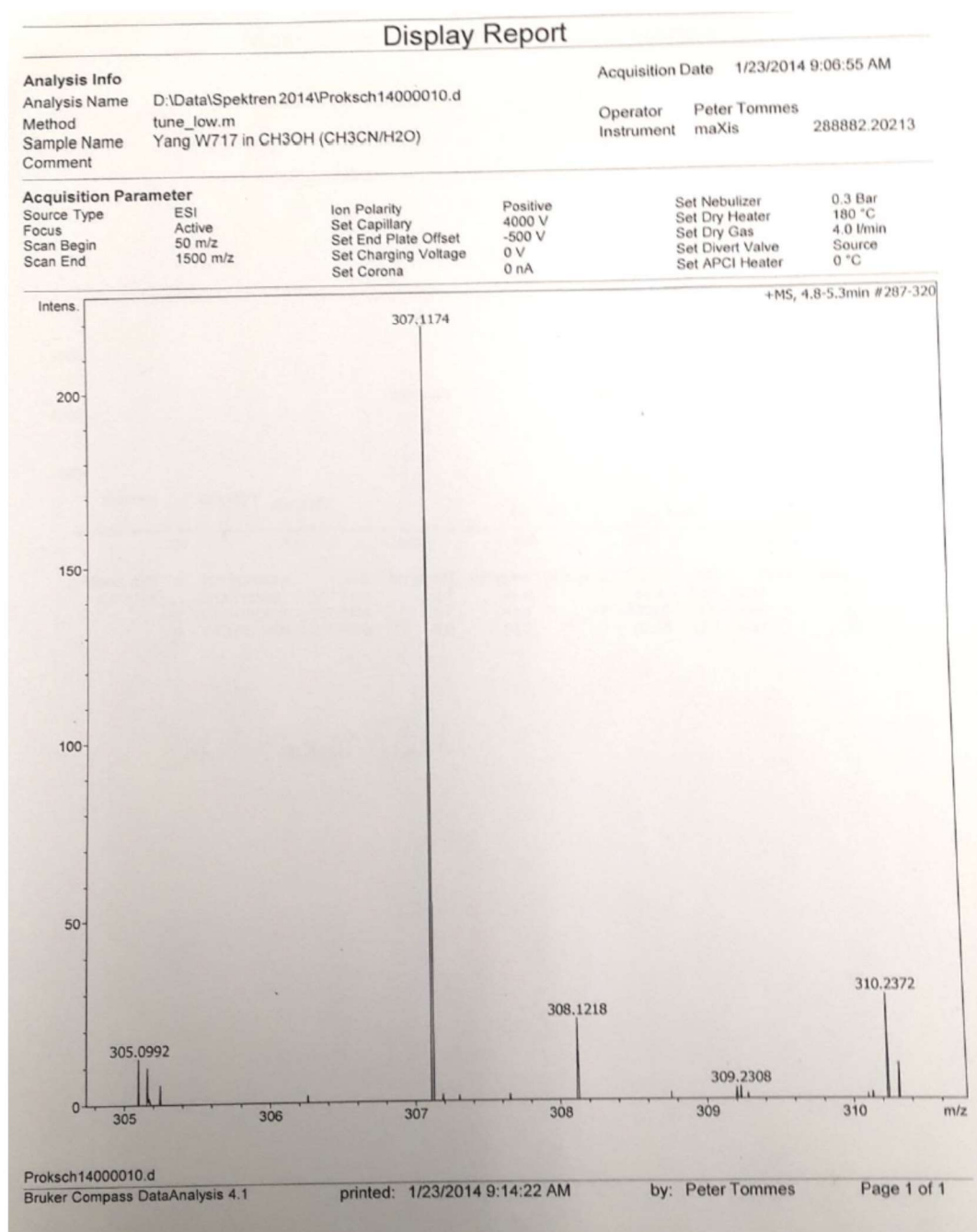


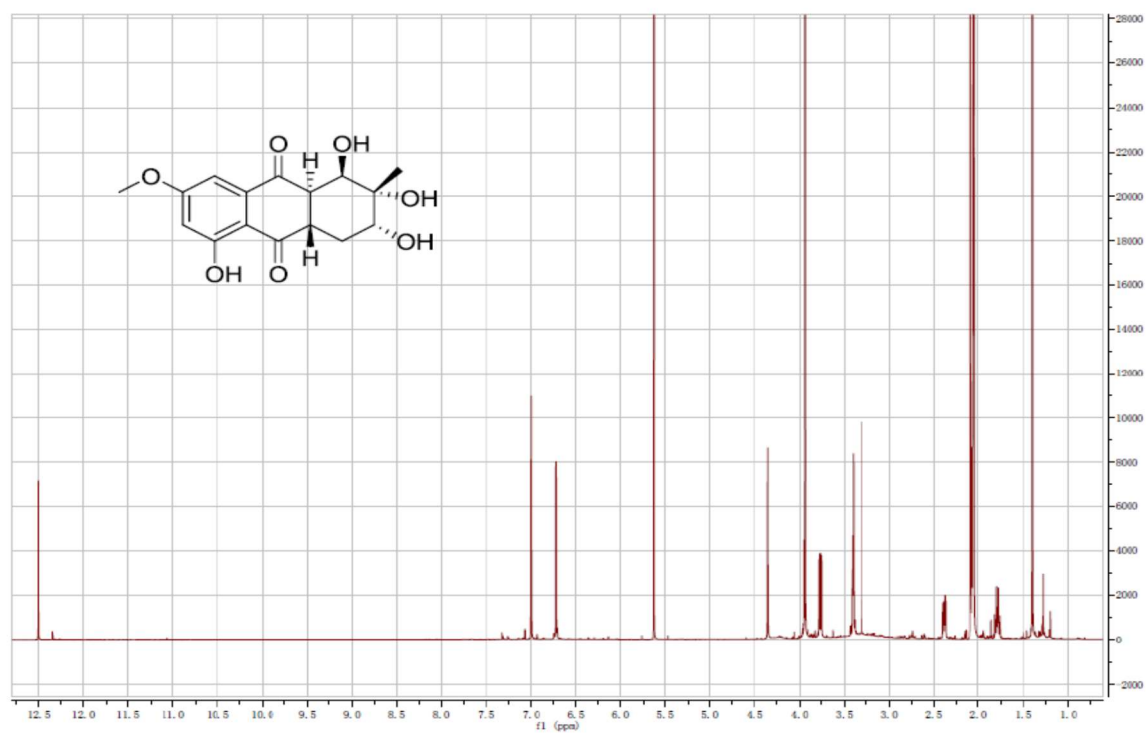
Figure S7 ^1H NMR spectrum of **2** (acetone- d_6 , 600 MHz)

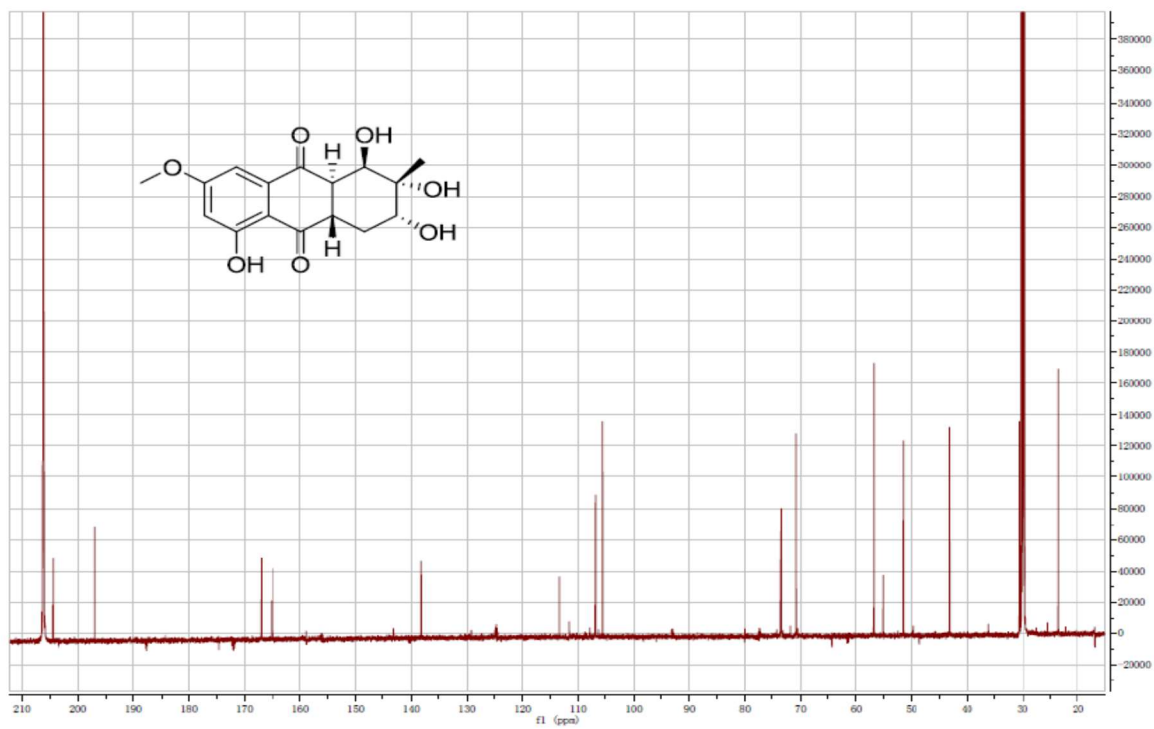
Figure S8 ^{13}C NMR spectrum of **2** (acetone- d_6 , 150 MHz)

Figure S9 HSQC spectrum of 2

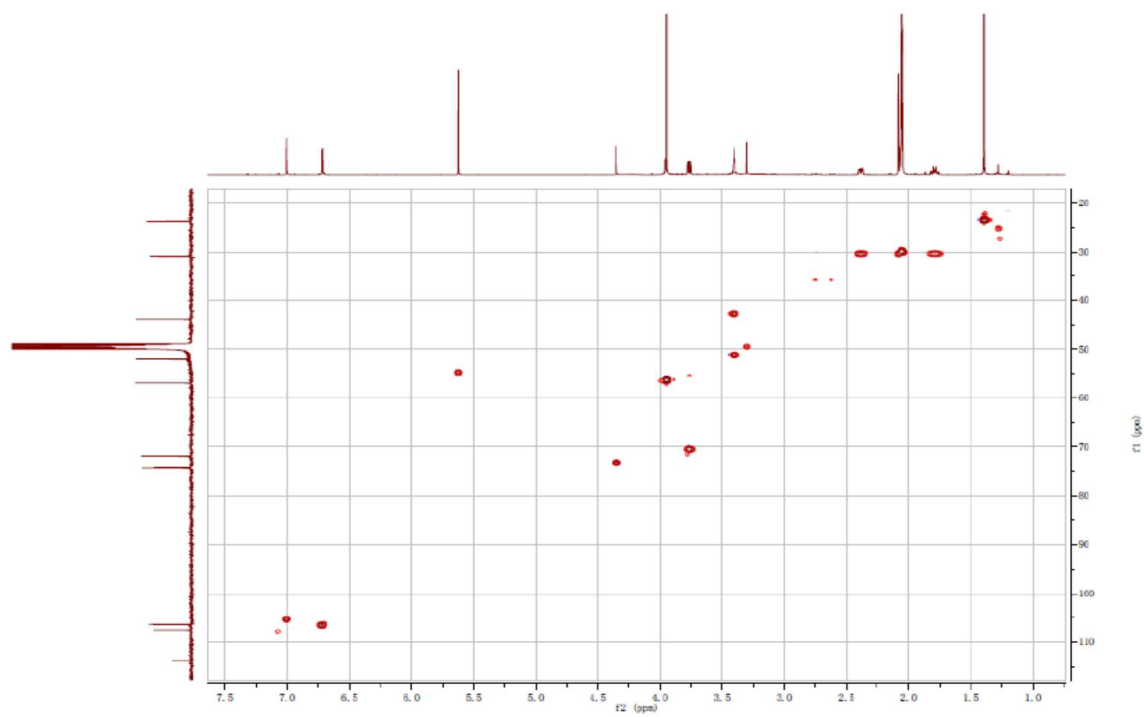


Figure S10 HMBC spectrum of 2

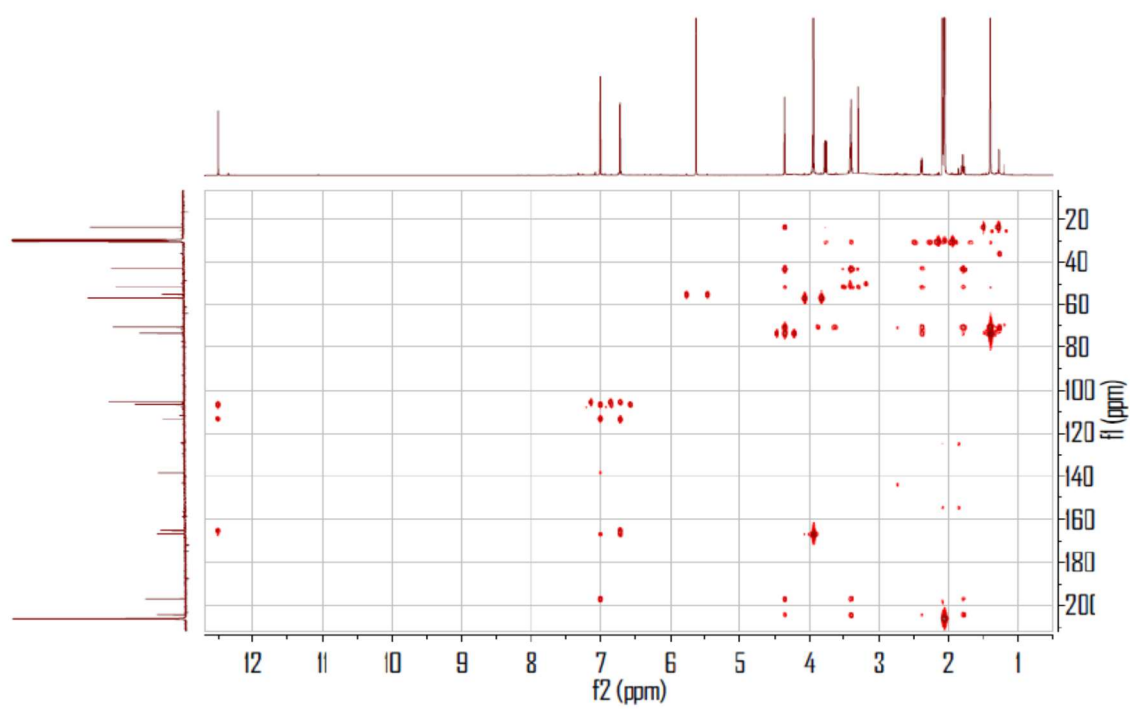


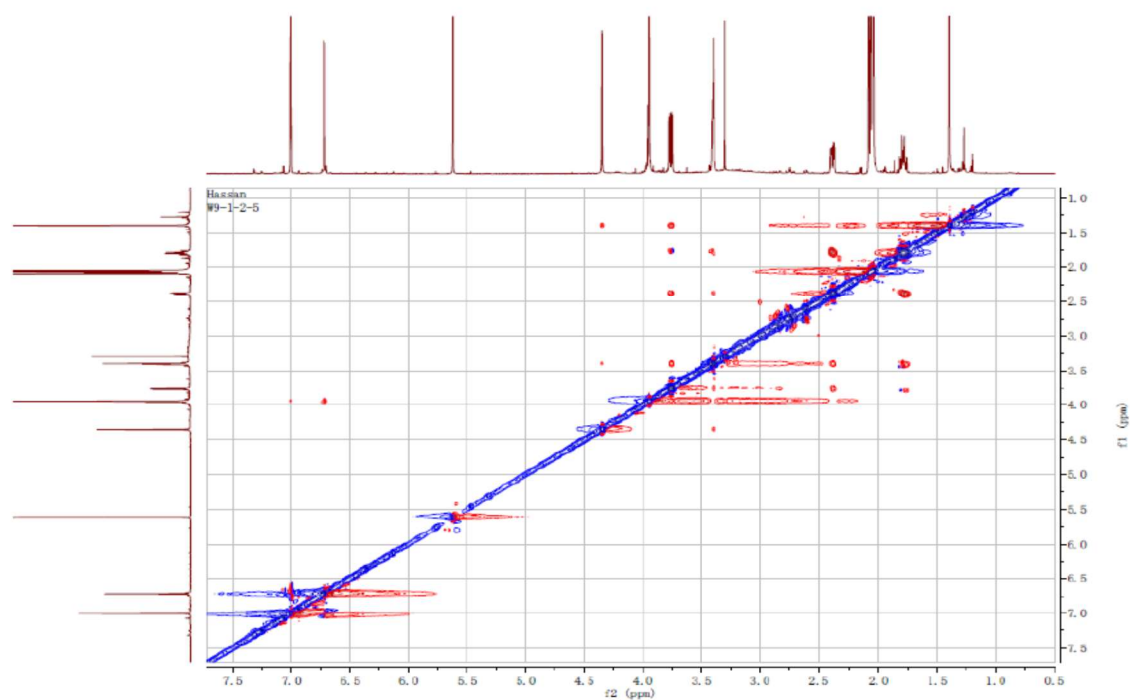
Figure S11 ROESY spectrum of **2**

Figure S12 HRESIMS spectrum of 2

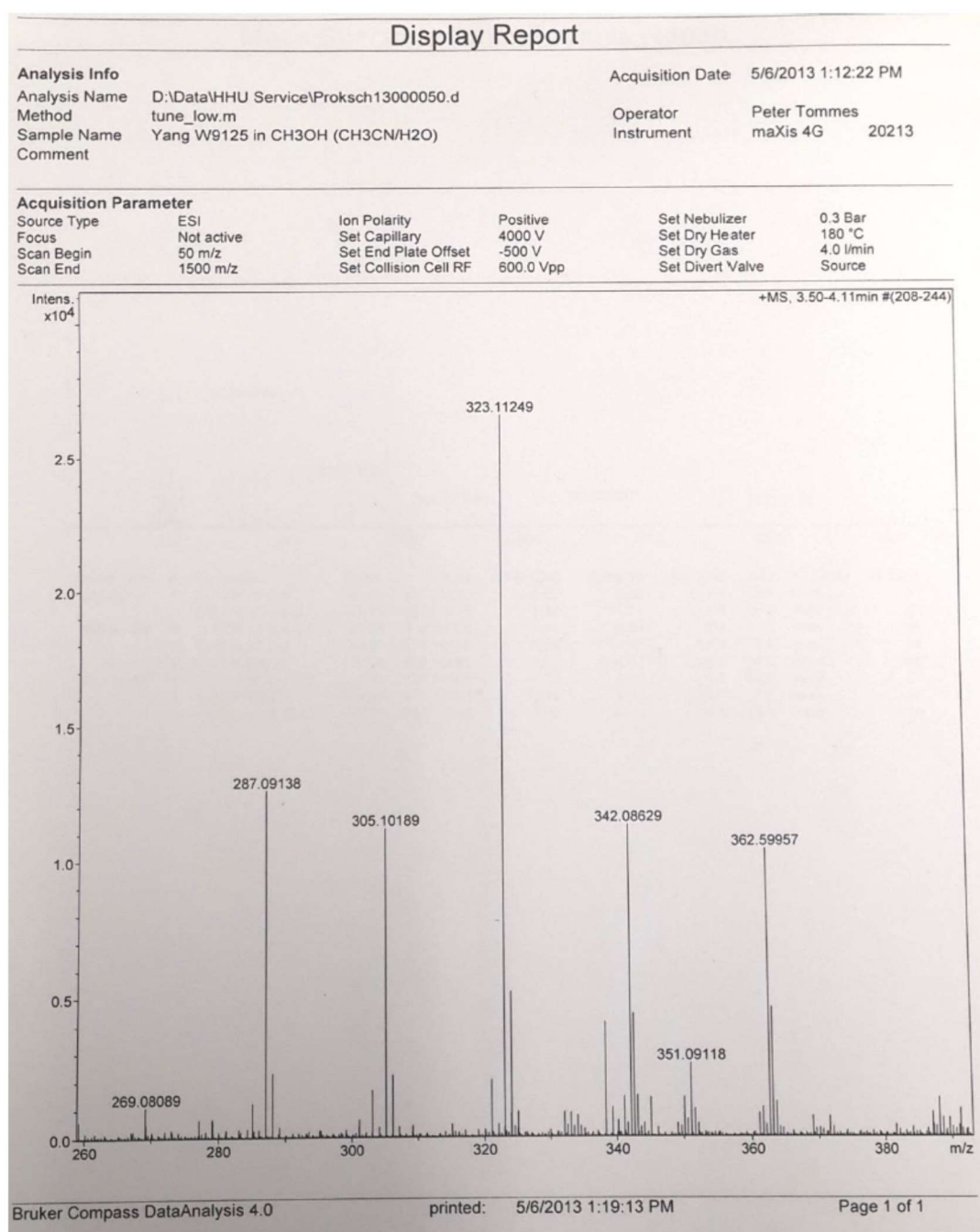


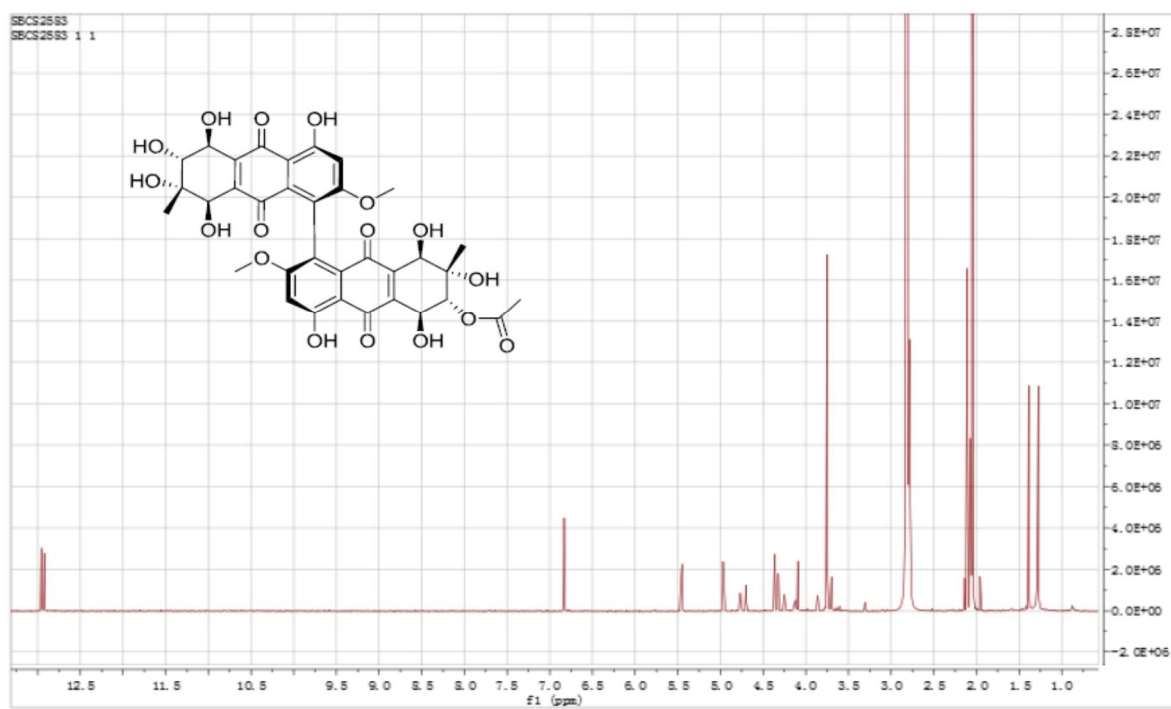
Figure S13 ^1H NMR spectrum of **3** (acetone- d_6 , 700 MHz)

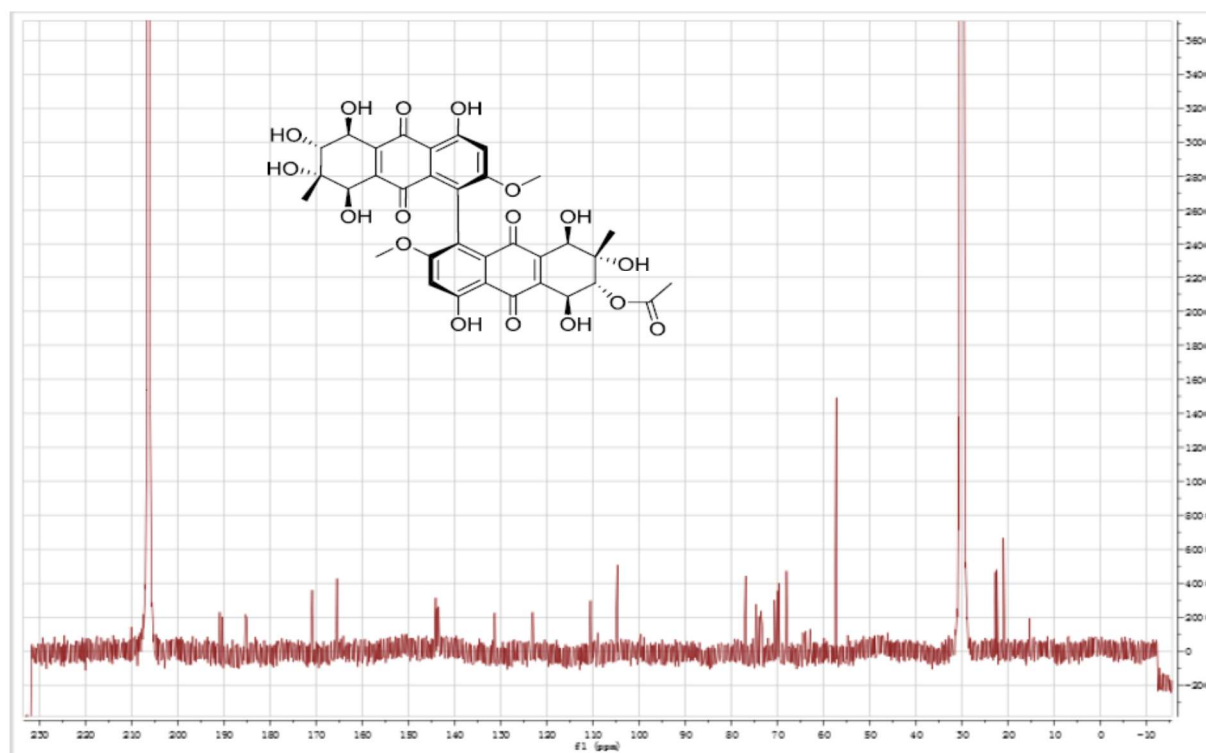
Figure S14 ^{13}C NMR spectrum of **3** (acetone- d_6 , 175 MHz)

Figure S15 HSQC spectrum of 3

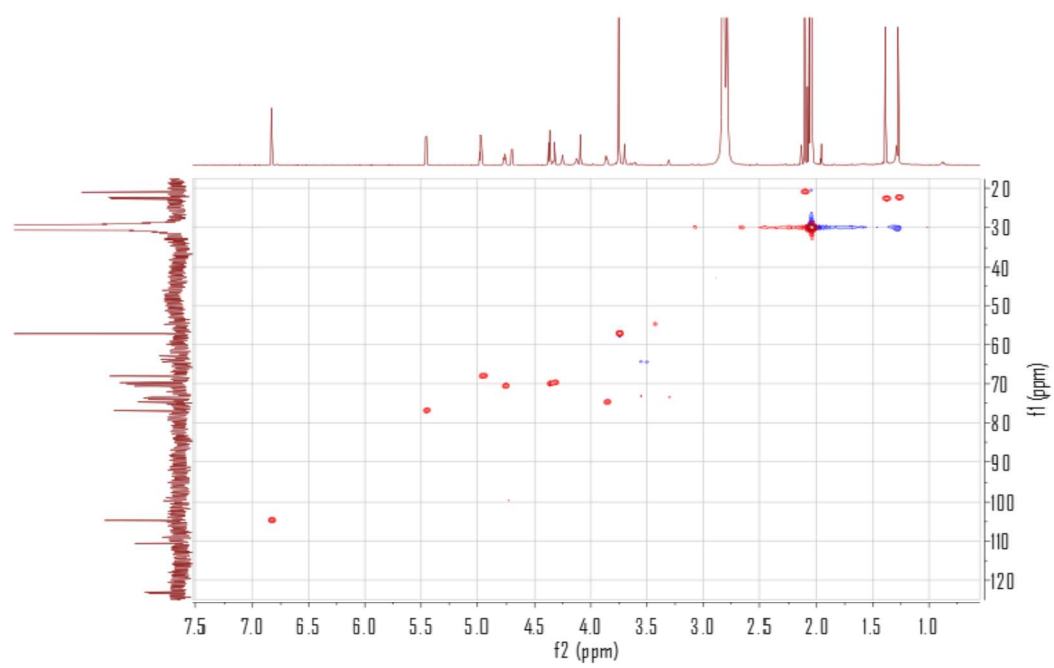


Figure S16 HMBC spectrum of 3

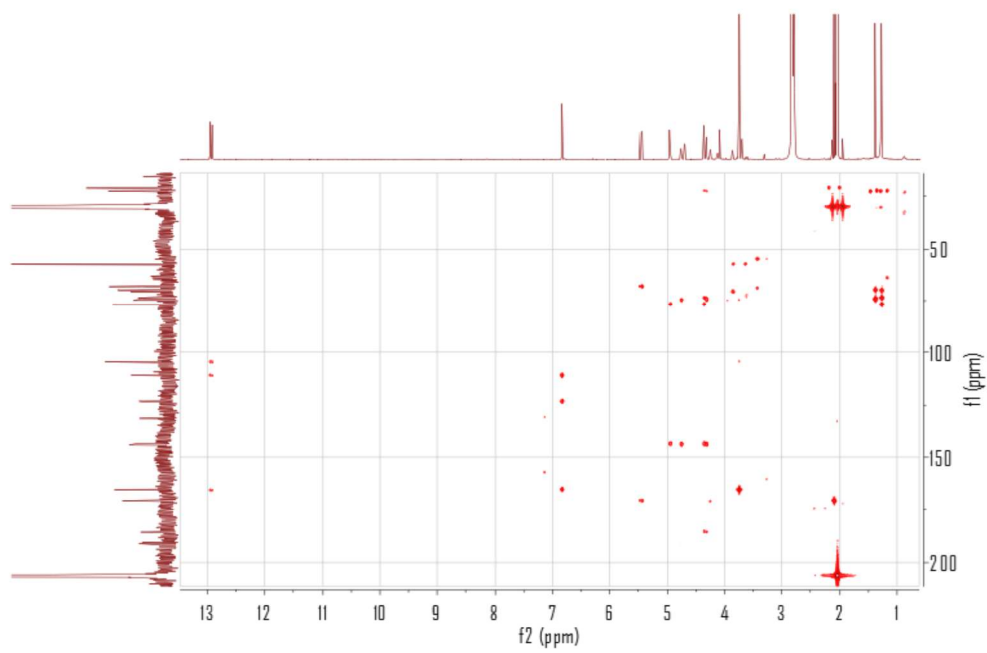


Figure S17 Roesy spectrum of 3

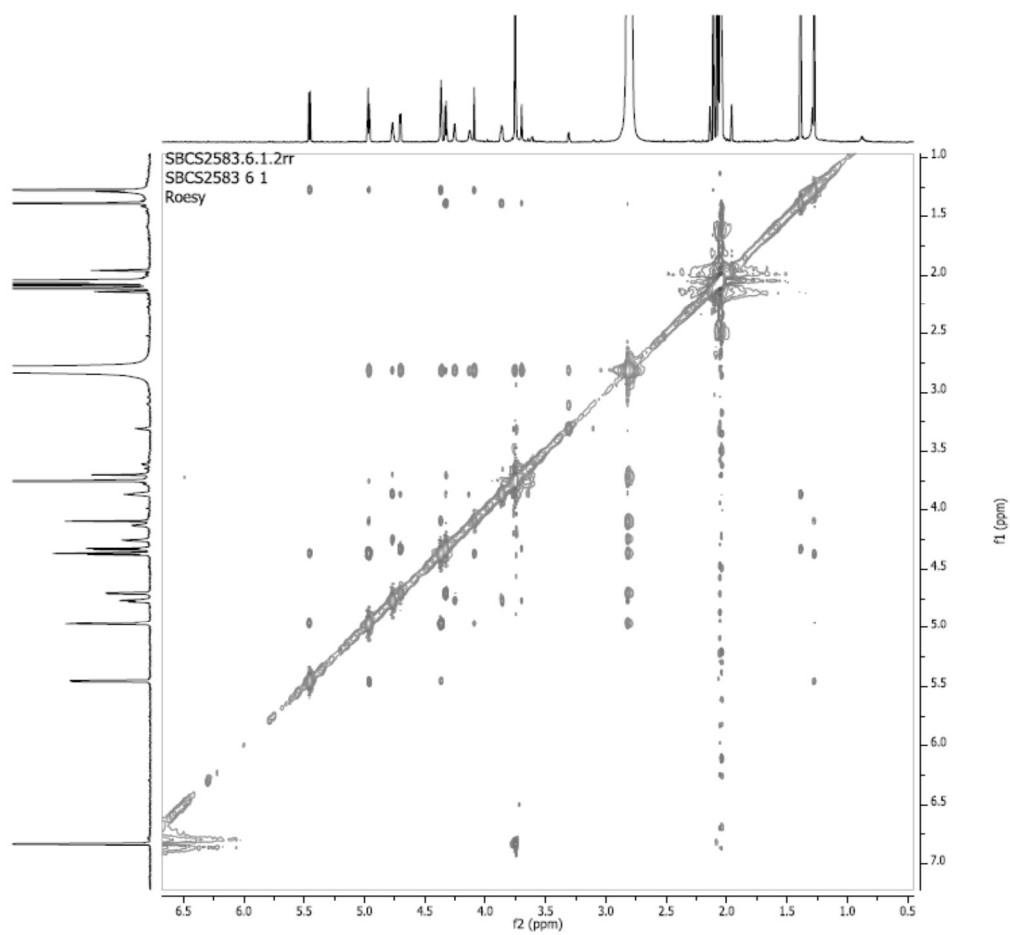


Figure S18 HRESIMS spectrum of 3

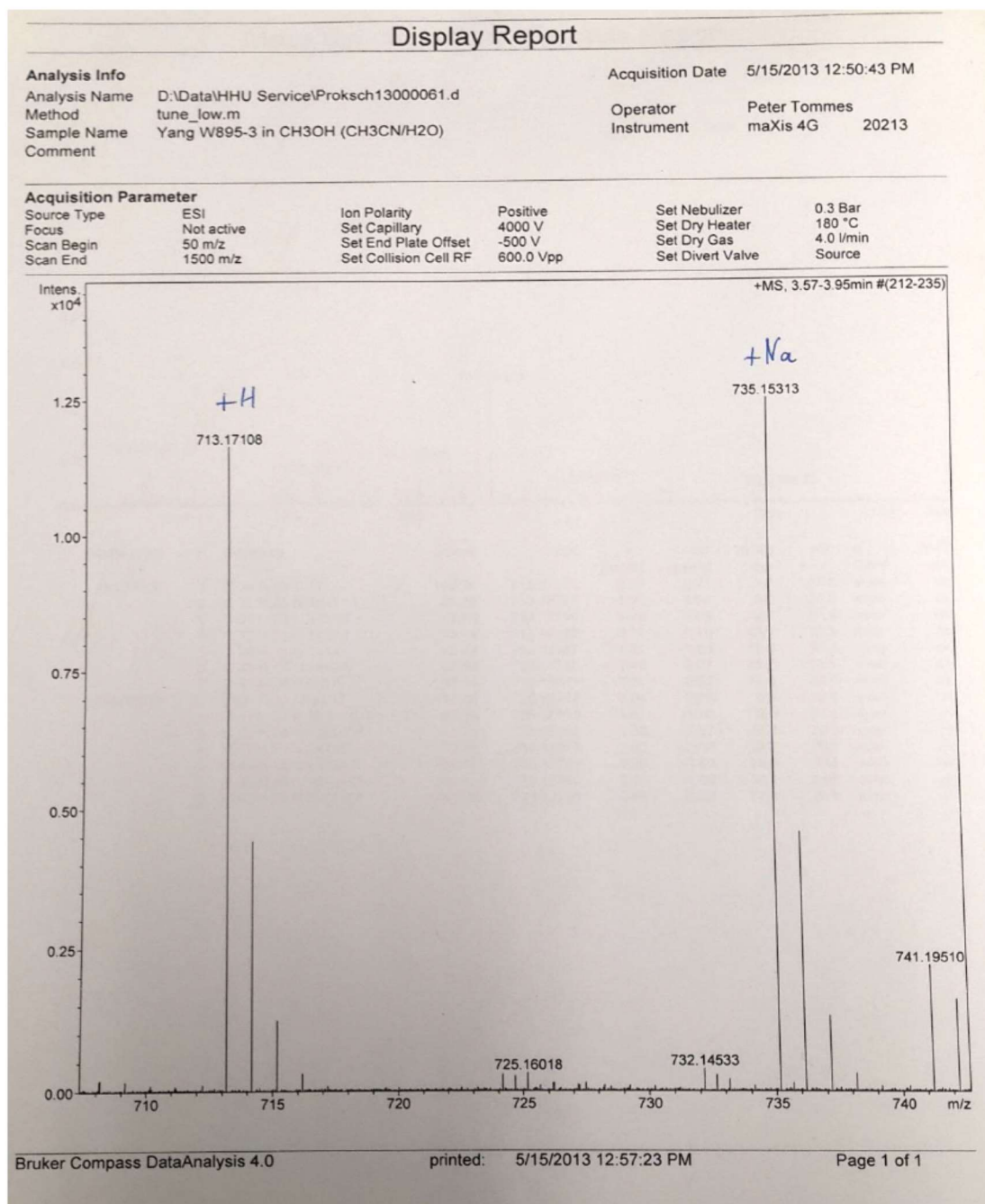


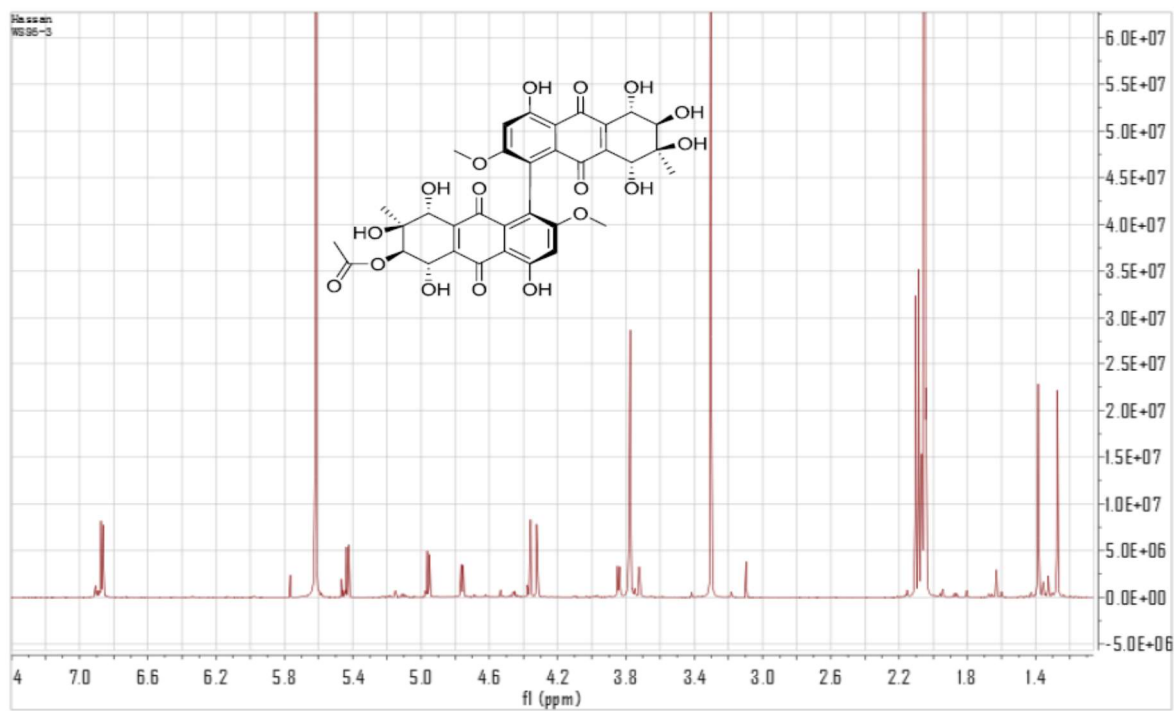
Figure S29 ^1H NMR spectrum of **4** (acetone- d_6 , 600 MHz)

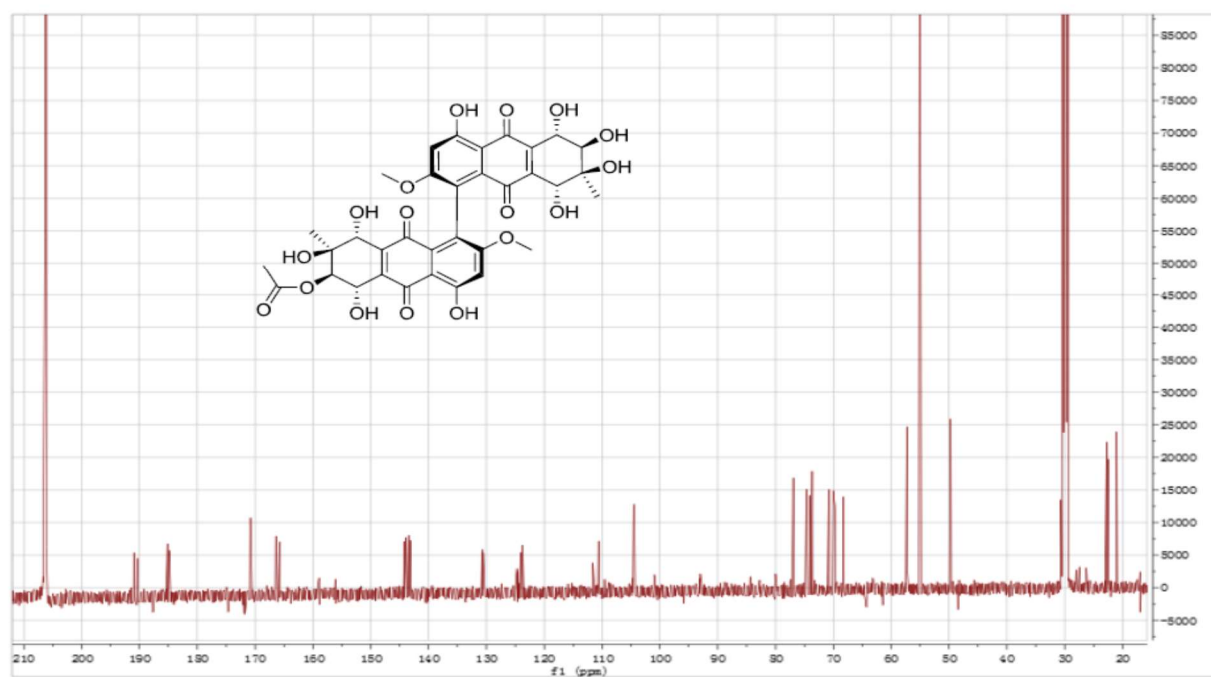
Figure S20 ^{13}C NMR spectrum of **4** (acetone- d_6 , 150 MHz)

Figure S21 HSQC spectrum of 4

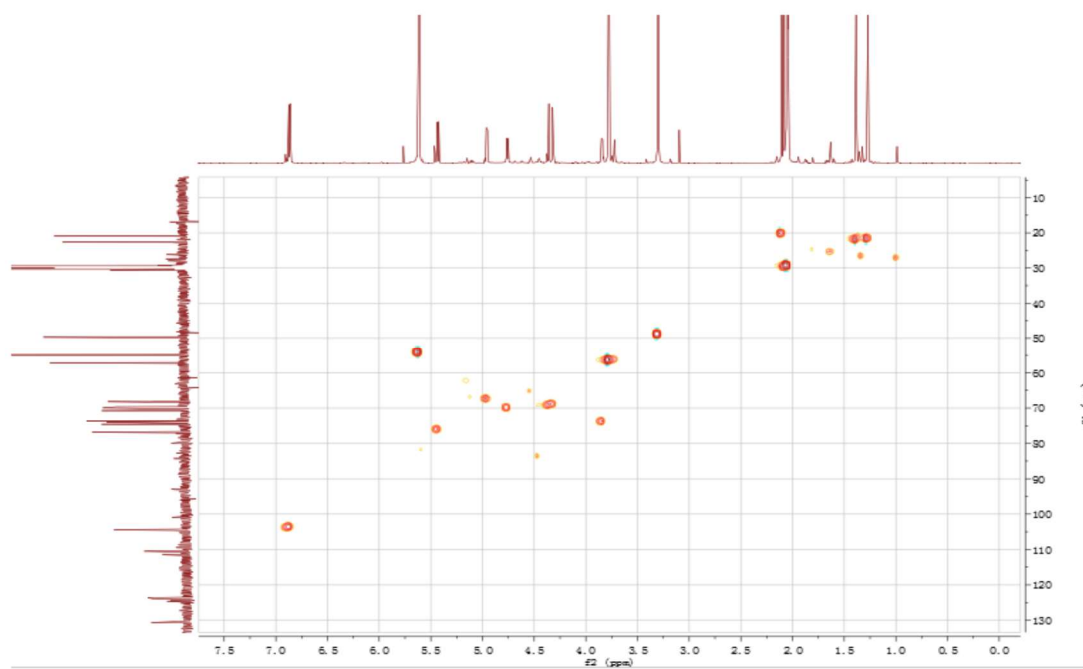


Figure S22 HMBC spectrum of 4

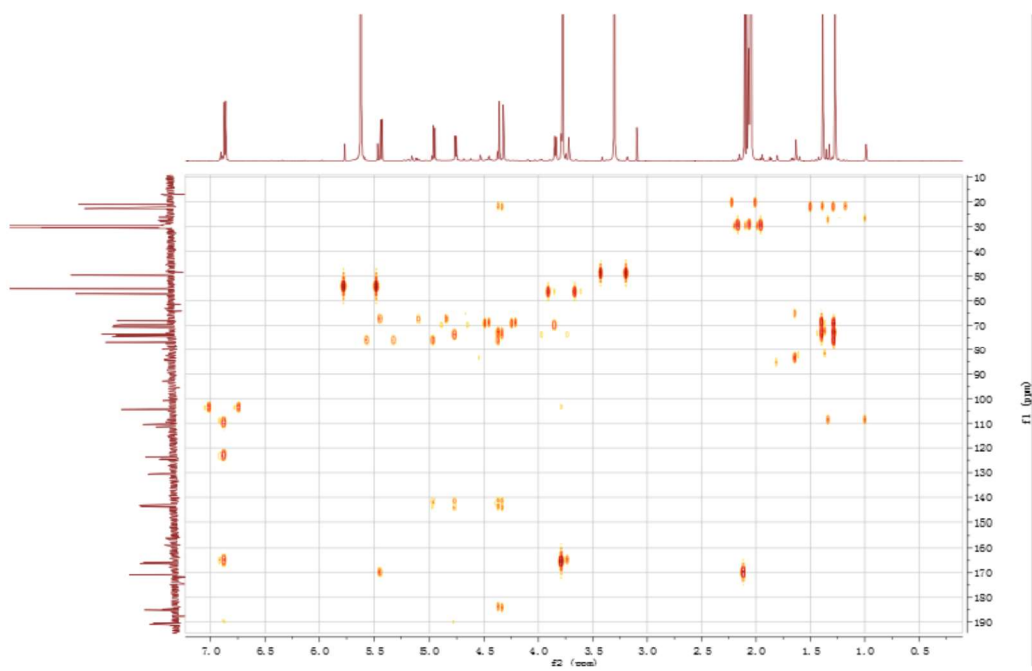


Figure S23 ROESY spectrum of 4

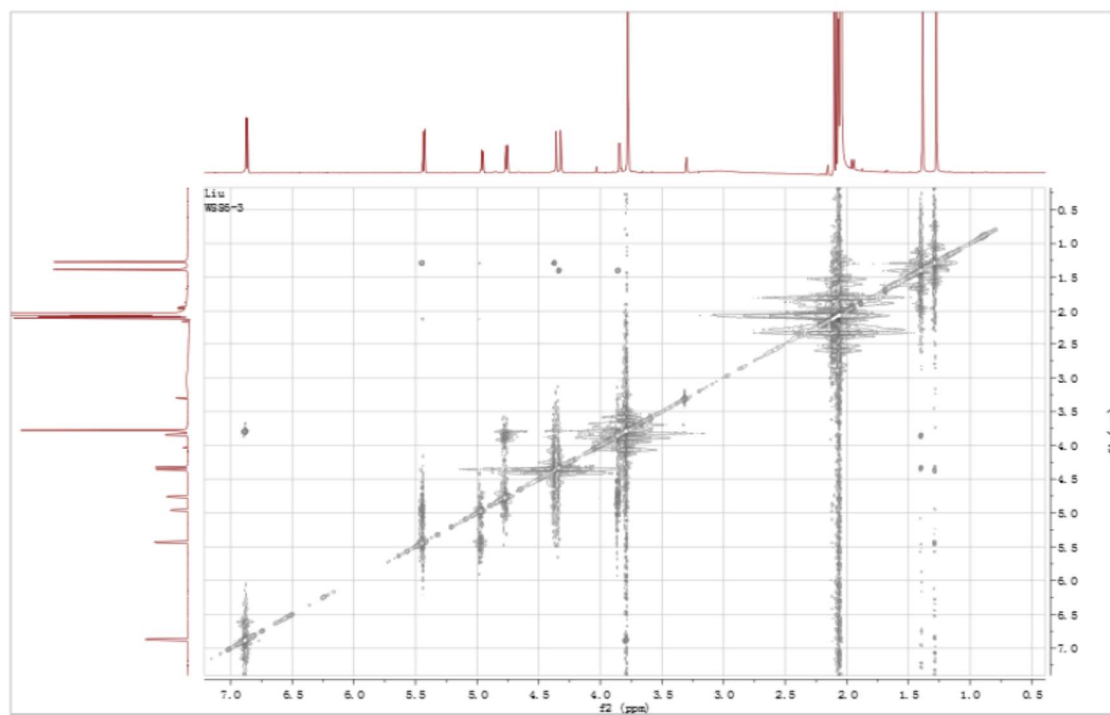
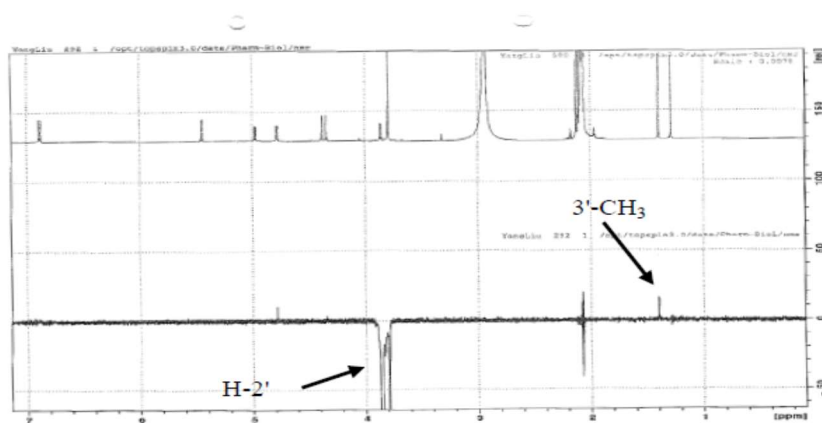


Figure S24 1D NOE spectrum of 4

a) Irradiating H-2' resonating at 3.84 ppm



b) Irradiating H-2 resonating at 5.43 ppm

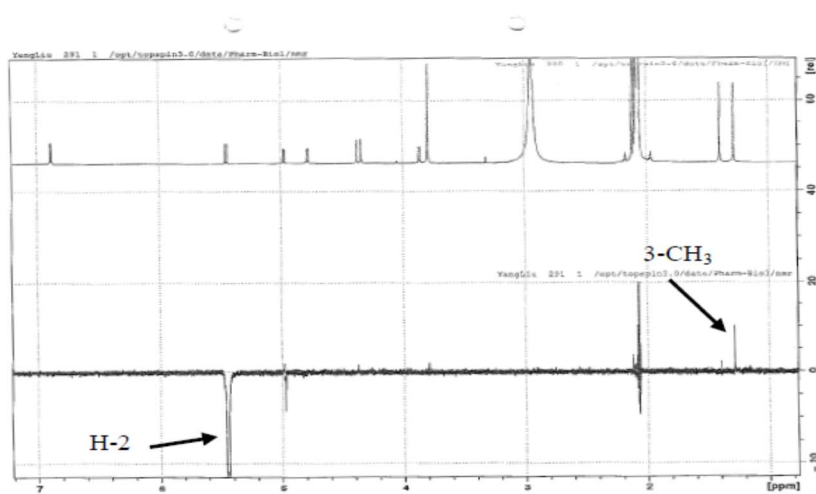


Figure S25 HRESIMS spectrum of 4

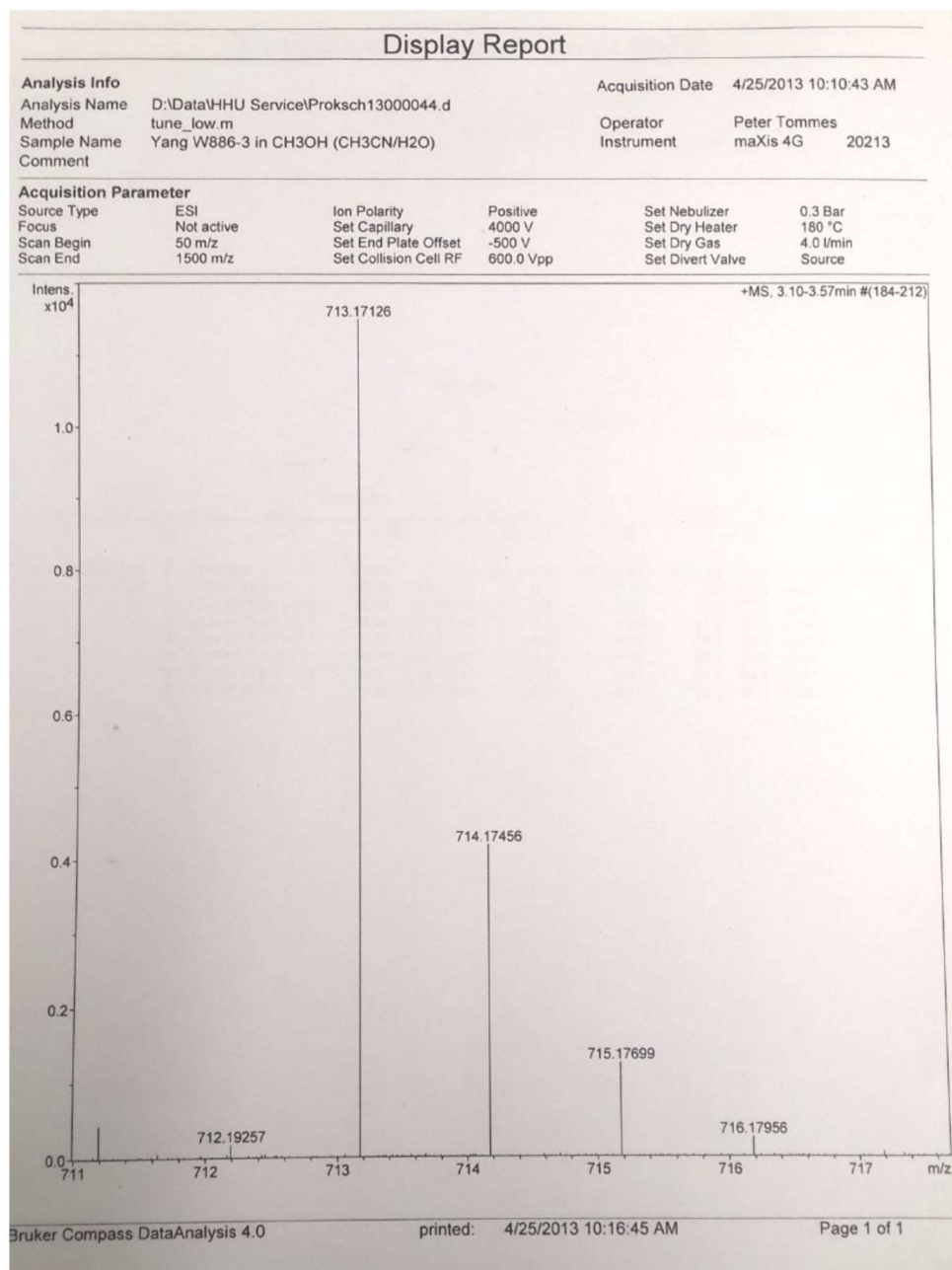


Figure S26 ECD spectra of **1** and **2** in acetonitrile.

dihydroaltersolanol B (**1**, black)

dihydroaltersolanol C (**2**, olive)

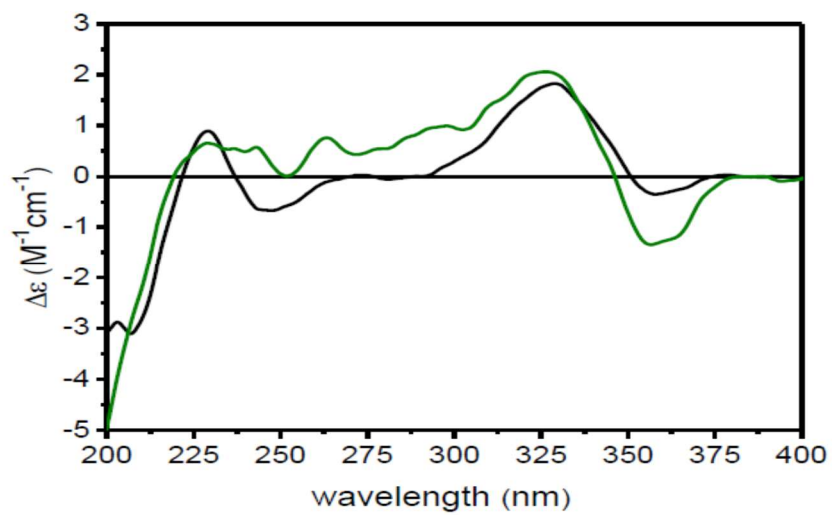


Figure S27 ECD spectra of **3**, **4**, **8**, and **9** in acetonitrile
acetylalterporriol D (**3**, red),
acetylalterporriol E (**4**, blue),
alterporriol D (**8**, black)
alterporriol E (**9**, green)

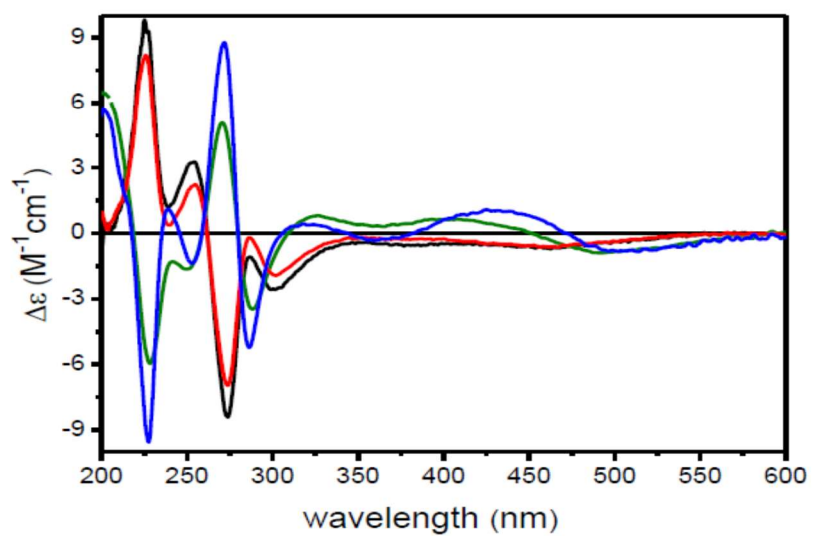
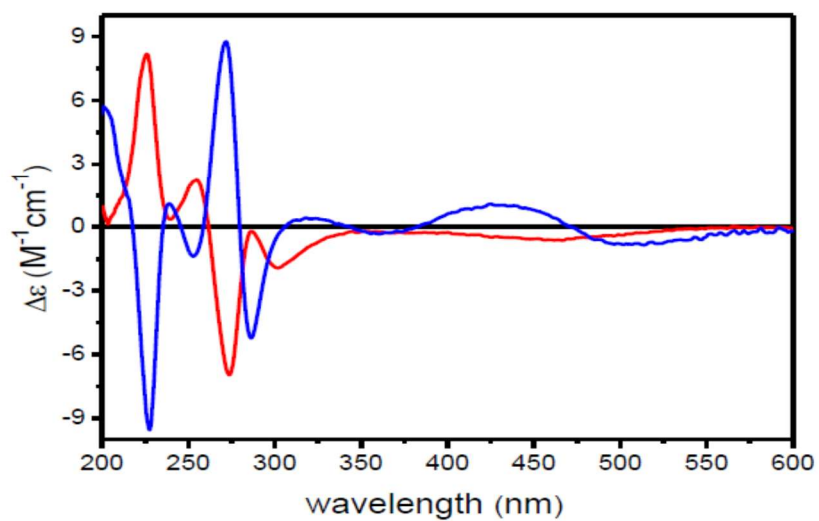


Figure S28 ECD spectra of **3** and **4** in acetonitrile
acetylalterporriol D (**3**, red)
acetylalterporriol E (**4**, blue).



4 Publication 3

4.1 Cladosporinone, a new viriditoxin derivative from the hypersaline lake derived fungus

Cladosporium cladosporioides

Intended for submission to “The Journal of Antibiotics”

Impact factor: 2.173

Contribution: 80%, first author, conducting most of the experiments, literature research, manuscript writing

Reprinted with permission from “Liu Y., Kurtán T., Wang C. Y., Lin W. H., Orfali R., Müller W. E. G., Daletos G., Proksch P. (2016) Cladosporinone, a new viriditoxin derivative from the hypersaline lake derived fungus *Cladosporium cladosporioides*.” The Journal of Antibiotics advance online publication, 24 February 2016. Copyright 2016 Japan Antibiotics Research Association



ORIGINAL ARTICLE

Cladosporinone, a new viriditoxin derivative from the hypersaline lake derived fungus *Cladosporium cladosporioides*

Yang Liu^{1,2}, Tibor Kurtán³, Chang Yun Wang², Wen Han Lin⁴, Raha Orfali⁵, Werner EG Müller⁶, Georgios Daletos¹ and Peter Proksch¹

A new cytotoxic viriditoxin derivative, cladosporinone (1), along with the known viriditoxin (2) and two viriditoxin derivatives (3 and 4) were obtained from the fungus *Cladosporium cladosporioides* isolated from the sediment of a hypersaline lake in Egypt. The structure of the new compound (1) was determined by 1D and 2D NMR measurements as well as by high-resolution ESIMS and electronic circular dichroism spectroscopy. All isolated compounds were studied for their cytotoxicity against the murine lymphoma cell line L5187Y and for their antibiotic activity against several pathogenic bacteria. Viriditoxin (2) was the most active compound in both bioassays. Compound 1 also exhibited strong cytotoxicity against the murine lymphoma cell line L5187Y with an IC₅₀ value of 0.88 μM, whereas its antibiotic activity was weak.

The Journal of Antibiotics advance online publication, 24 February 2016; doi:10.1038/ja.2016.11

INTRODUCTION

Since the discovery of penicillin by Sir Alexander Fleming in 1928, several fungal-derived natural products have been discovered and developed as new drugs, such as the antibacterial agent cephalosporin C from *Cephalosporium acremonium*,^{1–3} the immunosuppressive drug cyclosporine from *Tolypocladium inflatum*^{4,5} or the cholesterol-lowering agent lovastatin from *Aspergillus terreus*.⁶ However, the frequent re-isolation of known metabolites from fungi has turned the interest of natural product chemists to hitherto less investigated ecological niches, such as arctic glaciers, deep-sea hydrothermal vents or hypersaline lakes.^{7,8} Fungi that live at elevated temperatures, at an acidic or alkaline pH, high pressure, high-salt concentration and/or low-nutrient concentration are called extremophiles, and have developed unique metabolic mechanisms to produce bioactive secondary metabolites as a response to environmental stress.^{9–11} Thus, extremophilic fungi are attracting considerable attention in recent years as new promising sources for biologically active compounds with potential pharmaceutical applications.^{12–15}

During our ongoing search for new bioactive compounds from fungi,^{14–17} the extract of the fungus *Cladosporium cladosporioides*, isolated from the sediment of the hypersaline lake El Hamra located in Wadi el Natrun (Egypt), caused complete growth inhibition of the murine lymphoma cell line L5187Y when assayed at a dose of 10 μg ml⁻¹. Bioassay-guided fractionation of the extract afforded a

new viriditoxin derivative (1), together with viriditoxin (2) and two previously reported viriditoxin congeners (3 and 4).^{18,19} Viriditoxin (2) was first isolated from *Aspergillus viridinutans* as a mycotoxin, whereas it was later also obtained from *Aspergillus brevipes*, *Aspergillus fumigatus*, *Paecilomyces variotii* and *Spicaria divaricata*.^{18–20} Details on the isolation and structure elucidation of 1, its biological activity and the plausible biogenesis of the isolated compounds are reported herein.

RESULTS AND DISCUSSION

The ethyl acetate (EtOAc) extract of the sediment-derived fungus *C. cladosporioides* following cultivation on solid rice medium was partitioned between *n*-hexane and 90% aqueous methyl alcohol (MeOH). The resulting MeOH phase was fractionated by vacuum liquid chromatography on silica gel, followed by size exclusion chromatography over Sephadex LH-20 and separation on diol-functionalized silica. Final purification was achieved by semipreparative reversed-phase HPLC to yield a new viriditoxin derivative (1), along with three known compounds including viriditoxin (2) and its derivatives (3) and (4) (Figure 1).

Compound 1 was isolated as a red, amorphous powder. Its molecular formula was established as C₃₃H₃₀O₁₄ based on the prominent ion peak observed at *m/z* = 651.1706 [M+H]⁺ in the high-resolution ESIMS spectrum. The ¹H and ¹³C NMR data of 1

¹Institute of Pharmaceutical Biology and Biotechnology, Heinrich Heine University, Duesseldorf, Germany; ²Key Laboratory of Marine Drugs, The Ministry of Education of China, School of Medicine and Pharmacy, Ocean University of China, Qingdao, People's Republic of China; ³Department of Organic Chemistry, University of Debrecen, Debrecen, Hungary; ⁴State Key Laboratory of Natural and Biomimetic Drugs, Peking University, Beijing, People's Republic of China; ⁵Department of Pharmacognosy, Faculty of Pharmacy, King Saud University, Riyadh, KSA and ⁶Institute of Physiological Chemistry, University Medical Center of the Johannes Gutenberg University Mainz, Mainz, Germany

Correspondence: Dr G Daletos or Professor P Proksch, Institute of Pharmaceutical Biology and Biotechnology, Heinrich Heine University, Universitätsstrasse 1, Duesseldorf D-40225, Germany.

E-mail: georgios.daletos@uni-duesseldorf.de or proksch@uni-duesseldorf.de

Received 19 November 2015; revised 14 January 2016; accepted 20 January 2016

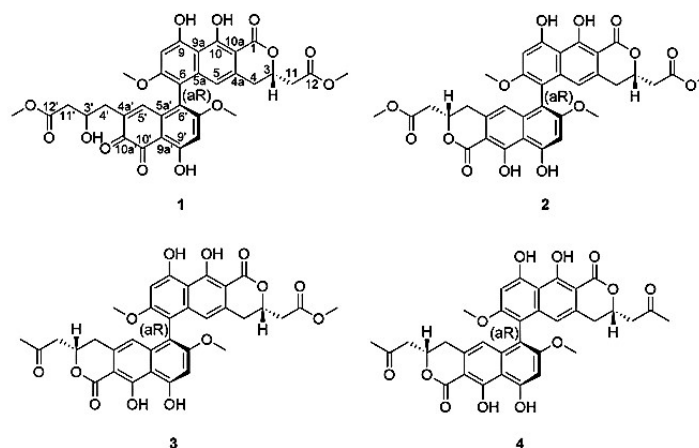


Figure 1 Structures of cladosporinone (1), viriditoxin (2) and viriditoxin derivatives (3 and 4).

Table 1 NMR spectroscopic data of **1** [DMSO- d_6] (^1H NMR in 600 MHz, ^{13}C NMR in 150 MHz, δ in p.p.m.)

<i>1</i>						
Position	δ_{H}	δ_{C}	HMBC	δ_{H}	δ_{C}	HMBC
1		169.90		9'-OH	12.81 s	C-8', 9', 9a'
3	4.94 m	75.7		3'	3.84 m	65.6
4	2.98 dd (16.4, 2.9) 2.89 dd (16.4, 11.8)	31.8	C-10a, 5, 11, 3	4'	2.36 dd (13.5, 5.3) 2.11 dd (13.5, 8.1)	37.1 C-3', 10a', 4a', 5', 11'
4a		133.9		4a'		136.4
5	6.41 s	112.8	C-4, 10a, 9a, 5a, 6	5'	6.58 s	138.7 C-4', 9a', 6', 10a', 4a'
5a		138.6		5a'		134.9
6		106.6 ^a		6'		120.3
7		160.1		7'		166.9
8	6.84 s	97.8	C-9, 6, 9a	8'	6.70 s	100.3 C-9a', 6', 9'
9		159.1 ^a		9'		168.0
9a		107.6		9a'		109.2
10		162.6		10'		179.9
10a		99.1		10a'		180.8
11	2.81 t (6.1)	38.7	C-4, 3, 12	11'	2.32 dd (15.2, 5.3) 2.13 dd (15.2, 8.6)	41.1 C-4', 12', 3'
12		169.87		12'		171.5
12-OCH ₃	3.63 s	51.7	C-12	12'-OCH ₃	3.49 s	51.1 C-12'
7-OCH ₃	3.77 s	56.1	C-7,	7'-OCH ₃	3.72 s	56.8 C-7'

^aAssignments may be interchanged.

(Table 1) were similar to those of the co-isolated viriditoxin (2). Accordingly, the ^1H NMR spectrum of **1** revealed signals corresponding to four methylene groups (H-4, δ_{H} 2.98 and 2.89; H-11, δ_{H} 2.81; H-4', δ_{H} 2.36 and 2.11 and H-11', δ_{H} 2.32 and 2.13), four methoxy groups (12-OCH₃, δ_{H} 3.63; 7-OCH₃, δ_{H} 3.77; 12'-OCH₃, δ_{H} 3.49 and 7'-OCH₃, δ_{H} 3.72), two oxymethine protons (H-3, δ_{H} 4.94 and H-3', δ_{H} 4.94) and four singlets in the aromatic region (H-8, δ_{H} 6.84; H-8', δ_{H} 6.70, H-5', δ_{H} 6.58 and H-5, δ_{H} 6.41) (Table 1). In addition, one exchangeable proton detected at δ_{H} 12.81 was attributable to a chelated hydroxy group. The ^{13}C and DEPT spectra revealed the presence of 19 sp^2 quaternary carbons, including five carbonyl groups (δ_{C} 169.90, C-1; δ_{C} 169.87, C-12; δ_{C} 179.9, C-10'; δ_{C} 180.8, C-10a' and δ_{C} 171.5, C-12').

Further inspection of the 2D NMR (COSY, HSQC and HMBC) data allowed us to establish the planar structure of **1**. The HMBC correlations from H-8 to C-9, C-9a and C-6, from H-5 to C-4, C-9a, C-10a, C-5a and C-6, and from H₂-4 to C-10a, C-5, C-11 and C-3 indicated the presence of a 3,4-dihydro- α -naphthopyrone structure. Further correlations from 7-OCH₃ to C-7, from 12-OCH₃ to C-12 and from H₂-11 to C-4, C-3 and C-12 fully supported the semi-viriditoxin moiety in the structure of **1** (Figure 2). Analysis of the 1D and 2D NMR data revealed that **1** also contained a 1,2-naphthoquinone moiety as confirmed by the HMBC correlations from H-8' to C-6', C-9' and C-9a' and from H-5' to C-9a', C-6', C-10a', C-4' and C-4a'. In addition, a 3'-OH-methyl butyrate side chain was located at C-4a' of the 1,2-benzoquinone ring, as supported by the COSY

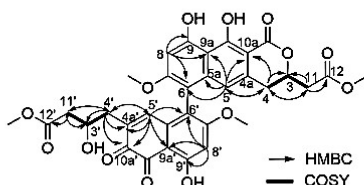


Figure 2 Selected HMBC and COSY correlations of **1**.

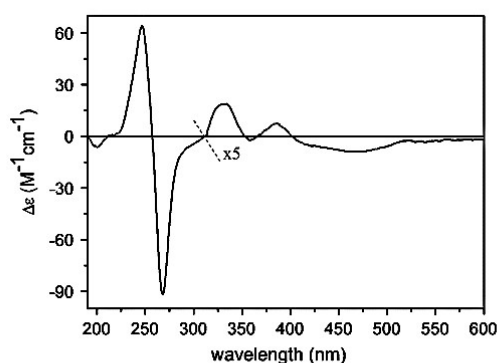


Figure 3 ECD spectrum of **1** in acetonitrile. $\Delta\epsilon$ values were multiplied by 5 above 314 nm for better visualization.

correlations from H-3' to H₂-4' and H₂-11', and by the HMBC correlations from H-4' to C-3', C-4a', C-10a', C-5' and C-11', from H-11' to C-3', C-4' and C-12', and from 12'-OCH₃ to C-12' (Figure 2). In a similar manner to viriditoxin, the HMBC correlations from 7'-OCH₃ to C-7' and from the chelated proton 9'-OH to C-8', C-9' and C-9a', indicated the presence of 7'-methoxy and 9'-hydroxy substituents in the aromatic ring, leaving only C-6' for the connection of the two monomers through a 6',6'-biaryl linkage. Thus, the planar structure of **1** was elucidated as shown in Figure 2.

In an attempt to determine the absolute configuration of C-3', the modified Mosher's method was applied, however, this reaction failed to give the corresponding Mosher's ester, probably, due to the chelated hydroxy group. The axial chirality of **1** was determined by comparing its electronic circular dichroism (ECD) spectrum (Figure 3) with that of the related viriditoxin (**2**), which had a negative exciton couplet (275 nm -194.7 , 255 nm $+174.0$) in chloroform.¹⁸ The negative couplet of viriditoxin derives from coupling of the two ¹B_b transitions of the interacting 6,6'-linked naphthopyrone chromophores having a counter-clockwise twist with a dihedral angle of about 90°. Although one of the naphthalene ring is replaced by a 1,2-naphthoquinone residue in **1**, the alignment of the interacting electric transition moments are not expected to alter significantly, and thus similarly to viriditoxin, the negative exciton couplet of **1** derives from (aR) axial chirality of the biaryl system. As the ECD spectrum is governed predominantly by the axial chirality element, the central chirality of the fused α -pyrone ring of **1** could not be determined from ECD. However, this configuration was determined earlier for semi-viriditoxin, the naphthopyrone monomer of viriditoxin, as (S)²¹ and it was also confirmed by stereoselective synthesis.²² Thus, **1** was identified as a new natural heterodimer for which the name cladosporinone is proposed.

The known compounds viriditoxin (**2**) and its analogs (**3** and **4**) were identified on the basis of NMR, mass spectrometry and optical rotation data analysis, as well as by comparison with the literature.^{18,19} The axial chirality of **3** and **4** had been deduced earlier as (aR) by comparison of their ECD curves with those of **2**.^{18–20} Several attempts were undertaken to influence the pattern of metabolites produced by *C. cladosporioides* either by changing the medium (OSMAC approach²³) or by co-culturing the fungus in the presence of several bacteria, such as *Bacillus subtilis* 168 trpC2, *Bacillus cereus* T, *Streptomyces lividans* TK24 and *Streptomyces coelicolor* A2(3). Mixed fermentation of fungi and bacteria has repeatedly been shown to activate silent fungal biogenetic gene clusters, thus causing the accumulation of compounds not detected in axenic fungal cultures.^{24,25} However, none of these attempts caused a significant change in the metabolite pattern on *C. cladosporioides* as shown by HPLC analysis of the respective extracts and by comparison to extracts of the fungus grown only on rice.

A plausible biogenetic pathway of compounds **1–4** includes a head-to-tail combination of one acetyl-CoA (starter unit) and seven malonyl-CoA (extender units) moieties, a process that is catalyzed by multidomain enzymes called polyketide synthases. Then, the octaketide chain would undergo regiospecific aromatization, reduction or cyclization reactions to form precursor B. Dehydration and lactonization of the latter (B) and subsequent methoxylation would afford the monomeric precursors C and D, respectively. Oxidative coupling of the different monomers at C-6/C-6' would result in the formation of **2–4**, as shown in Figure 4. An alternative biosynthetic route would include oxidative decarboxylation of precursor B to form the 1,2-naphthoquinone monomer, followed by oxidative coupling with monomer D to afford the new metabolite **1** (Figure 4).²⁶

Compounds **1–4** were assayed for their cytotoxicity toward L5178Y (murine lymphoma) cells. Viriditoxin (**2**) exhibited the most potent cytotoxicity against the tested cell line, with an IC₅₀ of 0.1 μM , followed by compound **3** with an IC₅₀ of 0.25 μM and the new compound **1** with an IC₅₀ of 0.88 μM (Table 2). Compound **4** was inactive in the bioassay. The loss of one or both methylated carboxyl groups at C-12 and C-12' as in **3** and **4** weakens the cytotoxicity of the respective derivatives when compared to **2**. Hydrolysis of one of the two lactone rings followed by oxidative decarboxylation as in **1** likewise attenuates the cytotoxicity as evident when compared to **2**. In addition, compounds **1–4** were evaluated for their antimicrobial activities against *Staphylococcus aureus* ATCC 29213, *Escherichia coli* ATCC 25213, and *Pseudomonas aeruginosa* ATCC 27853 (Table 2). Interestingly, all compounds showed selective activity against *S. aureus* ATCC 29213, with viriditoxin (**2**) being by far the most active compound exhibiting a MIC of 0.015 $\mu\text{g ml}^{-1}$ (0.023 μM), thus confirming the results of earlier studies.^{27–29}

EXPERIMENTAL PROCEDURE

General experimental procedures

Optical rotations were determined on a Perkin-Elmer-241 MC polarimeter (Perkin-Elmer, Waltham, MA, USA). ¹H, ¹³C, and 2D NMR spectra were recorded at 25 °C in DMSO-*d*₆ on Bruker AVANCE DMX 600 NMR spectrometers (Bruker BioSpin GmbH, Rheinstetten, Germany). Chemical shifts were referenced to the solvent residual peaks, $\delta_{\text{H}} = 2.50$ p.p.m. for ¹H and $\delta_{\text{C}} = 39.51$ p.p.m. for ¹³C. Mass spectra (ESI) were recorded with a Finnigan LCQ Deca mass spectrometer (Thermo Fisher Scientific GmbH, Bremen, Germany), and HRMS (ESI) spectra were obtained with a FTHRMS-Orbitrap (Thermo-Finnigan) mass spectrometer (Thermo Fisher Scientific GmbH). Solvents were distilled before use and spectral grade solvents were



of the medium to 9 or 11 by adding sodium hydroxide. In addition, co-cultivation experiments of *C. cladosporioides* with *B. subtilis* 168 trpC2, *B. cereus* T, *S. lividans* TK24 and *S. coelicolor* A2(3) were performed on rice medium as described before.^{24,25}

Extraction and isolation

Fungal cultures were extracted with EtOAc. The crude extract was evaporated to dryness, and then subjected to liquid-liquid partitioning between *n*-hexane and 90% aqueous MeOH. The 90% MeOH fraction amounted to 4.9 g, and was further separated by vacuum liquid chromatography (4.5 × 30 cm) on silica gel, using solvents in a gradient of increasing polarity—*n*-hexane-ethyl acetate-dichloromethane-methanol—to obtain a total of 11 fractions. The fractions eluted with *n*-hexane-ethyl acetate (30:70–100% EtOAc, 126 mg) and DCM-MeOH (90:10, 153 mg) were then subjected to column chromatography (3.5 × 60 cm) using Sephadex LH-20 as stationary phase and DCM-MeOH (50:50v/v) as mobile phase to remove pigments. The bioactive fraction (87 mg) was further subjected to column chromatography (2.5 × 50 cm) over diol-functionalized silica using DCM-MeOH (99:1v/v) as eluting solvent. Fractions were combined according to TLC monitoring (53 mg) and purified by reversed-phase HPLC (silica-based, semipreparative column), with gradient elution MeOH-H₂O from 50:50 to 60:40 in 30 min, to yield the four compounds 1 (5.3 mg), 2 (21 mg), 3 (4.4 mg) and 4 (3.9 mg).

Cladosporinone (1): red, amorphous powder; $[\alpha]_D^{25} = -154^\circ$ (*c* 0.35, MeOH); UV (MeCN) λ_{max} log ϵ : 440sh (2.8), 383 (3.1), 334sh (2.9), 264 (3.9), 222sh (3.7). ECD (MeCN, λ (nm) ($\Delta\epsilon$), *c* = 2.56×10^{-4} M): 471 (−1.8), 386 (1.5), 359 (−0.4), 333 (3.8), 289sh (−9.1), 268 (−91.6), 246 (64.3), 200 (−6.2); ¹H (600 MHz) and ¹³C (150 MHz) NMR, see Table 1; ESI-MS *m/z* 651.0 [M+H]⁺, 649.4 [M−H][−]; HRESIMS *m/z* 651.1706 [M+H]⁺ (calcd for C₃₃H₃₁O₁₄, 651.1708).

CONFLICT OF INTEREST

The authors declare no conflict of interest.

ACKNOWLEDGEMENTS

The financial support by the German Federal Ministry of Education and Support (BMBF; Bundesministerium für Bildung und Forschung) granted to PP and by the Ministry of Science and Technology (MOST) to WHL are gratefully acknowledged. YL wishes to thank the China Scholarship Council and the Ministry of Education of China for awarding her with a scholarship. The authors are indebted to Prof. MS Abdel-Aziz (National Research Center, Egypt) for his help during the collection of sediment from the hypersaline lake El Hamra in Egypt and to Prof. H Brötz-Oesterhelt (University of Tuebingen, Germany) for performing the antibacterial assays.

- Aoki, H. & Okuhara, M. Natural β -lactam antibiotics. *Ann. Rev. Microbiol.* **34**, 159–181 (1980).
- Abraham, E. Selective reminiscences of β -lactam antibiotics: early research on penicillin and cephalosporins. *BioEssays* **12**, 601–606 (1990).
- Muñiz, C. C., Zelaya, T. E. C., Esquivel, G. R. & Fernández, F. J. Penicillin and cephalosporin production: a historical perspective. *Rev. Latinoam. Microbiol.* **49**, 88–98 (2007).

- Traber, R., Hofmann, H. & Kobel, H. Cyclosporins—new analogues by precursor directed biosynthesis. *J. Antibiot.* **42**, 591–597 (1989).
- Murthy, M. V. R., Mohan, E. V. S. & Sadhukhan, A. K. Cyclosporin-A production by *Tolypocladium inflatum* using solid state fermentation. *Process Biochem.* **34**, 269–280 (1999).
- Alberts, A. W. Discovery, biochemistry and biology of lovastatin. *Am. J. Cardiol.* **62**, 10J–15J (1988).
- Wilson, Z. E. & Brimble, M. A. Molecules derived from the extremes of life. *Nat. Prod. Rep.* **26**, 44–71 (2009).
- Kingston, D. G. I. Modern natural products drug discovery and its relevance to biodiversity conservation. *J. Nat. Prod.* **74**, 496–511 (2011).
- Maetzko, Y. & Blum, P. Survival of the fittest: overcoming oxidative stress at the extremes of acid, heat and metal. *Life* **2**, 229–242 (2012).
- Ma, Y., Galinski, E. A., Grant, W. D., Oren, A. & Ventosa, A. Halophiles 2010: life in saline environments. *Appl. Environ. Microbiol.* **76**, 6971–6981 (2010).
- Satyanarayana, T., Raghukumar, C. & Shivaji, S. Extremophilic microbes: diversity and perspectives. *Curr. Sci.* **89**, 78–90p (2005).
- Jalgaonwala, R. E., Mohite, B. V. & Mahajan, R. T. A review: natural products from plant associated endophytic fungi. *J. Microbiol. Biotech. Res* **1**, 21–32 (2011).
- Demain, A. L. Importance of microbial natural products and the need to revitalize their discovery. *J. Ind. Microbiol. Biotechnol.* **41**, 185–201 (2014).
- Liu, Y. *et al.* Tetrahydroanthraquinone derivatives from the endophytic fungus *Stemphylium globuliferum*. *Eur. J. Org. Chem* **12**, 2646–2653 (2015).
- Liu, Y. *et al.* Trimeric anthracenes from the endophytic fungus *Stemphylium globuliferum*. *J. Nat. Prod.* **77**, 1734–1738 (2014).
- Okoye, F. B. C. *et al.* A phenylidilactone, bisnorsesquiterpene, and cytotoxic phenolics from *Maytenus senegalensis* leaves. *Tetrahedron Lett.* **55**, 3756–3760 (2014).
- Chen, H. *et al.* A new cytotoxic cytochalasin from the endophytic fungus *Trichoderma harzianum*. *Nat. Prod. Commun.* **10**, 585–587 (2015).
- Suzuki, K., Nozawa, K., Nakajima, S. & Kawai, K. Structure revision of mycotoxin, viriditoxin, and its derivatives. *Chem. Pharm. Bull.* **38**, 3180–3181 (1990).
- Mizuba, S., Hsu, C. & Jiu, J. A third metabolite from *Spicaria divaricata* NRRL 5771. *J. Antibiot.* **30**, 670–672 (1977).
- Jiu, J. & Mizuba, S. Metabolic products from *Spicaria divaricata* NRRL 5771. *J. Antibiot.* **27**, 760–765 (1974).
- Ayer, W. A., Craw, P. A. & Nozawa, K. Two 1H-naphtho[2,3-c]pyran-1-one metabolites from the fungus *Paecilomyces variotii*. *Can. J. Chem.* **69**, 189–191 (1991).
- Tan, N. P. H. & Donner, C. D. Total synthesis and confirmation of the absolute stereochemistry of semiviriditoxin, a naphthopyranone metabolite from the fungus *Paecilomyces variotii*. *Tetrahedron* **65**, 4007–4012 (2009).
- Bode, H. B., Bethe, B., Höfs, R. & Zecek, A. Big effects from small changes: possible ways to explore nature's chemical diversity. *ChemBioChem* **3**, 619–627 (2002).
- Chen, H. *et al.* Inducing secondary metabolite production by the soil-dwelling fungus *Aspergillus terreus* through bacterial co-culture. *Phytochem. Lett.* **12**, 35–41 (2015).
- Ola, A. R. B., Thomy, D., Lai, D., Brötz-Oesterhelt, H. & Proksch, P. Inducing secondary metabolite production by the endophytic fungus *Fusarium tricinctum* through coculture with *Bacillus subtilis*. *J. Nat. Prod.* **76**, 2094–2099 (2013).
- Donner, C. D. Naphthopyranones— isolation, bioactivity, biosynthesis and synthesis. *Nat. Prod. Rep.* **32**, 578–604 (2015).
- Anderson, D. E. *et al.* Comparison of small molecule inhibitors of the bacterial cell division protein FtsZ and identification of a reliable cross-species inhibitor. *ACS Chem. Biol.* **7**, 1918–1928 (2012).
- Foss, M. H. *et al.* Inhibitors of bacterial tubulin target bacterial membranes in vivo. *Med. Chem. Comm* **4**, 112–119 (2013).
- Wang, J. *et al.* Discovery of a small molecule that inhibits cell division by blocking FtsZ, a novel therapeutic target of antibiotics. *J. Biol. Chem.* **278**, 44424–44428 (2003).
- Okoye, F. B. C., Nworuc, C. S., Debbaba, A., Esimone, C. O. & Proksch, P. Two new cytochalasins from an endophytic fungus, KL-1.1 isolated from *Psidium guajava* leaves. *Phytochem. Lett.* **14**, 51–55 (2015).
- Wang, S. *et al.* Chaetopyranin, a benzaldehyde derivative, and other related metabolites from *Chaetomium globosum*, an endophytic fungus derived from the marine red alga *Polysiphonia urceolata*. *J. Nat. Prod.* **69**, 1622–1625 (2006).

Supplementary Information accompanies the paper on The Journal of Antibiotics website (<http://www.nature.com/ja>)

Cladosporinone, a new viriditoxin derivative from the hypersaline lake derived fungus *Cladosporium cladosporioides*

Yang Liu^{1,2}, Tibor Kurtán³, Chang Yun Wang², Wen Han Lin⁴, Raha Orfali⁵, Werner E. G. Müller⁶, Georgios Daletos¹, and Peter Proksch¹

¹ Institute of Pharmaceutical Biology and Biotechnology, Heinrich Heine University, Universitaetsstrasse 1, D-40225 Duesseldorf, Germany.

² Key Laboratory of Marine Drugs, The Ministry of Education of China, School of Medicine and Pharmacy, Ocean University of China, Qingdao 266003, P. R. China

³ Department of Organic Chemistry, University of Debrecen, P. O. B. 20, 4010 Debrecen, Hungary

⁴ State Key Laboratory of Natural and Biomimetic Drugs, Peking University, Beijing 100191, P. R. China

⁵ Pharmacognosy Department, Faculty of Pharmacy, King Saud University, Riyadh, KSA.

⁶ Institute of Physiological Chemistry, University Medical Center of the Johannes Gutenberg University Mainz, Duesbergweg 6, D-55128 Mainz, Germany

Correspondence: Dr. G. Daletos, E-mail: georgios.daletos@uni-duesseldorf.de;

Professor P. Proksch, E-mail: proksch@uni-duesseldorf.de

Contents

Figure S1 ^1H NMR spectrum of **1** (DMSO- d_6 , 600 MHz)

Figure S2 ^{13}C NMR spectrum of **1** (DMSO- d_6 , 150 MHz)

Figure S3 COSY spectrum of **1**

Figure S4 HSQC spectrum of **1**

Figure S5 HMBC spectrum of **1**

Figure S6 HRESIMS spectrum of **1**

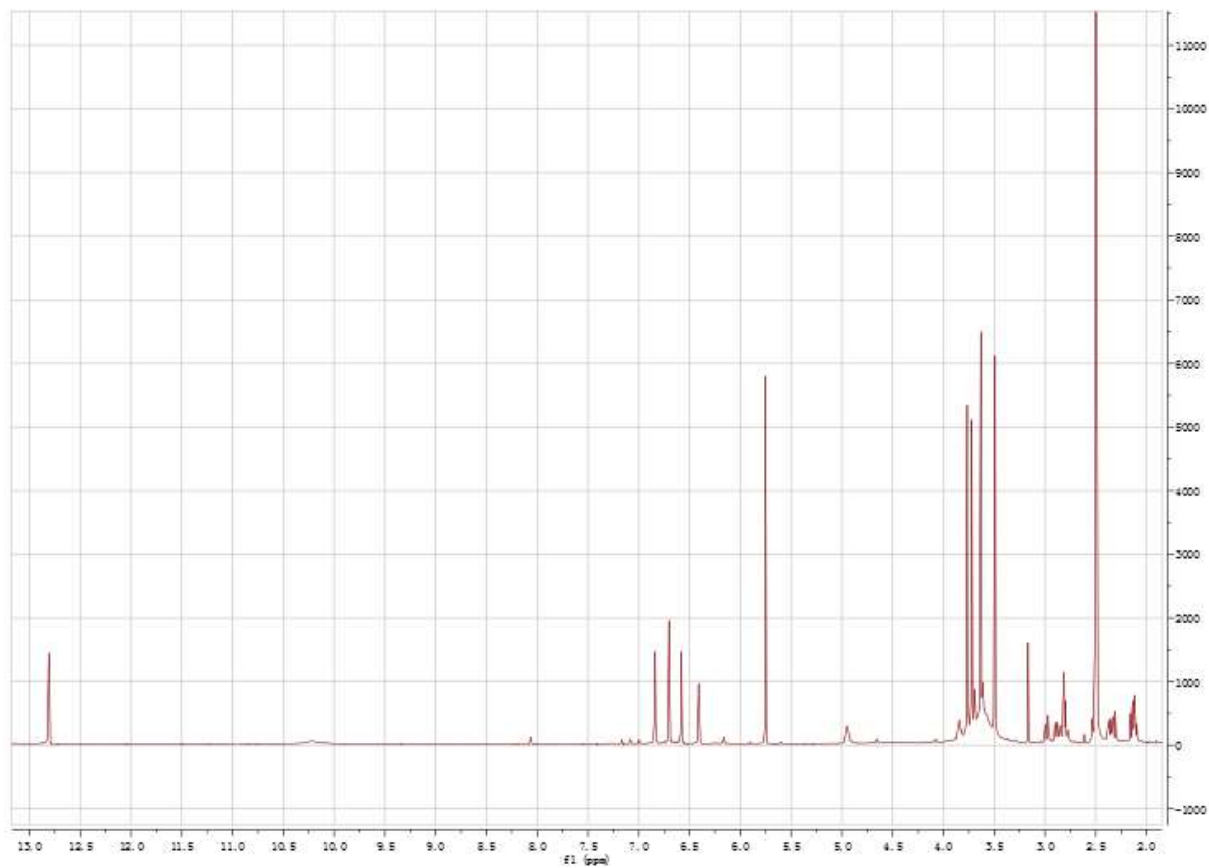
Figure S1 ^1H NMR spectrum of **1** (DMSO- d_6 , 600 MHz)

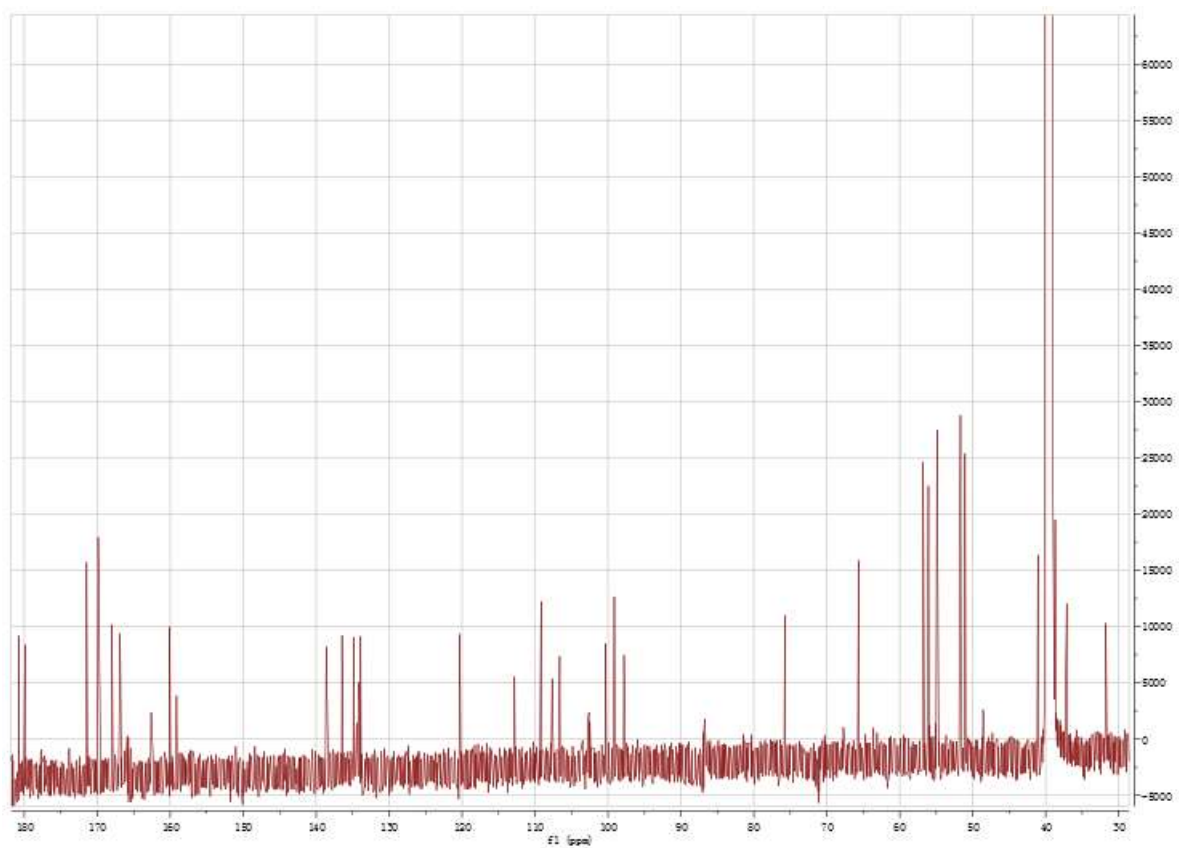
Figure S2 ^{13}C NMR spectrum of **1** (DMSO, 150 MHz)

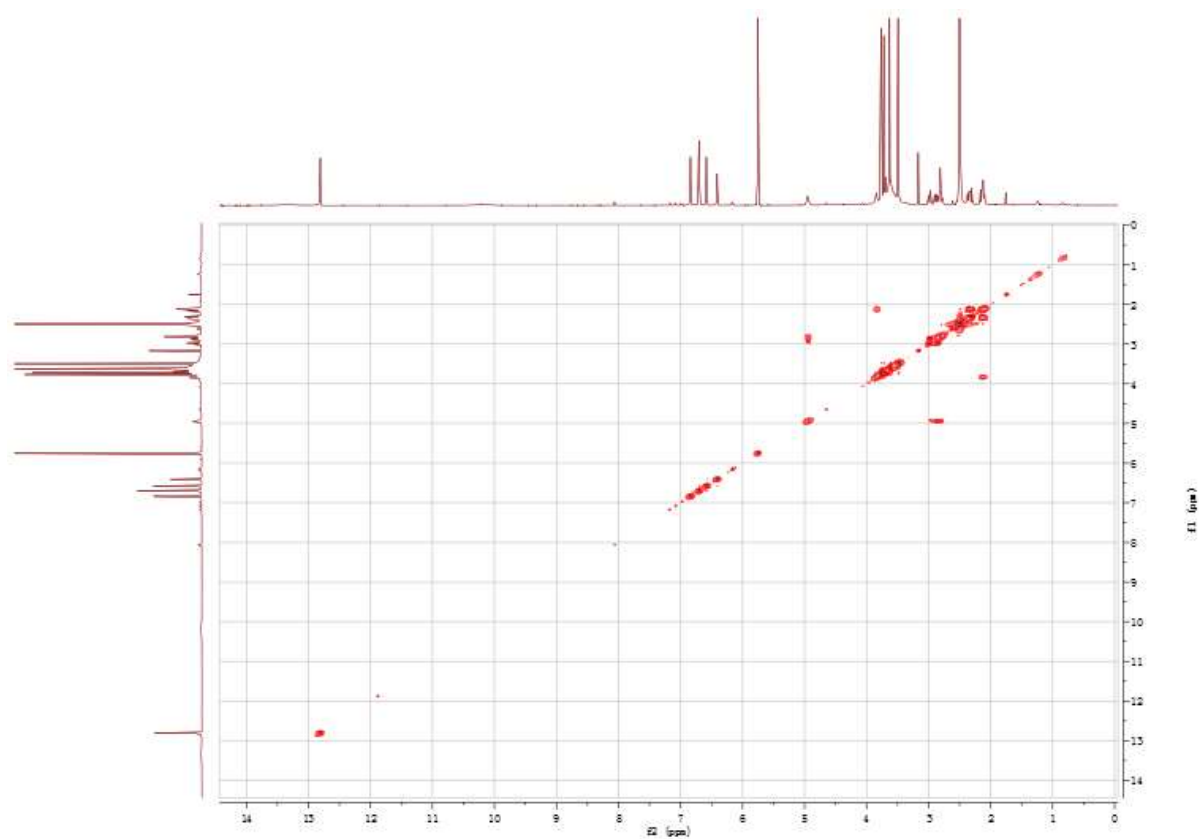
Figure S3 COSY spectrum of **1**

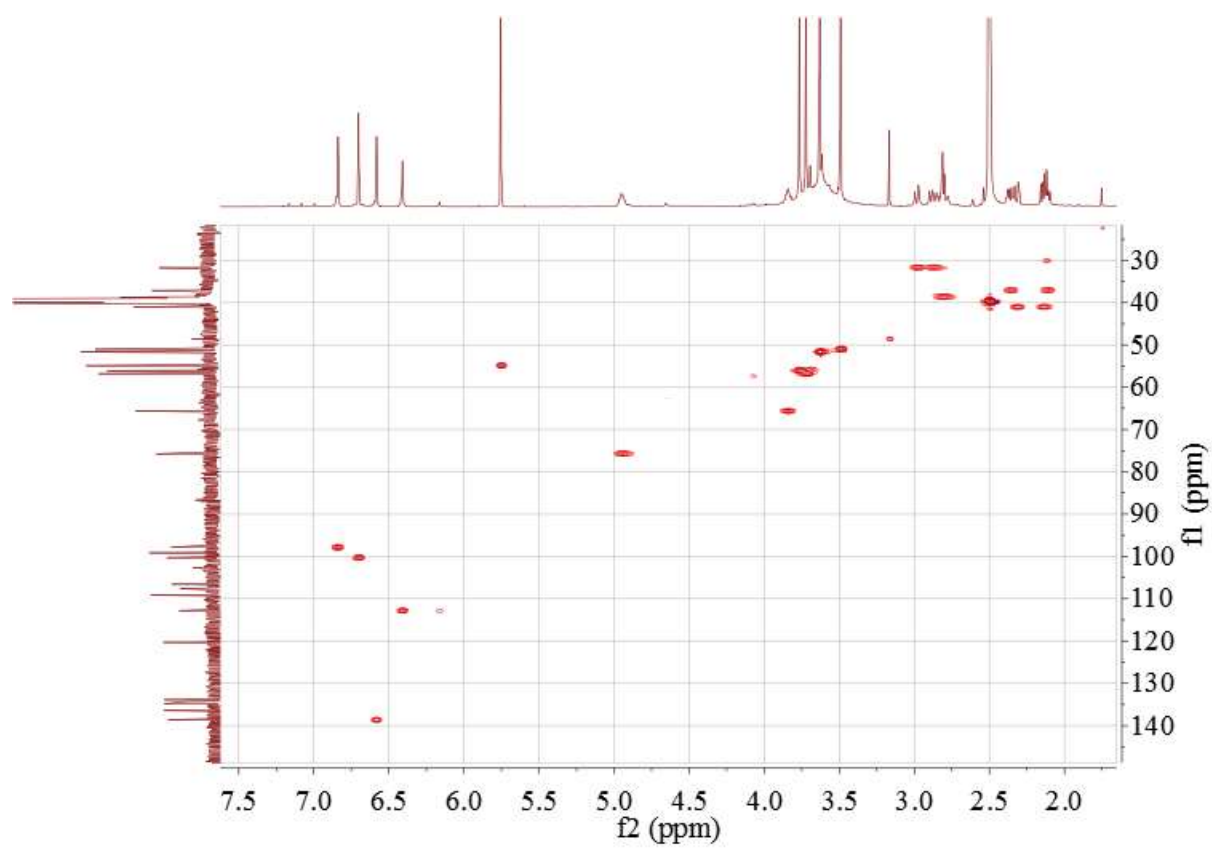
Figure S4 HSQC spectrum of **1**

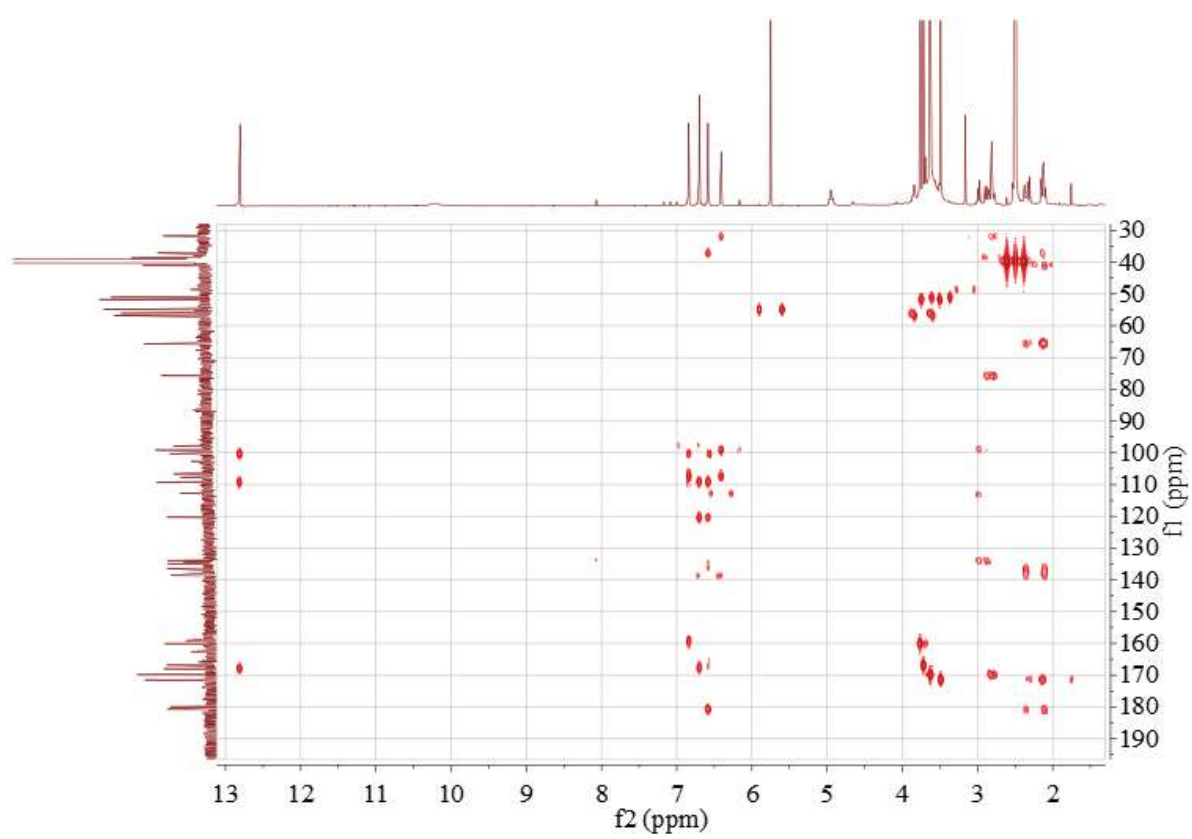
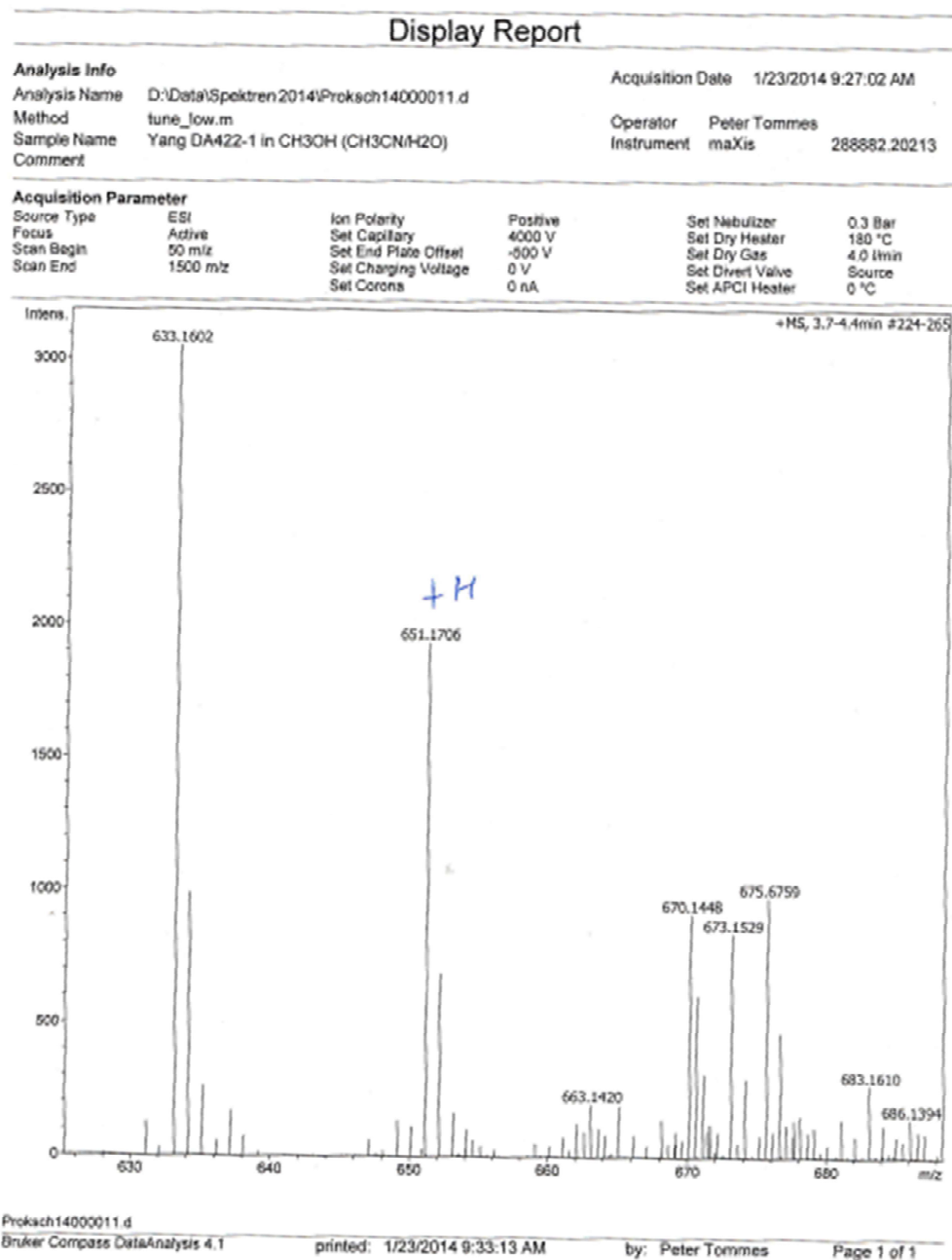
Figure S5 HMBC spectrum of **1**

Figure S6 HRESIMS spectrum of 1



5 Publication 4

5.1 Benzo[j]fluoranthene Metabolites from the Mangrove-Derived Endophytic Fungus *Annulohyphoxylon* sp.

Submitted to: “Journal of Natural Products”

Impact factor: 3.662

Contribution: 70 %, first author, conducting most of the experiments, literature research, manuscript writing.

Benzo[j]fluoranthene Metabolites from the Mangrove Derived Endophytic Fungus

Annulohypoxylon sp.

Yang Liu^{†§}, Fabian Stuhldreier[‡], Tibor Kurtán[¶], Attila Mándi[¶], Sathishkumar Arumugam[‡], Changyun Wang[§], Wenhan Lin[#], Sebastian Wesselborg[‡], Horst Weber[†], Birgit Henrich[†], Georgios Daletos^{†*}, and Peter Proksch^{†*}

[†] Institute of Pharmaceutical Biology and Biotechnology, Heinrich Heine University, Universitaetsstrasse 1, D-40225 Duesseldorf, Germany.

[§] Key Laboratory of Marine Drugs, The Ministry of Education of China, School of Medicine and Pharmacy, Ocean University of China, Qingdao 266003, P. R. China

[‡] Institute of Molecular Medicine, Heinrich Heine University, Universitaetsstrasse 1, D-40225 Duesseldorf, Germany

[¶] Department of Organic Chemistry, University of Debrecen, P. O. B. 20, 400, 4002 Debrecen, Hungary

[‡] Centre of Advanced Study in Marine Biology, Annamalai University, Parangipettai 608502, Tamilnadu, India.

[#] State Key Laboratory of Natural and Biomimetic Drugs, Beijing University, Beijing 100191, P. R. China

[†] Institute of Pharmaceutical and Medicinal Chemistry, Heinrich Heine University, Universitaetsstrasse 1, D-40225 Duesseldorf, Germany

[†] Institute of Medical Microbiology and Hospital Hygiene, University Clinic of the Heinrich Heine University, D-40225 Duesseldorf, Germany

Abstract: Two new benzo[j]fluoranthene metabolites, daldinones E, G (**1** and **3**), and the likewise undescribed artefact, daldinone F (**2**), along with six known compounds (**4-9**) were

isolated from the endophytic fungus *Annulohyphoxylon* sp. that was obtained from the Mangrove plant *Rhizophora racemosa* collected in Cameroon. The structures of the new compounds were elucidated by 1D and 2D NMR as well as by HRESIMS and ECD spectra analysis. Co-cultivation of this fungus with the actinomycetes *Streptomyces lividans* or with *Streptomyces coelicolor* resulted in an up to 38-fold increase of 1-hydroxy-8-methoxynaphthalene (**9**), while no significant induction was detected when the fungus was co-cultivated either with *Bacillus subtilis* or with *Bacillus cereus*. Compound **2** exhibited strong to moderate cytotoxicity against Ramos and Jurkat J16 cells with IC₅₀ values of 8.5 and 13.9 μ M, respectively. Mechanistic studies indicated that **2** induces apoptotic cell death caused by induction of intrinsic apoptosis. Moreover, **2** potently blocks autophagy, a potential pro-survival pathway for cancer cells. A proposed biogenetic pathway for the analyzed compounds involves oxidative coupling of 1,3,8-trihydroxynaphthalene (3HN) and/or 1,8-dihydroxynaphthalene (DHN). Feeding experiments with DHN led to an enhanced accumulation of daldinone B (**6**), which supported this hypothesis.

Introduction

Endophytes are microorganisms that colonize asymptotically the intercellular and/or intracellular parts of healthy plants^{1,2} and play an important role in drug discovery.³ In recent years, the increased re-isolation of known substances from fungi has turned the interest of natural product chemists to hitherto less investigated ecological niches such as Mangrove swamps for bioprospecting of fungi.⁴⁻⁶ Mangroves, also called halophytes, inhabit (sub)tropical coastal regions and are exposed to various stress factors, such as intense light and high salinity followed by tidal range alterations.^{7,8} In these harsh conditions, endophytic fungi have developed unique metabolic mechanisms and are described to have a positive influence on their hosts by providing nutrients and/or chemical defense.⁹ Mangrove-derived

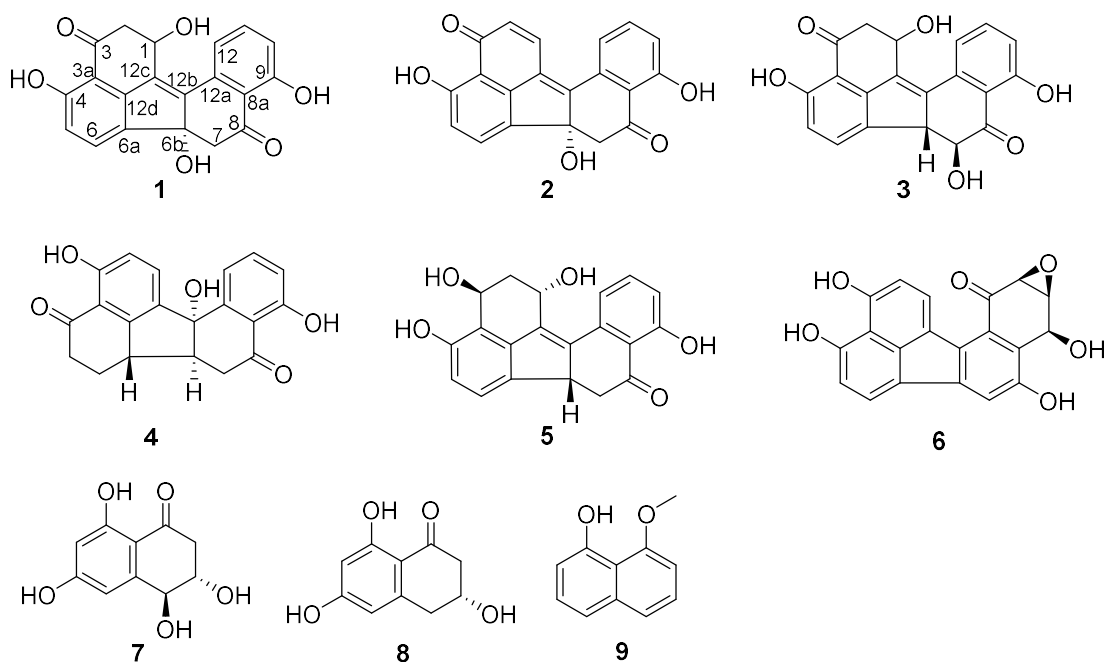
endophytic fungi have been shown to produce a plethora of new compounds with some of them showing pronounced biological activities as exemplified by the tetrahydroxanthone derivative phomoxanthone A that was recently isolated by our group from a Mangrove endophyte and showed strong anticancer activity against cisplatin resistant cancer cells in addition to immunostimulant activity.^{6,10}

During our ongoing search for new bioactive secondary metabolites from endophytic fungi,¹¹⁻¹³ an endophytic fungus was isolated from the Mangrove plant *Rhizophora racemosa*, collected in Cameroon. Several approaches, such as ITS sequencing and enlarged 18S-28S rDNA sequencing, were used to narrow the identity of the fungus. BlastN search in NCBI-databases revealed 76.4% highest homology to the fungus *Annulohypoxylon artrorseum* (acc.-no U32411), and massBLASTer analysis by unite (Unified system for the DNA based fungal species linked to the classification Ver. 7.0)¹⁴ revealed 97.75% homology of the sequence region of fungus from nt 2415 – nt 3906 to *Annulohypoxylon* spp. (acc-no JQ747656). Therefore, we assume that the fungus investigated in this study belongs to the genus *Annulohypoxylon* and it was nominated accordingly. *Annulohypoxylon*, which has been named *Hypoxylon* sect. *Annulata* before, is considered a new genus separated from *Hypoxylon* recently based on a report of Hsieh.¹⁵⁻¹⁸ *Annulohypoxylon* is believed to show the same evolutionary lineage as the genera *Hypoxylon* and *Daldinia*.¹⁹ Previous chemical investigations of taxa of *Annulohypoxylon* sp. yielded several metabolites including cohaerins A-K,¹⁷⁻¹⁹ daldinone A,¹⁶ truncatone,¹⁸ and truncaquinones A and B.¹⁶ Subsequent fractionation of *Annulohypoxylon* sp. investigated in this study afforded two new benzo[*j*]fluoranthene-based metabolites, daldinones E and G (**1** and **3**, respectively), and a hitherto undescribed artefact, daldinone F (**2**) that originated by rapid conversion of **1** during chromatographic isolation, along with six known compounds daldinone C (**4**), hypoxylonol C (**5**), daldinone B (**6**), 3,4-dihydro-3,4,6,8-trihydroxy-1(2H)-naphthalenone (**7**), (R)-scytalone

(**8**), and 1-hydroxy-8-methoxynaphthalene (**9**). Co-cultivation of this fungus with the actinomycetes *Streptomycetes lividans* or *Streptomyces coelicolor* resulted in an up to 38-fold increase of **9**. However, when co-culturing the fungus with either *Bacillus subtilis* or with *Bacillus cereus*, no significant induction in the accumulation of constitutively present metabolites was observed. Compound **2** showed pronounced cytotoxicity against Ramos and Jurkat J16 cell lines with IC₅₀ values of 8.5 and 13.9 μ M, respectively due to induction of intrinsic apoptosis. Moreover, **2** potently blocks autophagy, a potential pro-survival pathway for cancer cells. A proposed biogenetic pathway for the compounds isolated in this study was corroborated by feeding 1,8-dihydroxynaphthalene to the fungal culture which caused a pronounced increase of daldinones E and B.

Results and Discussion

The EtOAc extract of the fungus following cultivation on solid rice medium was partitioned between n-hexane and 90% aqueous MeOH. The resulting MeOH phase afforded two new benzo[*j*]fluoranthene secondary metabolites (**1** and **3**), and the likewise hitherto undescribed artefact (**2**) that rapidly originated from **1** during chromatographic isolation. In addition six known compounds including daldinone C, hypoxylonol C, daldinone B, 3,4-dihydro-3,4,6,8-trihydroxy-1(2H)-naphthalenone, (R)-scytalone, and 1-hydroxy-8-methoxynaphthalene (**4** – **9**) were likewise obtained.



Compound **1** was isolated as a red, amorphous powder. Its molecular formula was established as $C_{20}H_{14}O_6$ based on the prominent pseudomolecular ion peak observed at m/z 351.0865 $[M+H]^+$ in the HRESIMS spectrum, corresponding to 14 degrees of unsaturation. The 1H and COSY spectra revealed aromatic signals representative for a 1,2,3-trisubstituted benzene ring at δ_H 6.98 (H-10), 7.64 (H-11), and 7.51 (H-12), two *ortho*-coupled protons at δ_H 6.77 (H-5, $J = 8.1$ Hz) and 7.64 (H-6, $J = 8.1$ Hz), two sets of methylene groups at δ_H 3.39/2.74 (H₂-7), and 3.14/2.94 (H₂-2), as well as an oxymethine proton at δ_H 5.16 (H-1). In the HMBC spectrum of **1**, the correlations from H-5 to C-3a, C-6a, and C-4, from H-6 to C-4 and C-12d, from H-2 to C-1, C-3, C-12c, and C-3a, and from H-1 to C-3, C-12c, C-12d, suggested the presence of a vermelone^{20,21} moiety in the molecule (Figure 1). The HMBC spectrum verified the presence of a second vermelone subunit as deduced by the correlations observed from H-10 to C-8a, C-9, and C-12, from H-11 to C-9 and C-12a, from H-12 to C-8a, C-10, and C-12b, as well as from H-7 to C-6b, C-8, C-12b, and C-8. The connection of the two substructures at C-6a and C-6b was established on the basis of the HMBC correlation from H-6 to C-6b (Figure 1). These functionalities accounted for 13 of the 14 degrees of

unsaturation, thus leaving only C-12b to C-12c for connection between the two units, rationalizing the remaining degree of unsaturation. Hence, **1** was identified as a new natural product and was named daldinone E.

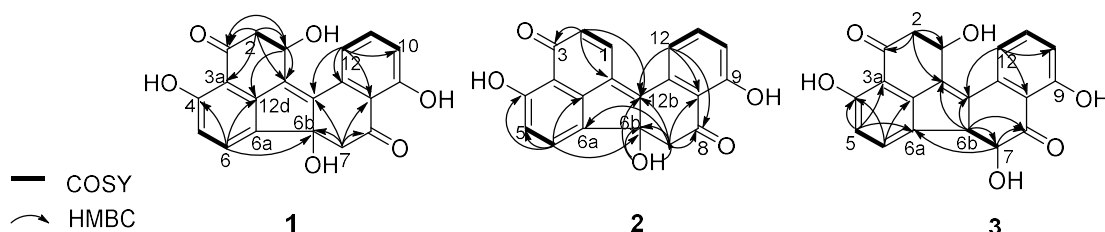


Figure 1. Selected HMBC correlations of **1-3**

The relative configuration of the two chirality centers of **1** could not be determined due to the lack of characteristic NOE correlations. For the stereochemical studies, ECD measurement and calculations were carried out, which first required the HPLC separation of **1** from its dehydration product **2**, since **1** was isolated as a 1:1 mixture with **2**. Compounds **1** and **2** could be base-line separated using Chiralpack IA column and the HPLC-ECD spectrum of **1** was recorded, which was used for comparison in the ECD calculations. A pure sample of **2** was available and TDDFT-ECD calculation determined its absolute configuration as (6b*R*), which suggested (6b*R*) absolute configuration for its precursor **1** as well (*vide infra*).

In order to determine the absolute configuration of **1**, the TDDFT-ECD protocol^{22,23} was applied on the (1*R*,6b*R*) and (1*S*,6b*R*) diastereomers of **1**. The Merck Molecular Force Field (MMFF) conformational search produced 5 low-energy conformers for both diastereomers in a 21 kJ/mol energy window which were reoptimized at four different DFT levels [B3LYP/6-31G(d) *in vacuo*, B97D/TZVP^{24,25} PCM/MeCN, B3LYP/TZVP PCM/MeCN and CAM-B3LYP/TZVP PCM/MeCN]. The ¹H NMR spectrum of **1** showed a small value of the ³*J*_{1-H,2-H} (4.9 and 1.9 Hz), which suggested the preferred equatorial orientation of 1-H in solution. The computed B3LYP/6-31G(d) *in vacuo* conformers of (1*R*,6b*R*)-**1** had preference for the

axial orientation of 1-H (see Fig. S10, Table S1 in the Supporting Information), while those of (1*S*,6*bR*)-**1** had larger population for the conformers with equatorial 1-H (see Fig. S12, Table S2 in the Supporting Information). This result would have afforded the assignment of the relative configuration and hence the absolute configuration as (1*S*,6*bR*). However, the three solvent model DFT optimizations (B97D/TZVP PCM/MeCN (Figure 2 and 4), B3LYP/TZVP PCM/MeCN and CAM-B3LYP/TZVP PCM/MeCN) showed that 1-H preferably adopts equatorial orientation in both the (1*R*,6*bR*) and the (1*S*,6*bR*) diastereomer and thus the correlation of the coupling constant ($^3J_{1-H,2-H}$) with the geometry of the computed conformers could not result in an unambiguous assignment of the relative configuration.

ECD spectra were computed for the low-energy ($\geq 2\%$) B3LYP/6-31G(d) *in vacuo* (Figure S2) and B97D/TZVP PCM/MeCN conformers of (1*R*,6*bR*)-**1** and (1*S*,6*bR*)-**1** with various functionals (B3LYP, BH&HLYP and PBE0) and TZVP basis set, and they reproduced well the main features of the experimental spectrum but there was no sufficient difference among the computed ECD spectra of the diastereomers to distinguish them. The agreement of the computed ECDs confirmed the configurational assignment of C-6b as (*R*).

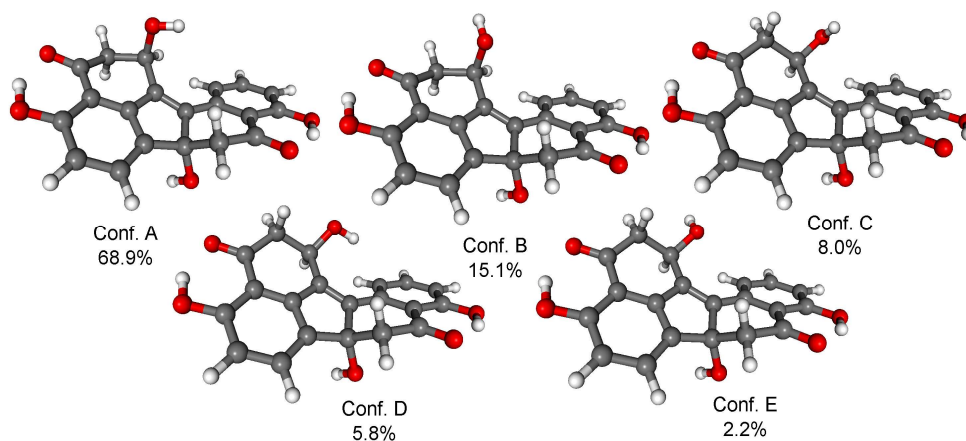


Figure 2. Structure and population of the low-energy B97D/TZVP PCM/MeCN conformers ($>2\%$) of (1*R*,6*bR*)-**1** diastereomer. Populations of the same conformers at B3LYP/TZVP PCM/MeCN level are 65.5%, 20.5%, 7.0%, 3.2% and 3.8% (order of last two conformers changed) while at CAM-B3LYP/TZVP PCM/MeCN level are 63.4%, 21.0%, 7.3%, 4.3% and 4.0%.

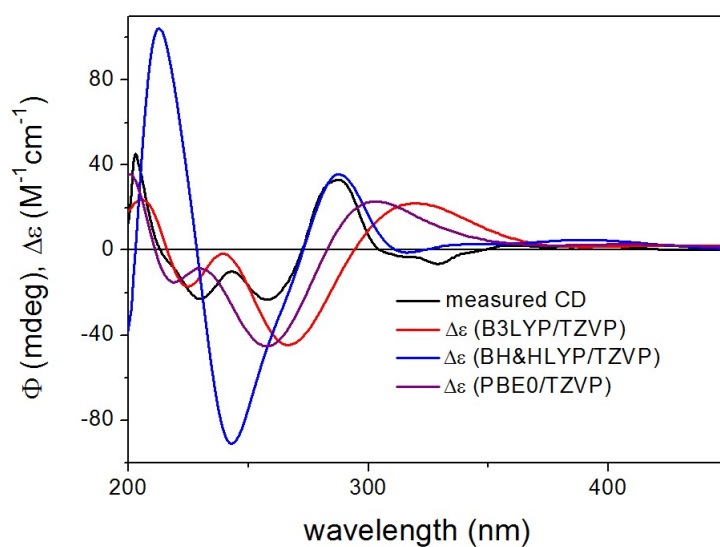


Figure 3. Experimental ECD spectrum of **1** compared with the Boltzmann-weighted ECD spectra computed for the B97D/TZVP PCM/MeCN low-energy conformers of (1*R*,6*R*)-**1** at various levels.

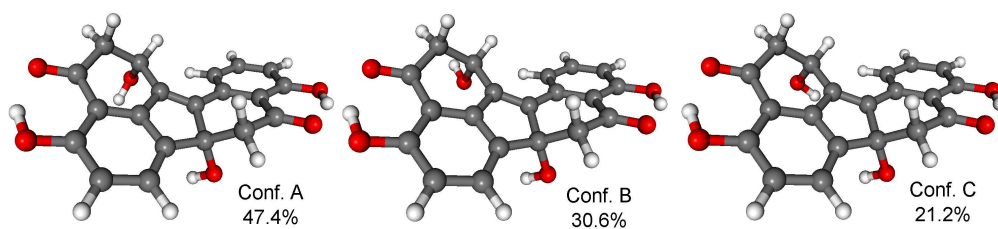


Figure 4. Structure and population of the low-energy B97D/TZVP PCM/MeCN conformers (>2%) of (1*S*,6*bR*)-**1** diastereomer. Populations of the same conformers at B3LYP/TZVP PCM/MeCN level are 33.0%, 47.2% and 18.4% (order of first two conformers changed) while at CAM-B3LYP/TZVP PCM/MeCN level are 25.9%, 53.2% and 19.0%.

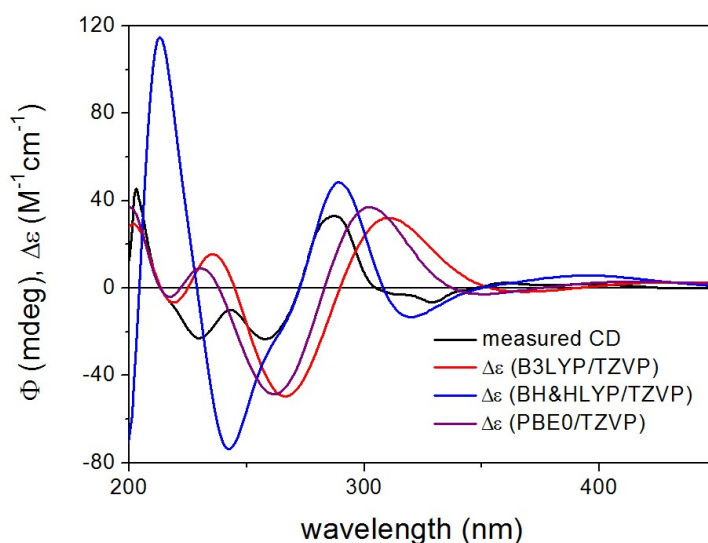


Figure 5. Experimental ECD spectrum of **1** compared with the Boltzmann-weighted ECD spectra computed for the B97D/TZVP PCM/MeCN low-energy conformers of (1*S*,6*bR*)-**1** at various levels.

ECD spectra computed for the B3LYP/6-31G(d) *in vacuo* and B97D/TZVP PCM/MeCN conformers performed better over 300 nm for the (1*S*,6*bR*) diastereomer, while the two negative Cotton effects (CEs) below 280 nm were reproduced better for the (1*R*,6*bR*) diastereomer. ECD spectra were also calculated for B3LYP/TZVP PCM/MeCN and CAM-B3LYP/TZVP^{26,27} PCM/MeCN conformers but these results were found similar to that of the B97D/TZVP PCM/MeCN method and the absolute configuration of C-1 could not be determined unambiguously.

Compound **2** was isolated as a red, amorphous powder. Its molecular formula was established as C₂₀H₁₂O₅ based on the prominent pseudomolecular ion peak observed at *m/z* 333.0756 [M+H]⁺ in the HRESIMS spectrum. The ¹H and ¹³C NMR data of **1** were similar to those of **2**, except for the deshielded signals resonating at δ_H 6.75 (δ_C 133.3, CH-1) and 8.23 (δ_C 134.7, CH-2), indicating that **2** is the dehydration product of **1** bearing an additional C1/2 double bond. In the HMBC spectrum of **2**, the correlations from H-2 to C-12b, C-12c, and C-3, as well as from H-1 to C-12c and C-3a corroborated this assumption. Notably, **1** was

observed to rapidly transform into **2** during the isolation procedure. Since **2** was not detected in the crude fungal extract, it is suggested to be an artefact arising from **1** during the isolation procedure. For compound **2** the name daldinone F is suggested.

The initial MMFF conformational search of the arbitrarily selected (*R*)-**2** resulted in a single conformer in a 21 kJ/mol energy window (Figure 6), which was reoptimized at B3LYP/6-31G(d) *in vacuo* level followed by ECD calculations at different levels. The calculated ECD spectra gave excellent agreement with the experimental one indicating (*R*) absolute configuration. Due to the nice agreement and limited conformational freedom, there was no need to use solvent model calculations in this case.

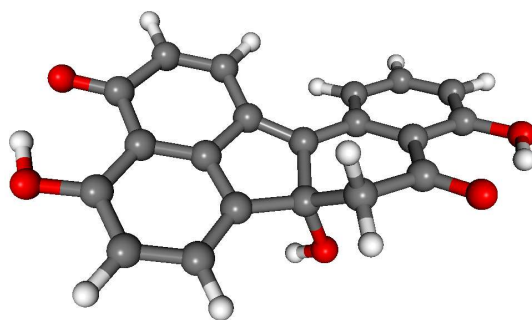


Figure 6. Structure of the computed conformer of (*R*)-**2** at B3LYP/6-31G(d) *in vacuo* level.

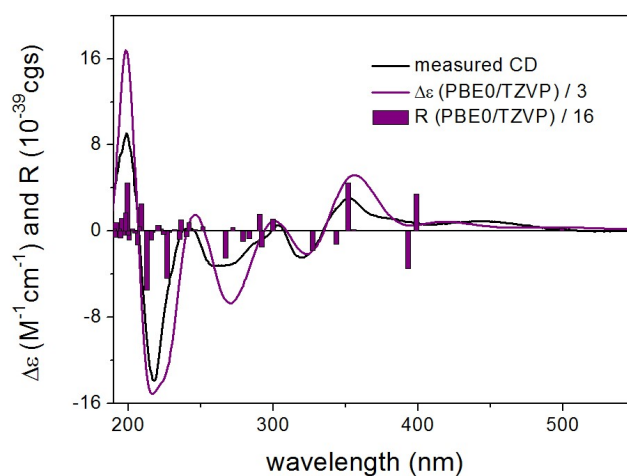


Figure 7. Experimental ECD spectrum of **2** in MeCN compared with the PBE0/TZVP PCM/MeCN ECD spectrum of the single conformer of (*R*)-**2** computed for the B3LYP/6-31G(d) optimized conformer. Bars represent the rotational strength of conformer A.

Compound **3** was isolated as a red, amorphous powder and displayed a very similar UV spectrum as **1**. Moreover, the HRESIMS exhibited a prominent ion peak at m/z 351.0862 $[M+H]^+$, indicating that both compounds shared the same molecular formula ($C_{20}H_{14}O_6$). Comparison of the 1H and ^{13}C NMR data of **3** to those of **1** revealed close similarity between both compounds, apart from the absence of the methylene group at δ_H 3.39/2.74 (δ_C 50.4, CH_2 -7 in **1**) and the presence of two vicinal methine signals at δ_H 4.13 (δ_C 58.7, CH-6b) and 3.99 (δ_C 77.7, CH-7) in **3** instead, as supported by the COSY spectrum. The above spectroscopic differences suggested that **3** is a positional isomer of **1** with the hydroxy group (6b-OH in **1**) located at C-7. This assumption was further corroborated by the HMBC correlations from H-6b to C-12a, C-12c, C-7, and C-8, as well as from H-7 to C-8 and C-6a. In addition, the large coupling constant between H-6b and H-7 ($^3J_{6b,7}=12.1$ Hz) suggested their *trans* relationship. Hence, **3** was identified as a new natural product and was named daldinone G.

Similarly to **1**, the relative configuration of C-1 could not be determined in the lack of characteristic NOE correlations, but a triplet signal for 1-H with 3.7 Hz coupling constant, suggested that 1-H preferably adopts equatorial orientation. The initial MMFF conformational searches were performed for the diastereomeric (1*R*,6*bS*,7*R*)- and (1*S*,6*bS*,7*R*)-**3** yielding 5 conformers for each in a 21 kJ/mol energy window. Similarly to the conformational analysis of **1**, the reoptimization of the MMFF conformers was carried at four levels of theory [B3LYP/6-31G(d) *in vacuo*, B97D/TZVP PCM/MeCN (Figure 8 and 10), B3LYP/TZVP PCM/MeCN and CAM-B3LYP/TZVP PCM/MeCN). The B3LYP/6-31G(d) *in vacuo* conformers of (1*R*,6*bS*,7*R*)-**3** showed that 1-H adopts preferably axial orientation, while those of (1*S*,6*bS*,7*R*)-**3** had larger population for conformers with equatorial 1-H. This difference diminished in the solvent model calculations, in which the conformers with equatorial 1-H were identified as the major ones for both diastereomers.

ECD spectra computed for B3LYP/6-31G(d) *in vacuo* and B97D/TZVP PCM/MeCN reoptimized conformers at various levels were nearly mirror-image to the experimental one for both diastereomers indicating (6*bR*,7*S*) absolute configuration. The C-1 chirality center has minor contribution to the ECD data and thus C-1 diastereomers could not distinguished by ECD calculations. The large negative specific rotation value of **3** prompted us to run OR calculations for the diastereomers. Similarly to the ECD calculations, the OR calculations of the diastereomers confirmed the (6*bR*,7*S*) absolute configuration but they were not suitable to determine the absolute configuration of C-1. Although both **1** and **3** had (6*bR*) absolute configuration, the geometry of their annulations is different as reflected by the opposite signs of the corresponding CEs. The (6*bR*) absolute configuration of **3** compares well with the reported absolute configuration of hypoxylonol C (**5**),²⁸ which may also suggest (1*S*) absolute configuration for **3**.

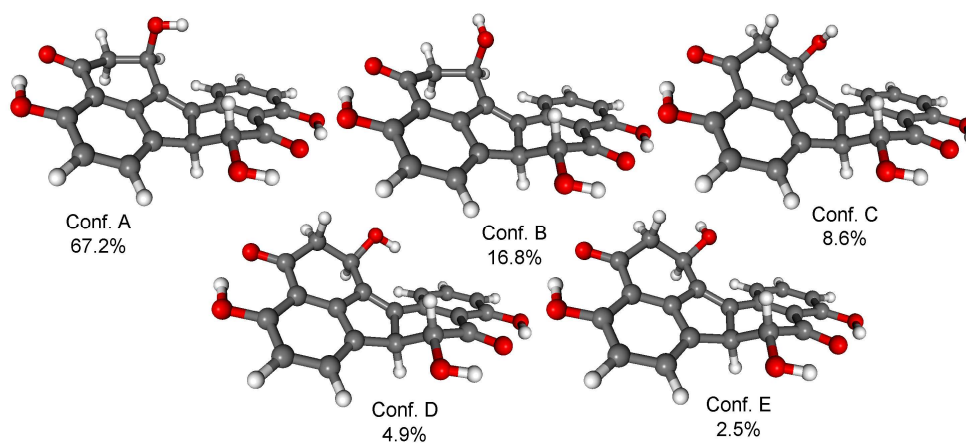


Figure 8. Structure and population of the low-energy B97D/TZVP PCM/MeCN conformers (>2%) of (1*R*,6*bS*,7*R*)-**3** diastereomer. Populations of the same conformers at B3LYP/TZVP PCM/MeCN level are 63.2%, 22.5%, 7.7%, 2.4% and 4.1% (order of last two conformers changed) while at CAM-B3LYP/TZVP PCM/MeCN level are 61.8%, 22.6%, 8.0%, 3.2% and 4.3%.

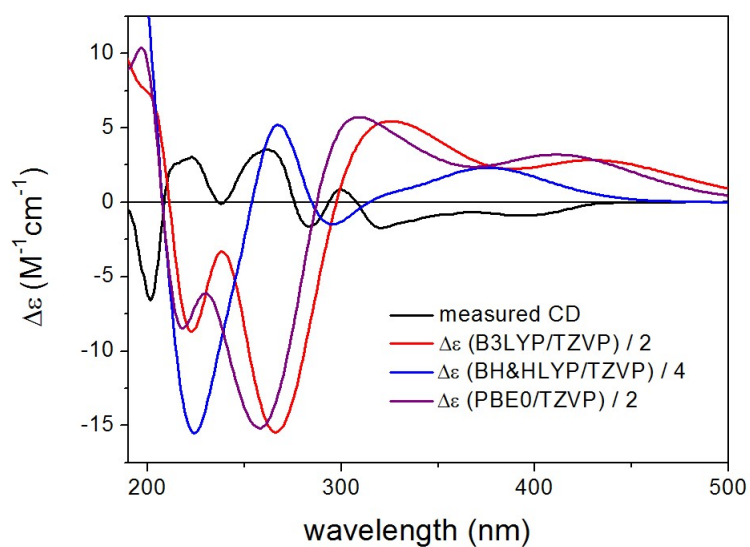


Figure 9. Experimental ECD spectrum of **3** compared with the Boltzmann-weighted ECD spectra computed for the B97D/TZVP PCM/MeCN low-energy conformers of (1R,6bS,7R)-**3** at various levels.

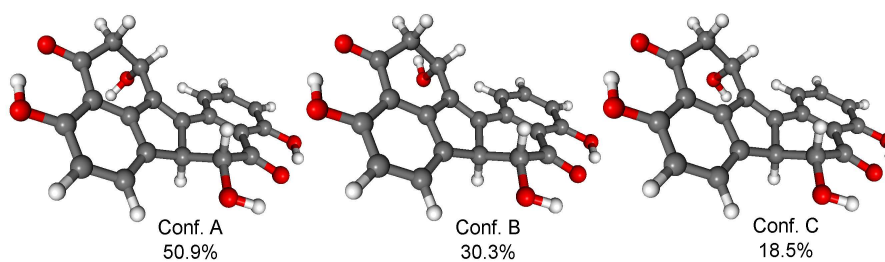


Figure 10. Structure and population of the low-energy B97D/TZVP PCM/MeCN conformers (>2%) of (1S,6bS,7R)-**3** diastereomer. Populations of the same conformers at B3LYP/TZVP PCM/MeCN level are 37.0%, 45.7% and 16.6% (order of first two conformers changed) while at CAM-B3LYP/TZVP PCM/MeCN level are 30.3%, 51.3% and 17.6%.

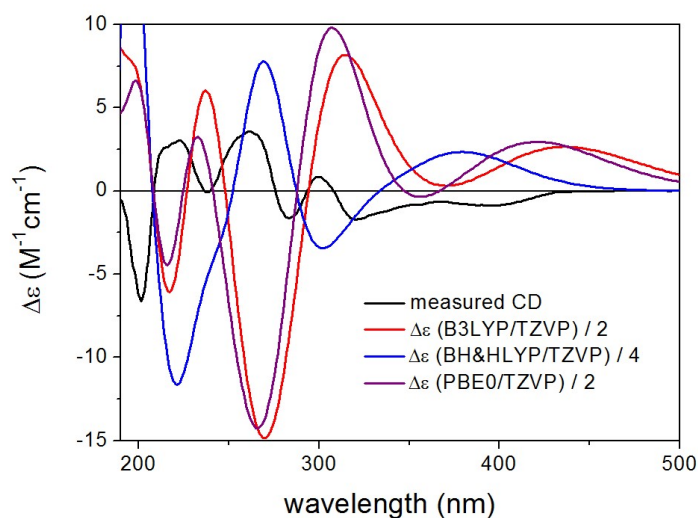


Figure 11. Experimental ECD spectrum of **3** compared with the Boltzmann-weighted ECD spectra computed for the B97D/TZVP PCM/MeCN low-energy conformers of (1*S*,6*bS*,7*R*)-**3** at various levels.

Table 1. NMR spectroscopic data of **1-3**

position	1^a		2^b		3^a	
	δ_C , type ^c	δ_H (<i>J</i> in Hz)	δ_C , type	δ_H (<i>J</i> in Hz)	δ_C , type ^c	δ_H (<i>J</i> in Hz)
1	63.5, CH	5.16, dd (4.9, 1.9)	133.3, CH	6.75 d (9.8)	63.6, CH	5.77, t (3.7)
2	47.8, CH ₂	3.14, dd (17.2, 4.9) 2.94, dd (17.2, 1.9)	134.7, CH	8.23 d (9.8)	47.2, CH ₂	3.20, dd (17.1, 3.7) 2.96, dd (17.1, 3.7)
3	201.7, C		188.3, C		200.9, C	
3a	114.1, C		113.4, C		112.0, C	
4	160.6, C		159.0, C		158.5, C	
5	115.2, CH	6.77, d (8.1)	114.5, CH	6.93 d (8.1)	114.8, CH	6.78, d (8.3)
6	131.0, CH	7.64, d (8.1)	128.7, CH	7.75 d (8.1)	133.8, CH	7.82, d (8.3)
6a	138.2, C		136.5, C		134.4, C	
6b	84.7, C		84.4, C		58.7, CH	4.13, d (12.1)
7	50.4, CH ₂	3.39, d (16.3) 2.74, d (16.3)	49.3, CH ₂	3.45 d (16.3) 2.97 d (16.3)	77.7, CH	3.99, d (12.1)
8	205.2, C		204.4, C		204.7, C	
8a	115.6, C		114.9, C		113.8, C	
9	163.3, C		162.1, C		162.6, C	
10	119.1, CH	6.98, d (8.0)	120.2, CH	7.15, dd (7.5, 0.5)	118.4, CH	6.95 dd, (7.0, 1.0)
11	137.7, CH	7.64, t (8.0)	137.6, CH	7.76, d (7.5)	138.3, CH	7.61 t, (7.0)

5 Publication 4

12	120.3, CH	7.51, d (8.0)	120.7, CH	7.64, dd (7.5, 0.5)	119.0, CH	7.53 dd, (7.0, 1.0)
12a	137.9, C		134.6, C		137.2, C	
12b	144.5, C		152.2, C		139.0, C	
12c	134.0, C		127.0, C		136.8, C	
12d	147.0, C		144.5, C		148.1, C	
4-OH				10.65, s		
6b-OH				6.23, s		
9-OH				12.34, s		

^aMeasured in CH₃OH-*d*₄ at 600 (¹H) and 150 (¹³C) MHz. ^bMeasured in DMSO-*d*₆ at 600 (¹H) and 150 (¹³C) MHz. ^cData extracted from HMBC and HSQC spectra.

The known compounds were identified as daldinone C (**4**),²⁹ hypoxylonol C (**5**),²⁸ daldinone B (**6**),³⁰ 3,4-dihydro-3,4,6,8-trihydroxy-1(2H)-naphthalenone (**7**),^{31,32} (R)-scytalone (**8**),²⁰ and 1-hydroxy-8-methoxynaphthalene (**9**)³³ based on their NMR and MS spectroscopic data and by comparison with the literature.

Co-cultivation of fungi and bacteria has repeatedly been shown to activate silent fungal biogenetic gene clusters, thus triggering the expression of compounds which are not detected in axenic fungal cultures or to enhance the accumulation of constitutively present metabolites cultures.³⁴ Several attempts were undertaken in this study to influence the pattern of fungal metabolites through co-cultivation of the fungus with bacteria, such as *Bacillus subtilis* 168 trpC2, *Bacillus cereus* T, *Streptomyces lividans* TK24 or *Streptomyces coelicolor* A2(3).^{35,36} Co-cultivation of the fungus with either *S. lividans* or *S. coelicolor* resulted in an up to 38-fold increase in the accumulation of the known compound 1-hydroxy-8-methoxynaphthalene (**9**) as shown by HPLC analysis. On the other hand, when the fungus was co-cultured with *B. subtilis* or with *B. cereus*, no effect on natural product accumulation was observed, hinting at a specificity of the fungal response towards different bacteria (see supporting information Fig. S20).

The isolated compounds (**2-5**, **7-9**) - apart from **1** and **6**, due to their chemical instability - were investigated for their antibacterial activity toward *Staphylococcus aureus* ATCC 25923, *Acinetobacter baumannii* ATCC BAA747, and *Mycobacterium tuberculosis*, however, none of them showed detectable activity when assayed at a dose of 10 μM . Initial screenings for cytotoxicity of the respective compounds in different cancer cell lines revealed that only compound **2** inhibited growth of the human lymphoma cell lines Jurkat J16 and Ramos in a dose-dependent manner. After 48 h of treatment, the determined IC_{50} values of compound **2** against Jurkat J16 and Ramos cells were 13.9 and 8.5 μM , respectively (Figure 12). Apparently, Burkitt's lymphoma (Ramos) cells are particularly sensitive toward its mode of action.

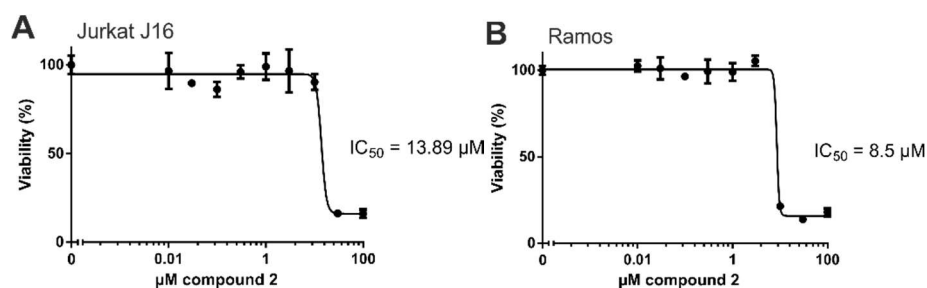


Figure 12. Cytotoxic effect of compound **2** on human lymphoma cell lines measured by MTT assay.

(A) Jurkat J16 cells (T-cell lymphoma cells) and (B) Ramos cells (Burkitt's lymphoma B lymphocytes) were seeded at a density of 0.5×10^6 cells/mL and incubated with increasing concentrations of compound **2**. Cells treated with DMSO (0.1% v/v) for 48 h were used as negative control. After incubation period of 48 h cell viability was monitored using the MTT Assay as described in methods. Relative viability in DMSO treated control cells was set to 100%. Data points shown are the mean of triplicates, error bars=SD. Viability and IC_{50} values (IC_{50} =half maximal inhibitory concentration) were calculated using Prism 6 (GraphPad Software).

To evaluate the potential contribution of proapoptotic mechanisms of compound **2** with regard to the observed cytotoxicity, we analyzed activation of caspase-3 through two different methods - on the one hand by immunoblotting of the caspase-3 substrate PARP and on the other hand by measuring the fluorescence of the profluorescent caspase-3 substrate

Ac-DEVD-AMC. Apoptosis is a programmed form of cell death, which is generally characterized by distinct activation of cysteine-dependent aspartate-directed proteases (caspases), leading to DNA fragmentation and finally to cell death. First we detected cleavage of PARP after treatment with compound **2** for 24 h via immunoblotting. In both Jurkat J16 and Ramos cells the treatment with 10 μ M of **2** for 24 h lead to an explicit cleavage of PARP, indicating activation of caspases and therefore induction of apoptosis (Figure 13). To ensure caspase dependency of the observed cleavage of PARP, the cells were co-incubated with the pan-caspase inhibitor N-(2-Quinolyl)-L-valyl-L-aspartyl-(2,6-difluorophenoxy) methylketone (QVD). This co-incubation entirely abrogates compound **2**-induced cleavage of PARP. In the next step, activation of caspase-3 was detected fluoroscopically, to confirm compound **2**-related induction of apoptosis. Treatment with **2** at concentrations up to 10 μ M leads to cleavage of the profluorescent caspase-3 substrate Ac-DEVD-AMC within a few hours (Figure 14), indicating once again activation of caspases and induction of apoptosis by compound **2**. In Ramos cells, the kinetic of **2**-induced activation of caspase-3 appears to be as fast as the kinetic of activation by the extremely potent apoptosis inducer staurosporine.

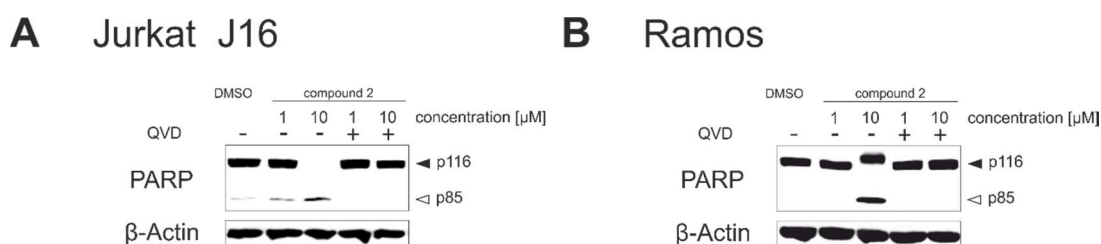


Figure 13. Compound **2** induces apoptosis.

(A) Jurkat J16 cells (T-cell lymphoma cells) and (B) Ramos cells (Burkitt's lymphoma B lymphocytes) were treated with the indicated concentrations of **2** in the absence or presence of the caspase inhibitor QVD-OPh (10 μ M) for 24 h. After incubation period cleavage of Poly (ADP-ribose) polymerase-1 (PARP) was determined by Western blot analysis. Solid arrowheads indicate the uncleaved form of PARP, open arrowheads indicate the cleaved form. The expression of β -actin was determined as protein loading control. Shown is the result of a representative blot.

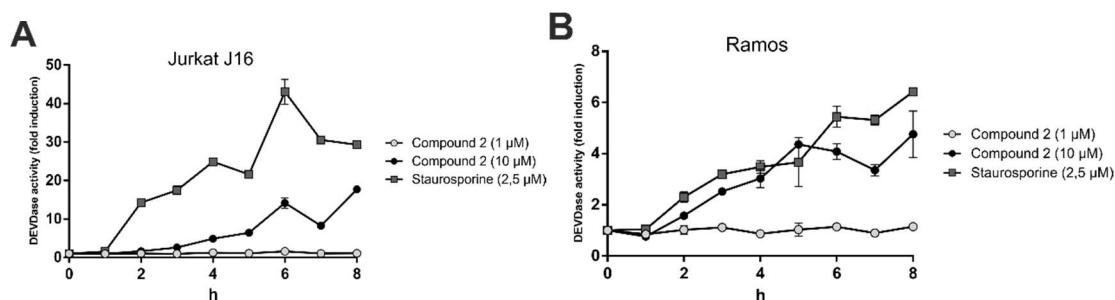


Figure 14. Compound **2** activates caspase-3 with rapid kinetics.

The kinetics of Caspase-3 activation in (A) Jurkat cells (T-cell lymphoma cells) and (B) Ramos cells (Burkitt's lymphoma B lymphocytes) after treatment with indicated concentrations of **2** were compared to those of staurosporine (STS, 2.5 μ M), a well-established inducer of apoptosis. Caspase-3 activity was measured by the rate of cleavage of the profluorescent Caspase-3 substrate Ac-DEVD-AMC. Relative caspase-3 activity in DMSO (0.1% v/v) treated control cells was set to 1. Data shown are the mean \pm SD from a representative experiment performed in triplicate.

In order to characterize the proapoptotic effect of **2** more precisely, we performed flow cytometry based analyses with caspase-9 deficient and caspase-9 reconstituted Jurkat cells. The signaling network of induction and execution of apoptosis is highly complex and consists of many regulatory pathways, but the extrinsic (death receptor) pathway and the intrinsic (mitochondrial) pathway are canonically considered as the two core pathways to induce apoptosis. While caspase-8 is the key player of the extrinsic pathway, caspase-9 is the corresponding key player of the intrinsic pathway.³⁷ Therefore, experiments with cells lacking these key players can shed light on the pathway triggered by **2** in more detail. To determine caspase-related degradation of DNA by **2**, we measured the amount of hypodiploid nuclei after treatment with **2** for 24 h. Comparative experiments in Jurkat cells lacking caspase-9 and in Jurkat cells, reconstituted with caspase-9 revealed that caspase-9 is indispensable for execution of **2**-induced apoptosis (Figure 15). Thus, **2** apparently induces intrinsic, but not extrinsic apoptosis.

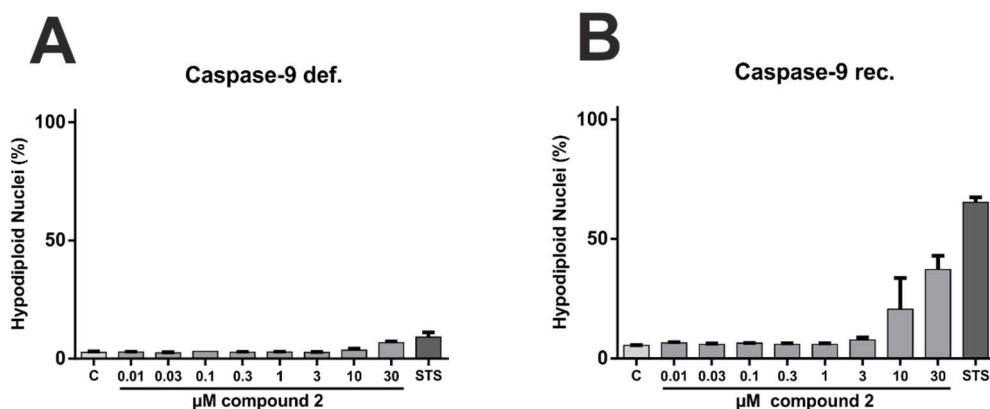


Figure 15. Compound 2-induced apoptosis in caspase-9 dependent.

Induction of apoptosis by **2** in (A) caspase-9 deficient and in (B) caspase-9 reconstituted Jurkat JMR cells (T-cell lymphoma cells) was assessed by flow cytometry to detect apoptotic DNA fragmentation, resulting in hypodiploid nuclei. After incubation period of 24 h cells were processed and measured as described in methods. Cells treated with staurosporine (STS, 2.5 μ M), a well-established inducer of apoptosis, served as positive control. Data shown are the mean \pm SD from a representative experiment performed in triplicate.

Autophagy is a major intracellular catabolic mechanism responsible for the degradation of cytosolic components through lysosomes and plays an important role in cellular homeostasis.³⁸ The ability to recycle unnecessary or dysfunctional components makes the process of autophagy essential for survival under conditions of starvation. Due to its crucial role regarding pro-survival signaling of fast proliferating cancer cells, suffering from starvation stress, autophagy is considered as a promising target in anticancer therapy.^{39,40} In order to determine potential effects of **2** regarding regulation of autophagy, we used MEF cells stably expressing mCitrine-hLC3B and analyzed lysosomal degradation of mCitrine-hLC3B upon starvation and treatment with either **2** or with the known autophagy inhibitor bafilomycin A1 via flow cytometry. LC3 is a major component of the double membraned structure called autophagosome, which delivers cytoplasmic components to the lysosomes and gets degraded by the lysosomal degradation system in the course of autophagy. Thereby, degradation of LC3 can be used as an indicator of autophagy. Incubation with **2** almost entirely blocked starvation-induced degradation of LC3, strongly indicating inhibition of autophagy by **2** (Figure 16).

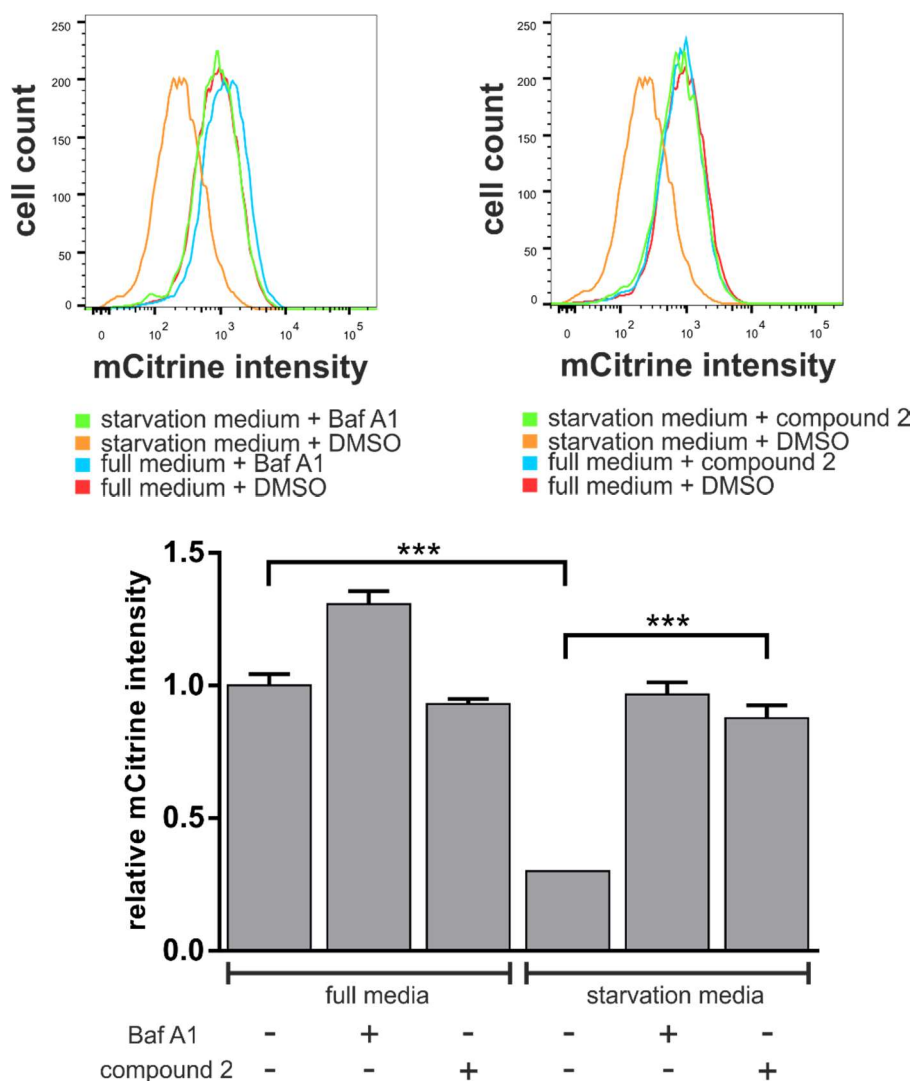


Figure 16. Compound 2 blocks amino acid starvation-induced autophagy.

Wild-type murine embryonic fibroblasts (MEFs) stably expressing mCitrine-hLC3B were cultivated in full medium or starvation medium (EBSS) with or without 10 nM bafilomycin A₁ (Baf A1) for 6 h. Total cellular mCitrine-hLC3B signals were analyzed by flow cytometry. (A) Representative FACS data from 3 independent experiments are shown. (B) The median of fluorescence intensity was plotted in a bar diagram. Values are normalized to DMSO (0.1 % v/v) treated cells cultivated in full medium (100 %) and represent mean \pm SD. ***P < 0.001 (Student's t-test, two-sample assuming unequal variances).

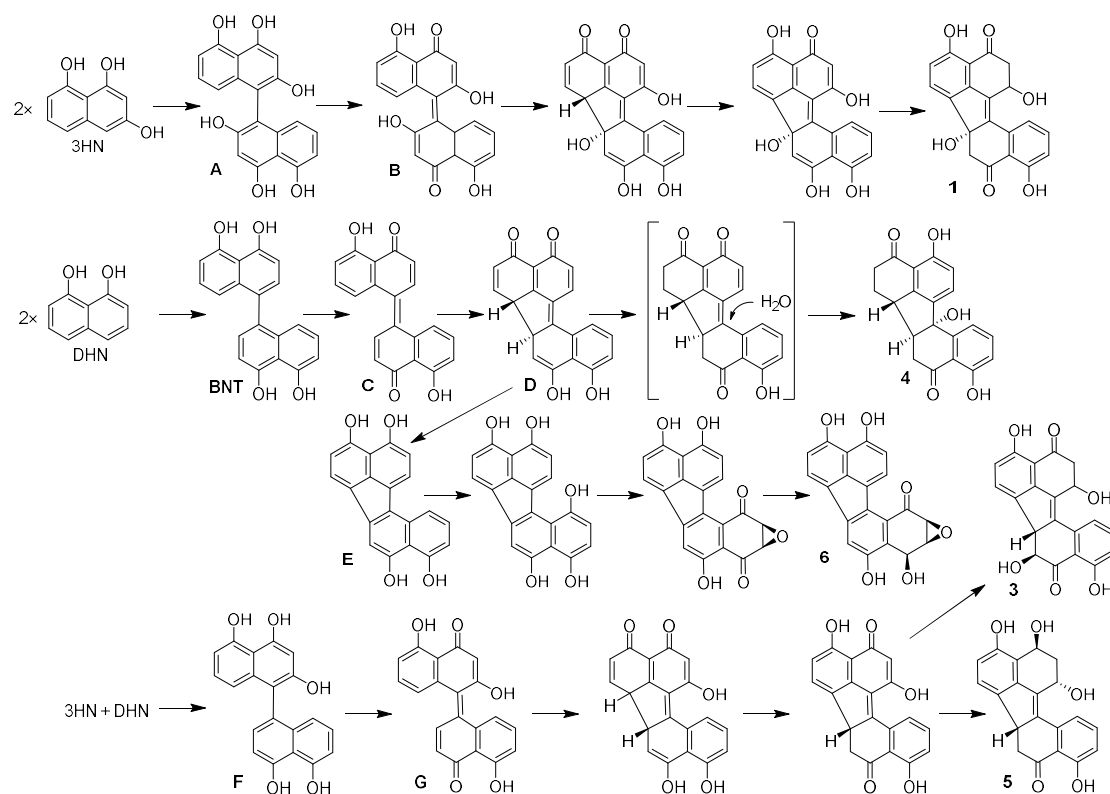


Figure 17. Proposed biogenetic pathway of isolated benzo[*j*]fluoranthene derivatives

A possible biogenetic pathway for the isolated compounds **1** and **3-6** includes a combination of one starter unit acetyl-CoA and four extender units malonyl-CoA to afford a polyketide, which undergoes condensation reactions to form 1,3,6,8-tetrahydroxynaphthalene (4HN). Moreover, it is known that 1,3,8-trihydroxynaphthalene (3HN) and 1,8-dihydroxynaphthalene (DHN) can be easily formed from 4HN under the tandem catalyses by 4HN and 3HN reductases.^{21,41} Oxidative coupling of two 3HN precursors could result in the formation of the binaphthalene derivative **A**, which is further oxidized to the dinaphthoquinone intermediate **B**. Spontaneous cyclization of the latter, resembling a Michael-addition reaction, would result in the formation of the benzo[*j*]fluoranthene-ring skeleton, and subsequent aromatization and hydrogenation would generate **1**. A second biogenetic route could include oxidative coupling of two DHN monomers to [1,1'-binaphthalene]-4,4',5,5'-tetrol (**BNT**), which can be transformed by oxidation and cyclization

reactions to generate intermediates **C** and **D**. The latter (**D**) would then undergo hydrogenation and water addition to form **4**. Complete aromatization of **D**, and subsequent oxidation and hydrogenation reactions would finally result in the formation of **6**. In a similar manner, the putative biosynthesis of **3** and **5** is suggested to start with an oxidative coupling of 3HN and DHN. The resulting binaphthalene **F** could be oxidized to **G**, which would then undergo cyclization, aromatization, oxidation, and hydrogenation reactions (Figure 17).

For an experimental support of the proposed biosynthetic route of the analyzed fungal constituents commercially available 1,8-dihydroxynaphthalene (DHN) was added to fungal cultures growing on solid rice medium at concentrations of 80mg, of 120mg or of 160mg per flask. Analysis of the resulting crude fungal extracts by HPLC revealed a pronounced increase of the accumulation of compounds **1** and **6** in a dose-dependent manner. The strongest increase of both compounds was observed in the presence of 120 mg DHN per flask. This induction of **6**, which is the main compound produced by the fungus, is in accordance with the proposed biosynthetic pathway, starting from oxidative coupling of two DHN units. Interestingly, the production of **1**, which is assumed to be biosynthesized from two 3HN units and was likewise enhanced, suggests a biochemical equilibrium between DHN and 3HN under catalysis of 3HN-reducases present in the metabolism of the fungus as described in Figure 18.

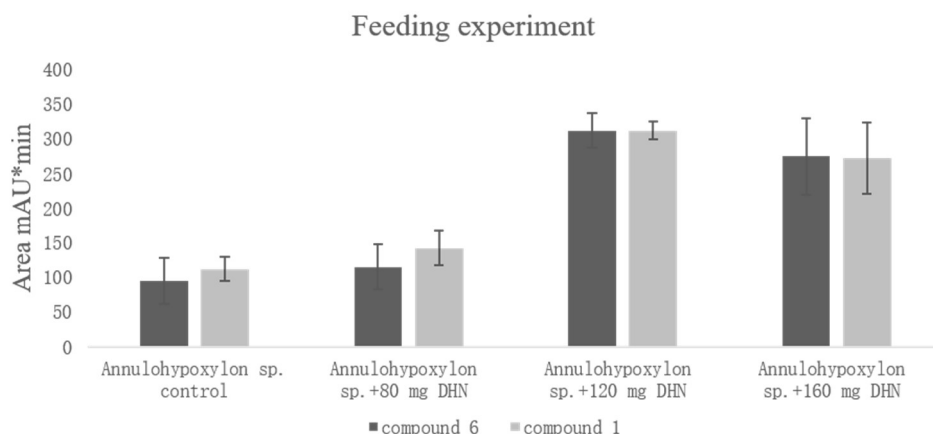


Figure 18. Feeding experiments of *Annulohypoxyton* sp. with 1,8-dihydroxynaphthalene (DHN) in three different concentrations 80 mg, 120 mg, and 160 mg. The yield per flask of **1** and **6** is indicated by the corresponding area of UV absorption. Data are means of three independent experiments (n=3)

Conclusion

The distinct cytotoxicity of **2** against human lymphoma cell lines was determined to be caused by induction of intrinsic apoptosis. Moreover it could be shown, that **2** potently blocks autophagy, a potential pro-survival pathway for cancer cells. Summing up, due to this dual activity regarding induction of apoptosis and inhibition of autophagy, compound **2** appears to be an interesting lead compound for further *in vivo* studies illuminating its usability in anticancer therapy. These subsequent studies could also shed more light on the mechanisms of compound **2**-related effects on apoptosis and autophagy.

Experimental Section

General Experimental Procedures: Optical rotations were determined on a Perkin-Elmer-241 MC polarimeter. ^1H , ^{13}C , and 2D NMR spectra were recorded at 25 °C in DMSO- d_6 and MeOD- d_4 on Bruker AVANCE DMX 600 NMR spectrometers. Chemical shifts were referenced to the solvent residual peaks, δ_{H} 2.50 (DMSO- d_6) and 3.31 (CH₃OH- d_4) ppm for

^1H , and δc 39.51 (DMSO- d_6) and 49.15 (CH₃OH- d_4) ppm for ^{13}C . Mass spectra (ESI) were recorded with a Finnigan LCQ Deca mass spectrometer, and HRMS (ESI) spectra were obtained with a FT-MS-Orbitrap (Thermo-Finnigan) mass spectrometer. Solvents were distilled prior to use and spectral grade solvents were used for spectroscopic measurements. HPLC analysis was performed with a Dionex UltiMate3400 SD with a LPG-3400SD Pump coupled to a photodiode array detector (DAD3000RS); routine detection was at 235 nm, 254 nm, 280 nm, and 340 nm. The separation column (125×4 mm) was pre-filled with Eurosphere-10 C18 (Knauer, Germany), and the following gradient was used (MeOH, 0.1% HCOOH in H₂O): 0 min (10% MeOH); 5 min (10% MeOH); 35 min (100% MeOH); 45 min (100% MeOH). Semipreparative HPLC was performed using a Merck Hitachi HPLC System (UV detector L-7400; Pump L-7100; Eurosphere-100 C18, 300×8 mm, Knauer, Germany). Column chromatography included LH-20 Sephadex and Merck MN Silica gel 60 M (0.04-0.063 mm). TLC plates with silica gel F254 (Merck, Darmstadt, Germany) were used to monitor fractions; detection was under UV at 254 nm and 366 nm or by spraying the plates with anisaldehyde reagent followed by heating. Bacterial growth was monitored by measuring the OD₆₀₀ in a Tecan microtiter plate reader (InfiniteM200, Tecan). ECD spectra were recorded on a J-810 spectropolarimeter. HPLC separations of **1** and **2** were performed with a Jasco HPLC system using Chiralpak IA column with 250 mm x 4.6 mm i.d., 5 μm (Daicel, Chemical Industries, Ltd.) and *n*-hexane/propan-2-ol eluent at a flow rate of 1.0 mL/min). HPLC-UV chromatograms were recorded with Jasco MD-910 multiwavelength detector. The on-line ECD and UV spectra of **1** were measured simultaneously by stopping the flow at the UV absorption maximum of each peak. The values of the ECD ellipticity (ϕ) were not corrected for the concentration.

Microbial Material: The endophytic fungus was isolated from fresh fruits of the mangrove *Rhizophora racemosa* collected in Cameroon in September 2013. The isolation was

performed as described before,⁴² and the fungus was identified by using a molecular biological protocol by DNA amplification and sequencing of the 18S-28S rDNA region.⁴³ The identification of the fungus was done by sequencing 3,952 bp of the 18S-28S rDNA region, followed by BlastN search in the NCBI-database. A phylogenetic tree that covers the highest number of homologous sequences in the database was generated. The 18S-28S rDNA sequence from nt 28 – nt 3357 exhibited 64.5% homology to a sequence of respective length of *Xylariaceae* sp. YX28 (e.g. accession number DQ022414), suggesting that the fungus belongs to the class of Xylariales (see Fig. S1 in the Supporting Information). The BlastN analysis of the 18S rDNA sequence from nt 54 – nt 1400 that comprised a region more commonly sequenced and thus more often found in the database in full length, showed 76.4% homology to *Annulohypoxyton artroroseum* (e.g. accession number U32411) of the order Xylariales, and from nt 2415 – nt 3906 a 97.75% homology to *Annulohypoxyton* sp. (acc-no JQ747656). Based on these data we nominate this fungus as *Annulohypoxyton* sp. (see Fig. S2 in the Supporting Information). A voucher strain was kept at one of the authors' laboratory (P.P.). The bacterial strains used for co-cultivation were standard laboratory strains: *Bacillus subtilis* 168 trpC2, *Bacillus cereus* T, *Streptomyces lividans* TK24, and *Streptomyces coelicolor* A2(3).

Fermentation: The fungus was cultivated on solid rice medium in twelve Erlenmeyer flasks. Solid rice medium was prepared by adding demineralized water (110 mL) to rice (100 g) in an Erlenmeyer flask, followed by autoclaving (121 °C, 20 min). The fungus, which nearly covered the whole surface of a petri dish, was inoculated onto this sterile rice medium under the clean bench and was allowed to grow (20 °C) for 25 days.

Co-cultivation experiments of RH with *B. subtilis* 168 trpC2 and *B. cereus* T

The fungal and bacterial strains were cultivated on solid rice media involving 15 Erlenmeyer flasks (3 flasks for *Annulohyphoxylon* sp. control, 3 flasks for *B. subtilis* control, 3 flasks for *B. cereus* control, 3 flasks for co-cultivation of *Annulohyphoxylon* sp. with *B. subtilis*, 3 flasks for co-cultivation of *Annulohyphoxylon* sp. with *B. cereus*). Each flask (1 L) containing 110 mL of distilled water and 100 g of commercially available milk rice (Milch-Reis, ORYZA) was autoclaved before inoculating the fungus and the bacteria.

B. subtilis and *B. cereus* were grown in lysogeny broth (LB) medium. Overnight cultures of *B. subtilis* and *B. cereus* were used to inoculate prewarmed LB medium (1:20), which was then incubated at 37 °C with shaking at 200 rpm to mid exponential growth phase (optical density at 600 nm (OD₆₀₀) of 0.2–0.4). An amount of 10 ml *B. subtilis* (6 flasks) and *B. cereus* (6 flasks) respectively was inoculated to rice medium and the inoculated flasks were kept in an incubator (37 °C) for 4 days. After this preincubation, to each flask containing *B. subtilis* or *B. cereus* 5 pieces (1 × 1 cm²) of *Annulohyphoxylon* sp. growing on malt agar were added to the rice medium.

Co-cultivation and axenic cultures of the fungus and bacterial control were kept at room temperature (20 °C) until they reached their stationary phase of growth (3 weeks for controls of the fungus and 4 weeks for co-cultivation). Then 500 mL of EtOAc was added to the cultures to stop the growth of cells followed by shaking of the flasks at 150 rpm for 8 h. The cultures were then left overnight and filtered on the following day using a Büchner funnel. EtOAc was removed by a rotary evaporation. Each extract was then dissolved in 50 mL of MeOH, and 10 µL of this was injected into the analytical HPLC.

Co-cultivation experiments of the fungus with *S. coelicolor* A2(3) and *S. lividans* TK24

Fifteen Erlenmeyer flasks (3 flasks for *Annulohypoxyton* sp. control, 3 for co-cultivation of *Annulohypoxyton* sp. and *S. coelicolor*, 3 for co-cultivation of *Annulohypoxyton* sp. and *S. lividans*, 3 for *S. coelicolor* control, 3 for *S. lividans* control) containing 110 mL of Yeast Malt (YM) medium and 100 g of commercially available milk rice (Milch-Reis, ORYZA) were autoclaved before inoculating the fungus and bacteria. An overnight culture of *S. coelicolor* or of *S. lividans* was used to inoculate prewarmed YM medium (1:20), which was then incubated at 30 °C with shaking at 200 rpm to mid exponential growth phase. This preculture was then incubated in fresh YM medium overnight to reach mid exponential growth phase. A volume of 10 ml *S. coelicolor* (6 flasks) and *S. lividans* (6 flasks) respectively was inoculated to rice medium and incubated (30 °C) for 4 days. Then the same process was carried out as described for the experiment of co-cultivation of the fungus with *B. subtilis* or with *B. cereus*.

Feeding experiments of 1,8-dihydroxynaphthalene

Twelve Erlenmeyer flasks containing 90 mL demineralized water and 100 g of commercially available milk rice (Milch-Reis, ORYZA) were autoclaved. Afterwards, three different amounts (80mg, 120mg, 160mg) of 1,8-dihydroxynaphthalene (DHN) were dissolved in 20 ml autoclaved water and each added to the autoclaved rice medium by sterile filtration (n = 3). Controls were only treated with autoclaved water. Next, the fungus was inoculated onto the medium. Flasks treated with DHN or controls lacking DHN were allowed to grow in the incubator (30 °C) for two weeks.

Cell lines and reagents

T-cells (Jurkat J16, no. ACC-282) and Burkitt's lymphoma B cells (Ramos, no. ACC-603) were obtained from the German Collection of Microorganisms and Cell Cultures

(DSMZ, Germany). Wild-type murine embryonic fibroblasts (MEFs, kindly provided by Xiaodong Wang)⁴⁴ expressing mCitrine-hLC3B were generated by retroviral gene transfer using pMSCVpuro/mCitrine-hLC3B. To generate pMSCVpuro/mCitrine-hLC3B, full-length human *MAP1LC3B* cDNA was cloned into pMSCVpuro/mCitrine vector (kindly provided by Michael Engelke, University of Göttingen, Germany). Caspase-9-deficient Jurkat JMR cells stably transfected with vector control or caspase-9 were previously described.⁴⁵ All cell lines were grown at 37 °C under humidified air supplemented with 5% CO₂ in RPMI 1640 (Jurkat J16, Jurkat JMR, Jurkat JMR reconstituted with caspase-9, Ramos) or DMEM (mCitrine-hLC3B-MEF) containing 10% fetal calf serum, 1% HEPES, 120 IU/mL penicillin, and 120 µg/mL streptomycin. The broad-range caspase inhibitor N-(2-Quinolyl)-L-valyl-L-aspartyl-(2,6-difluorophenoxy) methylketone [(QVD), #SML0063], the autophagy inhibitor bafilomycin A1 [(Baf A1), #B1793] and the kinase inhibitor Staurosporine [(STS), #S5921], used as positive control for induction of apoptosis, were obtained from Sigma-Aldrich. The profluorescent caspase-3 substrate Ac-DEVD-AMC was purchased from Biomol (# ABD-13402).

Determination of cell viability

Jurkat J16 cells and Ramos cells were seeded at a density of 2.5×10^5 cells/mL and incubated with different concentrations of compound **2** for 48 h. Cells treated with DMSO (0.1% v/v) for 48 h were used as negative control. After incubation for 48 h MTT (3-(4,5-Dimethyl-2-thiazolyl)-2,5-diphenyl-2H-tetrazolium Bromide; Calbiochem #475989) was added to the cells to a final concentration of 1 mg/mL, the cells were incubated further for 60 min and then centrifuged at 600 rcf for 5 min. The medium was aspirated and 100 µL DMSO were added to each well to extract the formazan product from the cells. After 25 min of incubation on a shaker at room temperature, the absorbance at 650 nm (reference wavelength)

and 570 nm (test wavelength) was measured using a multiplate reader (Synergy Mx, BioTek). Viability and IC₅₀ values (IC₅₀ = half maximal inhibitory concentration) were calculated using Prism 6 (GraphPad Software). Relative viability of DMSO (0.1 % v/v) treated control cells was set to 100%.

Western blot analysis

Ramos and Jurkat J16 cells were treated with the indicated concentrations of compound **2**. Coincubation with the caspase inhibitor Q-VD-OPh at a concentration of 10 μ M was used as proof of caspase-dependency of the observed effects. After incubation time of 24 h, cells were pelleted at 600 rcf at 4 °C for 5 min, washed with PBS and frozen in liquid nitrogen. The cells were lysed in ice-cold lysis buffer [(20 mM Tris-HCl, pH 7.5, 150 mM NaCl, 0.5 mM EDTA, 1% Triton X-100, 10 mM NaF, 2.5 mM Na₄P₂O₇, 10 μ M Na₂MoO₄, 1 mM Na₃VO₄, protease inhibitors (Sigma #P2714)]. The lysates were cleared from cell debris by centrifugation at 11,000 rcf at 4°C for 15 min and the total protein concentration was measured by Bradford assay and adjusted to equal concentrations. After loading with Laemmli buffer and heating to 95 °C for 5 min, 25 μ g of the protein extract was separated by SDS-PAGE [8 % tris-glycine polyacrylamide gel (v/v)] and transferred to a PVDF membrane by Western blotting according to a standard protocol. Analysis of proteins of interest was performed using primary mouse antibodies to Poly (ADP-ribose) polymerase-1 (Enzo Life Sciences #BML- SA250) or β -actin (Sigma-Aldrich #A5316) and IRDye800-conjugated secondary antibodies (LI-COR Biosciences #926-32210/11). Signals were detected with an infrared imaging system.

Caspase-3 activity assay

Jurkat J16 cells and Ramos cells were seeded at a density of 1×10^6 cells/mL in 96-well microtiter plates and incubated with different concentrations of compound **2** for the indicated

times. Cells treated with DMSO (0.1% v/v) were used as negative control. After incubation period, cells were harvested by centrifugation at 600 rcf at 4°C and lysed by incubation with ice-cold lysis buffer (20 mM HEPES, 84 mM KCl, 10 mM MgCl₂, 200 μM EDTA, 200 μM EGTA, 0.5% NP-40, 1 μg/mL Leupeptin, 1 μg/mL Pepstatin, 5μg/mL Aprotinin) for 10 minutes. After addition of 150 μl reaction buffer (50 mM HEPES, 100 mM NaCl, 10% Sucrose, 0.1% CHAPS, 2 mM CaCl₂, 13.35 mM DTT, 70 μM DEVD-AMC) per well, fluorescence (Ex 360nm, Em450 nm) was measured at 37 °C over a time course of 150 min using a multiplate reader (Synergy Mx, BioTek). Caspase activity was determined as the slope of the resulting linear regressions. Data points shown are the mean of triplicates, error bars=SD. Values are normalized to DMSO (0.1 v/v) treated cells (fold change = 1.00).

FACS-based analysis of apoptotic cell death

Caspase-9-deficient Jurkat cells stably transfected with vector control or caspase-9 cDNA were treated with the indicated concentrations of compound **2** for 24 h. Cells treated with DMSO (0.1 % v/v) served as negative control and cells treated with the kinase inhibitor staurosporine (2.5 mM) as positive control. After incubation period nuclei were prepared by lysing cells in hypotonic lysis buffer (1% sodium citrate, 0.1% Triton X-100, 50 μg/ mL propidium iodide) at 4 °C overnight. Subsequently, DNA content was analyzed by flow cytometry. Nuclei with a DNA content below that of nuclei of healthy G0/G1 cells were considered as apoptotic.⁴⁶ Data points shown are the mean of triplicates, error bars=SD.

FACS-based analysis of autophagy

MEF cells stably expressing mCitrine-hLC3B were cultured in the indicated medium for 6 h with or without bafilomycin A1 or compound **2**, harvested with 0.05% trypsin-EDTA, and washed once with phosphate-buffered saline. Subsequently, the intensity of mCitrine

fluorescence was analyzed by flow cytometry using FACSDiva software. Reduction of mCitrine-hLC3B compared to medium control indicates autophagy induction.

Extraction and Isolation: The crude extract of fungal cultures was subjected to liquid-liquid separation between *n*-hexane and 90% aqueous MeOH. The resulting MeOH fraction (8.2 g) was separated by vacuum liquid chromatography on silica gel, using solvents in a gradient of increasing polarity – *n*-hexane-ethyl acetate-dichloromethane-methanol – to generate 6 fractions. Each fraction was submitted to Sephadex LH-20 and eluted with DCM-MeOH (1:1) to remove black pigments. Final purification was carried out by semipreparative HPLC to yield **1** (1:1 mixture with **2**, 4.2 mg), **2** (14.7 mg), **3** (1.1 mg), **4** (3.2 mg), **5** (4.6 mg), **6** (4.4 mg), **7** (11.2 mg), **8** (20.6 mg), **9** (5.5 mg).

Daldinone E (**1**): red powder; UV [MeOH, photodiode array (PDA)]: $\lambda_{\max} = 200, 242, 292, 397$ nm. ^1H (600 MHz) and ^{13}C (150 MHz) NMR, see Table 1; ESI-MS m/z 351.2 $[\text{M}+\text{H}]^+$, 349.1 $[\text{M}-\text{H}]^-$; HRESIMS m/z 351.0865 $[\text{M}+\text{H}]^+$ (calcd for $\text{C}_{20}\text{H}_{15}\text{O}_6$, 351.0863). (6*bR*)-**1**: $t_{\text{R}} = 7.07$ min on a Chiralpak IA column (hexane/2-propanol 80:20); HPLC-ECD {hexane/2-propanol 80:20, λ [nm] (ϕ)}.

Daldinone F (**2**): red powder; $[\alpha]_{\text{D}}^{20} = -154$ (c 0.35, MeOH); UV [MeOH, photodiode array (PDA)]: $\lambda_{\max} = 201, 235, 335, 462$ nm; ECD {acetonitrile, λ [nm] ($\Delta\epsilon$)}; ^1H (600 MHz) and ^{13}C (150 MHz) NMR, see Table 1; ESI-MS m/z 333.1 $[\text{M}+\text{H}]^+$, 331.0 $[\text{M}-\text{H}]^-$; HRESIMS m/z 333.0756 $[\text{M}+\text{H}]^+$ (calcd for $\text{C}_{20}\text{H}_{12}\text{O}_5$, 333.0757).

Daldinone G (**3**): red powder; $[\alpha]_{\text{D}}^{20} = -180$ (c 0.25, MeOH) (c 0.25, MeOH); UV [MeOH, photodiode array (PDA)]: $\lambda_{\max} = 201, 242, 292, 398$ nm; ECD {acetonitrile, λ [nm] ($\Delta\epsilon$)}; ^1H (600 MHz) and ^{13}C (150 MHz) NMR, see Table 1; ESI-MS m/z 351.3 $[\text{M}+\text{H}]^+$, 349.1 $[\text{M}-\text{H}]^-$; HRESIMS m/z 351.0862 $[\text{M}+\text{H}]^+$ (calcd for $\text{C}_{20}\text{H}_{15}\text{O}_6$, 351.0863).

Computational section

Mixed torsional/low-frequency mode conformational searches were carried out by means of the Macromodel 9.9.223 software using the Merck Molecular Force Field (MMFF) with an implicit solvent model for CHCl_3 .⁴⁷ Geometry reoptimizations were carried out at the B3LYP/6-31G(d) level *in vacuo*, B3LYP/TZVP, B97D/TZVP^{24,25} and CAM-B3LYP/TZVP^{26,27} levels with the PCM solvent model for MeCN or MeOH. TDDFT ECD and OR calculations were run with various functionals (B3LYP, BH&HLYP, CAM-B3LYP, PBE0) and the TZVP basis set as implemented in the Gaussian 09 package with the same or no solvent model as in the preceding DFT optimization step.⁴⁸ ECD spectra were generated as sums of Gaussians with 2100-3000 cm^{-1} widths at half-height (corresponding to ca. 15-22 nm at 270 nm), using dipole-velocity-computed rotational strength values.⁴⁹ Boltzmann distributions were estimated from the ZPVE-corrected B3LYP/6-31G(d) energies in the gas-phase calculations and from the B3LYP/TZVP, B97D/TZVP and CAM-B3LYP/TZVP energies in the solvated ones. The MOLEKEL software package was used for visualization of the results.⁵⁰

Acknowledgements: The financial support of the Manchot Foundation granted to P. P. and by the Ministry of Science and Technology (MOST) to W. H. L. are gratefully acknowledged. T.K. thanks the Hungarian National Research Foundation (OTKA K105871) for financial support and the National Information Infrastructure Development Institute (NIIFI 10038) for CPU time. The authors are indebted to Prof. R. Kalscheuer (Heinrich-Heine-University, Duesseldorf) for performing the antibacterial assays.

Author information

Corresponding authors

*Tel.: +49 211 81 14173; fax: +49 211 81 11923, E-Mail: georgios.daletos@uni-duesseldorf.de (G. Daletos).

*Tel.: +49 211 81 14163; fax: +49 211 81 11923, E-Mail: proksch@uni-duesseldorf.de (P. Proksch).

Notes

The authors declare no competing financial interest.

References

1. Faeth, S. H. *Oikos* **2002**, *98*, 25–36.
2. Wilson, D. *Oikos* **1995**, *73*, 274–276.
3. Aly, A. H.; Debbab, A.; Proksch, P. *Appl. Microbiol. Biotechnol.* **2011**, *90*, 1829–1845.
4. Wilson, Z. E. and Brimble, M. A. *Nat. Prod. Rep.* **2009**, *26*, 44–71.
5. Kingston, D. G. I. *J. Nat. Prod.* **2011**, *74*, 496–511.
6. Rösberg, D.; Debbab, A.; Mándi, A.; Vasylyeva, V.; Böhler, P.; Stork, B.; Engelke, L.; Hamacher, A.; Sawadogo, R.; Diederich, M.; Wray, V.; Lin, W.; Kassack, M. U.; Janiak, C.; Scheu, S.; Wesselborg, S.; Kurtán, T.; Aly, A. H.; Proksch, P. *J. Org. Chem.* **2013**, *78*, 12409–12425.
7. Thatoi, H.; Behera, B. C.; Mishra R. R. *Mycology* **2013**, *4*, 54–71.

8. Zhu, F.; Chen, X.; Yuan, Y.; Huang, M.; Sun, H.; Xiang, W. *Open Nat. Prod. J.* **2009**, *2*, 24–32.
9. Saikkonen, K.; Saari, S.; Helander, M. *Fungal Divers.* **2010**, *41*, 101–113.
10. Frank, M.; Niemann, H.; Böhler, P.; Stork, B. Wesselborg, S.; Lin, W.; Proksch, P. *Curr. Med. Chem.* **2015**, *22*, 3523–3532.
11. Liu, Y.; Wray, V.; Abdel-Aziz, M. S.; Wang, C. Y.; Lai, D.; Proksch, P. *J. Nat. Prod.* **2014**, *77*, 1734–1738.
12. Liu, Y.; Marmann, A.; Abdel-Aziz, M. S.; Wang, C. Y.; Müller, W. E. G.; Lin, W. H.; Mándi, A.; Kurtán, T.; Daletos, G.; Proksch, P. *Eur. J. Org. Chem.* **2015**, *12*, 2646–2653.
13. Liu, Y.; Kurtán, T.; Wang, C. Y.; Lin, W. H.; Orfali, R.; Müller, W. E. G.; Daletos, G.; Proksch, P. *J. Antibiot.* **2016**, 1–5. doi: 10.1038/ja.2016.11
14. Kõljalg, U.; Nilsson, R. H.; Abarenkov, K.; Tedersoo, L.; Taylor, A. F. S.; Bahram, M.; Bates, S. T.; Bruns, T. D.; Bengtsson-Palme, J.; Callaghan, T. M.; Douglas, B.; Drenkhan, T.; Eberhardt, U.; Dueñas, M.; Grebenc, T.; Griffith, G. W.; Hartmann, M.; Kirk, P. M.; Kohout, P.; Larsson, E.; Lindahl, B. D.; Lücking, R.; Martín, M. P.; Matheny, P. B.; Nguyen, N. H.; Niskanen, T.; Oja, J.; Peay, K. G.; Peintner, U.; Peterson, M.; Pöldmaa, K.; Saag, L.; Saar, I.; Schüßler, A.; Scott, J. A.; Senés, C.; Smith, M. E.; Suija, A.; Taylor, D. L.; Telleria, M. T.; Weiß, M.; Larsson, K. H. *Mol. Ecol.* **2013**, *22*, 5271–5277.
15. Hsieh, H.M.; Ju, Y. M.; Rogers, J. D. *Mycologia* **2005**, *97*, 844–865.
16. Surup, F.; Wiebach, V.; Kuhnert, E.; Stadler, M. *Tetrahedron Lett.* **2016**, *57*, 2183–2185.
17. Surup, F.; Mohr, K. I.; Jansen, R.; Stadler, M. *Phytochemistry* **2013**, *95*, 252–258.
18. Quang, D. N.; Hashimoto, T.; Nomura, Y.; Wollweber, H.; Hellwig, V.; Fournier, J.; Stadler, M.; Asakawa, Y. *Phytochemistry* **2005**, *66*, 797–809.
19. Quang, D. N.; Stadler, M.; Fournier, J.; Tomita, A.; Hashimoto, T. *Tetrahedron* **2006**, *62*, 6349–6354.

-
20. Husain, S. M.; Schätzle, M. A.; Lüdeke, S.; Müller, M. *Angew. Chem. Int. Ed.* **2014**, *53*, 9806–9811.
21. Thompson, J. E.; Fahnestock, S.; Farrall, L.; Liao, D.; Valent, B.; Jordan, D. B. *J. Biol. Chem.* **2000**, *275*, 34867–34872.
22. Tian, Z.; Sun, P.; Yan, Y.; Wu, Z.; Zheng, Q.; Zhou, S.; Zhang, H.; Yu, F.; Jia, X.; Chen, D.; Mándi, A.; Kurtán, T.; Liu, W. *Nat. Chem. Biol.*, **2015**, *11*, 259–265.
23. Mándi, A.; Mudianta, I. W.; Kurtán, T.; Garson, M. J. *J. Nat. Prod.* **2015**, *78*, 2051–2056.
24. Grimme, S. *J. Comput. Chem.*, **2006**, *27*, 1787–1799.
25. Sun, P.; Xu, D. X.; Mándi, A.; Kurtán, T.; Li, T. J.; Schulz, B.; Zhang, W. *J. Org. Chem.* **2013**, *78*, 7030–7047.
26. Yanai, T.; Tew, D.; Handy, N. *Chem. Phys. Lett.* **2004**, *393*, 51–57.
27. Pescitelli, G.; Bari, L. D.; Berova, N.; *Chem. Soc. Rev.* **2011**, *40*, 4603–4625.
28. Fukai, M.; Tsukada, M.; Miki, K.; Suzuki, T.; Sugita, T.; Kinoshita, K.; Takahashi, K.; Shiro, M.; Koyama, K. *J. Nat. Prod.* **2012**, *75*, 22–25.
29. Gu, W.; Ge, H. M.; Song, Y. C.; Ding, H.; Zhu, H. L.; Zhao, X. A.; Tan, R. X. *J. Nat. Prod.* **2007**, *70*, 114–117.
30. Du, L.; King, J. B.; Cichewicz, R. H. *J. Nat. Prod.* **2014**, *77*, 2454–2458.
31. Iwasaki, S.; Muro, H.; Sasaki, K.; Woe, S.; Okuda, S. *Tetrahedron Lett.* **1973**, *37*, 3537–3542.
32. Pittayakhajonwut, P.; Sohsomboon, P.; Dramaee, A.; Suvannakad, R.; Lapanun, S.; Tantichareon, M. *Planta. Med.* **2008**, *74*, 281–286.
33. Nadeau A. K.; Sorensen J. L. *Tetrahedron Lett.* **2011**, *52*, 1697–1699.
34. Marmann, A.; Aly, A. H.; Lin, W.; Wang, B.; Proksch, P. *Mar. Drugs* **2014**, *12*, 1043–1065.

35. Chen, H.; Daletos, G.; Abdel-Aziz, M. S.; Thomy, D.; Dai, H.; Broetz-Oesterhelt, H.; Lin, W. H.; Proksch, P. *Phytochem. Lett.* **2015**, *12*, 35–41.
36. Ola, A. R. B.; Thomy, D.; Lai, D.; Broetz-Oesterhelt, H.; Proksch, P. *J. Nat. Prod.* **2013**, *76*, 2094–2099.
37. Taylor, R. C.; Cullen, S. P.; Martin, S. J. *Nat. Rev. Mol. Cell Biol.* **2008**, *9*, 231–241.
38. Mizushima, N. *Genes. Dev.* **2007**, *21*, 2861–2873.
39. Degenhardt, K.; Mathew, R.; Beaudoin, B.; Bray, K.; Anderson, D.; Chen, G.; Mukherjee, C.; Shi, Y.; Gélinas, C.; Fan, Y.; Nelson, D. A.; Jin, S.; White, E. *Cancer Cell* **2006**, *10*, 51–64.
40. Guo, J. Y.; Chen, H. Y.; Mathew, R.; Fan, J.; Strohecker, A. M.; Karsli-Uzunbas, G.; Kamphorst, J. J.; Chen, G.; Lemons, J. M.; Karantza, V.; Coller, H. A.; Dipaola, R. S.; Gélinas, C.; Rabinowitz, J. D.; White, E. *Genes Dev.* **2011**, *25*, 460–470.
41. Fang, W.; Ji, S.; Jiang, N.; Wang, W.; Zhao, G. Y.; Zhang, S.; Ge, H. M.; Xu, Q.; Zhang, A. H.; Zhang, Y. L.; Song, Y. C.; Zhang, J.; Tan, R. X. *Nat. Commun.* **2012**, *3*, 1039–1048.
42. Okoyea, F. B. C.; Nworuc, C. S.; Debbaba, A.; Esimone, C. O.; Proksch, P. *Phytochem. Lett.* **2015**, *14*, 51–55.
43. Akone, S. H.; Rahn, S.; Henrich, B.; Daletos, G.; Vardamides, J. C.; Nkengfack, A. E.; Lin, W.; Lai D.; Proksch, P. *Phytochem. Lett.* **2014**, *10*, 184–188.
44. Shang, L.; Chen, S.; Du, F.; Li, S.; Zhao, L.; Wang, X. *Proc. Natl. Acad. Sci. USA* **2011**, *108*, 4788–4793.
45. Manns, J.; Daubrawa, M.; Driessen, S.; Paasch, F.; Hoffmann, N.; Löffler, A.; Lauber, K.; Dieterle, A.; Alers, S.; Iftner, T.; Schulze-Osthoff, K.; Stork, B.; Wesselborg, S. *FASEB J.* **2011**, *25*, 3250–3261.
46. Nicoletti, I.; Migliorati, G.; Pagliacci, M. C.; Grignani, F.; Riccardi, C. *J. Immunol. Methods* **1991**, *139*, 271–279.

47. MacroModel; Schrödinger, LLC, 2012, <http://www.schrodinger.com/MacroModel>.
48. Frisch, M. J.; Trucks, G. W.; Schlegel, H. B.; Scuseria, G. E.; Robb, M. A.; Cheeseman, J. R.; Scalmani, G.; Barone, V.; Mennucci, B.; Petersson, G. A.; Nakatsuji, H.; Caricato, M.; Li, X.; Hratchian, H. P.; Izmaylov, A. F.; Bloino, J.; Zheng, G.; Sonnenberg, J. L.; Hada, M.; Ehara, M.; Toyota, K.; Fukuda, R.; Hasegawa, J.; Ishida, M.; Nakajima, T.; Honda, Y.; Kitao, O.; Nakai, H.; Vreven, T.; Montgomery, J. A. J.; Peralta, J. E.; Ogliaro, F.; Bearpark, M.; Heyd, J. J.; Brothers, E.; Kudin, K. N.; Staroverov, V. N.; Kobayashi, R.; Normand, J.; Raghavachari, K.; Rendell, A.; Burant, J. C.; Iyengar, S. S.; Tomasi, J.; Cossi, M.; Rega, N.; Millam, J. M.; Klene, M.; Knox, J. E.; Cross, J. B.; Bakken, V.; Adamo, C.; Jaramillo, J.; Gomperts, R.; Stratmann, R. E.; Yazyev, O.; Austin, A. J.; Cammi, R.; Pomelli, C.; Ochterski, J. W.; Martin, R. L.; Morokuma, K.; Zakrzewski, V. G.; Voth, G. A.; Salvador, P.; Dannenberg, J. J.; Dapprich, S.; Daniels, A. D.; Farkas, O.; Foresman, J. B.; Ortiz, J. V.; Cioslowski, J.; Fox, D. J. Gaussian 09, revision B.01; Gaussian, Inc.: Wallingford, CT, 2010.
49. Stephens, P. J.; Harada, N. *Chirality* **2010**, *22*, 229–233.
50. Varetto, U. MOLEKEL, v. 5.4; Swiss National Supercomputing Centre: Manno, Switzerland, 2009.

Benzo[j]fluoranthene Metabolites from the Mangrove-Derived Endophytic Fungus *Annulohyphoxylon* sp.

Yang Liu[§], *Fabian Stuhldreier*[‡], *Tibor Kurtán*[¶], *Attila Mándi*[¶], *Sathishkumar Arumugam*[†],
Changyun Wang[§], *Wenhan Lin*[#], *Sebastian Wesselborg*[‡], *Horst Weber*[†], *Birgit Henrich*[⊥],
Georgios Daletos^{†*}, and *Peter Proksch*^{†*}

[†] Institute of Pharmaceutical Biology and Biotechnology, Heinrich Heine University,
Universitaetsstrasse 1, D-40225 Duesseldorf, Germany.

[§] Key Laboratory of Marine Drugs, The Ministry of Education of China, School of Medicine
and Pharmacy, Ocean University of China, Qingdao 266003, P. R. China

[‡] Institute of Molecular Medicine, Heinrich Heine University, Universitaetsstrasse 1, D-
40225 Duesseldorf, Germany

[¶] Department of Organic Chemistry, University of Debrecen, P. O. B. 20, 400, 4002
Debrecen, Hungary

[†] Centre of Advanced Study in Marine Biology, Annamalai University, Parangipettai 608502,
Tamilnadu, India.

[#] State Key Laboratory of Natural and Biomimetic Drugs, Beijing University, Beijing
100191, P. R. China

[†] Institute of Pharmaceutical and Medicinal Chemistry, Heinrich Heine University,
Universitaetsstrasse 1, D-40225 Duesseldorf, Germany

[⊥] Institute of Medical Microbiology and Hospital Hygiene, University Clinic of the Heinrich
Heine University, D-40225 Duesseldorf, Germany

Contents

- Fig. S1** Phylogenetic tree based on part of the 18S-28S rDNA (28-3357 bp)
- Fig. S2** Phylogenetic tree based on part of the 18S rDNA (54-1400 bp)
- Fig. S3** ^1H NMR (600 MHz, $\text{CH}_3\text{OH-}d_4$) spectrum of the new compound **1**
- Fig. S4** Expanded ^1H NMR (600 MHz, $\text{CH}_3\text{OH-}d_4$) spectrum of the new compound **1**
- Fig. S5** COSY spectrum of the new compound **1**
- Fig. S6** HSQC spectrum of the new compound **1**
- Fig. S7** HMBC spectrum of the new compound **1**
- Fig. S8** Expanded HMBC spectrum of the new compound **1**
- Fig. S9** HRESIMS spectrum of the new compound **1**
- Fig. S10** Structure and population of the low-energy B3LYP/6-31G(d) *in vacuo* conformers (>2%) of (1*R*,6*bR*)-**1** diastereomer
- Fig. S11** Experimental ECD spectrum of **1** compared with the Boltzmann-weighted ECD spectra computed for the B3LYP/6-31G(d) *in vacuo* low-energy conformers of (1*R*,6*bR*)-**1** at various levels
- Fig. S12** Structure and population of the low-energy B3LYP/6-31G(d) *in vacuo* conformers (>2%) of (1*S*,6*bR*)-**1** diastereomer
- Fig. S13** Experimental ECD spectrum of **1** compared with the Boltzmann-weighted ECD spectra computed for the B3LYP/6-31G(d) *in vacuo* low-energy conformers of (1*S*,6*bR*)-**1** at various levels
- Fig. S14** Experimental ECD spectrum of **1** compared with the Boltzmann-weighted ECD spectra computed for the B3LYP/TZVP PCM/MeCN low-energy conformers of (1*R*,6*bR*)-**1** at various levels
- Fig. S15** Experimental ECD spectrum of **1** compared with the Boltzmann-weighted ECD spectra computed for the B3LYP/TZVP PCM/MeCN low-energy conformers of (1*S*,6*bR*)-**1** at various levels
- Fig. S16** Experimental ECD spectrum of **1** compared with the Boltzmann-weighted ECD spectra computed for the CAM-B3LYP/TZVP PCM/MeCN low-energy conformers of (1*R*,6*bR*)-**1** at various levels

Fig. S17 Experimental ECD spectrum of **1** compared with the Boltzmann-weighted ECD spectra computed for the CAM-B3LYP/TZVP PCM/MeCN low-energy conformers of (1*S*,6*bR*)-**1** at various levels

Table S1. Populations of conformers with equatorial and axial 1-H for (1*R*,6*bR*)-**1** at various levels of theory

Table S2. Populations of conformers with equatorial and axial 1-H for (1*S*,6*bR*)-**1** at various levels of theory

Fig. S18 ¹H NMR (600 MHz, DMSO-*d*₆) spectrum of the new compound **2**

Fig. S19 Expanded ¹H NMR (600 MHz, DMSO-*d*₆) spectrum of the new compound **2**

Fig. S20 COSY spectrum of the new compound **2**

Fig. S21 ¹³C NMR (150 MHz, DMSO-*d*₆) spectrum of the new compound **2**

Fig. S22 Expanded ¹³C NMR (150 MHz, DMSO-*d*₆) spectrum of the new compound **2**

Fig. S23 HSQC spectrum of the new compound **2**

Fig. S24 HMBC spectrum of the new compound **2**

Fig. S25 Expanded HMBC spectrum of the new compound **2**

Fig. S26 HRESIMS spectrum of the new compound **2**

Fig. S27 ¹H NMR (600 MHz, CH₃OH-*d*₄) spectrum of the new compound **3**

Fig. S28 Expanded ¹H NMR (600 MHz, CH₃OH-*d*₄) spectrum of the new compound **3**

Fig. S29 COSY spectrum of the new compound **3**

Fig. S30 HSQC spectrum of the new compound **3**

Fig. S31 HMBC spectrum of the new compound **3**

Fig. S32 HRESIMS spectrum of the new compound **3**

Fig. S33 Structure and population of the low-energy B3LYP/6-31G(d) *in vacuo* conformers (>2%) of (1*R*,6*bS*,7*R*)-**3** diastereomer

Fig. S34 Experimental ECD spectrum of **3** compared with the Boltzmann-weighted ECD spectra computed for the B3LYP/6-31G(d) *in vacuo* low-energy conformers of (1*R*,6*bS*,7*R*)-**3** at various levels

Fig. S35 Structure and population of the low-energy B3LYP/6-31G(d) conformers (>2%) of (1*S*,6*bS*,7*R*)-**3** diastereomer

Fig. S36 Experimental ECD spectrum of **3** compared with the Boltzmann-weighted

ECD spectra computed for the B3LYP/6-31G(d) *in vacuo* low-energy conformers of (1*S*,6*bS*,7*R*)-**3** at various levels

Fig. S37 Experimental ECD spectrum of **3** compared with the Boltzmann-weighted

ECD spectra computed for the B3LYP/TZVP PCM/MeCN low-energy conformers of (1*R*,6*bS*,7*R*)-**3** at various levels

Fig. S38 Experimental ECD spectrum of **3** compared with the Boltzmann-weighted

ECD spectra computed for the B3LYP/TZVP PCM/MeCN low-energy conformers of (1*S*,6*bS*,7*R*)-**3** at various levels

Fig. S39 Experimental ECD spectrum of **3** compared with the Boltzmann-weighted

ECD spectra computed for the CAM-B3LYP/TZVP PCM/MeCN low-energy conformers of (1*R*,6*bS*,7*R*)-**3** at various levels

Fig. S40 Experimental ECD spectrum of **3** compared with the Boltzmann-weighted

ECD spectra computed for the CAM-B3LYP/TZVP PCM/MeCN low-energy conformers of (1*S*,6*bS*,7*R*)-**3** at various levels

Fig. S41 HPLC chromatograms of EtOAc extracts from co-culture experiments

Fig. S1 Phylogenetic tree based on part of the 18S-28S rDNA (28-3357 bp)

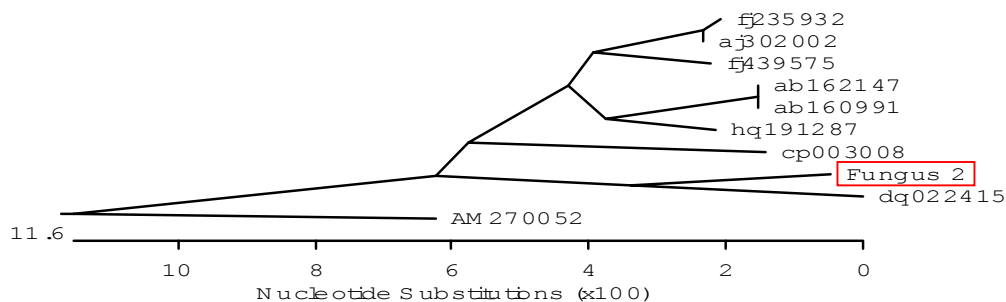
3,952 bp ribosomal rRNA Gene Sequence (18S – 28S):

TTGTCTCAAAGATTAAGCCATGCATGTCTAaGTATAAGCaATTTACTGCGAAACTGCGAATGGCTCATTAAATC
 AGTTATCGTTTATTTGATAGTACCTTACTACTTGGATAACCGTGGTAATTCTAGAGCTAATACATGCTAAAAATCCC
 GACTTACGGAGGGATGTATTTATTAGATTAAAAACCAATGCCCTTCGGGGCTCTCTGGTGATTATAATAACTTCT
 CGAATCGCATGGCCTTGCCCGGCGATGGTTCATTCAAATTTCTGCCCTATCAACTTTCGATGGCAGGGTCTTGG
 CCTGCCATGGTTACAACGGGTAACGGAGGGTTAGGGCTCGACCCCGGAGAAGGAGCCTGAGAAAACGGCTACTA
 CATCCAAGGAAGgCAGgCAGgCGCGCaAATTACCCAATTCGGATACGGAGAGGTAGTGACGATAAATACTGATACA
 GGGCTCTTTTGGGTCTTGTAATTGGAATGAGTACAATTTAAATCCCTTAACGAGGAACAATTGGAGGGCAAGTCT
 GGTGCCAGCAGCCGCGGTAATTCCAGCTCCAATAGCGTATATTAAGTTGTTGCAGTTAAAAAGCTCGTAGTTGA
 ACCTTGGGCTGGCTGGCCGGTCCGCTCACCGCGTGTACTGGTTCGGCCGGGCTTTCCCTCTGGGGAACCTC
 ATGCCCTTCACTGGGTGTGCTGGGGAACCAGGACTTTTACTGTGAAAAAATTAGAGTGTTCAAAGCAGGCCTAT
 GCTCGAATACATCAGCATGGAATAATAGAATAGGACGTGCGGTTCTATTTTGTGGTTTCTAGGACCGCCGTAAT
 GATTAATAGGGACAGTCGGGGGCATCAGTATTCAATTGTCAGAGGTGAAATTCTTGGATTTATTGAAGACTAACT
 ACTGCGAAAGCATTGTCAAGGATGTTTTCATTAATCAGGAACGAAAGTTAGGGGATCGAAGACGATTAATCTG
 GTCGTCCACAGTTAGGCGAGAGCCTAGCTAGTCCGCTGTAACGGCGTTACAGCGGGCGACACCGTCAAATTGC
 GGGTACCTCCTTAGAGCCCTCACACACCCTACCGCTAGAAATAGCGGCAGGTCGTAACAGTGTGGGGGATTGG
 ACCATCCGAGCCAAGCCCGCAAAACCTACCCGGTAGGTTAGGGTGCAGTTCACAGACTAAACGTCGGTGGGA
 ACTTAGTTCTTAAGATATAGTCGACCCGCGCCTGAAAAGGTGACGACAAGCGCTGAGGGTAGCGCTGTAAATCG
 CAGATACCGTCGTAGTCTTAACCATAAACTATGCCGACTAGGGATCGGACGATGTTATTTTTTACTCGTTCGGC
 ACCTTACGAGAAATCAAAGTTTTTGGGTTCTGGGGGAGTATGGTCGCAAGGCTGAAACTTAAAGAAATTGAC
 GGAAGGGCACCACCAGGGGTGGAGCCTGCGGCTTAATTTACTCAACACGGGGAAACTCACAGGTCCAGAC
 ACAATGAGGATTGACAGATTGAGAGCTCTTCTTGATTTTGTGGGTGGTGGTGCATGgCCGTCTTAGTTGGTGG
 AGTGATTTGTCTGCTTAATTGCGATAACGAACGAGACCTTAACCTGCTAAATAGCCCGTATTGCTTTGGCAGTAC
 GCTGGCTTCTTAGAGGGACTATCCGCTCAAGCGGATGGAAGTTTGGAGCAATAACAGGTTGAATTCACAGGCCT
 GTAAAAGTAAAGCCTCGTTAAAGAAGTACTAGTCCAGTACCTTTATCTCTTTTGGGGAAGCCCCCTTCTATCGGG
 AAGAGACGCAGCGCTGAAAAGCACTGCTTGGTACGGGCGACACTACCTGGTACAGGGAACGCTTCAGGCGCTA
 CAGCGCCTAAGCCGATCCTGTGGCGAGTCCGTTTAGCGCCGACCGTCGCAACGCGCGGAAAGGAGTGGGTTA
 GGCTACAAGGCCTAGCTTAAGGTACGTGCTAATCCCTCGAGAAATCGAGCCCCTATAATTAAGCCCGATAGGCT
 GAAGTATAGGGGGGCCTGAGATCTTCAGGCTGGTGTTTTTACTGCTGTGATGCCCTTAGATGTTCTGGGCCGCAC
 GCGGTTACTACTGACAGAGCCAGCGAGTACTTCTTGGTAGAAATACCCGGGTAATCTTGTTAAACTCTGTCTG
 GCTGGGGATAGAGCATTGCAATTATTGCTCTTCAACGAGGAATCCCTAGTAAGCGCAAGTCATCAACTTGCCTTG
 ATTACGTCCCTGCCCTTTGTACACACCCGCCGTCGCTACTACCGATTGAATGGCTCAGTGAGGCTATCGGACTGG
 CCTAGAGGAGTCGGCAACGACACCTCGGGCCGGAAAGTTATCCAAACTCGGTCATTTAGAGGAAGTAAAAGT
 CGTAACAAGGTCTCCGTTGGTGAACCAGCGGAGGGATCATTACTGAGTTATCAAAACTCCAACCTATGTGaAC
 CTTACCTCTGTTTCCCTCGGCCAACTGCAAAGGCTTACCCTATAGGGGGTTACCCTGTAGGGAGGTGCCCGATGAC
 GCTATCCAACCCCTGCCTCGGGGAGGTTAGCTGAGGGCCCCTCCAAGCCGGCCGACGCGCCGATCGAAAAAA
 ACCTTTTCGAAAAACTTTGTCCAACCTTACCCTATAGAGCTAATCGTTTCGAAAAAATCTCTTATCTCGAGGCTT
 TTCTTTGCCTTGGGGCTGAGGCTTTTCCTTGCCTTGCCTTTCTAATCAGTTCGAATATGTTCCCGGTTGGAATTT
 TTGCTCGAAGTTTACGATGTTACGACCTTACGAATGCCTTCGCGTGAAATGTTACCCTGTACCAACAGATCCCTT
 TCGCTCGAATGTATTTCCCGGTTGGAATTTTTGCTCGAGTTTAATTTCTTTCTGTACTAATACTGTTTTTGTTC
 TGTTGAAAGTCTTTCCCGGTTGGAATTTTTGCTCGAGTTCTATTTAATAGAGTCTGAATTGCATCAAAACA
 AATTTTGTGAAAACAACTTGTATCAAACTTTCAACAACGGATCTCTTGGTTCTGGCATCGATGAAGAACGCA
 GCGAAATGCGATAAGTAATGTGAATTGCAGAATTCAGTGAATCATGAATCTTTGAACGCACATTGCGCCCATTA

GTATTCTAGTGGGCATGCCTATTTCGAGCGTCATTACAACCCTTAAGCCCTGTTGCTTAGCGTTGGGAATCTACGG
 CTTAGGCGTAGTTCCTTAAAATTAGTGGCGGAGTTATAGCACTCTCAGCGTAGTAATTTGCCTCGCTTCTGAGTA
 GCTATAGCTGCCTGCCGTAAACCCCTATACTTCTAGTGGTtGACCTCGGATTAGGTAGGAATACCCGCTGAACCT
 AAGCATATCAATAAGCGGAGGAAAAGAAACCAACAGGGATTGCCCTAGTAACGGCGAGTGAAGCGGCAACAG
 CTCAAATTTGAAATCTGGCCCTAGCGGTCCGAGTTGTAATTTGCAGAGGATGCTTTTGGTGCGGTGCCTCCGAG
 TTCCCTGGAACGGGACGCCAGAGAGGGTGAGAGCCCCGTACGGTTGGACACCTACCCTATATATAGCTCCTTCG
 ACGAGTCGAGTAGTTTGGGAATGCTGCTCTAAATGGGAGGTAAATTTCTTCTAAAGCTAAATACCGGCCAGAGA
 CCGATAGCGCACAAGTAGAGTGATCGAAAGATGAAAAGCACTTTGAAAAGAGGGTTAAATAGCACGTGAAATT
 GTTAAAAGGGAAGCGTTTTCGACCAGACCTTTTCCAGGCGGATCATCCGGTGTCTCACCGGTGCACCTCGCCT
 GGTTTAGGCCAGCATCGGTTTCTTAGGGGGATAAAGGCTTGGGGAACGTAGCTCTTTAGGGAGTGTTATAGCC
 CCTTGCGTAATACCCCTCGGGGGACCGAGGACCGCGCTCTGCAAGGATGCTGGCGTAATGGTCGTAACGACCC
 GTCTTGA

Of these 3,952 nucleotides which were used for BlastN search in the NCBI-database, region of nt 28- nt 3357 showed the highest number of homologous sequences and was thus used for the generation of a phylogenetic tree with the highest homologue sequences of the databases that cover the same sequence region (Species Abbr. and Acc. numbers are indicated). The 18S-28S rDNA from nt 28- nt 3357 region of the titled fungus exhibited 64.5% homology to the respective length of *Xylariaceae* sp. YX28 (e.g. accession number DQ022414), suggesting that the fungus belongs to the order of Xylariales

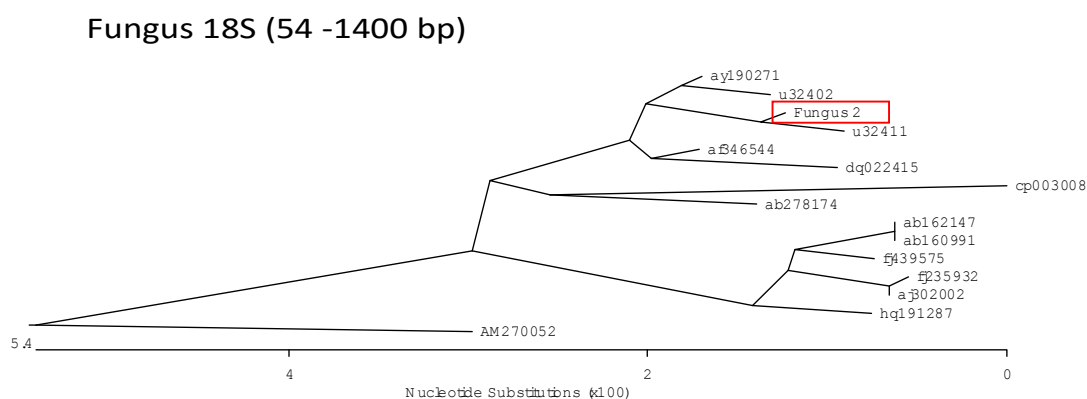
Fungus 18S-28S rDNA (28-3357 bp)



Acc-No	Spezies	Ordnung	Klasse
AB162147	Claviceps purpurea	Hypocreales	Sordariomycetes
AB160991	Claviceps purpurea		
FJ439575	Hypocreales sp. GMG C1		
FJ235932	Myrothecium roridum		
AJ302002	Myrothecium atroviride		
HQ191287	Sordariomycetes sp.		
CP003008	Myceliophthora thermophila	- Sordariales	
Fungus 2			
DQ022415	Xylariaceae sp. YX 28	Xylariales	
AM270052	Aspergillus	- Eurotiales	Eurotiomycetes

Fig. S2 Phylogenetic tree based on part of the 18S rDNA (54-1400 bp)

Of these 3330 nucleotides, the BlastN analysis of the 18S rDNA sequence from the region of nt 54-nt 1750 showed the highest number of homologous sequences and was thus used for the generation of a phylogenetic tree with the highest homologue sequences of the databases (Species abbr. and Acc. numbers are indicated). The 18S rDNA sequence from nt 54 – nt 1400 showed 76.4% homology to *Annulohypoxyton artroroseum* (e.g. accession number U32411) of the order Xylariales, and from nt 2415-3906 a 97.75% homology to *Annulohypoxyton spp.* (acc-no JQ747656). Based on this data we assumed that the fungus belongs to and nominate this fungus as *Annulohypoxyton sp.*



Acc-No	Spezies	Ordnung	Klasse
AY190271	Sordariomycete sp. G7-R280	Xylariales	Sordariomycetes
U32402	Daldinia concentrica		
Fungus 2	!Annulohypoxyton spp.		
U32411	Annulohypoxyton artroroseum		
AF346544	Hypoxyton submonticulosum		
DQ022415	Xylariaceae sp. YX 28		
CP003008	Myceliophthora thermophila	- Sordariales	Sordariomycetes
AB278174	Togninia minima	- Calosphaerales	
AB162147	Claviceps purpurea	Hypocreales	Eurotiomycetes
AB160991	Claviceps purpurea		
FJ439575	Hypocreales sp. GMG C1		
FJ235932	Myrothecium roridum		
AJ302002	Myrothecium atroviride		
HQ191287	Sordariomycetes sp.		
AM270052	Aspergillus	- Eurotiales	

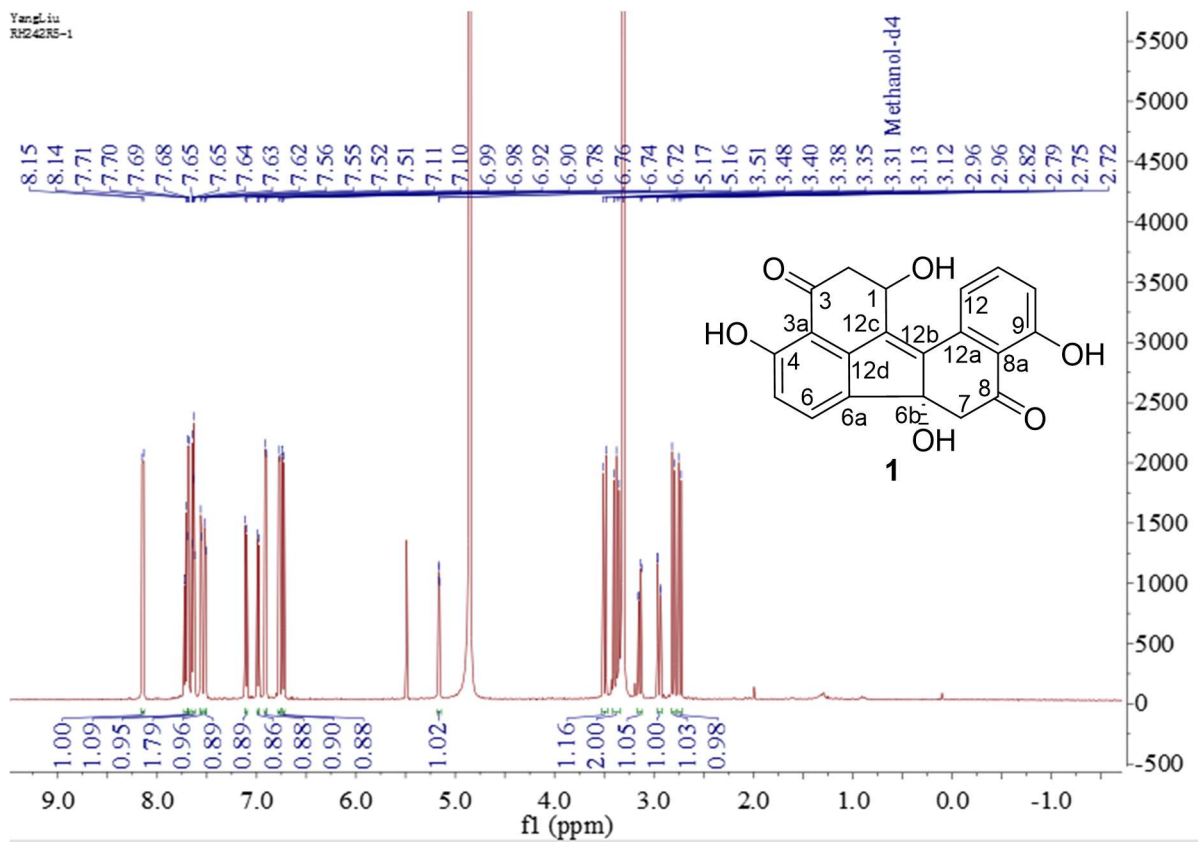
Fig. S3 ^1H NMR (600 MHz, $\text{CH}_3\text{OH}-d_4$) spectrum of the new compound **1**

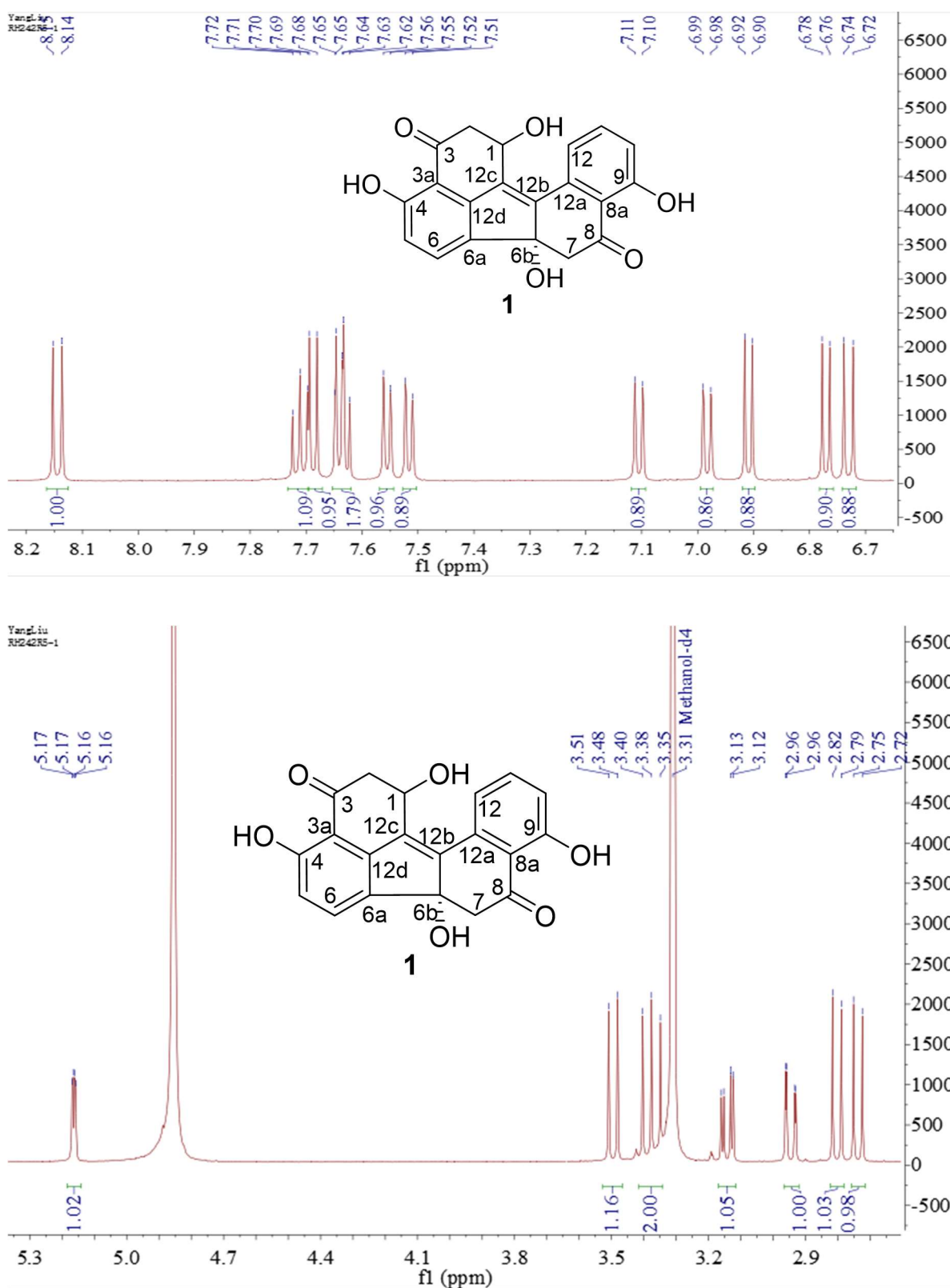
Fig. S4 Expanded ^1H NMR (600 MHz, $\text{CH}_3\text{OH}-d_4$) spectrum of the new compound **1**

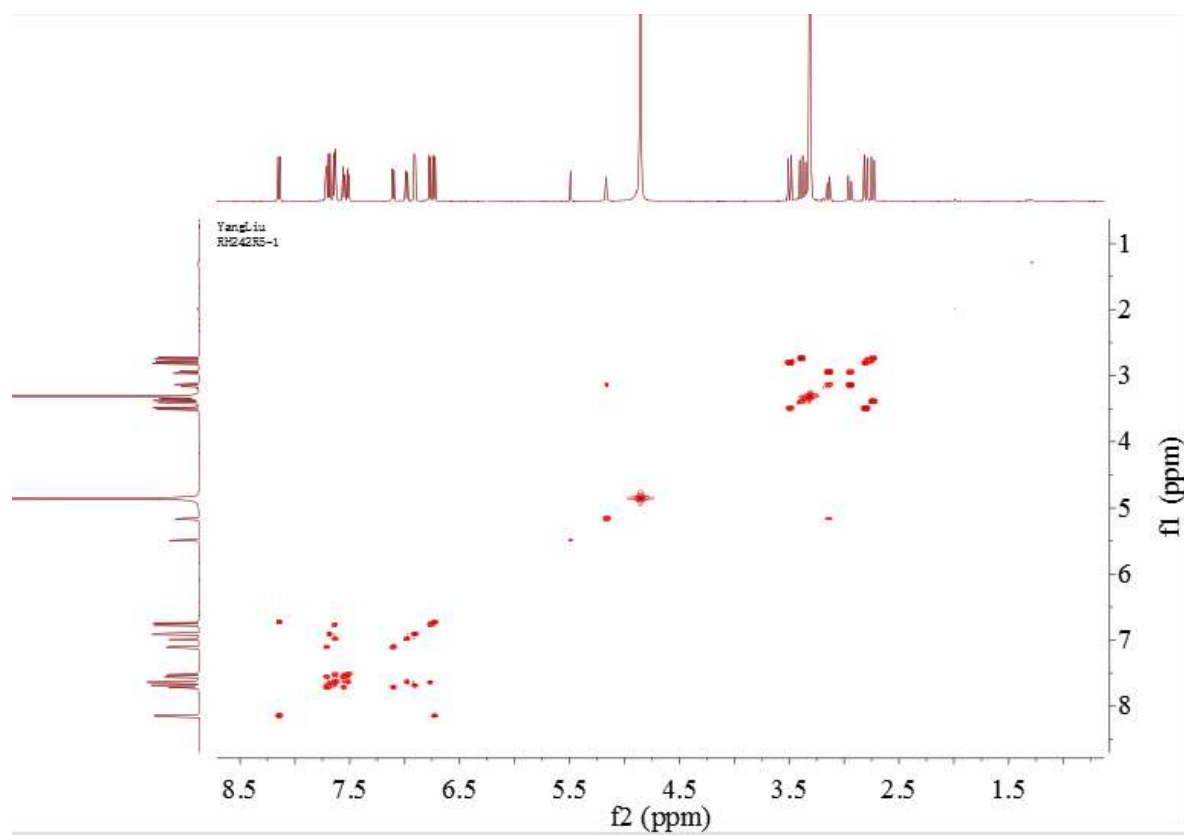
Fig. S5 COSY spectrum of the new compound **1**

Fig. S6 HSQC spectrum of the new compound 1

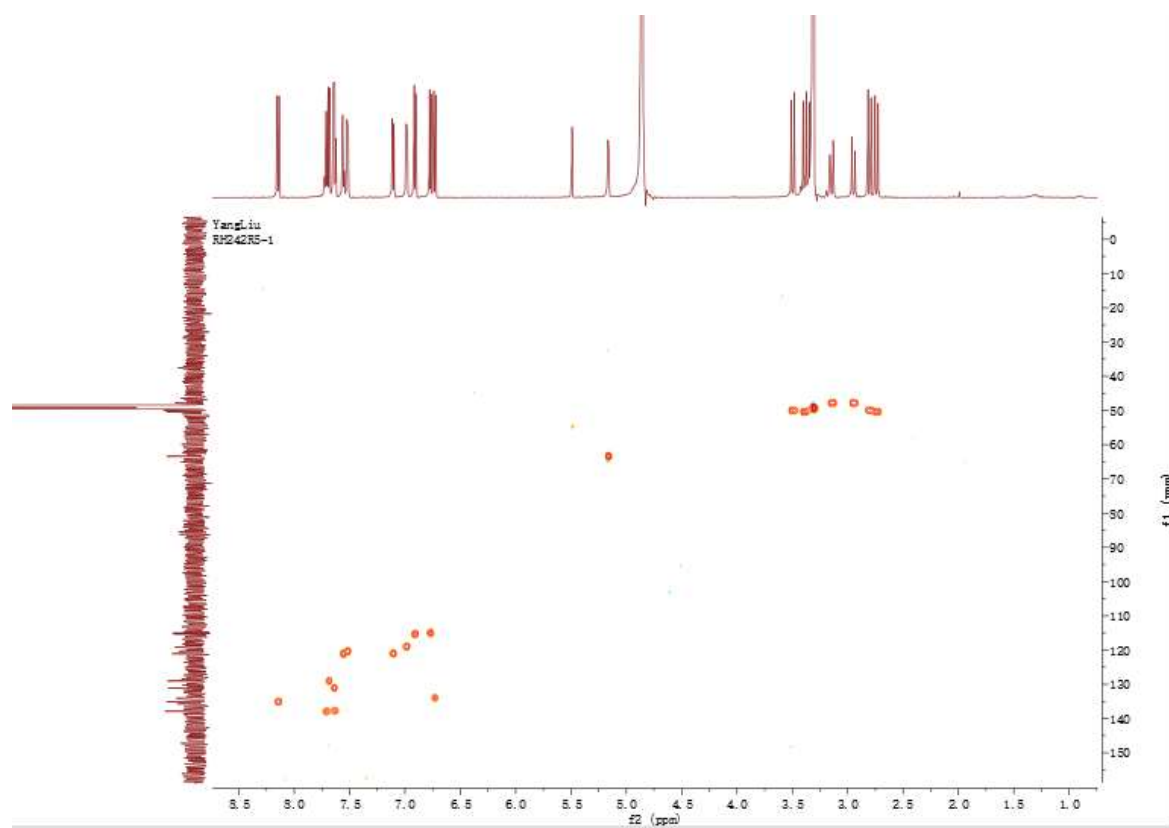


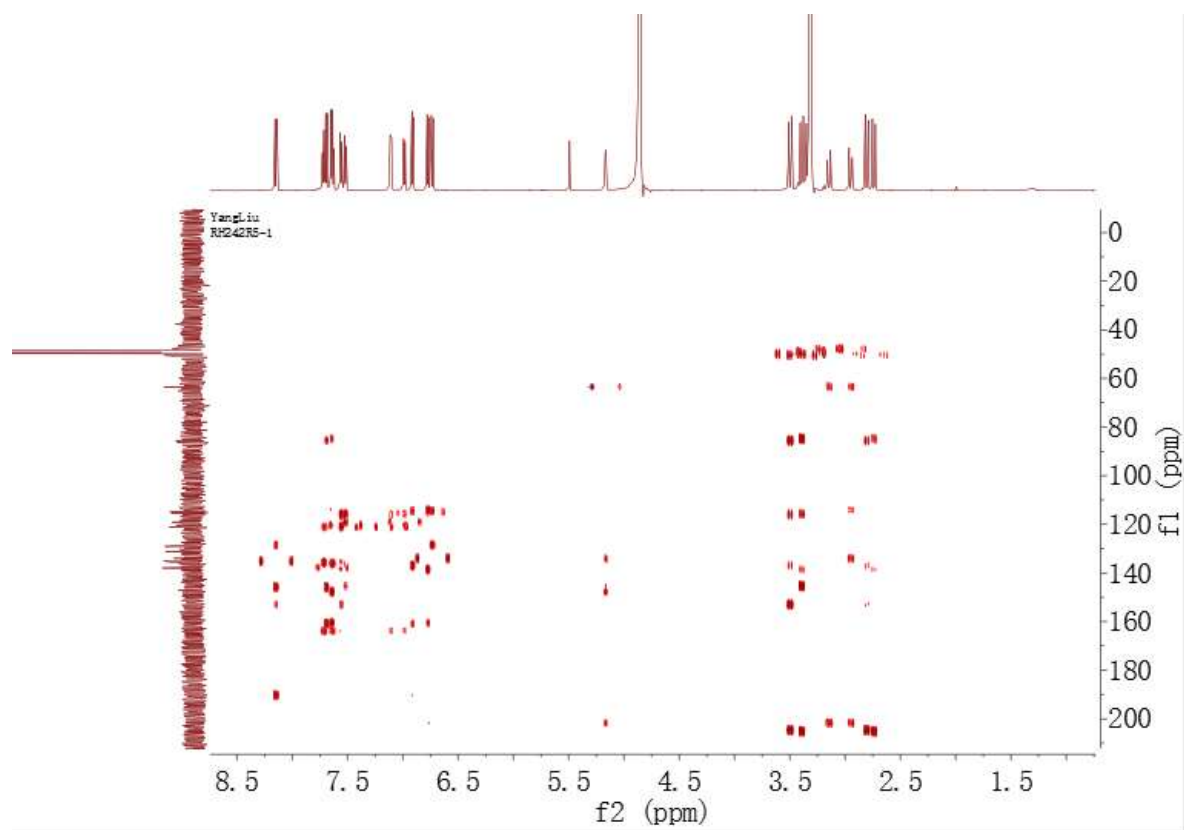
Fig. S7 HMBC spectrum of the new compound **1**

Fig. S8 Expanded HMBC spectrum of the new compound 1

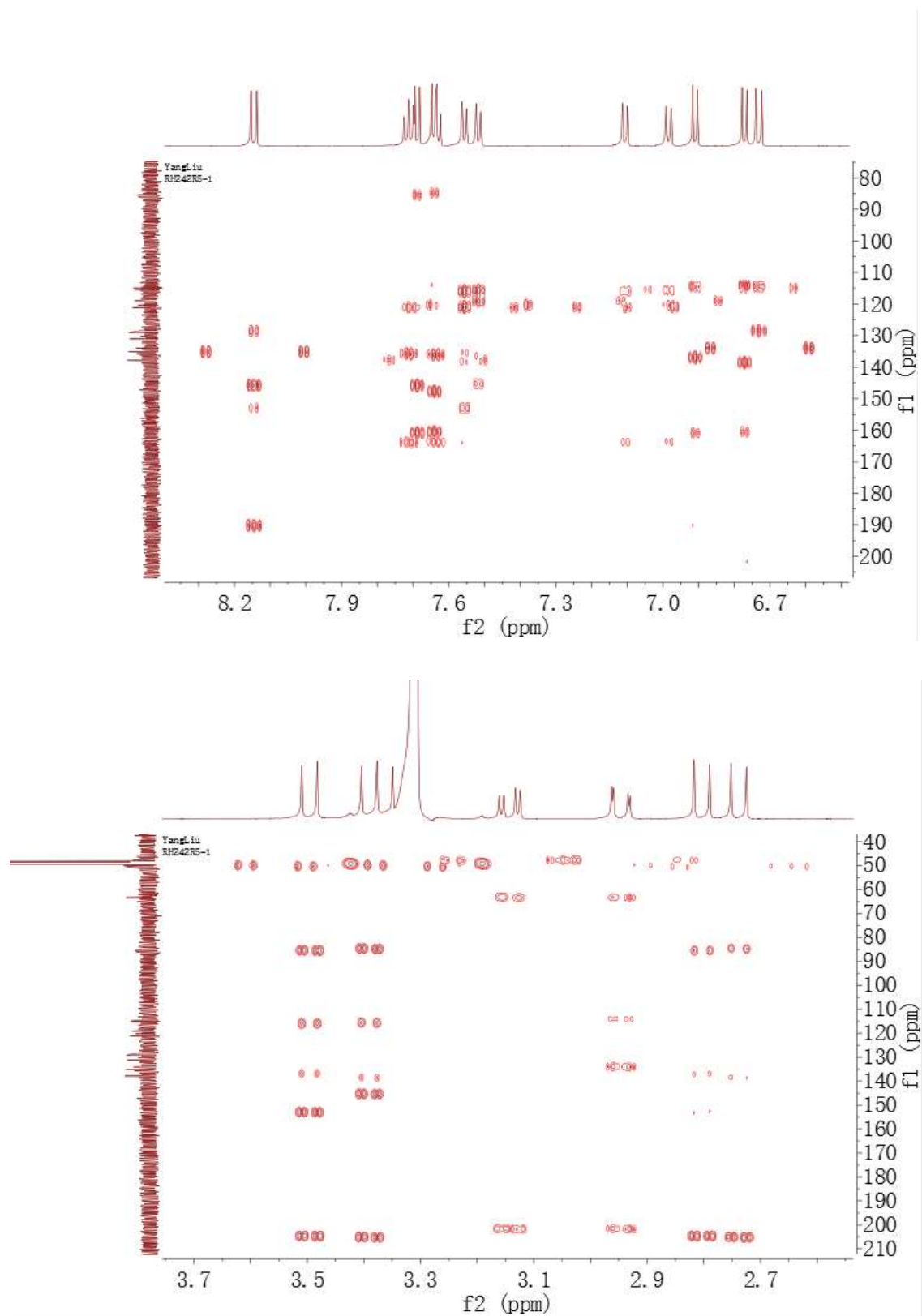


Fig. S9 HRESIMS spectrum of the new compound 1

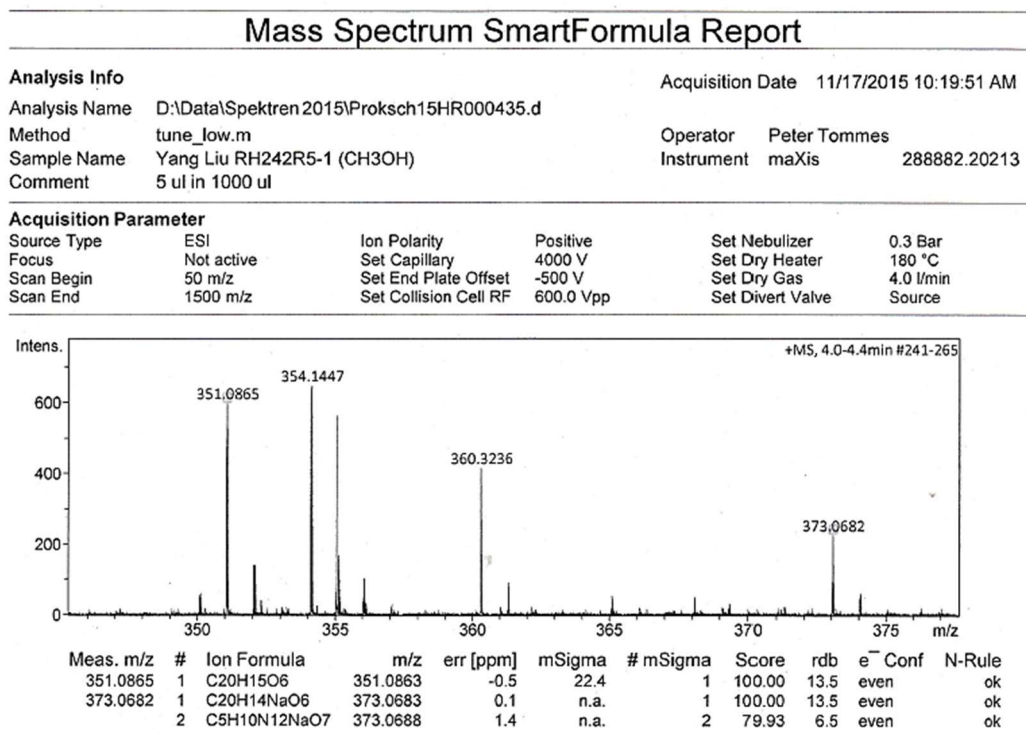


Fig. S10 Structure and population of the low-energy B3LYP/6-31G(d) *in vacuo* conformers (>2%) of (1*R*,6*bR*)-**1** diastereomer

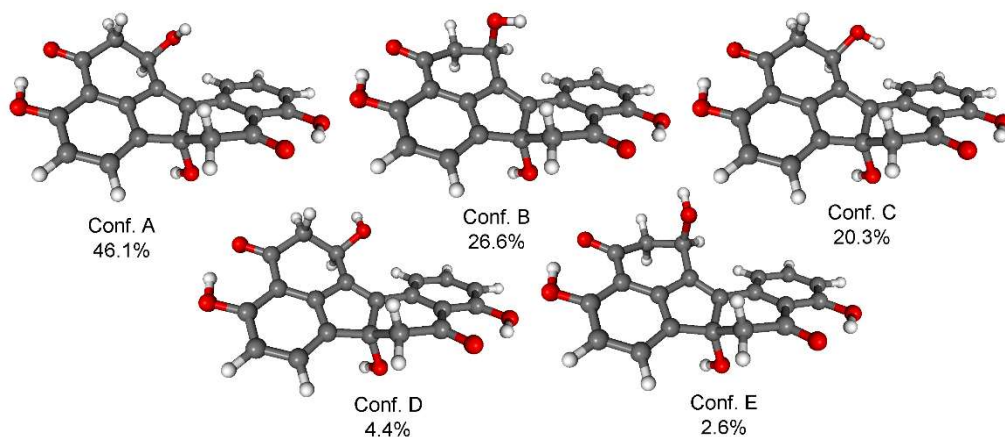


Fig. S11 Experimental ECD spectrum of **1** compared with the Boltzmann-weighted ECD spectra computed for the B3LYP/6-31G(d) *in vacuo* low-energy conformers of (1*R*,6*bR*)-**1** at various levels

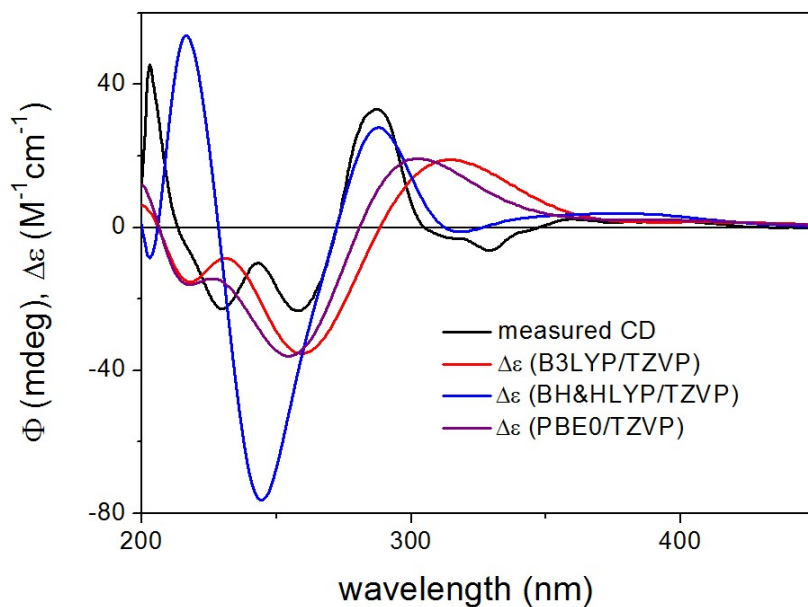


Fig. S12 Structure and population of the low-energy B3LYP/6-31G(d) *in vacuo* conformers (>2%) of (1*S*,6*bR*)-**1** diastereomer

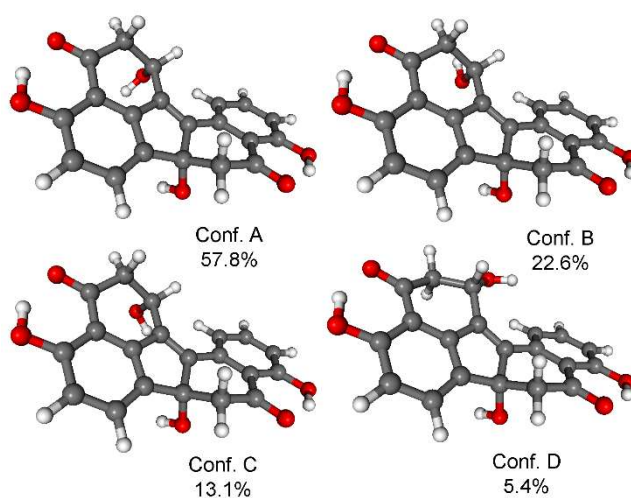


Fig. S13 Experimental ECD spectrum of **1** compared with the Boltzmann-weighted ECD spectra computed for the B3LYP/6-31G(d) *in vacuo* low-energy conformers of (1*S*,6*bR*)-**1** at various levels

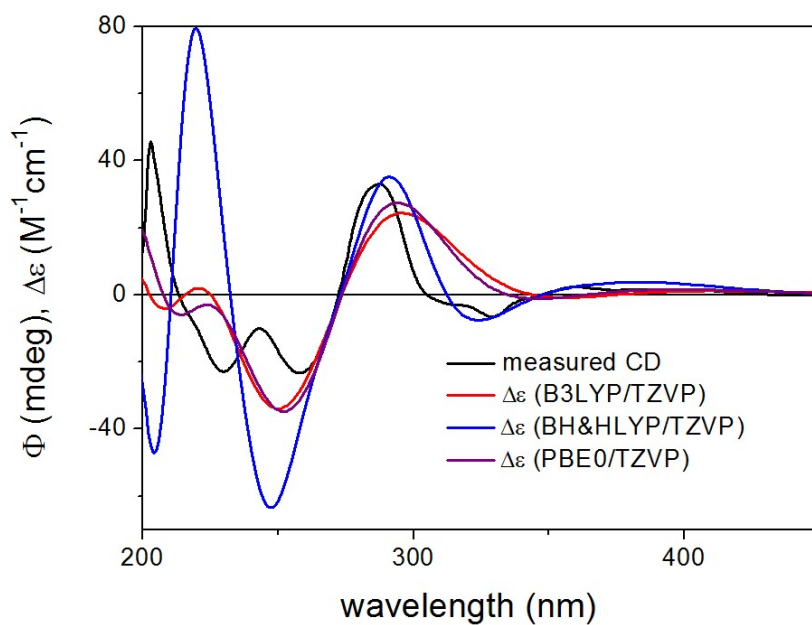


Fig. S14 Experimental ECD spectrum of **1** compared with the Boltzmann-weighted ECD spectra computed for the B3LYP/TZVP PCM/MeCN low-energy conformers of (1*R*,6*bR*)-**1** at various levels

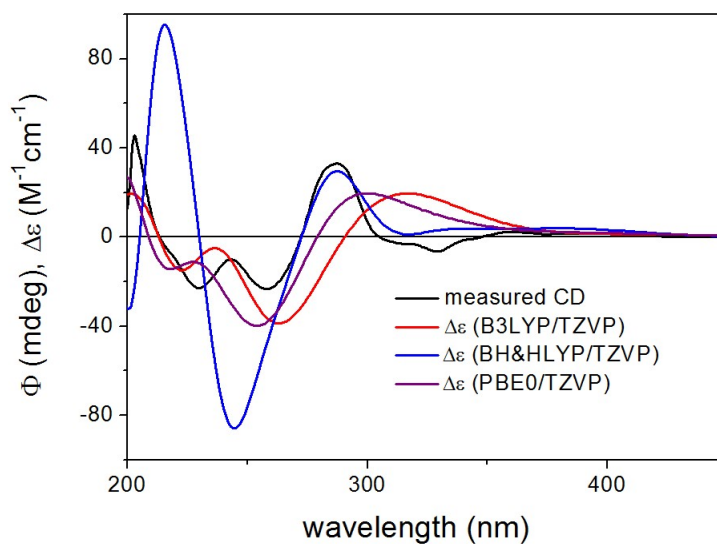


Fig. S15 Experimental ECD spectrum of **1** compared with the Boltzmann-weighted ECD spectra computed for the B3LYP/TZVP PCM/MeCN low-energy conformers of (1*S*,6*bR*)-**1** at various levels

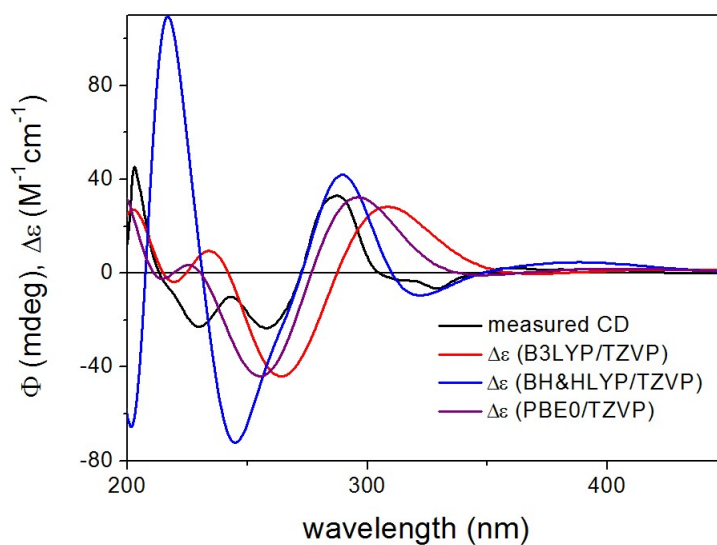


Fig. S16 Experimental ECD spectrum of **1** compared with the Boltzmann-weighted ECD spectra computed for the CAM-B3LYP/TZVP PCM/MeCN low-energy conformers of (1*R*,6*bR*)-**1** at various levels

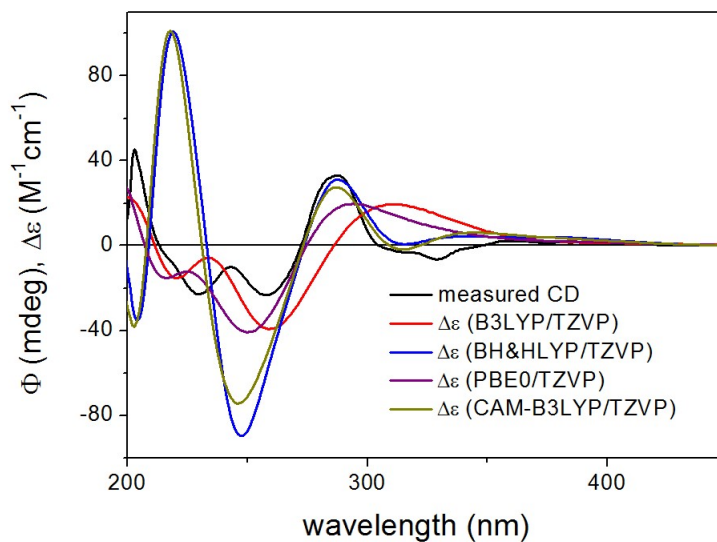


Fig. S17 Experimental ECD spectrum of **1** compared with the Boltzmann-weighted ECD spectra computed for the CAM-B3LYP/TZVP PCM/MeCN low-energy conformers of (1*S*,6*bR*)-**1** at various levels

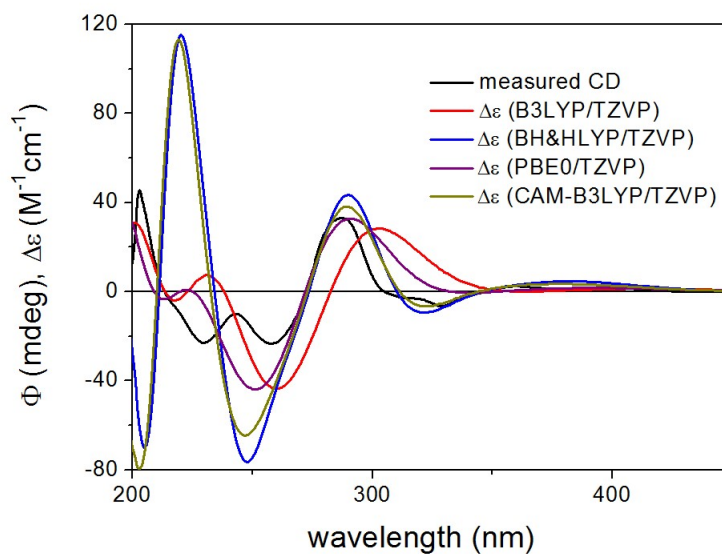


Table S1 Populations of conformers with equatorial and axial 1-H for (1*R*,6*bR*)-**1** at various levels of theory

	B3LYP/6-31G(d) Boltzmann population / ax. or eq.	B3LYP/TZVP PCM/MeCN Boltzmann population / ax. or eq.	B97D/TZVP PCM/MeCN Boltzmann population / ax. or eq.	CAM-B3LYP/TZVP PCM/MeCN Boltzmann population / ax. or eq.
Conf. A	46.1% / ax.	65.5% / eq.	68.9% / eq.	63.4% / eq.
Conf. B	26.6% / eq.	20.5% / eq.	15.1% / eq.	21.0% / eq.
Conf. C	20.3% / ax.	7.0% / ax.	8.0% / ax.	7.3% / ax.
Conf. D	4.4% / ax.	3.8% / ax.	5.8% / ax.	4.3% / ax.
Conf. E	2.6% / eq.	3.2% / ax.	2.2% / ax.	4.0% / ax.
ax./eq.	71/29	14 / 86	16/84	16 / 84

Table S2 Populations of conformers with equatorial and axial 1-H for (1*S*,6*bR*)-**1** at various levels of theory

	B3LYP/6-31G(d) Boltzmann population / ax. or eq.	B3LYP/TZVP PCM/MeCN Boltzmann population / ax. or eq.	B97D/TZVP PCM/MeCN Boltzmann population / ax. or eq.	CAM-B3LYP/TZVP PCM/MeCN Boltzmann population / ax. or eq.
Conf. A	57.8% / eq.	47.2% / eq.	47.4% / eq.	53.2% / eq.
Conf. B	22.6% / eq.	33.0% / eq.	30.6% / eq.	25.9% / eq.
Conf. C	13.1% / eq.	18.4% / eq.	21.2% / eq.	19.0% / eq.
Conf. D	5.4% / ax.	0.8% / ax.	0.6% / eq.	1.1% / eq.
Conf. E	1.1% / ax.	0.7% / ax.	0.1% / eq.	0.8% / eq.
ax./eq.	6/94	1 / 99	1/99	2 / 98

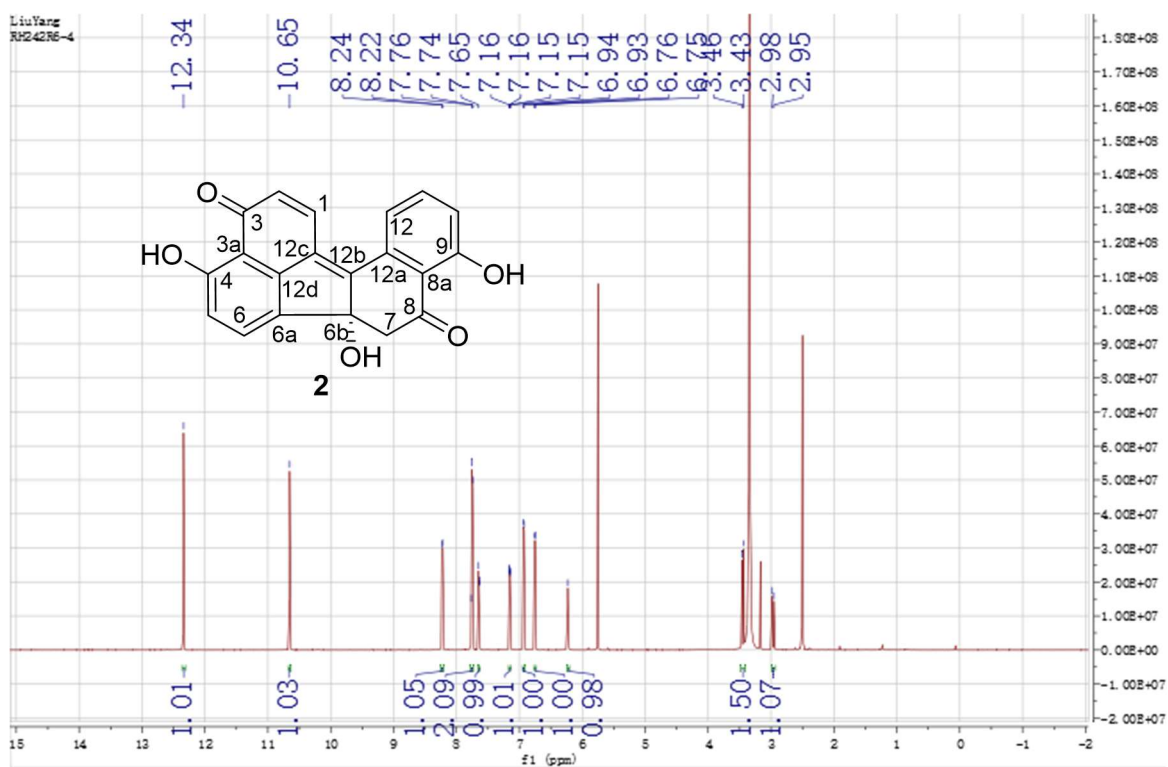
Fig. S18 ^1H NMR (600 MHz, $\text{DMSO-}d_6$) spectrum of the new compound **2**

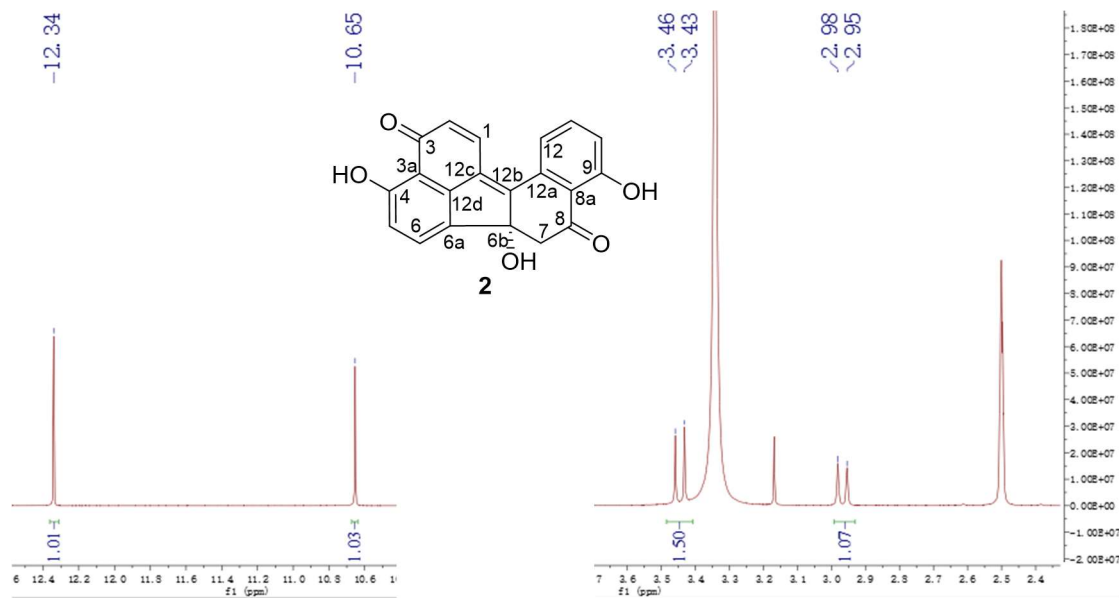
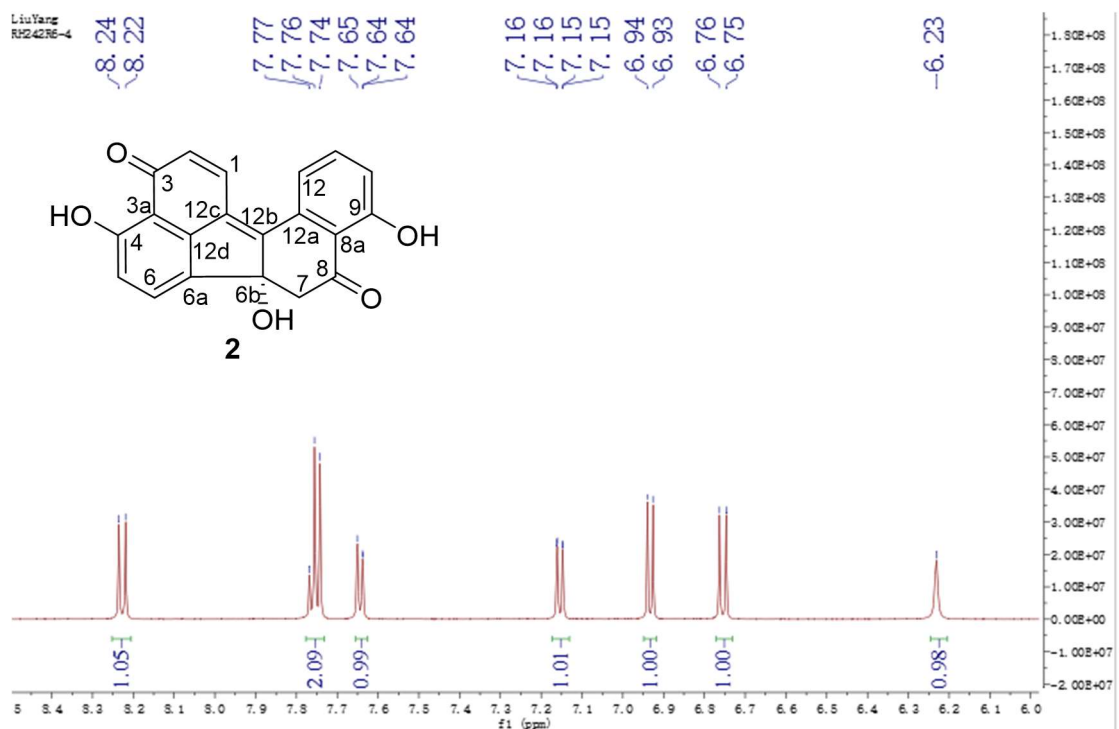
Fig. S19 Expanded ^1H NMR (600 MHz, $\text{DMSO-}d_6$) spectrum of the new compound **2**

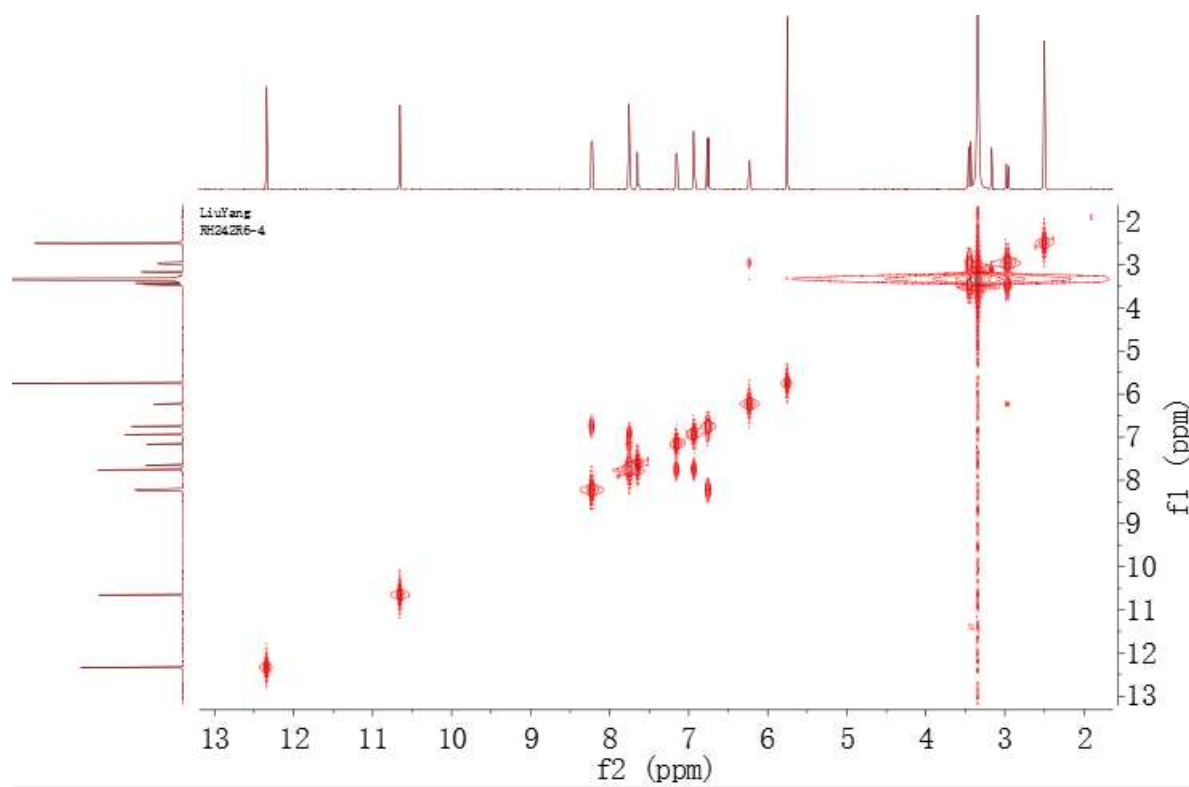
Fig. S20 COSY spectrum of the new compound **2**

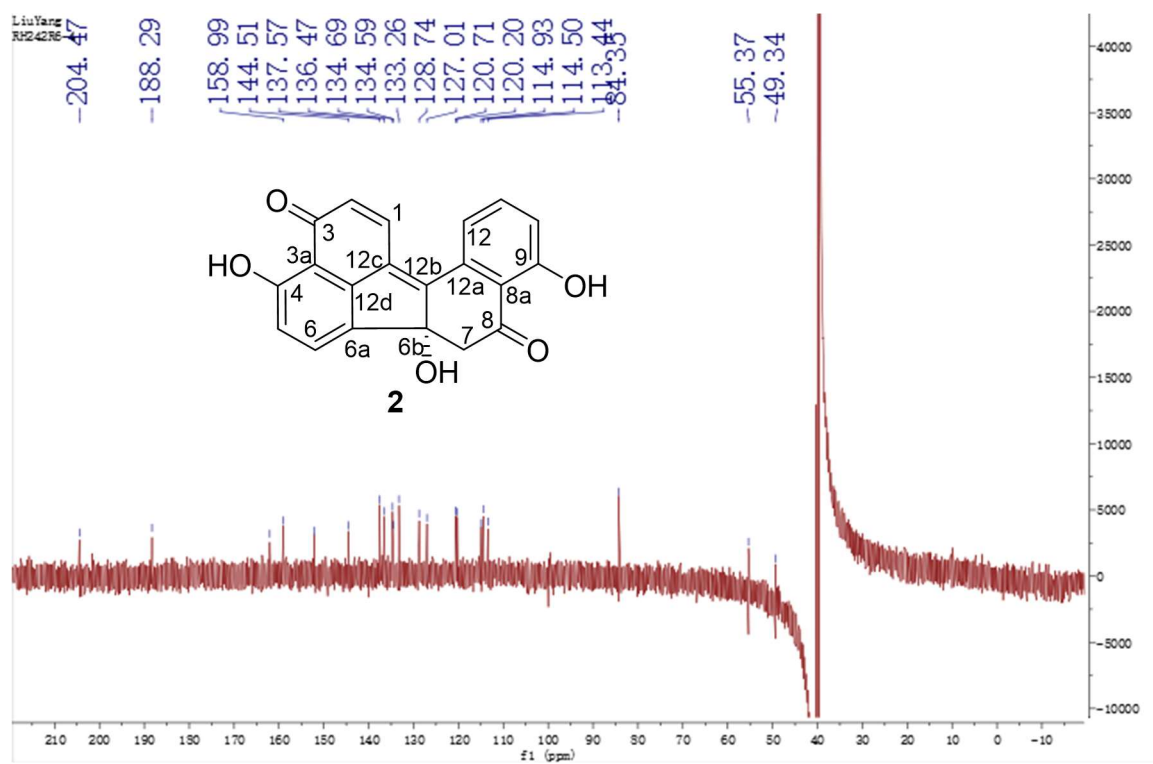
Fig. S21 ^{13}C NMR (150 MHz, $\text{DMSO-}d_6$) spectrum of the new compound **2**

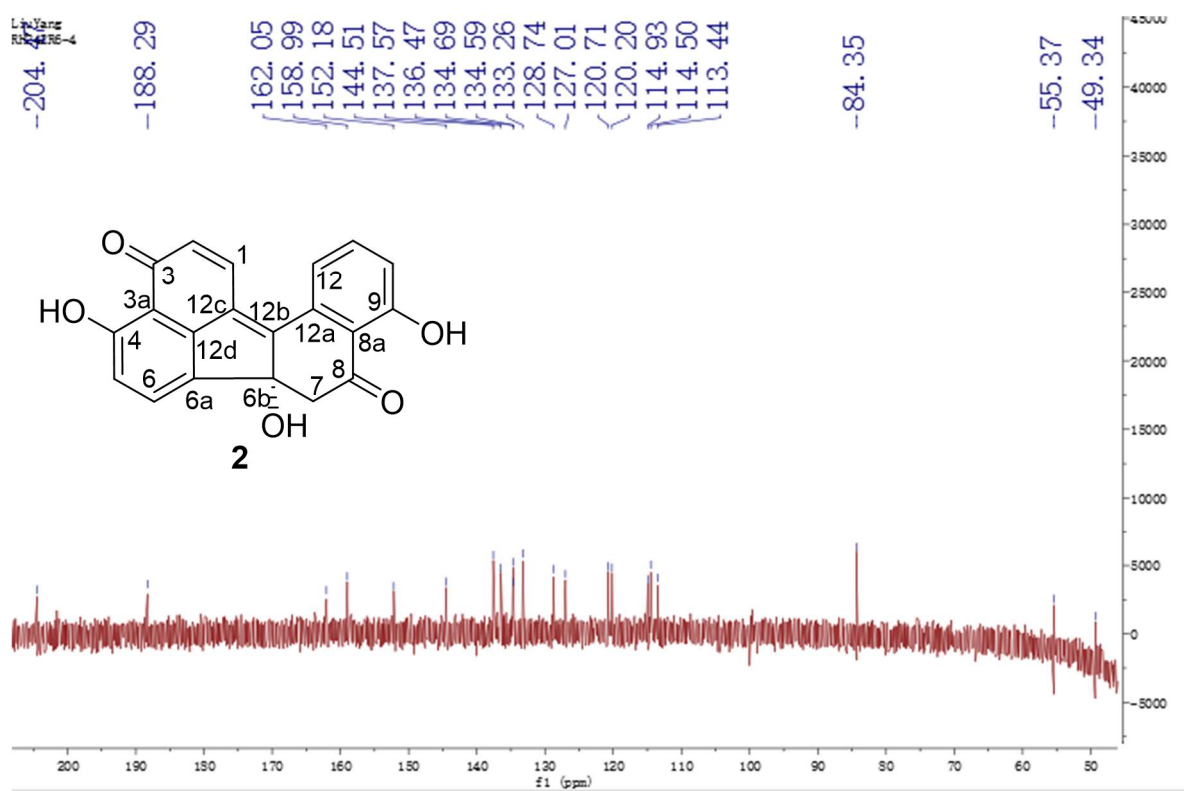
Fig. S22 Expanded ^{13}C NMR (150 MHz, $\text{DMSO-}d_6$) spectrum of the new compound **2**

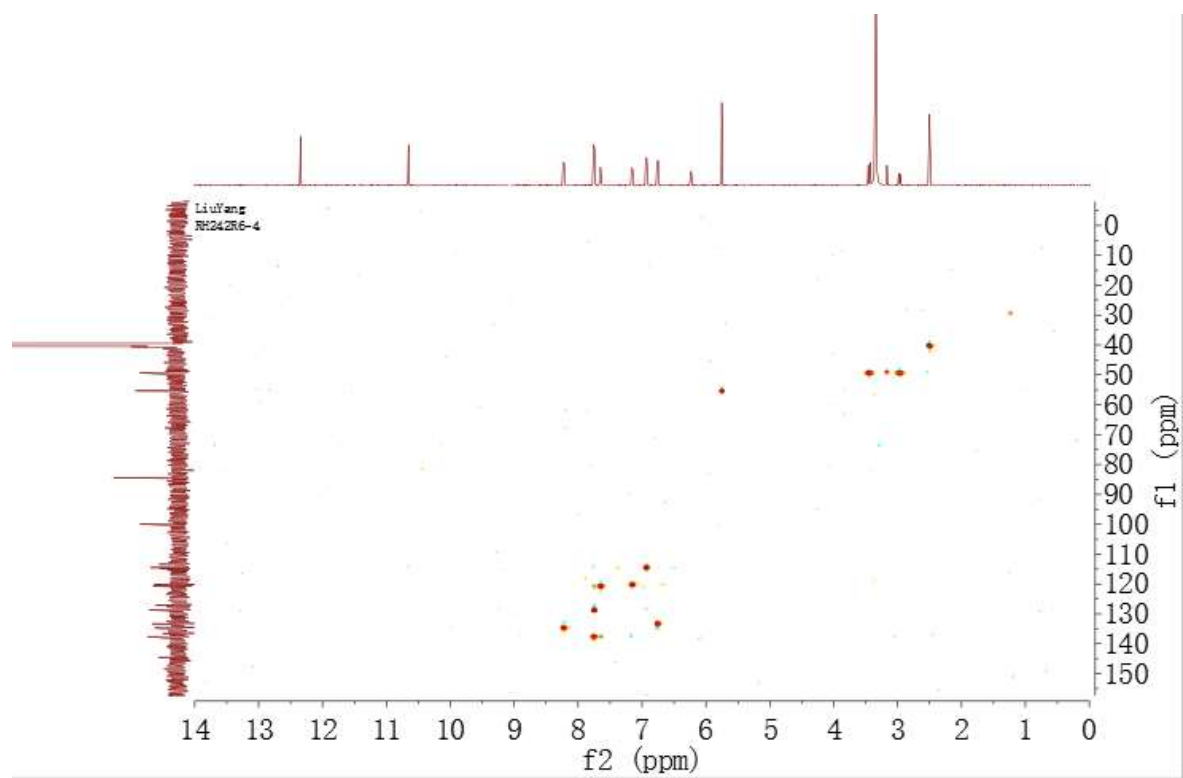
Fig. S23 HSQC spectrum of the new compound **2**

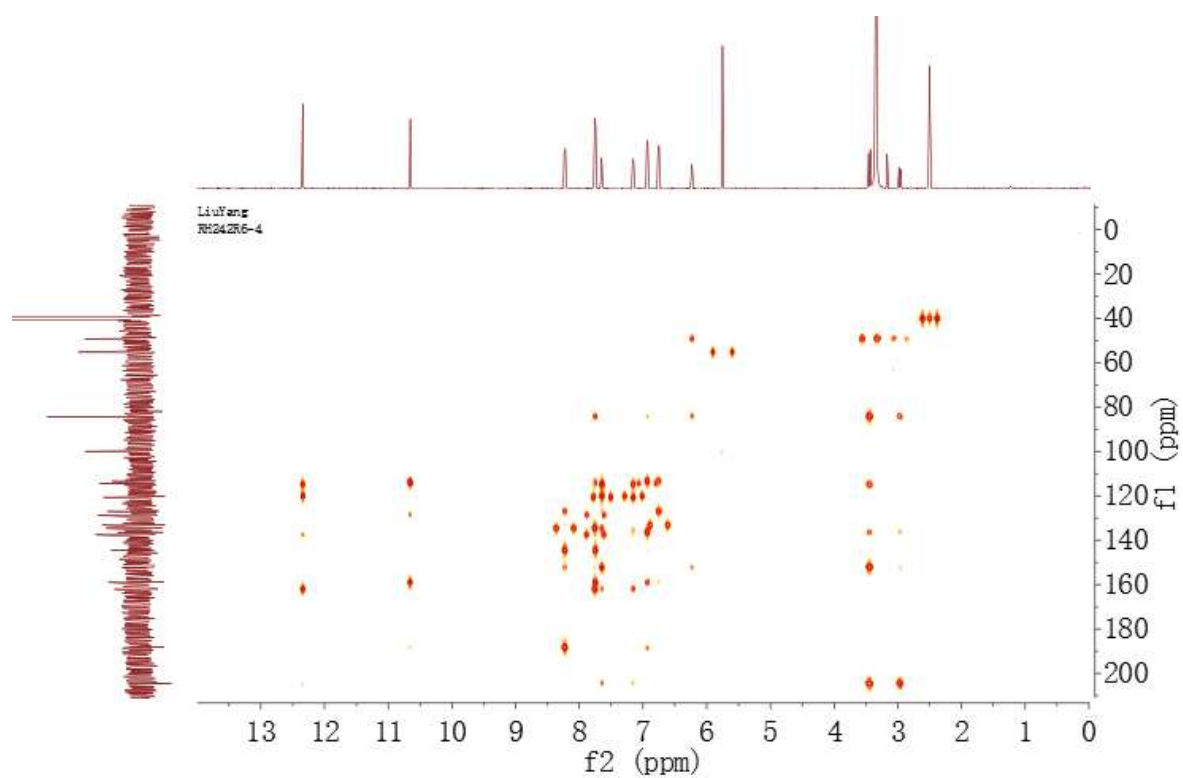
Fig. S24 HMBC spectrum of the new compound **2**

Fig. S25 Expanded HMBC spectrum of the new compound 2

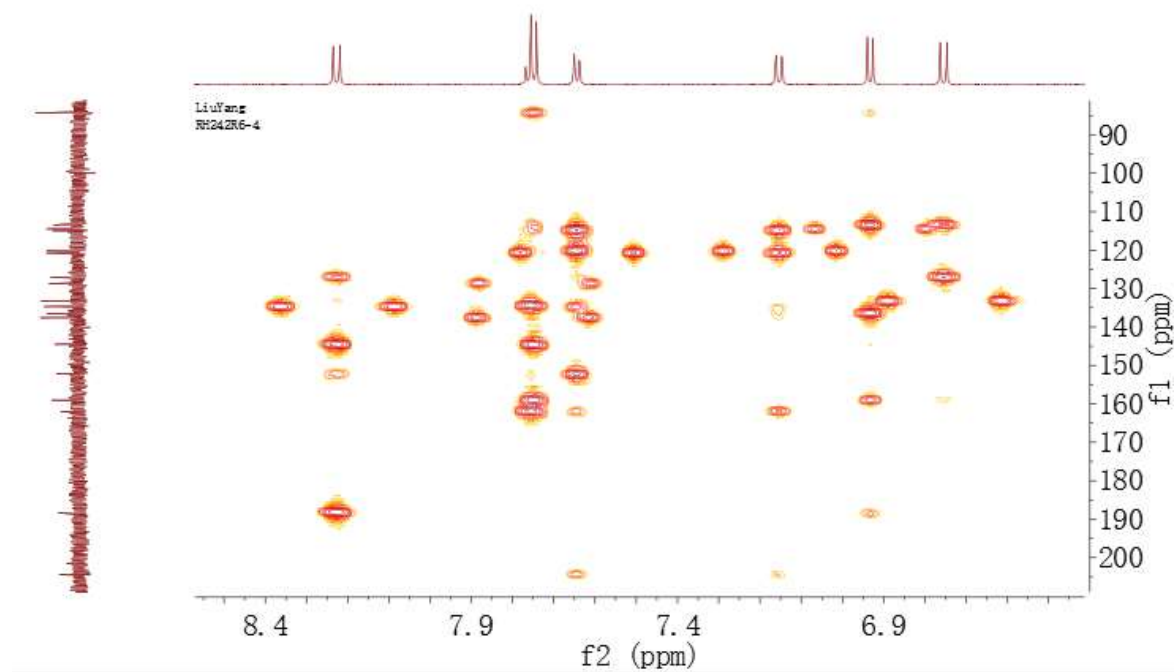


Fig. S26 HRESIMS spectrum of the new compound 2

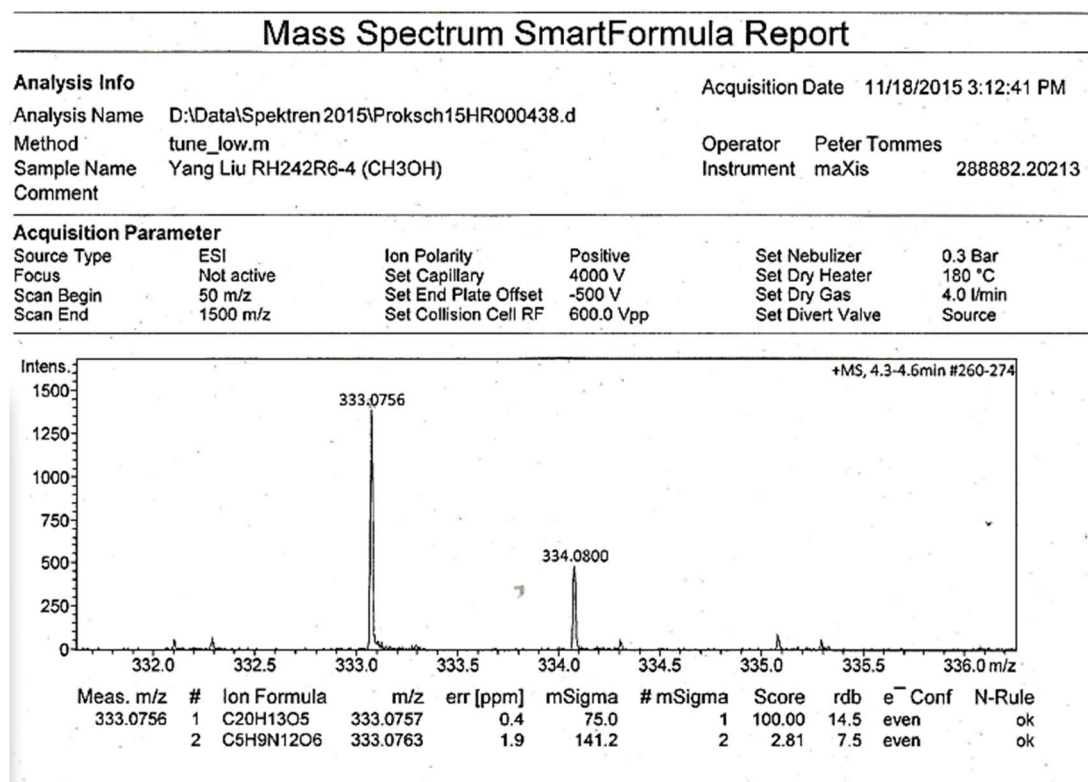


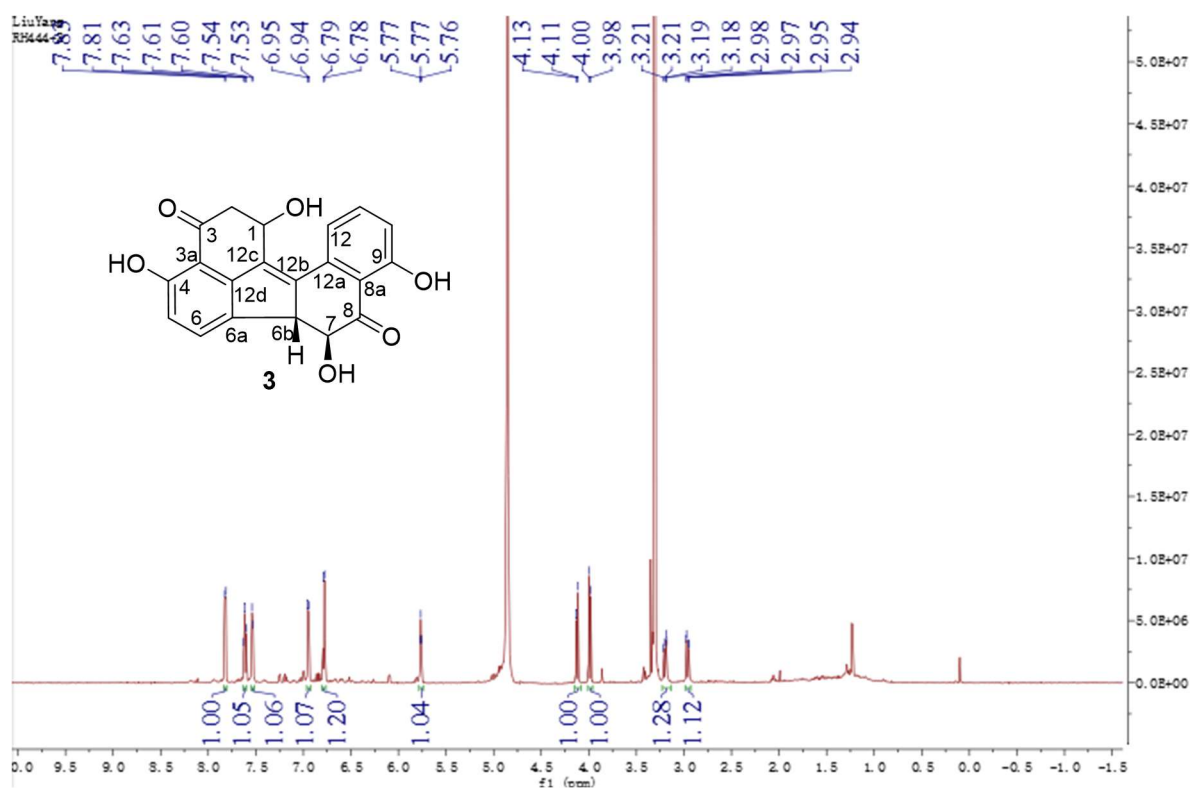
Fig. S27 ^1H NMR (600 MHz, $\text{CH}_3\text{OH}-d_4$) spectrum of the new compound **3**

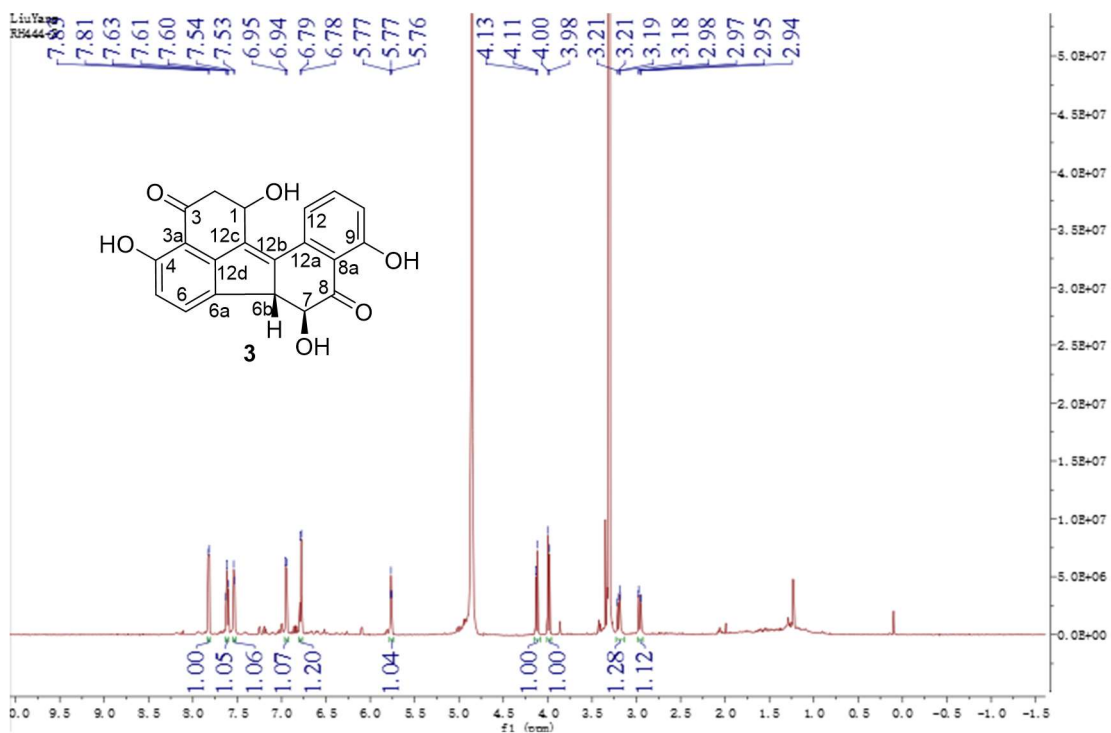
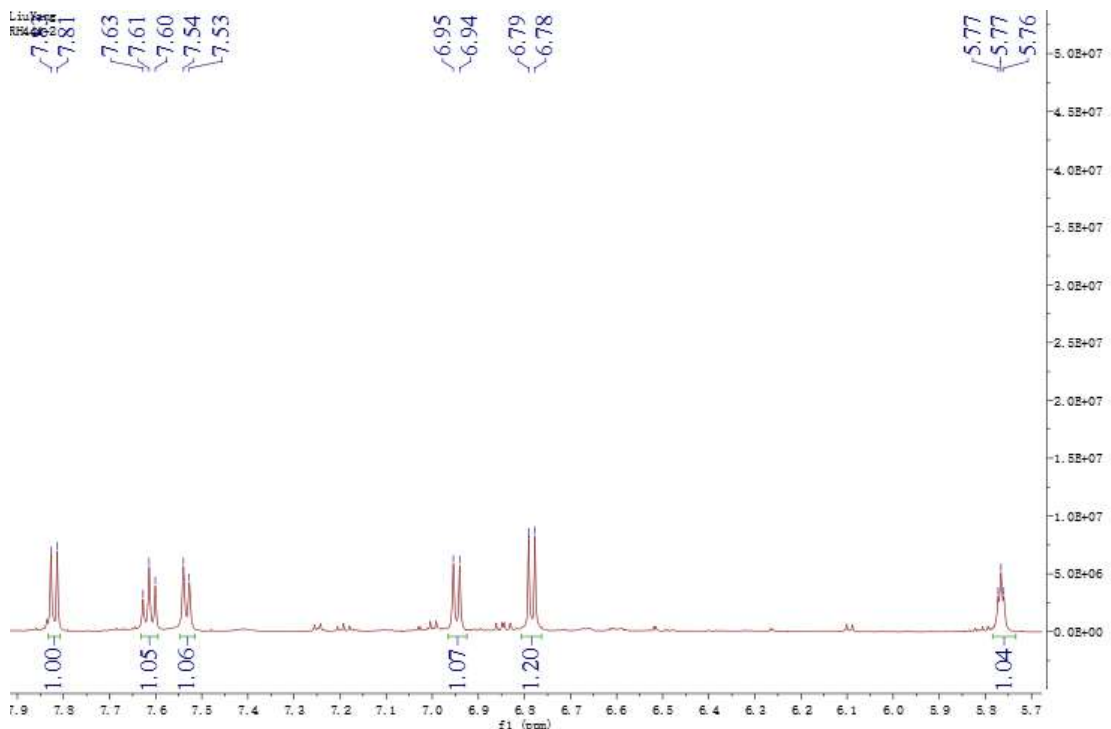
Fig. S28 Expanded ^1H NMR (600 MHz, $\text{CH}_3\text{OH}-d_4$) spectrum of the new compound **3**

Fig. S29 COSY spectrum of the new compound 3

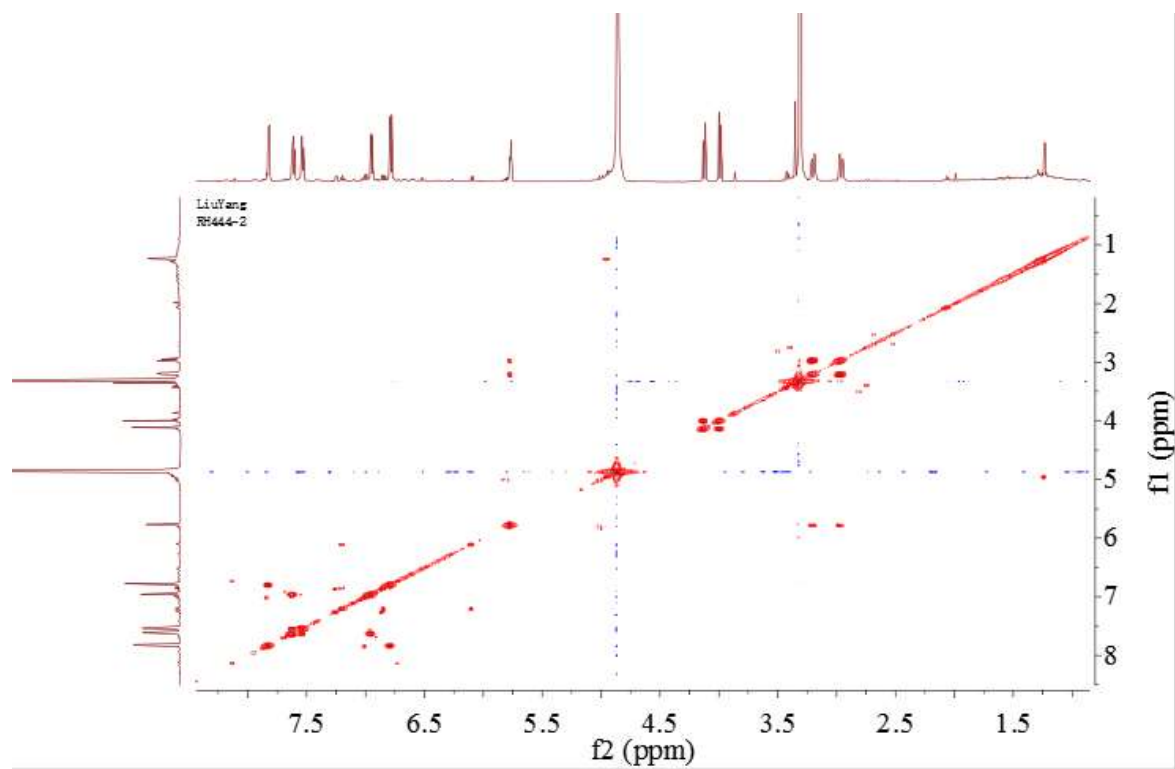


Fig. S30 HSQC spectrum of the new compound 3

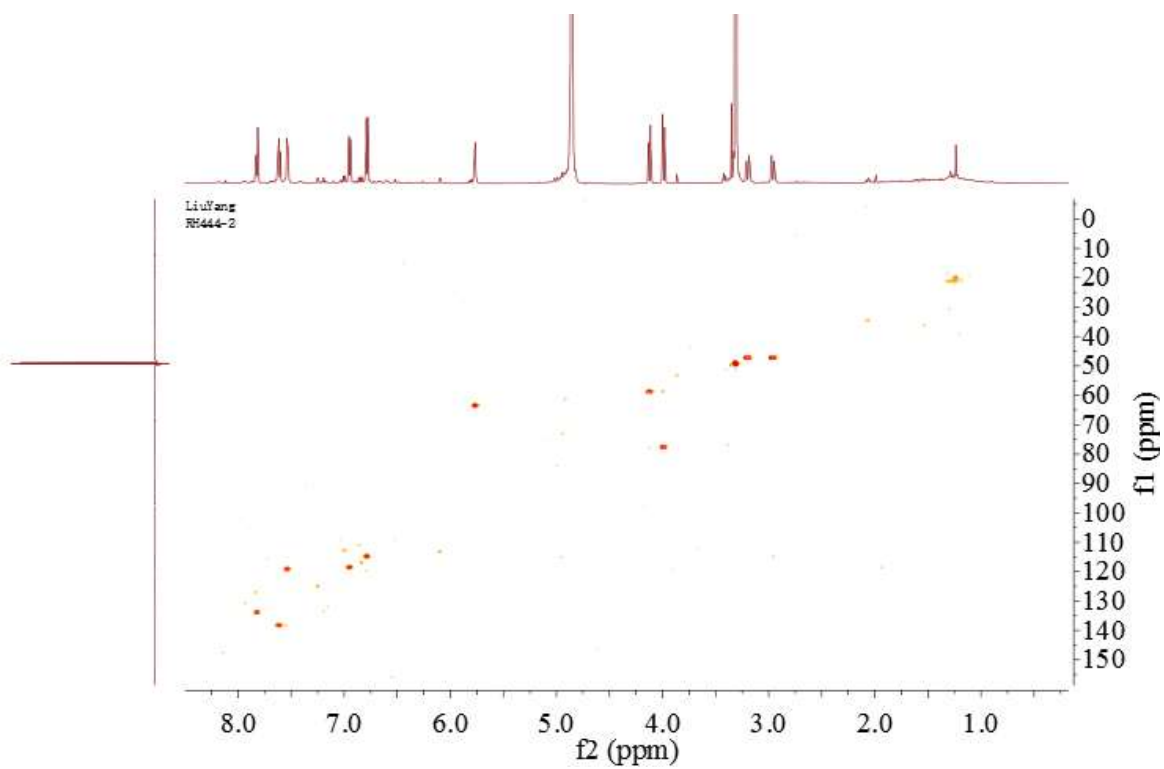


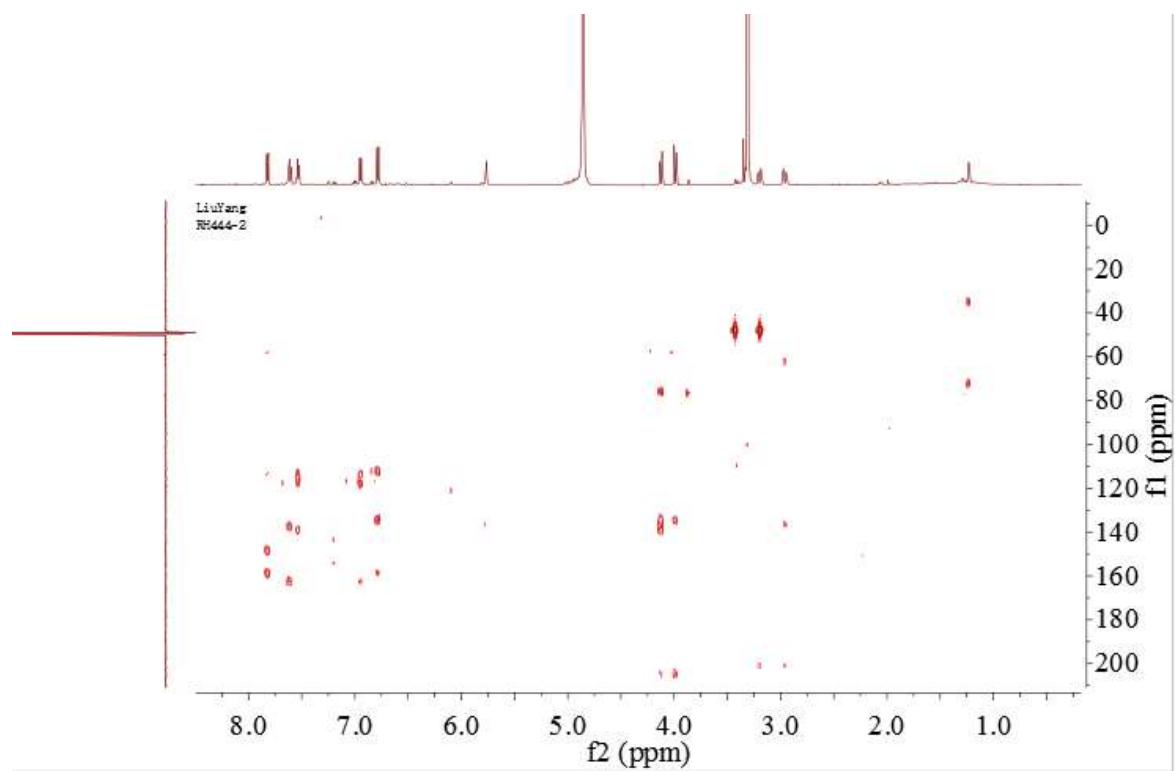
Fig. S31 HMBC spectrum of the new compound **3**

Fig. S32 HRESIMS spectrum of the new compound 3

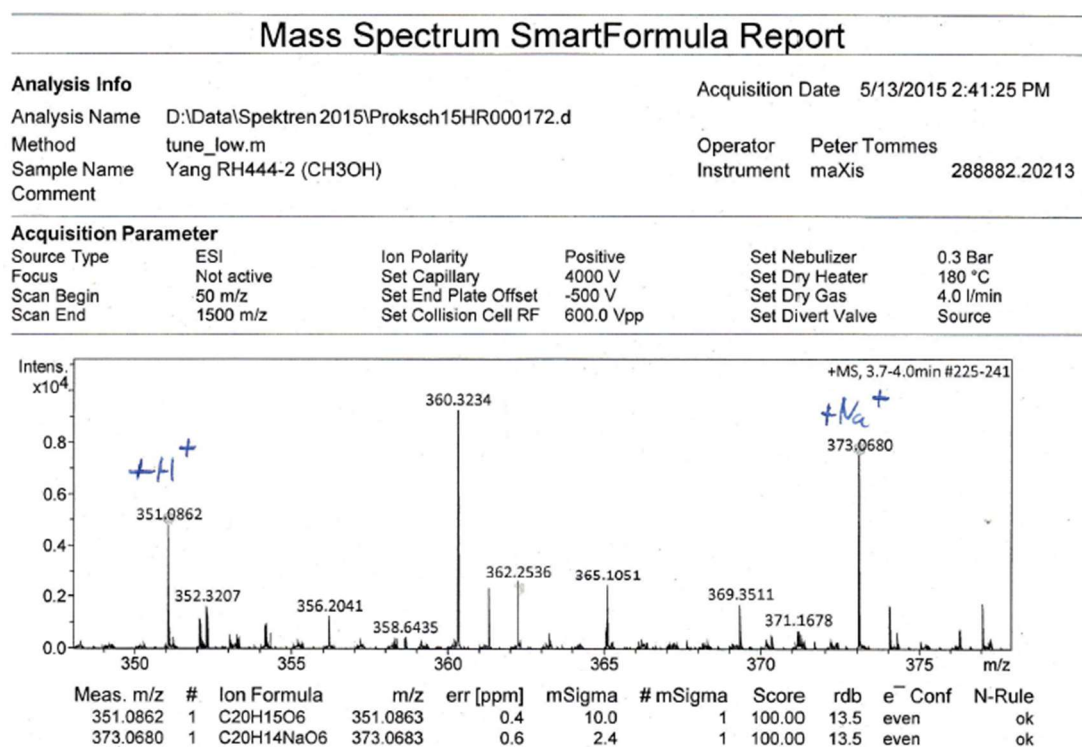


Fig. S33 Structure and population of the low-energy B3LYP/6-31G(d) *in vacuo* conformers (>2%) of (1*R*,6*bS*,7*R*)-**3** diastereomer

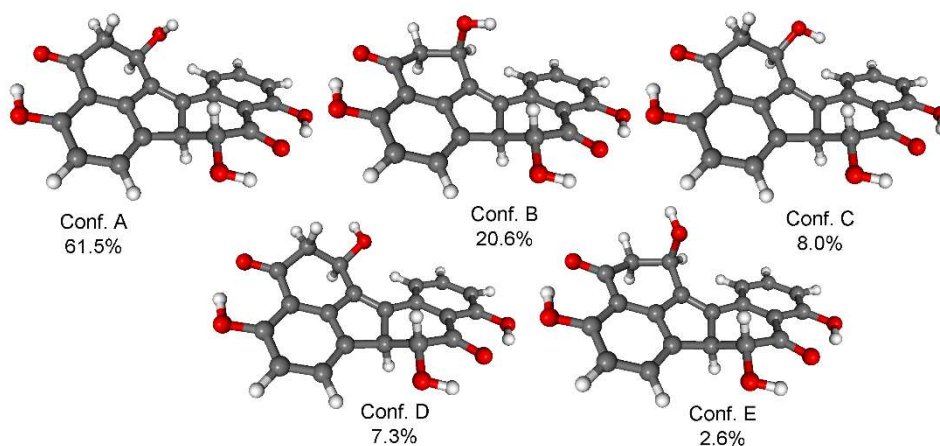


Fig. S34 Experimental ECD spectrum of **3** compared with the Boltzmann-weighted ECD spectra computed for the B3LYP/6-31G(d) *in vacuo* low-energy conformers of (1*R*,6*bS*,7*R*)-**3** at various levels

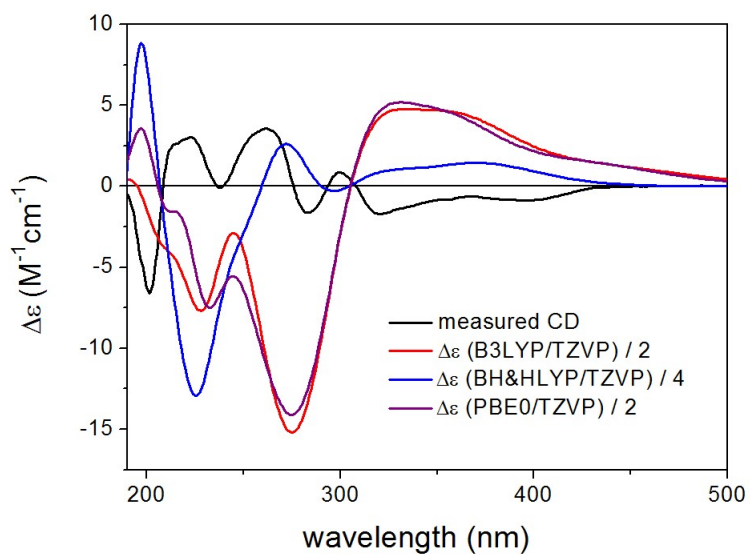


Fig. S35 Structure and population of the low-energy B3LYP/6-31G(d) conformers (>2%) of (1*S*,6*bS*,7*R*)-**3** diastereomer

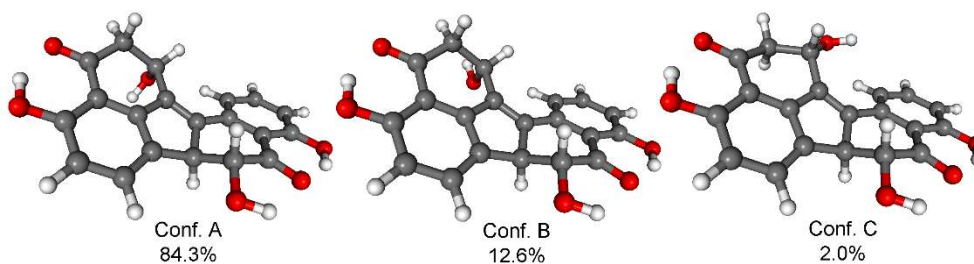


Fig. S36 Experimental ECD spectrum of **3** compared with the Boltzmann-weighted ECD spectra computed for the B3LYP/6-31G(d) *in vacuo* low-energy conformers of (1*S*,6*bS*,7*R*)-**3** at various levels

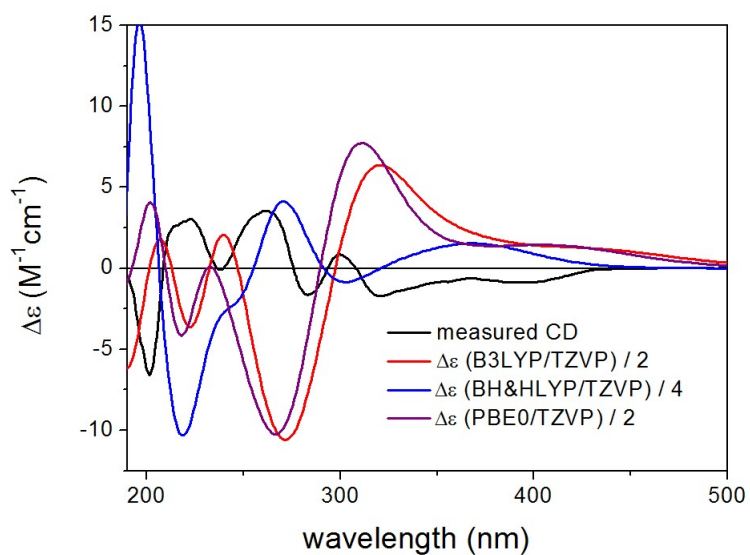


Fig. S37 Experimental ECD spectrum of **3** compared with the Boltzmann-weighted ECD spectra computed for the B3LYP/TZVP PCM/MeCN low-energy conformers of (1*R*,6*bS*,7*R*)-**3** at various levels.

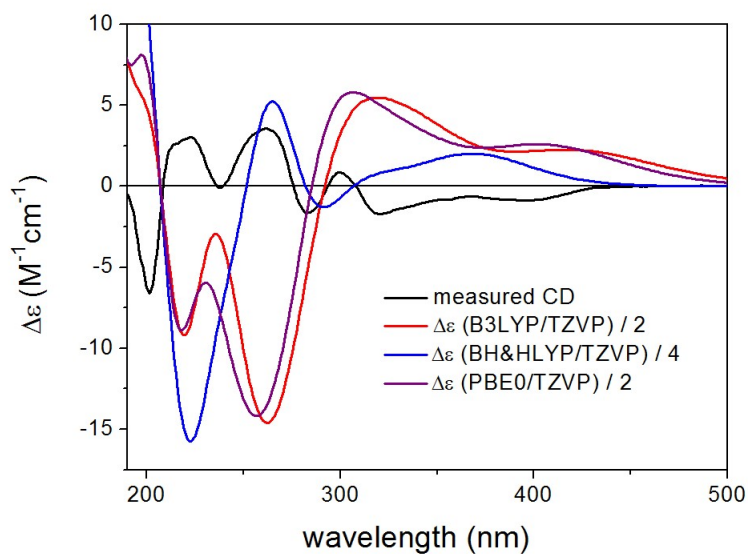


Fig. S38 Experimental ECD spectrum of **3** compared with the Boltzmann-weighted ECD spectra computed for the B3LYP/TZVP PCM/MeCN low-energy conformers of (1*S*,6*bS*,7*R*)-**3** at various levels

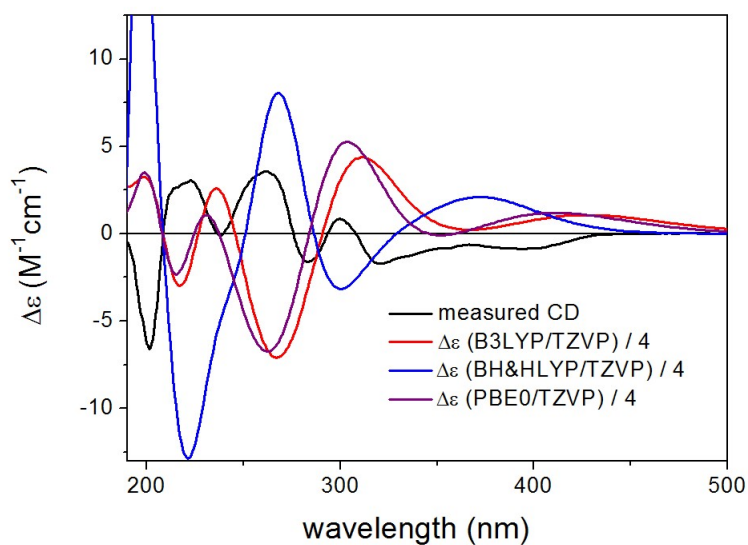


Fig. S39 Experimental ECD spectrum of **3** compared with the Boltzmann-weighted ECD spectra computed for the CAM-B3LYP/TZVP PCM/MeCN low-energy conformers of (1*R*,6*bS*,7*R*)-**3** at various levels

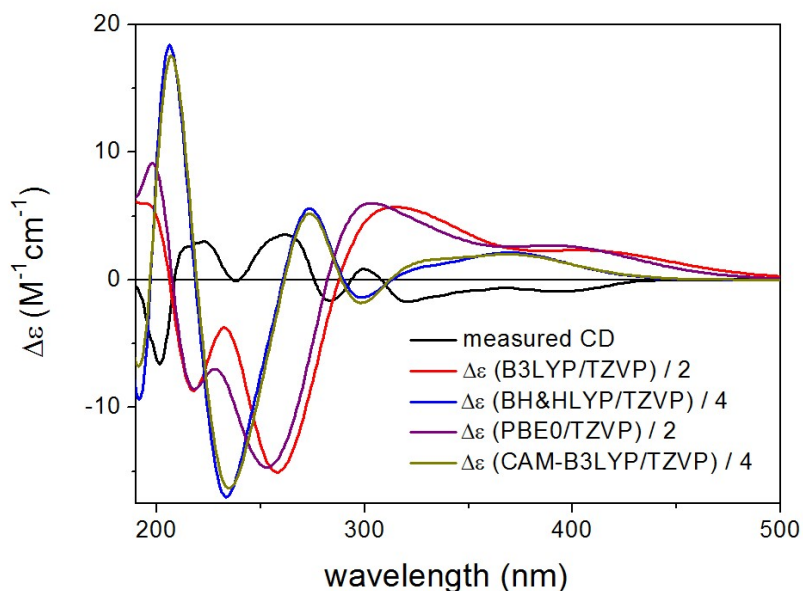


Fig. S40 Experimental ECD spectrum of **3** compared with the Boltzmann-weighted ECD spectra computed for the CAM-B3LYP/TZVP PCM/MeCN low-energy conformers of (1*S*,6*bS*,7*R*)-**3** at various levels.

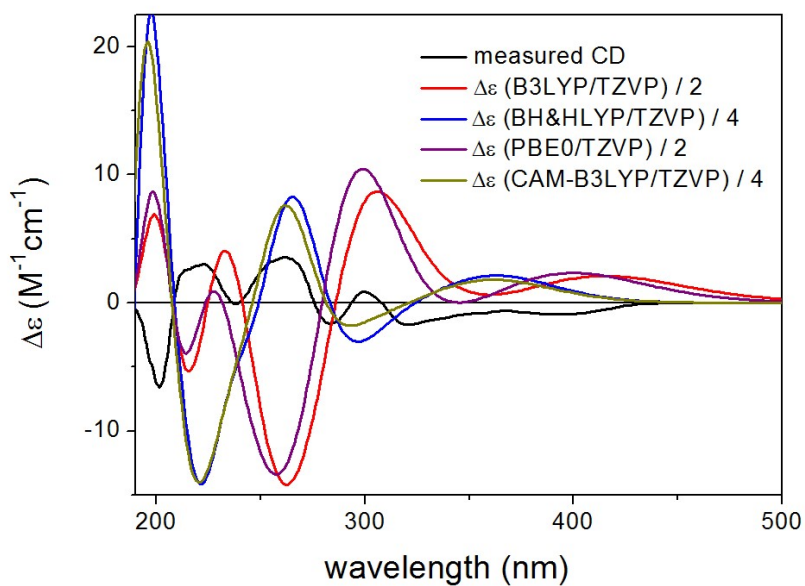
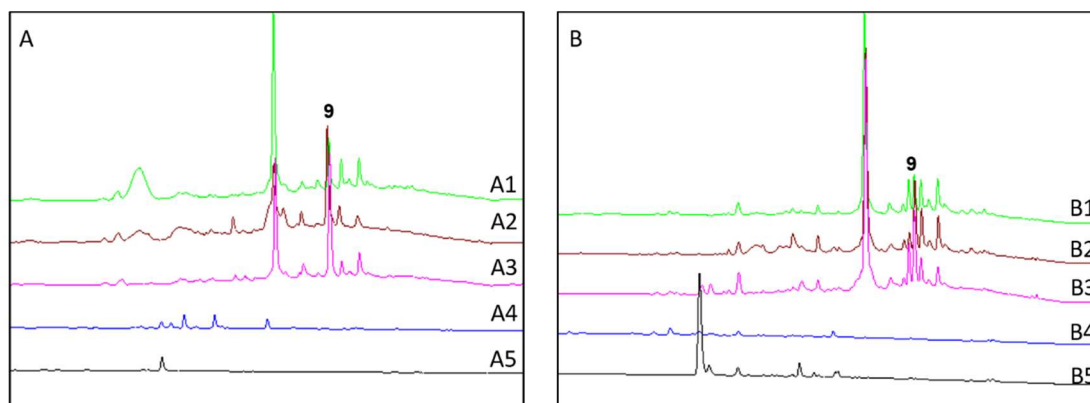


Fig. S41 HPLC chromatograms of EtOAc extracts from co-culture experiments (detection at UV 235 nm)



A: (A1) *Annulohypoxyylon* sp. control, (A2) co-cultivation of *Annulohypoxyylon* sp. with viable *S. coelicolor*, (A3) co-cultivation of *Annulohypoxyylon* sp. with viable *S. lividans*, (A4) *S. coelicolor* control, (A5) *S. lividans* control;

B: (B1) *Annulohypoxyylon* sp. control, (B2) co-cultivation of *Annulohypoxyylon* sp. with viable *B. cereus*, (B3) co-cultivation of *Annulohypoxyylon* sp. with viable *B. subtilis*, (B4) *B. cereus* control, (B5) *B. subtilis* control

6 General Discussion

6.1 Endophytic fungi produce secondary metabolites through the polyketide biogenetic pathway

Endophytic fungi produce a wide range of biologically active secondary metabolites for pharmaceutical and agricultural applications (Kumar *et al.*, 2014). Fungal metabolites continue to attract the attention of natural product researchers for chemical synthesis, mode of action, biosynthesis, and drug discovery studies (Zhang *et al.*, 2015). Polyketides, one of the largest groups of secondary metabolites, are widely produced by plants, bacteria, and fungi, and exhibit interesting biological and/or pharmaceutical properties (Zhang *et al.*, 2004; Hertweck, 2009).

Polyketides are biosynthetically derived from condensation of acetyl-CoA and malonyl-CoA units under catalysis of polyketide synthases (PKSs). PKSs have a single polypeptide chain with multiple catalytic domains that catalyze the polyketide biosynthesis *in vivo*. Polyketide biosynthesis can be detected by adding ^{13}C - or ^{14}C -labeled acetate in the medium followed by NMR/MS analysis of the labeled patterns (Simpson, 1987; Chooi and Tang, 2012).

The anthraquinone-based secondary metabolites isolated from the endophytic fungus *Stemphylium globuliferum* biogenetically arise from the polyketide biosynthetic pathway. Accordingly, the biosynthesis is suggested to start with the condensation of one starter unit acetyl-CoA and seven extender malonyl-CoA units to form the polyketide chain, which then undergoes condensation, decarboxylation, hydrogenation, and methylation reactions to yield intermediate A. The latter undergoes hydrogenation and oxidation reactions to generate macrosporin, as well as altersolanols A, B, and C. Altersolanols B and C could then be hydrogenated to form dihydroaltersolanol B and dihydroaltersolanol C, respectively. Subsequent oxidative coupling of two altersolanol A units would result in the formation of the atropisomers alterporriols D and E, possessing an *aS* or *aR* configuration, respectively. Likewise, oxidative coupling of one macrosporin and two altersolanol A units would afford the trimers stemphylanthranols A and B, as shown in Fig. 1.

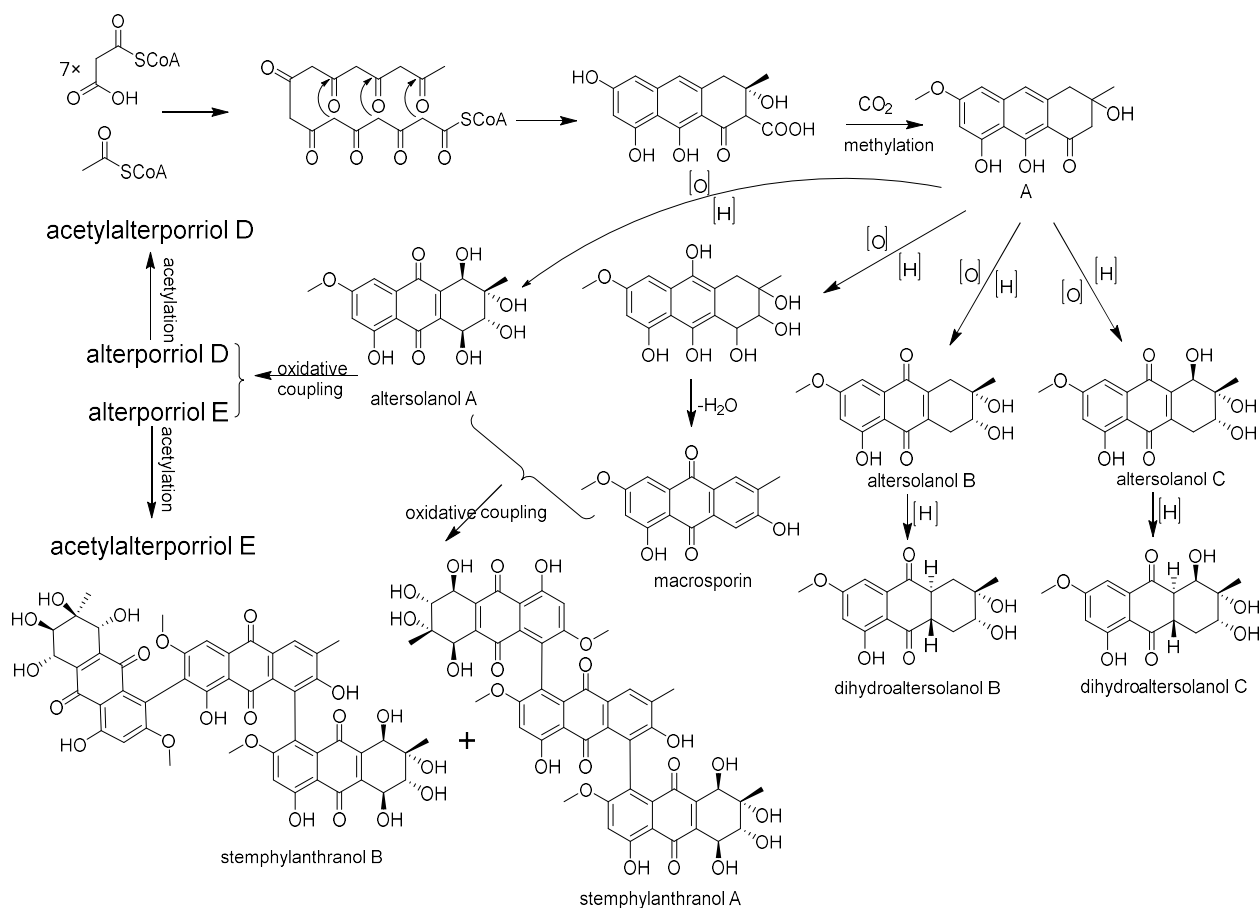


Fig. 1 Proposed biosynthetic pathway of isolated anthraquinone derivatives

In a similar manner, the naphthopyranone derivatives, isolated from the hypersaline soil fungus *C. cladosporioides*, are considered to biogenetically arise from condensation of one starter unit acetyl-CoA and seven extender malonyl-CoA units. The resulting octaketide chain would then undergo specific aromatization, reduction, and cyclization reactions to generate the intermediate B. Dehydration and lactonization of the latter followed by methoxylation would afford the monomeric precursors C and D, respectively. Oxidative coupling of the different monomers would then result in the formation of viriditoxin and its derivatives (Fig. 2). An alternative biosynthetic route would include oxidative decarboxylation of precursor B to form the 1,2-naphthoquinone monomer followed by oxidative coupling with monomer D to afford cladosporinone, as shown in Fig. 2.

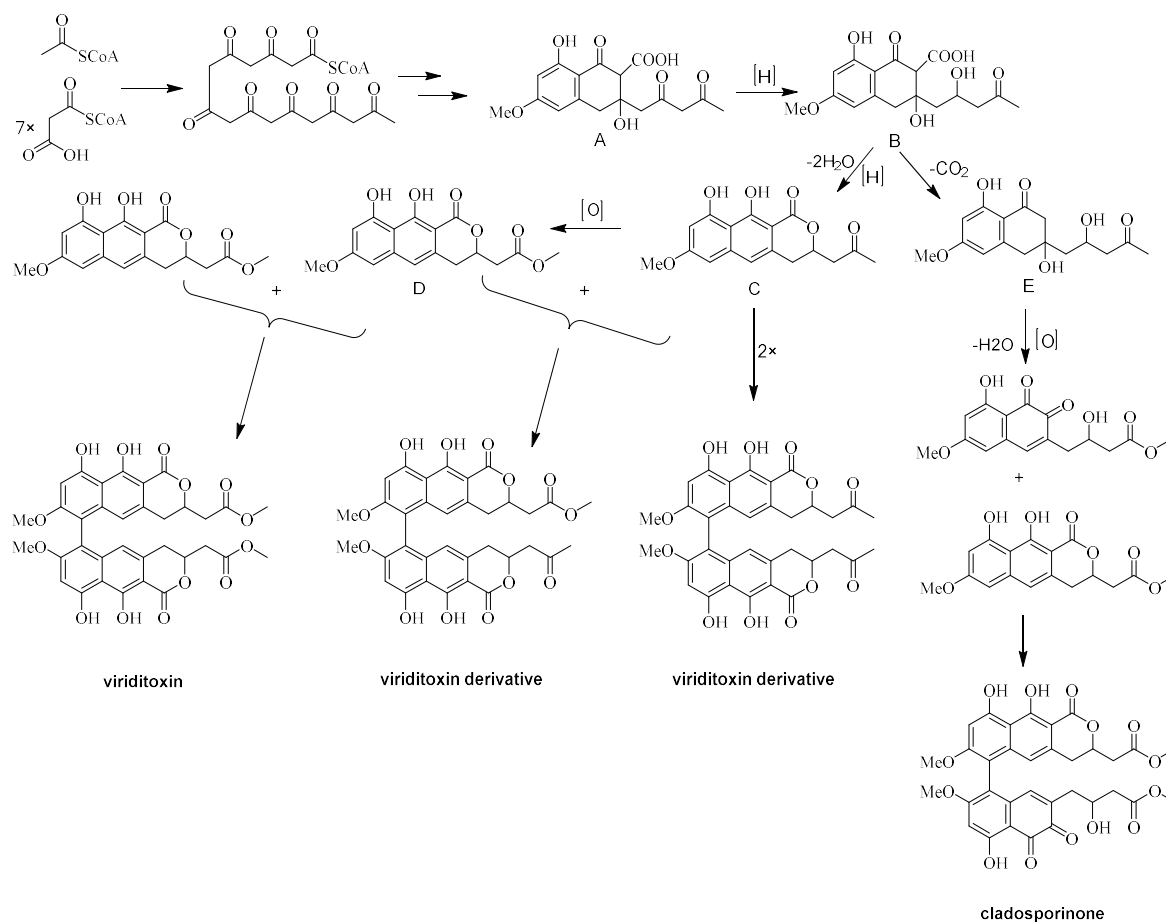


Fig. 2 Proposed biosynthetic pathway of naphthopyranones

Another example of polyketide-derived metabolites are the benzo[*j*]fluoranthene derivatives, isolated from an endophytic fungus of the genus *Annulohyphoxylon*. Their biosynthesis is suggested to start with condensation of one starter acetyl-CoA unit and four extender malonyl-CoA units to afford the precursors 1,3,8-trihydroxynaphthalene (3HN) and 1,8-dihydroxynaphthalene (DHN). Oxidative coupling of 3HN and/or DHN units would then afford the respective binaphthalene derivatives, which are further oxidized to dinaphthoquinone intermediates. Spontaneous cyclization of the latter, resembling a Michael-addition reaction, would result in the formation of the benzo[*j*]fluoranthene-ring skeleton. Finally, a series of oxidation, reduction, and water addition reactions would generate the obtained benzo[*j*]fluoranthene derivatives, as described in Fig. 3.

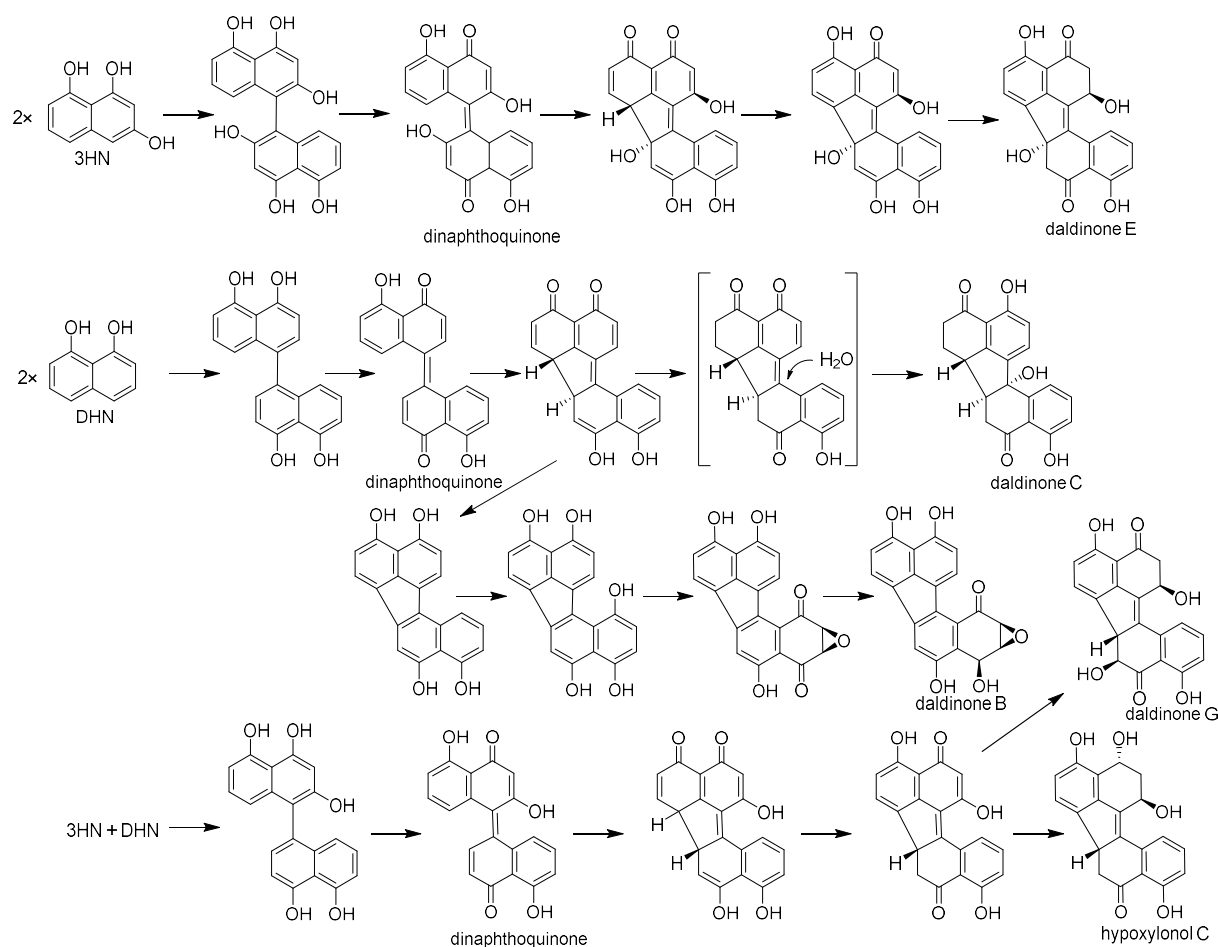


Fig. 3 Proposed biosynthetic pathway of benzo[*j*]fluoranthene derivatives

6.2 Co-cultivation: an ecological perspective to stimulate the secondary metabolites accumulation of the endophytic fungus *Annulohyphoxylon* sp.

Endophytes are described as microorganisms that thrive in the internal tissues of plants without causing any apparent disease symptoms (Faeth, 2002; Wilson, 1995). So far, more than 42,000 natural compounds have been identified from microbes, including endophytes (Ismed *et al.*, 2016; Kumar *et al.*, 2014; Rateb *et al.*, 2013; Shukla *et al.*, 2014). However, microbial genome sequence analyses suggest that most gene clusters, responsible for the production of secondary metabolites, remain silent under standard laboratory conditions (Chiang *et al.*, 2008; Schroeckha *et al.*, 2009; Tanaka *et al.*, 2013; Netzker *et al.*, 2015).

Several approaches can be employed to activate silent gene clusters, such as molecular-based techniques, OSMAC (One Strain MAny Compounds), chromatin modification or co-cultivation. The diversity of fungal secondary metabolites is largely influenced by different

cultural conditions, such as pH value, nutrition, salinity or oxygenation (Maezato and Blum, 2012), as well as by interaction between two or more microorganisms. In nature, numerous endophytes inhabit plants, and therefore they have developed unique biosynthetic pathways for the production of bioactive secondary metabolites, as a defense mechanism to fight for limited nutrients and space (Bertrand *et al.*, 2014). In these complex microbial communities, the assembly of metabolites is enhanced by secretion of chemical signals and/or by physical interaction between different microorganisms. Thus, co-cultivation is considered as a powerful tool to maximize the diversity of secondary metabolites under standard laboratory conditions, as inter-species crosstalk activates silent biosynthetic pathways in an ecological perspective (Marmann *et al.*, 2014).

In this study, three fungi were selected for co-cultivation experiments, including *Stemphylium globuliferum*, *Cladosporium cladosporioides*, and *Annulohyphoxylon* sp. These fungi were co-cultivated with the bacteria *Bacillus subtilis* 168 trpC2, *Bacillus cereus* T, *Streptomyces lividans* TK24, and *Streptomyces coelicolor* A2(3). Among the investigated fungi, only *Annulohyphoxylon* sp. showed interesting results in the co-cultivation experiments by comparing the chromatograms with those of the axenic fungal cultures as detected by HPLC analysis (Fig. 4). Particularly, co-cultivation of *Annulohyphoxylon* sp. with *Streptomyces lividans* TK24 or *Streptomyces coelicolor* A2(3) resulted in a 38-fold increase of 1-hydroxy-8-methoxynaphthalene (**9**). However, no significant induction was observed when *Annulohyphoxylon* sp. was co-cultivated with *Bacillus* species.

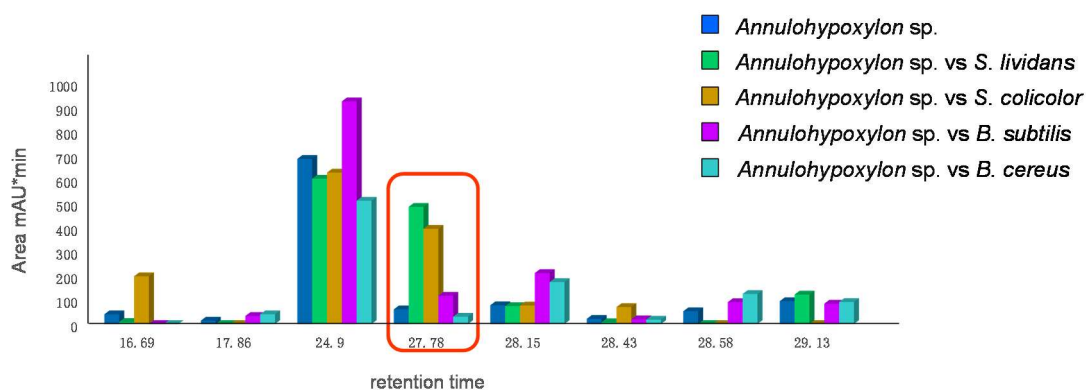


Fig. 4 HPLC chromatograms of the EtOAc extracts from different co-culture experiments (detection under UV 235 nm). The retention time of 1-hydroxy-8-methoxynaphthalene (**9**) is 27.78 min.

The high yield of 1-hydroxy-8-methoxynaphthalene (**9**) produced by *Annulohypoxyton* sp. under co-cultivation conditions suggested that **9** serves an ecological role under natural competitive conditions (Slattery *et al.*, 2001). Nevertheless, compound **9** showed no antibacterial activity against *Staphylococcus aureus* ATCC 25923, *Enterococcus faecalis* ATCC 29212 or *Mycobacterium tuberculosis*. In conclusion, mimicking the natural microbial environment through co-cultivation experiments resulted in the accumulation of constitutively present secondary metabolites, suggesting that for some fungi co-cultivation is a powerful tool for enhancing the chemical diversity of microorganisms (Rateb *et al.*, 2013).

6.3 Structure and activity relationships of the isolated compounds

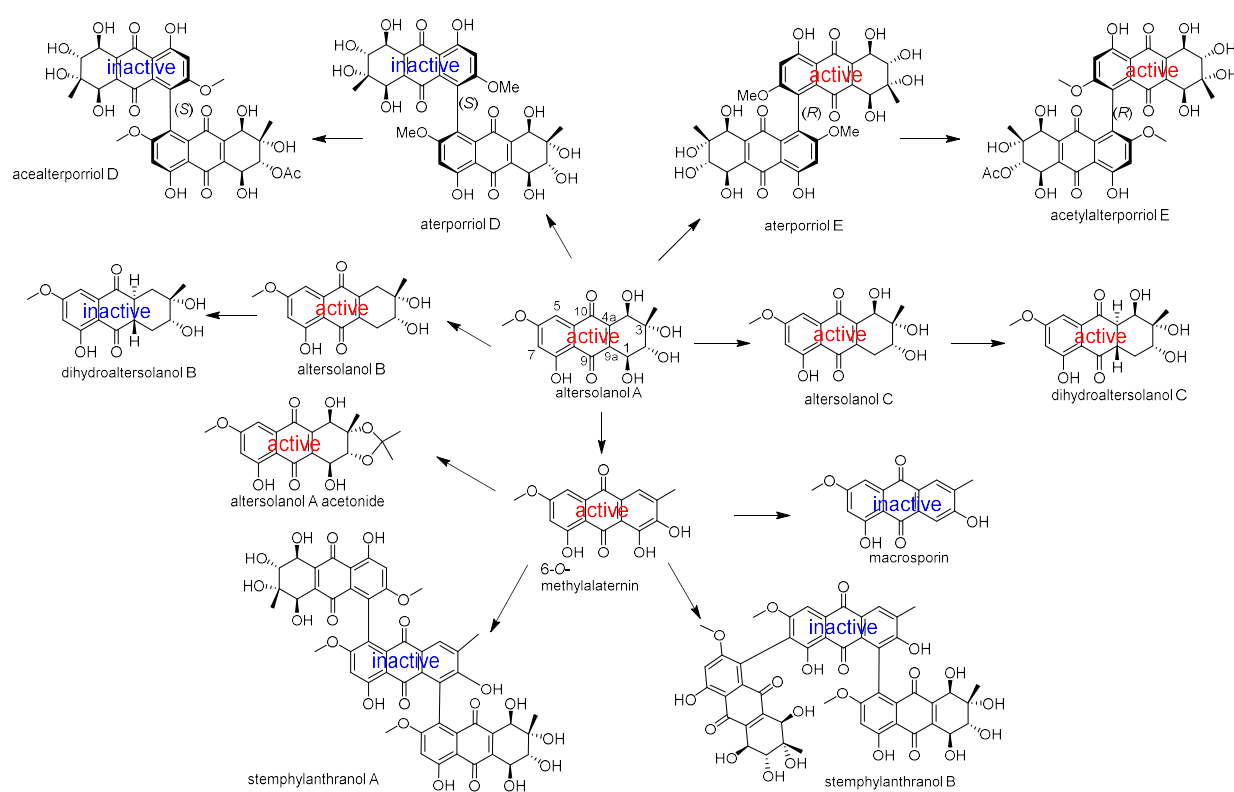
Endophytic fungi produce a wide range of bioactive secondary metabolites that can be used as drugs or drug lead compounds, such as paclitaxel, podophyllotoxin or camptothecin. These bioactive agents not only play an ecological role, but are also important from a biochemical and molecular standpoint (Kusari *et al.*, 2012). The structure-activity relationships of the isolated compounds are discussed herein.

6.3.1 Anthraquinone derivatives isolated from *Stemphylium globuliferum*

Stemphylium species are filamentous ascomycetes mainly isolated from plant hosts, but they are also known as plant pathogens or saprobes (Inderbitzin *et al.*, 2009). They produce a variety of anthraquinone derivatives, which are the largest group of natural pigments, displaying yellow, orange or brown color (Arnone and Nasini, 1986; Barash *et al.*, 1983; Manulis *et al.*, 1984; Debbab *et al.*, 2012; Debbab *et al.*, 2009; Aly *et al.*, 2010). Up to now, around 700 substances of this group have been isolated from plants and their associated microorganisms (Gessler *et al.*, 2013). Anthraquinones are well investigated natural products with a broad bioactivity spectrum, including anticancer (Huang *et al.*, 2007), antibacterial (Yang *et al.*, 2012), antifungal (Anke *et al.*, 1980), antimalarial, antituberculosis (Kanokmedhakul *et al.*, 2005), anti-osteoporotic (Wu *et al.*, 2009), and immunoinhibitory activities (Šterzl *et al.*, 1981).

The anthraquinone derivatives isolated from the endophytic fungus *S. globuliferum*, including altersolanols A-C, dihydroaltersolanol C, 6-*O*-methylalaternin, alterporriol E and

acetylalterporriol E, showed significant cytotoxicity against the murine lymphoma (L5178Y) cell line. A tentative suggestion on the structure-activity relationships of these derivatives is proposed. The reduced activity of altersolanol A acetonide compared to the cytotoxic compounds altersolanols A-C suggested that the hydroxy groups located at the aliphatic ring are not necessary for cytotoxicity. Moreover, in dihydroaltersolanols B and C, the hydroxy group located at C-4 was one of the key functional groups for mediating cytotoxicity. Likewise, 6-*O*-methylalternerin displayed strong cytotoxicity, whereas its analogue macrosporin was inactive, suggesting that the hydroxy group at C-1 is one of the functional groups for cytotoxicity. Interestingly, alterporriols E and acetylalterporriol E, consisting of two altersolanol A units that are connected through a 5, 5'-biaryl linkage with (aR) axial chirality, showed strong cytotoxicity, whereas their (aS)-congeners were inactive.

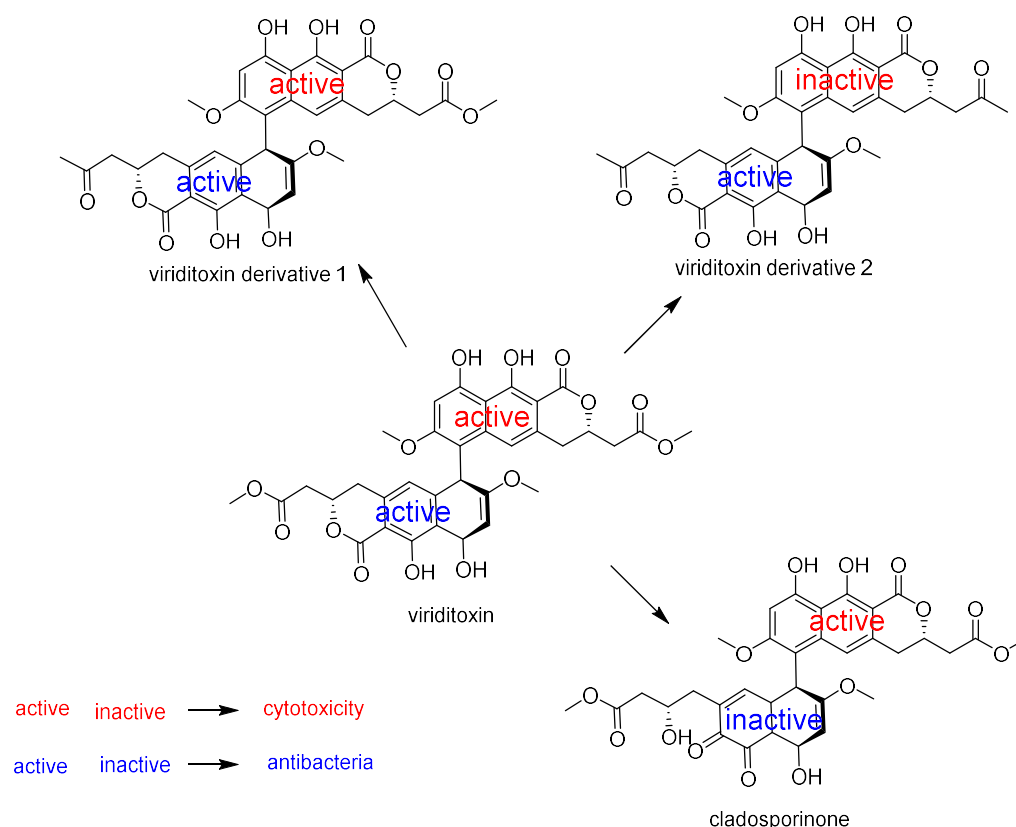


6.3.2 Naphthopyranone derivatives isolated from *Cladosporium cladosporioides*

The genus *Cladosporium* consists of more than 772 species (Dugan *et al.*, 2008). Fungi of this genus are widespread and are commonly found as endophytes, human pathogens, phytopathogens or saprobes (Crous *et al.*, 2007; Dugan *et al.*, 2008). Particularly,

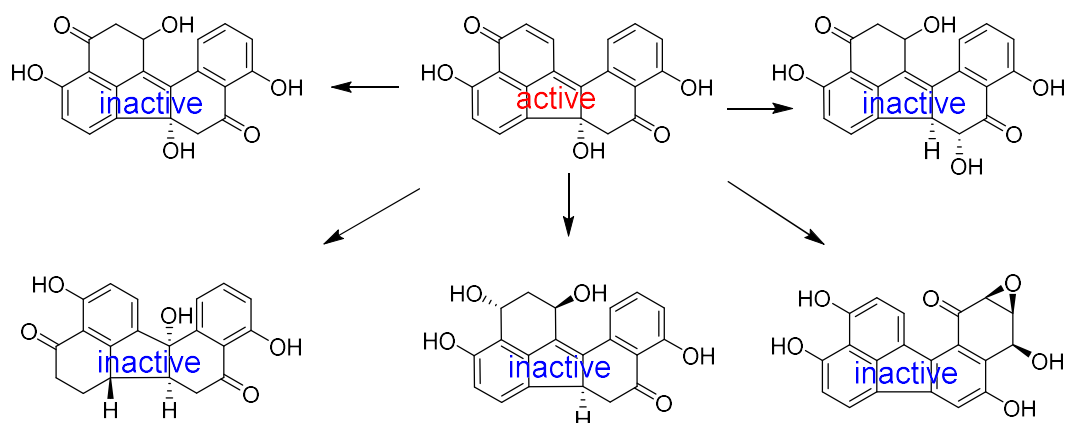
Cladosporium cladosporioides is a cosmopolitan saprobic species, which is often isolated from air, soil or necrotic parts of different plants (Bensch *et al.*, 2010). The well known antifungal and antibiotic secondary metabolite cladosporin, as well as the diastereoisomers cladosporin and isocladosporin, which showed growth inhibition of etiolated wheat coleoptiles, have been described from *Cladosporium cladosporioides* (Wang *et al.*, 2013; Anke and Zähler, 1978; Jacyno, 1993).

The naphthopyranone derivatives that are involved in this study were obtained from the fungus *C. cladosporioides*, isolated from the sediment of a hypersaline lake in Egypt. The known antibiotic viriditoxin showed potent inhibitory activity against *Staphylococcus aureus* with an MIC value of 0.023 μM . However, the new derivative, cladosporinone, exhibited only weak antibacterial activity (MIC = 97.86 μM) against the same cell line, suggesting that hydrolysis of one of the two lactone rings, followed by oxidative decarboxylation attenuates the antibacterial activity. Likewise, loss of the methylated carboxyl groups at the side chain weakens the antibacterial activity of the two viriditoxin derivatives (MIC values of 3.09 and 25.32 μM) when compared to viriditoxin. Interestingly, the latter displayed potent cytotoxicity against the murine lymphoma (L5178Y), A2780sens and A2780CisR cell lines with IC_{50} values of 0.15 μM , 0.12 μM , and 0.43 μM , respectively, whereas cladosporinone exhibited selective activity against the murine lymphoma (L5178Y) cell line with an IC_{50} value of 0.88 μM .



6.3.3 Benzo[*j*]fluoranthene derivatives isolated from *Annulohypoxyton* sp.

The benzo[*j*]fluoranthene-based secondary metabolites isolated from *Annulohypoxyton* sp. exhibited no significant cytotoxic or antibacterial activity. However, the artefact daldinone F, which is the dehydrated product of daldinone E, exhibited strong cytotoxicity against Ramos and Jurkat J16 cell lines with IC₅₀ values of 6.7 and 14 μM, respectively. Notably, mechanistic studies indicated that daldinone F induces apoptotic cell death through induction of intrinsic apoptosis. Moreover, daldinone F blocks autophagy, which is a potential pro-survival pathway for cancer cells, highlighting its usability in anticancer therapy.



7 Bibliography

1. Alberts A. W. (1988) Discovery, biochemistry and biology of lovastatin. *Am. J. Cardiol.*, 62, 10J-15J.
2. Aly A. H., Debbab A., Proksch P. (2011) Fungal endophytes: unique plant inhabitants with great promises. *Appl. Microbiol. Biotechnol.*, 90, 1829-1845.
3. Aly A. H., Debbab A., Edrada-Ebel R. A., Müller W. E. G., Kubbutat M. H. G., Wray V., Ebel R., Proksch P. (2010) Protein kinase inhibitors and other cytotoxic metabolites from the fungal endophytic *Stemphylium botryosum* isolated from *Chenopodium album*. *Mycosphere*, 1, 153-162.
4. Anke H., Kolthoum I., Laatsch H. (1980) Metabolic products of microorganisms. 192. The anthraquinones of *Aspergillus glaucus* group. II. Biological activity. *Arch. Microbiol.*, 126, 231-236.
5. Anke H. and Zähler H. (1978) Metabolic products of microorganisms 170. On the antibiotic activity of cladosporin. *Arch. Microbiol.*, 116, 253-257.
6. Antoraz S., Santamaría R. I., Díaz M., Sanz D., Rodríguez H. (2015) Toward a new focus in antibiotic and drug discovery from the *Streptomyces arsenal*. *Front. Microbiol.*, 6, 1-8.
7. Aoki H. and Okuhara M. (1980) Natural β -lactam antibiotics. *Ann. Rev. Microbiol.*, 34, 159-181.
8. Ariëns E. J. (1984) Stereochemistry, a basis for sophisticated nonsense in pharmacokinetics and clinical pharmacology. *Eur. J. Clin. Pharmacol.*, 26, 663-668.
9. Bailly C. (2003) Homocamptothecins: potent topoisomerase I inhibitors and promising anticancer drugs. *Crit. Rev. Oncol. Hematol.*, 45, 91-108.
10. Barash I., Manulis S., Kashman Y., Springer J. P., Chen M. H., Clardy J., Strobel G. A. (1983) Crystallization and x-ray analysis of stemphyloxin I, a phytotoxin from *Stemphylium botryosum*. *Science*, 220, 1065-1066.
11. Bensch K., Groenewald J. Z., Dijksterhuis J., Starink-Willemsse M., Andersen B., Summerell B. A., Shin H. D., Dugan F. M., Schroers H. J., Braun U., Crous P. W. (2010) Species and ecological diversity within the *Cladosporium cladosporioides* complex

- (Davidiellaceae, Capnodiales). *Stud. Mycol.*, 67, 1-94.
12. Bertolini F. (2011) Anti-angiogenesis in cancer; met and unmet goals-an interview with Robert Kerbel. *Int. J. Dev. Biol.*, 55, 395-398.
 13. Bertrand S., Bohni N., Schnee S., Schumpp O., Gindro K., Wolfender J. (2014) Metabolite induction via microorganism co-culture: A potential way to enhance chemical diversity for drug discovery. *Biotechnol. Adv.*, 32, 1180–1204.
 14. Bhanot A., Sharma R., Noolvi M. N. (2011) Natural sources as potential anti-cancer agents: A review. *Int. J. Phytomedicine*, 3, 9-26.
 15. Bhatnagar I. and Kim S. K. (2012) Pharmacologically prospective antibiotic agents and their sources: A marine microbial perspective. *Environ. Toxicol. Pharmacol.*, 34, 631-643.
 16. Bode H. B., Bethe B., Höfs R., Zeeck A. (2002) Big effects from small changes: possible ways to explore nature's chemical diversity. *ChemBioChem*, 3, 619-627.
 17. Bosch F. X., Manos M. M., Munoz N., Sherman M., Jansen A. M., Peto J., Schiffman M. H., Moreno V., Kurman R., Shah K.V. (1995) Prevalence of Human Papillomavirus in Cervical Cancer: a Worldwide Perspective. *J. Natl. Cancer. Inst.*, 87, 796-802.
 18. Butler M. S. (2004) The Role of Natural Product Chemistry in Drug Discovery. *J. Nat. Prod.*, 67, 2141-2153.
 19. Changediya V. (2010) The study of relevance of microbial coculture fermentation in biotechnology. *Int. J. Pharm. Sci. Rev. Res.*, 5, 5-13.
 20. Chiang Y., Szewczyk E., Nayak T., Davidson A. D., Sanchez, J. F., Lo H., Ho W., Simityan H., Kuo Eric., Praseuth A., Watanabe K., Oakley B. R., Wang C. C. C. (2008) Molecular Genetic Mining of the *Aspergillus* Secondary Metabolome: Discovery of the Emericellamide Biosynthetic Pathway. *Chemistry & Biology*, 15, 527-532.
 21. Chin Y. W., Balunas M. J., Chai H. B., Kinghorn A. D. (2006) Drug discovery from natural sources. *AAPS J.*, 8, E239-E253.
 22. Chooi Y. H. and Tang Y. (2012) Navigating the Fungal Polyketide Chemical Space: From Genes to Molecules. *J. Org. Chem.*, 77, 9933–9953.
 23. Cortés F., Pastor N., Mateos S., Domínguez I. (2003) Roles of DNA topoisomerases in chromosome segregation and mitosis. *Mutat. Res.*, 543, 59-66.

24. Cragg G. M., Newman D. J., Snader K. M. (1997) Natural products in drug discovery and development. *J. Nat. Prod.*, 60, 52-60.
25. Cragg G. M. (1998) Paclitaxel (Taxol®): A success story with valuable lessons for natural product drug discovery and development. *Inc. Med. Res. Rev.*, 18, 315-331.
26. Cragg G. M. and Newman D. J. (2003) Plants as a source of anti-cancer and anti-HIV agents. *Ann. appl. Biol.*, 143, 127-133.
27. Cragg G. M., Grothaus P. G., Newman D. J. (2009) Impact of Natural Products on Developing New Anti-Cancer Agents. *Chem. Rev.*, 109, 3012-3043.
28. Cragg G. M. and Newman D. J. (2013) Natural products: A continuing source of novel drug leads. *BBA-Gen. Subjects*, 1830, 3670-3695.
29. Crous P. W., Braun U., Schubert K., Groenewald J. Z. (2007) Delimiting *Cladosporium* from morphologically similar genera. *Stud. Mycol.*, 58, 33-56.
30. Debbab A., Aly A. H., Edrada-Ebel R., Wray V., Pretsch A., Pescitelli G., Kurtan T., Proksch P. (2012) New Anthracene Derivatives - Structure Elucidation and Antimicrobial Activity. *Eur. J. Org. Chem.*, 7, 1351–1359.
31. Debbab A., Aly A. H., Edrada-Ebel R. A., Wray V., Müller W. E. G., Totzke F., Zirrgiebel U., Schächtele C., Kubbutat M. H. G., Lin W. H., Mosaddak M., Hakiki A., Proksch P., Ebel R. (2009) Bioactive Metabolites from the Endophytic Fungus *Stemphylium globuliferum* Isolated from *Mentha pulegium*. *J. Nat. Prod.*, 72, 626-631.
32. Demain A. L. and Sanchez S. (2009) Microbial drug discovery: 80 years of progress. *J. Antibiot.*, 62, 5–16.
33. Demain A. L. (2014) Importance of microbial natural products and the need to revitalize their discovery. *J. Ind. Microbiol. Biotechnol.*, 41, 185-201.
34. Dewese J. E. and Osheroff N. (2009) The DNA cleavage reaction of topoisomerase II: wolf in sheep's clothing. *Nucleic Acids Res.*, 37, 738–748.
35. Dugan F. M., Braun U., Groenewald J. Z., Crous P. W. (2008) Morphological plasticity in *Cladosporium sphaerospermum*. *Persoonia*, 21, 9-16
36. Efferth T., Fu Y., Zu Y., Schwarz G., Konkimalla V. S. B., Wink M. (2007) Molecular target-guided tumor therapy with natural products derived from traditional Chinese medicine. *Curr. Med. Chem.*, 14, 2024-2032.

37. Faeth S. H. (2002) Are endophytic fungi defensive plant mutualists? *Oikos*, 98, 25-36.
38. Ganesan A. (2008) The impact of natural products upon modern drug discovery. *Curr. Opin. Chem. Biol.*, 12, 306–317.
39. Gessler N. N., Egorova A. S., Belozerskaya T. A. (2013) Fungal Anthraquinones. *Appl. Microbiol. Biotechnol.*, 49, 85-99.
40. Goodman M. and Mcgahren W. J. (1966) Plant antitumor agents. I. The isolation and structure of Camptothecin, a novel alkaloidal leukemia and tumor inhibitor from *Camptotheca acuminata*. *J. Am. Chem. Soc.*, 88, 3888-3890.
41. Gull K. and Trinci A. P. J. (1973) Griseofulvin inhibits fungal mitosis. *Nature*, 244, 292-294.
42. Guo B., Li H., Zhang L. (1998) Isolation of a fungus producing vinblastine. *J. Yunnan Univ.*, 20, 214-215.
43. Grabley S. and Thiericke R. (1999) Bioactive agents from natural sources: Trends in discovery and application. *Adv. Biochem. Eng. Biotechnol.*, 64, 101-154.
44. Hanahan D. and Weinberg R. A. (2000) The Hallmarks of Cancer. *Cell*, 100, 57-70.
45. Harzstark A. L., Rosenberg J. E., Weinberg V. K., Sharib J., Ryan C. J., Smith D. C., Pagliaro L. C., Beer T. M., Liu G., Small E. J. (2011) Ixabepilone, mitoxantrone, and prednisone for metastatic castration-resistant prostate cancer after docetaxel-based therapy. *Cancer*, 117, 2419-2425.
46. Hawksworth D. L. (1991) The fungal dimension of biodiversity: magnitude, significance, and conservation. *Mycol. Res.*, 95, 641-655.
47. Hawksworth D. L. (2004) Fungal diversity and its implications for genetic resource collections. *Stud. Mycol.*, 50, 9-18.
48. Helleday T., Petermann E., Lundin C., Hodgson B., Sharma R. A. (2008) DNA repair pathways as targets for cancer therapy. *Nat. Rev. Cancer.*, 8, 193-204.
49. Hertweck C. (2009). The Biosynthetic Logic of Polyketide Diversity. *Angew. Chem. Int. Ed.*, 48, 4688-4716
50. Huang Q., Lu G., Shen H. M., Chung M. C. M., Ong C. N. (2007) Anti-cancer properties of anthraquinones from rhubarb. *Med. Res. Rev.*, 27, 609-630.
51. Inderbitzin P., Mehta Y. R., Berbee M. L. (2009) Pleospora species with *Stemphylium*

- anamorphs*: a four locus phylogeny resolves new lineages yet does not distinguish among species in the Pleospora herbarum clade. *Mycologia*, 101, 329-339
52. Ismed F., Nofriani A., Haryenti R. S. Elsy A., Djamaan A. (2016) Fermentation and Antimicrobial Activity assay from *Aspergillus fumigatus* Isolated from Corncob. *Der Pharmacia Lettre*, 8, 153-157.
 53. Jacyno J. M. (1993) Isocladosporin, a biologically active isomer of cladosporin from *Cladosporium cladospriosides*. *J. Nat. Prod.*, 56, 1397-1401.
 54. Jalgaonwala R. E., Mohite B. V., Mahajan R. T. (2011) A review: Natural products from plant associated endophytic fungi. *J. Microbiol. Biotech. Res.*, 1, 21-32.
 55. Ji Y. T., Liu Y. N., Liu Z. P. (2015) Tubulin Colchicine Binding Site Inhibitors as Vascular Disrupting Agents in Clinical Developments. *Curr. Med. Chem.*, 22, 1348-1360.
 56. Kanokmedhakul K., Kanokmedhakul S., Phatchana R. (2005) Biological activity of anthraquinones and triterpenoids from *Prismatomeris fragrans*. *J. Ethnopharmacol.*, 100, 284-288
 57. Kato S. and Kikuchi A. (1998) DNA topoisomerase: the key enzyme that regulates DNA super structure. *Nagoya J. Med. Sci.*, 61.11-26.
 58. Kennedy M. and Krouse D. (1999) Strategies for improving fermentation medium performance: a review. *J. Ind. Microbiol. Biotechnol.*, 23, 456-475.
 59. Kerbel R. S. (2000) Tumor angiogenesis: past, present and the near future. *Carcinogenesis*, 21, 505-515.
 60. Kharwar R. N., Mishra A., Gond S. K., Stierle A., Stierle D. (2011) Anticancer compounds derived from fungal endophytes: their importance and future challenges. *Nat. Prod. Rep.*, 28, 1208-1228.
 61. Kingston D. G. I. (2009) Tubulin-Interactive Natural Products as Anticancer Agents. *J. Nat. Prod.*, 72, 507-515.
 62. Kitajima M., Yoshida S., Yamagata K., Nakamura M., Takayama H., Saito K., Seki H., Aimi N. (2002) Camptothecin-related alkaloids from hairy roots of *Ophiorrhiza pumila*. *Tetrahedron*, 58, 9169-9178.
 63. Klayman D. L. (1985) Qinghaosu Artemisinin): An Antimalarial Drug from China. *Science*, 228, 1049-1055.

64. Kumar A., Abnave P., Ahmad A. (2013) Culture morphological and molecular characterization of vinca alkaloids producing endophytic fungus *Fusarium solani* isolated from *Catharanthus roseus*. *Int. J. Bot. Res.*, 3, 1-12.
65. Kumar A., Patil D., Rajamohanan P. R., Ahmad A. (2013) Isolation, purification and characterization of vinblastine and vincristine from endophytic fungus *Fusarium oxysporum* isolated from *Catharanthus roseus*. *Plos One*, 8, e71805-e71815.
66. Kumar S., Aharwal R. P., Shukla H., Rajak R. C., Sandhu S. S. (2014) Endophytic fungi: as a source of antimicrobials bioactive compounds. *WJPPS*, 3, 1179-1197.
67. Kusari S., Zühlke S., Spiteller M. (2009) An endophytic fungus from *Camptotheca acuminata* that produces camptothecin and analogues. *J. Nat. Prod.*, 72, 2-7.
68. Kusari S., Hertweck C., Spiteller M. (2012) Chemical Ecology of Endophytic Fungi: Origins of Secondary Metabolites. *Chemistry & Biology*, 19, 792-798.
69. Lam K. S. (2007) New aspects of natural products in drug discovery. *Trends. Microbiol.*, 15, 279-289.
70. Laupacis A., Keown P. A., Ulan R. A., McKenzie N., Stiller, C. R. (1982). Cyclosporin A: a powerful immunosuppressant. *Can. Med. Assoc. J.*, 126, 1041-1046.
71. Lavergne O., Lesueur-Ginot L., Rodas F. P., Kasprzyk P. G., Pommier J., Demarquay D., Prévost G., Ulibarri G., Rolland A., Schiano-Liberatore A., Harnett J., Pons D., Camara J., Bigg D. C. H. (1998) Homocamptothecins: Synthesis and Antitumor Activity of Novel E-Ring-Modified Camptothecin Analogues. *J. Med. Chem.*, 41, 5410-5419.
72. Lee Y. M., Kim M. J., Li H., Zhang P., Bao B., Lee K. J., Jung J. H. (2013) Marine-Derived *Aspergillus* Species as a Source of Bioactive Secondary Metabolites. *Mar. Biotechnol.*, 15, 499-519.
73. Lorence A. and Nessler C. L. (2004) Camptothecin, over four decades of surprising findings. *Phytochemistry*, 65, 2735-2749.
74. Maezato Y. and Blum P. (2012) Survival of the fittest: overcoming oxidative stress at the extremes of acid, heat and metal. *Life*, 2, 229-242.
75. Manulis S., Kashman Y., Netzer D., Brash I. (1984) Phytotoxins from stemphylium botryosum: structural determination of stemphyloxin II, production in culture and interaction with iron. *Phytochemistry*, 23, 2193-2198.

76. Millward M., Mainwaring P., Mita A., Federico K., Lloyd G. K., Reddinger N., Nawrocki S., Mita M., Spear M. A. (2012) Phase 1 study of the novel vascular disrupting agent plinabulin (NPI-2358) and docetaxel. *Invest. New Drugs*, 30, 1065-1073.
77. Mita M. M., Spear Ma. A., Yee L. K., Mita A. C., Heath E. I., Papadopoulos K. P., Federico K. C., Reich S. D., Romero O., Malburg L., Pilat M., Lloyd G. K., Neuteboom S. T. C., Cropp G., Ashton E., LoRusso P. M. (2010) Phase 1 First-in-Human Trial of the Vascular Disrupting Agent Plinabulin (NPI-2358) in Patients with Solid Tumors or Lymphomas. *Clin. Cancer Res.*, 16, 5892-5899.
78. Netzker T., Fischer J., Weber J., Mattern D. J., König C. C., Valiante V., Schroeckh V., Brakhage A. A. (2015) Microbial communication leading to the activation of silent fungal secondary metabolite gene clusters. *Front. Microbiol.*, 6, 1-13.
79. Newman D. J., Cragg G. M., Snader K. M. (2000) The influence of natural products upon drug discovery. *Nat. Prod. Rep.*, 17, 215-234.
80. Newman D. J. and Cragg G. M. (2012) Natural products as sources of new drugs over the 30 years from 1981 to 2010. *J. Nat. Prod.*, 75, 311-335.
81. Nisa H., Kamili A. N., Nawchoo I. A., Shafi S., Shameem N., Bandh S. A. (2015) Fungal endophytes as prolific source of phytochemicals and other bioactive natural products: A review. *Microb. Pathogenesis*, 82, 50-59.
82. Nützmann H., Reyes-Domingue Y., Scherlach K., Schroeckh V., Horn F., Gacek A., Schumann J., Hertweck C., Strauss J., Brakhage A. A. (2011) Bacteria-induced natural product formation in the fungus *Aspergillus nidulans* requires Saga/Ada-mediated histone acetylation. *Proc. Natl. Acad. Sci.*, 108, 14282–14287.
83. Ola A. R. B., Thomy D., Lai D., Brötz-Oesterhelt H., Proksch P. (2013) Inducing secondary metabolite production by the endophytic fungus *Fusarium tricinctum* through coculture with *Bacillus subtilis*. *J. Nat. Prod.*, 76, 2094-2099.
84. Oliveira A. L. L., Felício R., Deboni H. M. (2012) Marine natural products: chemical and biological potential of seaweeds and their endophytic fungi. *Rev. Bras. Farmacogn.*, 22, 906-920.
85. Ortholand J. Y. and Ganesan A. (2004) Natural products and combinatorial chemistry: back to the future. *Curr. Opin. Chem. Biol.*, 8, 271–280.

86. Overy D. P., Bayman P., Kerr R. G., Bills G. F. (2014) An assessment of natural product discovery from marine (*sensu strictu*) and marine-derived fungi. *Mycology*, 5, 145-167.
87. Parker S. L., Tong T., Bolden S., Wingo P. A. (1996) Cancer Statistics, 1996. *CA-Cancer J. Clin.*, 65, 5-27.
88. Pimentel M. R., Molina G., Dionísio A. P., Junior M. R. M., Pastore G. M. (2011) The Use of Endophytes to Obtain Bioactive Compounds and Their Application in Biotransformation Process. *Biotechnol. Res. Int.*, 2011, 576286-576297
89. Pusztai L. (2007) Markers predicting clinical benefit in breast cancer from microtubule-targeting agents. *Ann. Oncol.*, 18, 15-20.
90. Rateb M. E. and Ebel R. (2011) Secondary metabolites of fungi from marine habitats. *Nat. Prod. Rep.*, 28, 290-344.
91. Rateb M. E., Hallyburton I., Houssen W. E. Bull A. T., Goodfellow M., Santhanam R., Jaspars M., Ebel R. (2013) Induction of diverse secondary metabolites in *Aspergillus fumigatus* by microbial co-culture. *RSC Adv.*, 3, 14444-14450.
92. Rehman S., Shawl A. S., Kour A., Andrabi R., Sudan P., Sultan P., Verma V., Qazi G. N. (2008) An endophytic *Neurospora* sp. from *Nothapodytes foetida* producing camptothecin. *Appl. Biochem. Microbiol.*, 44, 203–209.
93. Saleem M., Ali M. S., Hussain S., Jabbar A., Ashraf M., Lee Y. S. (2007) Marine natural products of fungal origin. *Nat. Prod. Rep.*, 24, 1142–1152.
94. Scherlach K. and Hertweck C. (2009) Triggering cryptic natural product biosynthesis in microorganisms. *Org. Biomol. Chem.*, 7, 1753-1760.
95. Schroeckh V., Scherlach K., Nützmann H., Shelest E., Schmidt-Heck W., Schuemann J., Martin K., Hertweck C., Brakhage A. A. (2009) Intimate bacterial–fungal interaction triggers biosynthesis of archetypal polyketides in *Aspergillus nidulans*. *Proc. Natl. Acad. Sci.*, 106, 14558-14563.
96. Shukla S. T., Habbu P. V., Kulkarni V. H., Jagadish K. S., Pandey A. R., Sutariya V. N. (2014) Endophytic microbes: A novel source for biologically/pharmacologically active secondary metabolites. *AJPT*, 2, 1-16.
97. Shweta S., Gurumurthy B. R., Ravikanth G., Ramanan U. S., Shivanna M.B. (2013) Endophytic fungi from *Miquelia dentata* Bedd., produce the anti-cancer

- alkaloid,camptothecine. *Phytomedicine*, 20, 337-342.
98. Singh A. V., Bandi M., Raje N., Richardson P., Palladino M. A., Chauhan D., Anderson K. C. (2011) A novel vascular disrupting agent plinabulin triggers JNK-mediated apoptosis and inhibits angiogenesis in multiple myeloma cells. *Blood*, 117, 5692-5700.
99. Slattery M. and Wesson R. K. (2001) Competition-mediated antibiotic induction in the marine bacterium *Streptomyces tenjimariensis*. *Microb. Ecol.*, 41, 90-96.
100. Soliman S. S. M., Trobacher C. P., Tsao R., Greenwood J. S., Raizada M. N. (2013) A fungal endophyte induces transcription of genes encoding a redundant fungicide pathway in its host plant. *BMC Plant. Biol.*, 13, 93-103.
101. Somjaipeng S., Medina A., Kwasna H., Ortiz J. O., Magan N. (2015) Isolation, identification, and ecology of growth and taxol production by an endophytic strain of *Paraconiothyrium variabile* from English yew trees (*Taxus baccata*). *Fungal Biol.*, 119, 1022-1031.
102. Sikora K., Advani S., Koroltchouk V., Magrath I., Levy L., Pinedo H., Schwartzmann G., Tattersall M., Yan S. (1999) Essential drugs for cancer therapy: A World Health Organization consultation. *Ann. Oncol.*, 10, 385-390.
103. Simpson T. J. (1987) Applications of Multinuclear NMR to Structural and Biosynthetic Studies of Polyketide Microbial Metabolites. *Chem. SOC. Rev.*, 16, 123-160.
104. Sirikantaramas S., Yamazaki M., Saito K. (2009) A survival strategy: The coevolution of the camptothecin biosynthetic pathway and self-resistance mechanism. *Phytochemistry*, 70, 1894-1898.
105. Slattery M., Rajbhandari I., Wesson, K. (2001) Competition-mediated antibiotic induction in marine bacterium *Streptomyces tenjimariensis*. *Microb. Ecol.*, 41, 90-96.
106. Sreekanth D., Sushim G. K., Syed A., Khan B. M., Ahmad A. (2011) Molecular and morphological characterization of a Taxol-producing endophytic fungus, *Gliocladium sp.*, from *Taxus baccata*. *Mycobiology*, 39, 151-157.
107. Šterzl J., Cudlín J., Steinerová N., Johanovská D., Milerová J. (1981) The immunoinhibitory and immunostimulatory effect of hydroxyanthra- and hydroxynaphthoquinone derivatives. *Folia Microbiol.*, 26, 169-175.
108. Stierle A., Strobel G., Stierle D. (1993) Taxol and Taxane Production by *Taxomyces*

- andreae*, an Endophytic Fungus of Pacific Yew. *Science*, 260, 214-216.
109. Stone E. A., Fung H. B., Kirschenbaum H. L. (2002) Caspofungin: An Echinocandin Antifungal Agent. *Clin. Ther.*, 24, 351-37.
110. Strobel G. and Daisy B. (2003) Bioprospecting for Microbial Endophytes and Their Natural Products. *Microbiol. Mol. Biol. Rev.*, 67, 491-502.
111. Subramani R. and Aalbersberg W. (2012) Marine actinomycetes: An ongoing source of novel bioactive metabolites. *Microbiol. Res.*, 167, 571- 580.
112. Suryanarayanan T. S., Thirunavukkarsu N., Govindarajulu M. B., Sasse F., Jansen R., Murali, T. S. (2009) Fungal endophytes and bioprospecting. *Fungal Biol. Rev.*, 23, 9-19.
113. Sweet R. M. and Dahl L. F. (1970) Molecular Architecture of the Cephalosporins. Insights into Biological Activity Based on Structural Investigations. *J. Am. Chem. Soc.*, 92, 5489-5507.
114. Tan R. X. and Zou W. X. (2001) Endophytes: a rich source of functional metabolites. *Nat. Prod. Rep.*, 18, 448-459.
115. Tanaka Y., Kasahara K., Hirose Y., Murakami K., Kugimiya R., Ochi K. (2013) Activation and Products of the Cryptic Secondary Metabolite Biosynthetic Gene Clusters by Rifampin Resistance (*rpoB*) Mutations in Actinomycetes. *J. Bioact.*, 195, 2959-2970.
116. Vasudev N. S. and Reynolds A. R. (2014) Anti-angiogenic therapy for cancer: current progress, unresolved questions and future directions. *Angiogenesis*, 17, 471-494.
117. Wang Z., Dabrosin C., Yin X., Fuster M. M., Arreola A., Rathmell W. K., Generali D., Nagaraju G. P., El-Rayes B., Ribatti D. i, Chen Y. C., Honoki K., Fujii H., Georgakilas A. G., Nowsheen S., Amedei A., Niccolai E., Amin A., Ashraf S. S., Helferich B., Yang X., Guha G., Bhakta D., Ciriolo M. R., Aquilano K., Chen S., Halicka D., Mohammed S. I., Azmi A. S., Bilsland A., Keith W. N., Jensen L. D. (2015) Broad targeting of angiogenesis for cancer prevention and therapy. *Seminars in Cancer Biology*, 35, S224-S243
118. Wang Y, Zhang H., Gigant B., Yu M, Wu Y., Chen X., Lai Q., Yang Z., Chen Q., Yang J. (2016) Structures of a diverse set of colchicine binding site inhibitors in complex with tubulin provide a rationale for drug discovery. *FEBS Journal*, 283, 102-111.
119. Wall, M. E. and Wani, M. C. (1996). Camptothecin and taxol: from discovery to clinic. *J. Ethnopharmacol.*, 51, 239-254.

120. Wang X., Radwan M. M., Taráwneh A. H., Gao J., Wedge D. E., Rosa L. H., Cutler H. G., Cutler S. J. (2013) Antifungal activity against plant Pathogens of metabolites from the endophytic fungus *Cladosporium cladosporioides*. *J. Agric. Food Chem.*, 61, 4551-4555.
121. Wani M. C., Taylor H. L., Wall M. E., Coggon P., McPhail A. T. (1971) Plant Antitumor Agents. VI. The Isolation and Structure of Taxol, a Novel Antileukemic and Antitumor Agent from *Taxus breoifolia*. *J. Am. Chem. Soc.*, 93, 2325-2327.
122. Wani M. C. and Horwitz S. B. (2014) Nature as a remarkable chemist: a personal story of the discovery and development of Taxol. *Anti-Cancer Drug.*, 25, 482-487.
123. Wilson D. (1995) Endophyte: the evolution of a term, and clarification of its use and definition. *Oikos*, 73, (2), 274-276
124. Wilson L., Creswell K. M., Chin D. (1975) The mechanism of action of Vinblastine. Binding of [acetyl-³H] Vinblastine to embryonic chick brain tubulin and Tubulin from sea Urchin sperm tail outer doublet microtubules. *Biochemistry*, 14, 5586-5592.
125. Wu Y. B., Zheng C. J., Qin L. P., Sun L. N., Han T., Jiao L., Zhang Q. Y., Wu J. Z. (2009) Antiosteoporotic activity of anthraquinones from *Morinda officinalis* on Osteoblasts and Osteoclasts. *Molecules*, 14, 573-583.
126. Xiong Z. Q., Yang Y. Y., Zhao N., Wang Y. (2013) Diversity of endophytic fungi and screening of fungal paclitaxel producer from Anglojap yew, *Taxus media*. *BMC Microbiol.*, 13, 71-81.
127. Yamazaki Y., Kido Y., Hidaka K., Yasui H., Kiso Y., Yakushiji F., Hayashi Y. (2011) Tubulin photoaffinity labeling study with a plinabulin chemical probe possessing a biotin tag at the oxazole. *Bioorg. Med. Chem.*, 19, 595-602
128. Yamazaki Y., Tanaka K., Nicholson B., Deyanat-Yazdi G., Potts B., Yoshida T., Oda A., Kitagawa T., Orikasa S., Kiso Y., Yasui H., Akamatsu M., Chinen T., Usui T., Shinozaki Y., Yakushiji F., Miller B. R., Neuteboom S., Palladino M., Kanoh K., Lloyd G. K., Hayashi Y. (2012) Synthesis and Structure–Activity Relationship Study of Antimicrotubule Agents Phenylahistin Derivatives with a Didehydropiperazine-2,5-dione Structure. *J. Med. Chem.*, 55, 1056-1071
129. Yang K. L., Wei M. Y., Shao C. L., Fu X. M., Guo Z. Y., Xu R. F., Zheng C. J., She Z.

- G., Lin Y. C., Wang C. Y. (2012) Antibacterial anthraquinone derivatives from a sea anemone-derived fungus *Nigrospora* sp. *J. Nat. Prod.*, 75, 935-941.
130. Yakushiji F., Tanaka H., Muguruma K., Iwahashi T., Yamazaki Y., Hayashi Y. (2011). Water-Soluble Prodrug of Antimicrotubule Agent Plinabulin: Effective Strategy with Click Chemistry. *Chem. Eur. J.*, 17, 12587-12590.
131. Zhang M., Hou X. F., Qi L. H., Yin Y., Li Q., Pan H. X., Chen X. Y., Tang G. L. (2015) Biosynthesis of trioxacarcin revealing a different starter unit and complex tailoring steps for type II polyketide synthase. *Chem. Sci.*, 6, 3440-3447.
132. Zhang Y. Q., Brock M., Keller N. P. (2004) Connection of Propionyl-CoA Metabolism to Polyketide Biosynthesis in *Aspergillus nidulans*. *Genetics*, 168, 785–794.
133. Zuma A. A., Cavalcanti D. P., Maia M. C.P., Souza W., Motta M. C. M. (2011) Effect of topoisomerase inhibitors and DNA-binding drugs on the cell proliferation and ultrastructure of *Trypanosoma cruzi*. *Int. J. Antimicrob. Agents*, 37, 449-456.

8 Abbreviations

A2780 CisR	Cisplatin resistance, human ovarian cancer cell line
A2780 Sens	Cisplatin sensitive, humane ovarian cancer cell line
br	broad signal
CD	Circular Dichroism
CDCl ₃	deuterated chloroform
CH ₂ Cl ₂	dichloromethane
CHCl ₃	chloroform
cm	centimeter
COSY	correlation spectroscopy
CoA	coenzyme A
d	doublet
DCM	dichloromethane
dd	doublet of doublet
DMSO	dimethyl sulfoxide
DNA	deoxyribonucleic acid
ED	effective dose
EI	electron impact ionization
ESI	electrospray ionization
et al.	et altera (and others)
EtOAc	ethyl acetate
eV	electronvolt
g	gram
HMBC	heteronuclear multiple bond connectivity
HMQC	heteronuclear multiple quantum coherence
H ₂ O	water
HPLC	high performance liquid chromatography
H ₃ PO ₄	phosphoric acid

HR-MS	high resolution mass spectrometry
Hz	Herz
L	liter
LC	liquid chromatography
LC/MS	liquid chromatography-mass spectrometry
m	multiplet
M	molar
MeOD	deuterated methanol
MeOH	methanol
mg	milligram
MHz	mega Herz
min	minute
mL	milliliter
MS	mass spectrometry
MTT	microculture tetrazolium assay
m/z	mass per charge
NaCl	sodium chloride
NADPH	nicotinamide adenine dinucleotide phosphate
NMR	nuclear magnetic resonance
NOE	nuclear Overhauser effect
NOESY	nuclear Overhauser and exchange spectroscopy
PCR	polymerase chain reaction
ppm	parts per million
q	quartet
ROESY	rotating frame overhauser enhancement spectroscopy
RP 18	reversed phase C 18
s	singlet
sp.	species (singular)

t	triplet
TFA	trifluoroacetic acid
THF	tetrahydrofuran
TLC	thin layer chromatography
UV	ultra-violet
VLC	vacuum liquid chromatography
μg	microgram
μL	microliter
μM	micromol
$[\alpha]_{\text{D}}^{20}$	specific rotation at the sodium D-line

9 Acknowledgements

It's my pleasure to have the chance to thank all the people that involved in my Ph.D research, without your help and support, I will be not successful to finish my study; without sharing the knowledge and happiness, I will not so enjoy all the time here. Those valuable time will be in my heart forever!

First of all, I sincerely pay the respects to Prof. Proksch for the valuable opportunity to study as Ph.D in the Institute of Pharmaceutical Biology and Biotechnology, Heinrich-Heine University Duesseldorf. My research will not be so successful without the support and guidance of Prof. Dr. Peter Proksch. I would like to express my heartfelt thanks to Prof. Proksch for the nice working conditions, as well as his scientific suggestions, valuable discussions, unforgettable support, meticulous care and attentions. Thank you so much Prof. Proksch!

I am deeply indebted to Prof. Dr. Changyun Wang (Key Laboratory of Marine Drugs, School of Medicine and Pharmacy, Ocean University of China) for his recommendation and support to do the doctoral researches in the group of Prof. Proksch, as well as his valuable suggestions and plans for my further career.

My deep gratitude to Prof. Dr. Rainer Kalscheuer, Institute of Pharmaceutical Biology and Biotechnology, Heinrich-Heine University Duesseldorf, as my second mentor during my study, and a lots of thanks for his kindly suggestions and helpful performing of antibiotic assay of the collaboration.

I want to express my cordial thanks to Prof. Dr. Wenhan Lin (State Key Laboratory of Natural and Biomimetic Drugs, Beijing University, Health Science Center) for his help to solve the difficulties during my doctoral research, as well as the valuable suggestions for my further researches.

I am very appreciate to Dr. Tibor Kurtán, Department of Organic Chemistry, University of Debrecen, Hungary, for the collaboration of my research to make the ECD calculation.

I want to give my special acknowledgement to Dr. Georgios Daletos for mentorship of sharing the knowledge with me, and the numerous help for the experimental suggestions, NMR elucidation, and the correction of my manuscript and the dissertation. I also want to give my thanks to Dr. Daowan Lai for his help and scientific advice during my first year study; Also many thanks to my colleague and friend Catalina Pérez Hemphill for guiding me to be familiar with the institute, and sharing a lot of happy time together.

I would like to thank Prof. W. E. G. Müller, Johannes Gutenberg University, Mainz, Germany, and Prof. Dr. Matthias Kassack, Institut of Pharmaceutical and Medicinal Chemistry, Heinrich-Heine University, Duesseldorf, for the cytotoxicity assays; Prof. Dr. Horst Weber, Institute of Pharmaceutical and Medicinal Chemistry, Heinrich Heine University, Duesseldorf, Germany, Fabian Stuhldreier from the group of Prof. Sebastian Wesselborg, Institute of Molecular Medicine, Heinrich Heine University, Duesseldorf, Germany for the further study of cytotoxic mechanism. Dr. Tommes, Mr. Bürgel, Ms. Karkoschke and Ms. Beuer for their NMR and MS measurements.

My deep appreciate to the my Chinese professors for their kindness and valuable suggestion and help, and for their professional discussion and suggestions. Prof. Dr. Bingui Wang, Laboratory of Experimental Marine Biology, Institute of Acknowledgements II Oceanology, Chinese Acedemy of Science, Qindao, China; Prof. Haofu Da, Key Laboratory of Biology and Genetic Resources of Tropical Crops, Ministry of Agriculture, Institute of Tropical Bioscience and Biotechnology, Chinese Academy of Tropical Agricultural Sciences

I would like to express my appreciation to our secretary Mrs. Claudia Eckelskemper, our technicians Mrs. Waltraud Schlag, Mrs. Simone Miljanovic, Mrs. Katja Friedrich, Mrs. Heike Goldbach-Gecke, Mrs. Simone Mönninghoff-Pützer, Mrs. Linda Wiegand, Institute of

Pharmaceutical Biology and Biotechnology, Heinrich-Heine University, Duesseldorf, for her various help and assistant for the help to solve my problems during the living and study whenever needed.

My deep appreciate to my former colleagues: Dr. Andreas Marmann, Dr. Hendrik Niemann, Dr. Cong-Dat Pham, Dr. Antonius R B Ola, Dr. Hammerschmidt Lena, Dr. Amal Hassan, Dr. Sherif Sayed Ebada, Dr. Mustapha ElAmrani, Dr. Festus Okoye, Dr. Mousa AlTarabeen, Dr. Huiqin Chen as well as my present colleagues: Dr. Weaam Ebrahim, Dr. Zhen Liu, Dr. Elena Ancheeva, Dr. Ramsay Kamdem, Rini Muharini, Hervé Sergi Akoné, Mi-Young Chung, Imke Form, Marian Frank, Amin Mokhlesi, Shuai Liu, Mariam Moussa, Hao Wang, Haiqian Yu, Nam Michael Tran-Cong, because of you, I have a really nice time during the study and sharing the happiness.

My great thankful to China Scholarship Council, the Ministry of Education of China for the financial support during my study.

At the end, I really wish to show my deepest thanks to my family for their encouraging, understanding and company for time I study here.

Yang Liu**Curriculum Vitae**

Date of Birth Dalian, 22 Feb. 1986, China

Address Institute of Pharmaceutical Biology and Biotechnology,
Heinrich-Heine-University,
40225, Duesseldorf

E-mail Address Yang.Liu@hhu.de or liuyangthink@163.com

EDUCATION

Qualification Doctoral Canditate (Sep. 2012 - Jan. 2016)

Instituion Heinrich Heine Universität Düsseldorf Germany

Discipline Microbial Natural Product Chemistry

Qualification Master (Sep. 2009 - Jul. 2012)

Institution Ocean University of China, China

Discipline Marine Natural Products Chemistry

Qualification Bachelor (Sep. 2005 - Sep. 2009)

Institution Shenyang University, China

Discipline Bioengineering

RESEARCH EXPERIENCE

A. Microbial Natural Product for Drug Discovery

- Isolation and identification of fungi from terrestrial and marine environment
- Isolation and identification of bioactive compounds from Endophytic Fungi

- Media cultivation experiments for enhancing chemical profile of endophytic fungi

B. New Approach for Activation Silent Biosynthetic Pathways in Microorganism

- Epigenetic experiment for enhancing chemical profile by using histone modifier
- Mix fermentation for natural product drug discovery (Co-cultivation experiment Bacteria vs Fungi and Fungi vs Fungi).
- The production of antibiotic fungal compounds through co-culture with bacteria

TECHNICAL SKILLS AND EXPERIENCE

Chemical Extraction and Separation

- Small-scale and large-scale extraction of biological material
- Liquid-liquid partitioning, Solid Phase extraction, Thin Layer Chromatography, Column Chromatography
- Preparative and analytical HPLC and LC-MS using UV-Vis (photodiode array) detection
- HPLC fault diagnosis and repairs
- Analytical GC and GC-MS

Fungal Isolation and Identification

- Isolated around 150 endophytic fungi from plant and sediment
- RNA isolation and PCR amplification and purification.

Spectroscopy and Structure Elucidation

- Interpretation of 1D and 2D NMR data for complete structure elucidation and assignment of chemical shifts
- Operation and interpretation of UV/Vis and FT-IR for assisting in structure elucidation

- Interpretation of ES-MS data for assisting in compound identifications
 - Interpretation of GC-MS for chemical compounds identification
-

PUBLICATIONS AND SUBMITTED MANUSCRIPT

Yang Liu, Tibor Kurtán, Chang Yun Wang, Wen Han Lin, Raha Orfali, Werner EG Müller, Georgios Daletos and Peter Proksch. Cladosporinone, a new viriditoxin derivative from the hypersaline lake derived fungus *Cladosporium cladosporioides*. *The Journal of Antibiotics*, 2016, advance online publication, 1–5.

Yang Liu, Andreas Marmann, Mohamed S. Abdel-Aziz, Chang Yun Wang, Werner E. G. Müller, Wen Han Lin, Attila Mándi, Tibor Kurtán, Georgios Daletos, and Peter Proksch. Tetrahydroanthraquinone Derivatives from the Endophytic Fungus *Stemphylium globuliferum*. *European Journal of Organic Chemistry*, 2015, 12, 2646-2653.

Yang Liu, Victor Wray, Mohamed S. Abdel-Aziz, Chang-Yun Wang, Daowan Lai, and Peter Proksch. Trimeric Anthracenes from the Endophytic Fungus *Stemphylium globuliferum*. *Journal of Natural Products*, 2014, 77, 1734–1738.

Yang Liu, Fabian Stuhldreier, Tibor Kurtán, Attila Mándi, Sathishkumar Arumugam, Chang Yun Wang, Wen Han Lin, Sebastian Wesselborg, Horst Weber, Birgit Henrich, Georgios Daletos, and Peter Proksch. Benzo[j]fluoranthene Metabolites from the Mangrove Derived Endophytic Fungus *Annulohyphoxylon* sp. *Journal of Natural Products*, 2016, (submitted).

Yang Liu, Jie Zhao, Shanglun Shao, Changyun, Wang. Review on the secondary metabolites from blue starfish *Linckia laevigata* and their bioactivities. *Chinese Journal of Marine Drugs*, 2011, 30, 52-58.

Chang-Yun Wang, Chang-Lun Shao, Xiu-Mei Fu, Mei-Yan Wei, **Yang Liu**. Marine Pharmacology[M]. Beijing Science Press, 2011.

Lingling Sun, **Yang Liu**, Gaifang Hou, Changlun Shao, Changyun Wang. Chemical constituents from *Chondrophyucus papillosus* C.Agerdh Garbary et Harper. Marine Drug Symposium Proceedings of the Tenth China[C], 2009, 322-325.

Xin Liu, Gaifang Hou, **Yang Liu**, Changlun Shao, Changyun Wang. Studies on the chemical constituents of *Sargassum pallidum* (Turn.) C.Ag. Marine Drug Symposium Proceedings of the Tenth China[C], 2009, 340-345.

Honors

Granted a full scholarship from Program of Governmental Graduate students Scholarship launched by China Scholarship Council (09. 2012-08. 2014)